Synthesis and Characterization of Some Nanofluids for Direct Absorption Solar Collectors

Thesis Submitted

By

Pritam Kumar Das

Doctor of Philosophy (Engineering)

Department of Power Engineering,

Faculty Council of Engineering and Technology

Jadavpur University

Kolkata, India

Year: 2018

JADAVPUR UNIVERSITY

KOLKATA – 700 032, INDIA

INDEX NO. 222/13/E

1. Title of the thesis:

Synthesis and Characterization of Some Nanofluids for Direct Absorption Solar Collectors

2. Name, Designation & Institution of the Supervisors:

Dr. Apurba Kumar Santra, Professor, Dept. of Power Engineering, Jadavpur University, Salt Lake Campus, Kolkata–700098.

Dr. Ranjan Ganguly, Professor, Dept. of Power Engineering, Jadavpur University, Salt Lake Campus, Kolkata–700098.

3. List of Publications (Journals):

i. **P.K. Das**, A.K. Mallik, A.K. Santra, R. Ganguly, Synthesis and characterization of TiO_2-water nanofluids with different surfactants, International Communications in Heat and Mass Transfer 75 (2016) 341–348.

ii. **P.K. Das**, N. Islam, A.K. Santra, R. Ganguly,Experimental investigation of thermophysical properties of Al_2O_3-water nanofluid: role of surfactants, Journal of Molecular Liquids 237 (2017) 304–312.

iii. **P.K. Das**, A.K. Mallik, A.K. Santra, R. Ganguly, Stability and thermophysical measurements of TiO_2 (anatase) nanofluids with different surfactants, Journal of Molecular Liquids 254 (2018) 98–107.

4. List of Patents: Nil

5. List of Presentation in National/International Conferences:

i. **P.K. Das**, A.K. Santra and R. Ganguly, Numerical Study of Forced Convective Heat Transfer of Nanofluids through a Long Straight Tube, International Conference on Frontiers in Chemical Engineering (*ICFCE 2013*), 9-11th December 2013, NIT Rourkela.

ii. **P.K. Das**, A.K. Santra, CFD Simulation on Laminar Forced Convection Heat Transfer of Cu-water Nanofluids inside a Vertical Tube, International Conference on Electronics

and Communication System (*ICECS 2014*), 13-14th February 2014, 978-1-4799-2320-5/14/$31.00 (c) 2014 IEEE.

iii. **P.K. Das**, A.K. Santra and R. Ganguly, Study of performance of direct absorption solar collector using nanofluids, 5th International Conference on Fluid Mechanics and Fluid Power (*FMFP-2014*), IIT Kanpur.

iv. **P.K. Das**, A.K. Santra and R. Ganguly, Numerical investigation of heat transfer coefficient of nanofluids flow through a vertical pipe, International Conference on Advanced Materials and Energy Technology (*ICAMET-2014*) 17-19th December 2014, BESU West Bengal.

v. **P.K. Das**, A.K. Santra and R. Ganguly, Performance analysis of direct absorption solar collector using multiphase model, Proceedings of the 23rd National Heat and Mass Transfer Conference and 1st International ISHMT-ASTFE Heat and Mass Transfer Conference (IHMTC-2015), 17-20th December 2015, Thiruvananthapuram, India.

vi. **P.K. Das**, R. Ganguly, A.K. Santra, Experimental investigation on thermal conductivity of TiO_2-water based nanofluids, 6th International and 43rd National Conference on Fluid Mechanics and Fluid Power (FMFP-2016), 15-17th December, 2016, MNNIT, Allahabad, U.P., India.

vii. **P.K Das**, N. Islam, K. Zakaria, B. Roy, A.K. Santra, R. Ganguly, Measurement of surface tension and contact angle of different nanofluids: An experimental study, 24th National and 2nd International ISHMT-ASTFE Heat and Mass Transfer Conference (IHMTC-2017), 27-30th December 2017.

CERTIFICATE FROM THE SUPERVISORS

This is to certify that the thesis entitled ***"Synthesis and Characterization of Some Nanofluids for Direct Absorption Solar Collectors"*** *submitted by* ***Shri Pritam Kumar Das****, who got his name registered on* ***23rd of October, 2013*** *for the award of the* ***Ph.D. (Engineering)*** *degree of Jadavpur University, is absolutely based upon his own work under the supervision of* ***Prof. Apurba Kumar Santra*** *and* ***Prof. Ranjan Ganguly, Jadavpur University,*** *and that neither his thesis nor any part of the thesis has been submitted for any degree/diploma or any other academic award anywhere before.*

Signature of the Supervisor
and date with office seal

Signature of the Supervisor
and date with office seal

Dedicated to my Parents
&
my Family

ACKNOWLEDGEMENT

I am feeling honoured to express my sincerest gratitude and indebtedness to Prof. Apurba Kumar Santra and Prof. Ranjan Ganguly, my supervisor for the valuable suggestions, exemplary guidance, monitoring and constant encouragements throughout the course of this dissertation work. It is impossible for me to express my gratitude in words for the immense emotional support he provided at different stages of this work.

I would like to express my sincere gratitude to Prof. Amitava Datta, Dept. of Power Engineering, Jadavpur University, for the technical as well as moral support during all time of this work.

I must confess that this work would not have culminated in a success if I did not have the support of Mr. Arnab mallik, Mr. Nurul Islam, Mr. Atmadeep Bhattacharya, Mr. Bijoy Das, Mr. Mithun Das, Mr. Sajjan Kumar, Mr. Atish Nandi and other scholars in my lab. Furthermore, I would also like to take this opportunity to thank Mr. Jitendra Patra, Dr. Prakash Ghosh for their initial support.

I would like to acknowledge the UGC-sponsored DRS program of the Department of Power engineering, Jadavpur University for its support provided to carry out the present research work and also acknowledges the additional support provided by TEQIP Phase-II in the form of a research fellowship. I would also acknowledge Prof. Kalyan K. Chattopadhyay of School of Materials Science & Nanotechnology, Jadavpur University, for the TEM data, CRNN, University of Calcutta for the DLS and viscosity measurement facility, Dr. Aparna Datta and Dr. Abhijit Saha of Inter University Consortium (IUC) for DLS and Zeta potential measurements and valuable insight on particle size distribution.

I would like to thank everyone in my family for their incessant support and encouragement. Moreover, I remember with gratitude the constant guidance, suggestions and encouragement forwarded by several respected persons and know very well that it is impossible to express my indebtedness for all those valuable assistances in this finite piece of paper. Following conventions, I therefore, acknowledge in this page, the assistance rendered by all of them.

List of Figures

List of tables

Abstract

Need for research in the area of harnessing renewable energy resources and conversion device has seen a drastic rise in the recent past in the face of depleting fossil fuel reserve and the burgeoning concern over the global warming. Harnessing solar energy with solar thermal collectors deploying advanced heat transfer materials has been pitched as a viable option by several researchers. Direct absorption solar collection (DASC) is a genre of solar thermal collector (STC), which allows direct absorption of solar energy in the heat transfer fluid. Nanofluids are the colloidal suspension of nanoparticles that have attracted much attention due to their enhanced heat transfer characteristics. It is therefore intuitive that the use of nanofluids with suitable thermophysical properties in DASC can augment the collector efficiency appropriately. However, such deployment would require a priori knowledge of the nanofluid properties like thermal stability, thermal conductivity, viscosity, etc.

The main aim of this research is to investigate the stability and characterize the properties of some nanofluids for a possible application in DASC. Different types of synthesis routes of nanofluids are discussed from the literature and their properties are compared. Theoretical models of thermal conductivity and viscosity are also summarized. Literature review clearly indicates a conflict amongst the reports by various groups on the thermophysical properties of different nanofluids – some of them are inconclusive and others describe contradicting trends while characterizing the effect of different parameters on thermal conductivity and viscosity of nanofluids. Stabilization of the nanofluid, which is also important for industrial applications, is addressed additionally. From the literature survey, the gap areas are identified on which the study is focused.

Three different types of nanoparticles (TiO_2, Al_2O_3, TiO_2-anatase) are chosen to prepare the nanofluids. Stability of the nanoparticle suspension with various surfactants, e.g., acetic acid (AA), oleic acid (OA), cetyl trimethyl ammonium bromide (CTAB), sodium dodecylbenzenesulfonate (SDBS), and sodium dodecyl sulfate (SDS), is investigated. CTAB and AA surfactants are found to provide stable suspensions for TiO_2 nanoparticles, SDBS works well for Al_2O_3 nanoparticles, while SDS and CTAB offer good stability for TiO_2 (anatase) nanoparticles. Transmission electron microscopy (TEM) measurement indicates the morphological behaviour of nanoparticles. Dynamic

light scattering (DLS) measurements shows particle size, clustering and polydispersity index of the suspension. Zeta potential techniques shows the stability of the nanofluids. The thermal conductivity, viscosity, and surface tension are measured using a KD2-Pro thermal conductivity meter; a Brookfield viscometer; and a standard tensiometer, respectively. Besides, the contact angle and pH of nanofluids are also measured under different levels of particle volume fraction φ and temperature T.

Thermal conductivity of the synthesized, stable nanofluids are measured for different φ (0.1–2.0 %) and T (20–60 °C). For all the nanofluids, thermal conductivity is found to increase with the increase in both φ and T. The observed thermal conductivity ratio of the nanofluid to base fluid (k_{nf}/k_f) match well with existing correlation in the literature for $\varphi > 1.0$ % but are underpredicted for lower range of φ. Modifications of existing property models are proposed to match the observed (k_{nf}/k_f) values. The difference between the experimentally observed k_{nf}/k_f values and those predicted from models can be attributed to the limitation in accounting for the dynamic factor. Dynamic effect becomes more tangible at very low φ. Viscosity, surface tension, pH and contact angle data of the prepared nanofluid are measured for the respective φ and T. Moreover, the effect of shear rate on viscosity of nanofluids are also studied. Viscosity of the nanofluid is found to increase with φ and decrease with T. TiO_2-AA and -CTAB nanofluids show slight shear thickening behavior for shear rates ranging between 76 to 760 s^{-1}. The value of critical shear rate depends on the particle loading and nanofluid temperature. It is observed that for a particular φ the critical shear rate decreases with increase in temperature. Surface tension and contact angle of the nanofluids decrease with increase in φ and T.

Besides experimental characterization of the thermophysical characteristics of the nanofluids, forced convective heat transfer in them under various configurations relevant to direct absorption solar collectors (DASC) is also studied numerically. The governing transport equations (continuity, momentum and energy) are solved numerically using a commercial CFD software, ANSYS FLUENT 13.0. Single phase and mixture phase models are employed to analyze heat transfer in the nanofluids. For laminar forced convection in Cu-water and Al_2O_3-water nanofluids inside vertical tubes with constant heat flux, the HTC and Nusselt number increase with increase in Re and φ. For the same Re

and φ, Cu-water nanofluid exhibits better heat transfer than that of Al_2O_3 nanofluid, while the wall shear stress is more for Al_2O_3 nanofluid at a particular condition. For flow of nanofluid through vertical pipe, Al_2O_3-water nanofluid shows better heat transfer than TiO_2-water nanofluid. However, the effect of φ becomes more important in the turbulent flow regime than the laminar one. Heat transfer and pressure drop in forced-flow arrangement are also investigated in DASC configuration. It is found that the average HTC increases with increase in φ and flow rate. For TiO_2-nanofluid, the mixture phase model shows better enhancement of *Nu* and average HTC compared to the single-phase model. Pressure drop is also increased with increase in φ and *Re*. Based on the simulation results, design of a DASC test rig is drawn for measurement of heat transfer performance of the device with different nanofluids.

Table of Contents

CHAPTER 1

1. INTRODUCTION

1.1. MOTIVATION AND BACKGROUND

The importance of investigation for alternative sources of energy has grown by leaps and bounds across the world over the last few decades as the conventional energy sources are decaying rapidly. In this scenario, researchers, scientists and inventors visualize solar energy as the most potent alternative source. Solar energy is currently one of the most important sources of inexhaustible, free and renewable energy with minimal environmental impact. Due to the limited availability of fossil fuels and environmental problems associated with them, the solar energy application has seen a steady increase over time. Solar thermal collectors (STC) are heat exchangers that transform solar radiation energy to internal energy of the transport medium. STC is one of the major components of any solar energy harvesting system, because this is the device which absorbs the incoming solar radiation, converts it into heat and transfers this heat to a fluid (air, water, or oil) flowing through the collector. There are two types of solar collectors: concentrating and non-concentrating [1]. Direct absorption solar collector (DASC) is a genre of STC which allows direct absorption of solar energy in the heat transfer fluid [2]. These have emerged as promising STC devices, since they have simple design requirements and high collector efficiency. The efficiency of DASC can be improved by enhancing the fraction of direct absorption of solar radiation in the working fluid. Use of nanofluids as the working medium in DASC has been proposed in this regard as nanofluids exhibits high absorption of solar radiation [2] and favourable thermophysical properties. Nanofluid-based solar collectors have the potential to harness solar radiant energy more efficiently compared to conventional solar collectors.

Nanofluids are comparatively recent innovation; they exhibit enhanced heat absorbing and heat transport ability. Besides STC, heat removal from different engineering appliances that deal with high power and small size is also a major concern for the industry. For example, in electronics cooling, the thermal heat loads and heat fluxes are growing rapidly, warranting high-quality cooling medium for effective thermal management. Selection of a convenient heat transfer fluid for heat dissipation is important for the design of heat exchangers. Low thermal conductivity of conventional

fluid is often a matter of concern for industrial applications. Therefore, improvising the fluid to develop a new class of fluids, which offer better cooling or heating performance for different thermal systems, is a highly relevant pursuit.

1.2. NANOFLUID

Nanofluid is a stable suspension of nanometer-sized (1-100 nm) materials (nanoparticles, nanofibers, nanotubes, nanowires, nanorods, and nanosheet) dispersed in conventional fluids. Since the first report of nanofluids by Choi [3] in 1995, several different types nanofluids have been prepared by researchers, by dispersing nanoparticles of copper (Cu), nickel (Ni), alumina (Al), Silver (Ag), metal oxides such as: titanium oxide (TiO_2), zirconium dioxide (ZrO_2), barium titanate ($BaTiO_3$), aluminium oxide (Al_2O_3), copper oxide (CuO), iron oxide (Fe_3O_4), silicon dioxide (SiO_2), zinc oxide (ZnO) and some other compounds such as; silicon carbide (SiC), carbon nanotube (CNT), aluminium nitride (AlN), graphene, calcium carbonate ($CaCO_3$) etc in different host liquids such as: water, ethylene glycol (EG), engine oil (EO), etc. [4]. Experimentally, nanofluids have shown to possess improved thermal properties, heat transfer coefficients (HTC) and higher energy efficiency in a variety of thermal exchange systems for different industrial applications and also in STCs. Convective heat transfer is one of the most widely investigated thermal phenomena in nanofluids, relevant to a number of engineering applications. The advent of high heat flow processes has created significant demand for new technologies to enhance heat transfer. For example, microprocessors have continually become smaller and more powerful; heat flux demands have steadily increased over time, leading to new challenges in thermal management. In an automotive system, improved heat transfer can lead to smaller heat exchangers, resulting in reduced weight of the vehicle. It is challenging to manage the high thermal loads with conventional coolants, since they often are crippled with inferior heat transfer characteristics. Nanofluids play an important role in all these areas of applications, which lead to a major impact in developing future generation of equipment for numerous engineering and medical applications. Nanofluids have, therefore, found widespread applications in several areas such as: electronic cooling [5, 6], heat transfer in microchannel cooling [7], minichannel [8], heat exchanger cooling [9], and industrial cooling [10], radiator cooling [11], engine cooling [12],

refrigerator [13], energy (storage, solar absorption) [14, 2, 15], mechanical (friction reduction, magnetic sealing) [16, 17], biomedical (antibacterial activity, nanodrug delivery, cancer theraupetics, nanocryosurgery) [18, 19, 20], and many more.

1.3. STATE OF THE ART

Deploying nanofluids in the above-mentioned engineering applications require an in-depth understanding of the procedure for synthesis of nanofluids, and the effect of different parameters on the thermophysical properties of nanofluids. A detailed account of the state of art on synthesis and characterization of nanofluids is provided in the following sections:

1.3.1. Synthesis of nanofluids

The foremost part in the study on nanofluids is identification of a viable method of synthesis where the nanofluid should be highly stable with no sedimentation and agglomeration to ensure its better utilization in industrial applications. Initially, Xuan and Li [21] suggested the basic methods for preparation of suspensions: (a) to change the pH value of suspensions, (b) to use surfactants or dispersants, (c) to use the ultrasonic vibration. These methods can change the surface properties of particles. The use of these techniques depends upon the application of nanofluids. Selection of suitable surfactants for stabilization depends mainly upon the properties of the base fluid and particles. Surfactants basically lower the surface tension between two liquids or between a solid and a liquid. Generally, there are mainly two techniques used to prepare the nanofluids – single or one-step method and two-step method.

1.3.1.1. Single-step method

Single step method is a process that combines the production of nanoparticles and their dispersion in the host fluid simultaneously. In one such method, called VEROS (Vacuum Evaporation onto a Running Oil Substrate, invented by Yatsuya et al. [22]) the nanoparticles are directly prepared by physical vapor deposition (PVD) technique or condensation of the nanoparticles from a vapour phase into a flowing low vapour-pressure fluid. In this technique, the processes of drying, storage, transportation, and dispersion of nanoparticles are not required, and hence, the agglomeration of nanoparticles can be minimized and the stability of nanofluids can be increased. Direct Evaporation

technique [23, 24] is a modified version of VEROS technique, in which vapours of metal condensed to nanoparticles and directly dispersed into the host fluid. This technique provides excellent control over size of nanoparticles and produce a stable nanofluid without using any additive [25]. Laser ablation (LA) [26, 27, 28, 29] is another method, which has been used to produce alumina nanofluids [30]. Pure chemical synthesis method is used to prepare copper nanofluids dispersed in EG [31]. The advantage of single step method is low agglomeration of nanoparticles, which leads to improved stability of nanofluids. Moreover, the cost of drying and dispersion can be avoided. Disadvantages of single-step method include (i) contamination by the residual reactants (impurities) that are left behind in the nanofluids due to the incomplete reaction, (ii) difficulty in scaling up due to high cost of production, and (iii) compatibility with only low vapour pressure base fluids [32]. Some other examples of single step processes are: chemical reduction [33, 34, 35, 36], microwave irradiation [37, 38], polyol process [39, 40, 41], submerged arc nanoparticle synthesis system (SANSS) [42, 43], and phase transfer method [44].

1.3.1.2. Two-step method

Two-step method is widely used by the researchers to prepare nanofluids. In this method, nanoparticles are first produced by either physical or chemical process (e.g., milling, grinding, sol-gel and vapour phase methods) in the form of dry powder. Then, in the second step, the produced nanoparticles are directly dispersed into the given base fluid with the help of dispersing device such as intensive magnetic stirrer, high-shear mixing, homogenizer, or by using ultrasonic devices like ultrasonic bath, and probe type ultrasonicator. Ultrasonication or stirring process decreases the particle agglomeration and sedimentation. Agglomeration is a major issue in synthesizing nanofluids. Two-step method is widely used for preparing nanofluids, due to large scalability and cost effectiveness. Moreover, it is also the most economical method for large-scale production of nanofluids in industrial applications. Manna [45] and Eastman et al. [24] suggested that the two-step method is more suitable for preparing nanofluids with oxide nanoparticles than with metallic nanoparticles. Nanoparticles tend to aggregate due to its high surface area and surface activity. Therefore, the nanoparticles are to be stabilized to prevent agglomeration [46] and hence, sonication

is required. Stability is the main issue for this method, as the nanopowder aggregate easily due to strong van der Waals force among the nanoparticles. Despite this issue, two-step methods are recognized as the most economical process for producing nanofluids.

1.3.2. Thermal conductivity of nanofluids

Thermal conductivity of materials plays a significant role in the cooling of electronics equipment, nanofluid-based thermal applications and many more. Thermal conductivity of cooling fluid can be enhanced by adding small percentage of nanoparticles in a base fluid [47]. It has widely been observed in the literature that thermal conductivity of nanofluids exceed those of their respective base fluids [48]. Several other researchers also observed that effective thermal conductivity of nanofluid increases with increase in nanoparticle concentration and suggested appropriate models [49] for effective thermal conductivity of nanofluid. Based on the following literature review, it may be found that thermal conductivity of nanofluid depends on several factors, e.g., particle volume fraction, temperature, pH, extent of sonication, type of surfactants, particle type, thermal conductivity shape and diameter of nanoparticles.

1.3.2.1. Effect of volume fraction

The main issue that can highly affect thermal conductivity of nanofluid is concentration or volume fraction (φ) of nanoparticles. From the past research conducted on nanofluids it was observed that the thermal conductivity increases with φ. Das et al. [50] measured the thermal conductivity of Al_2O_3-water and CuO-water nanofluids using temperature oscillation technique at different φ = 1–4 %. At φ = 1.0 %, the thermal conductivity enhancement increased from 2.0 % (21 °C) to 10.8 % (51 °C), whereas at φ = 4.0 % it increased from 9.4 % (21 °C) to 24.3 % (51 °C). Zhu et al. [51] showed that the thermal conductivity of Al_2O_3-water nanofluids increased up to 10.1 % with 0.15 wt. % nanoparticle compared to the host fluid. Liu et al. [36] studied the enhancement of thermal conductivity of water in presence of copper by using chemical reduction method. The results showed that Cu-water nanofluids with low φ of nanoparticles had higher thermal conductivities than those of the base fluid, and at φ = 0.1 % of Cu nanoparticles, thermal conductivity was improved upto 23.8 % compared to that of the base fluid. Wongwises [52] dispersed TiO_2 nanoparticles (diameters of 21 nm)

in water with φ = 0.2–2 % to prepare nanofluid and they observed an increment of thermal conductivity with an increase in φ. Murshed et al. [53] observed a nonlinear relationship of water-based nanofluids containing spherical and rod-shaped TiO_2 nanoparticles. Angayarkanni and Philip [54] studied Al_2O_3, TiO_2 and SiO_2 water-based nanofluids and found the thermal conductivity enhancement of 14, 16 and 9 %, at φ = 4 % respectively. An enhancement of 32.4 % was observed in the effective thermal conductivity of Al_2O_3-water-based nanofluids for φ = 4.3 % [55] and also found a linear relationship with φ. Mintsa et al. [56] investigated the effects of φ, temperature and particle size on thermal conductivity of Al_2O_3-water and CuO-water nanofluids. They observed that the effective thermal conductivity increased with an increase in φ. Enhancement between 1–8 % occurred in thermal conductivities for every 0.05 % increase in nanoparticle φ with Al_2O_3 having the highest enhancement. Cho et al. [57] reported an anomalous increase in thermal conductivity of 18 % with a very low φ of Ag nanoparticle of 10,000 ppm. At φ = 4 %, Fe_3O_4-water-based nanofluids exhibited 38 % enhancement in thermal conductivity. The measured thermal conductivities are higher than those predicted by existing models. The abnormal and nonlinear thermal conductivities of nanofluids were mainly due to the nanoparticle alignment and clustering [58]. Experimental and theoretical investigations of effective thermal conductivity of Al_2O_3-water nanofluid in the range of φ = 0.33–5 % were performed by Chandrasekar et al. [59]. They found that thermal conductivity of nanofluid increased with φ. They also proposed a new model that could be used for the prediction of thermal conductivity of Al_2O_3-water nanofluids. Lee et al. [60] observed more than 20 % of enhancement at φ = 4 % for CuO-EG based nanofluids. A linear increment in thermal conductivity was observed at low φ. Yoo et al. [61] found thermal conductivity enhancement of 16.5 % in EG based iron nanofluid for φ = 0.3 %, 4 % of enhancement with φ = 1.0 % of Al_2O_3 nanoparticles, 14.4 % of enhancement with φ = 1.0 % of TiO_2 nanoparticles, and 13.8 % of enhancement with φ = 0.3 % of WO_3 nanofluid. Hwang et al. [62] investigated thermal conductivity of different types of nanoparticle such as MWCNTs, CuO and SiO_2 dispersed in water and EG, to prepare nanofluid. The highest thermal conductivity enhancement was observed for an MWCNT-water nanofluid: 11.3 % at φ = 1 %. An increase in thermal conductivity with increase in φ was found for CuO-water, Al_2O_3-water, EG-CuO, and EG-Cu

based nanofluids [63]. A similar type of relationship was observed by Wang et al. [64] with Al_2O_3 and CuO nanoparticles in water and EG. Chopkar et al. [65] dispersed Al_2Cu and Ag_2Al nanoparticles in water and EG; an enhancement upto 100 % was observed at φ = 1.5 %. $Al_{70}Cu_{30}$ nanofluids was prepared by Chopkar et al. [66], who reiterated the same behavior of nanofluids and observed a dramatic enhancement of 200 % with 1.5 % addition of $Al_{70}Cu_{30}$ nanoparticles in EG. Karthikeyan et al. [67] observed an enhancement in thermal conductivity of 31.6 % and 54.0 % at φ = 1 % for CuO nanoparticles in water and EG respectively. Xuan and Li [21] performed studies by using Cu nanoparticles in water and transformer oil (TO); the ratio of thermal conductivity was varied from 1.24 to 1.78 as the φ increased from 2.5 to 7.5 %. Similar observations were reported by Eastman et al. [24], who dispersed Al_2O_3, CuO, and Cu in water and TO, to prepared nanofluids; they found 40 % enhancement in thermal conductivity at φ = 0.3 % for Cu-EG nanofluids. Methanol-based Al_2O_3, SiO_2 and TiO_2 nanofluids showed an increase in thermal conductivity with increase in φ (0.005–0.15 %) [68]. Lee et al. [69] prepared EG-based TiO_2 (anatase) nanofluids by one-step pulsed wire evaporation (PWE) method to measure the thermal conductivity. They observed that the enhancement ratio of thermal conductivity did not show any temperature dependency for all φ for anatase-EG nanofluid; they also found that the thermal conductivity of the nanofluid increased with φ and the enhancement ratio was 16.2 % at φ = 5.5 %. Yu et al. [70] studied nanofluids of graphene oxide nanosheets and found thermal conductivity enhancement of 30, 62 and 76 % at φ = 5 %, for three different base fluids, viz., water, propyl glycol and liquid paraffin, respectively. It can be concluded that thermal conductivity enhancement is a strong function of φ.

1.3.2.2. Effect of temperature

Researchers have found that temperature and thermal conductivity were directly related to each other, i.e. when temperature increases, thermal conductivity of nanofluid also increases. Temperature plays an important role in enhancement of thermal conductivity of nanofluids, as the base fluid and particle thermal conductivities are strong functions of temperature. It has been largely agreed by the researchers that thermal Brownian motion of the nanoparticles plays a very important role in increasing thermal conductivity of nanofluids [71]. The change of temperature affects the

Brownian motion and clustering of nanoparticles, which in turn results in dramatic changes of thermal conductivity of nanofluids. Mintsa et al. [56] experimentally observed that the effective thermal conductivity of Al_2O_3-water and CuO-water increases with increase in temperature. Duangthongsuk and. Wongwises [72] reported variation in thermal conductivity of TiO_2-water nanofluids of different φ (0.2–2 %) at different temperatures (15–35 °C). The results showed that the measured thermal conductivity of nanofluids increased with increase in nanofluids temperature and the experimental result did not match with existing correlations. Thermal conductivity of nanofluids containing Al_2O_3, SiO_2, and TiO_2 in water illustrates decreasing trend with temperature [55], whereas the increasing trend of thermal conductivity with temperature, was established for Al_2O_3-water and CuO-water nanofluid [73, 74]. Murshed et al. [75] measured the thermal conductivity of aqueous TiO_2 and Al_2O_3 nanofluids having 15 nm and 80 nm particles, respectively. Their result showed that the effective thermal conductivity of nanofluids increased with temperature as well as φ. Chon et al. [76] measured the thermal conductivity of Al_2O_3 nanofluid in the temperature range of 21–71 °C and nanoparticle size ranging between 11–150 nm (nominal diameters) using the transient hot wire method. They found that the thermal conductivity increased with temperature and decreased with nanoparticle size. A water-based Al_2O_3 nanofluids (φ = 1 %) showed a thermal conductivity enhancement from 2 to 10 % as the temperature was increased from 21 to 50 °C [77]. A constant thermal conductivity enhancement in hexadecane (HD) based Al_2O_3 nanofluid was observed in the temperature range of 25–50 °C [78]. Li and Peterson [79] performed a study by dispersing Al_2O_3 and CuO nanoparticles in water. An increase in mean temperature from 27 to 34.7 °C resulted in enhancement by almost threefold. The thermal conductivity ratio increased with temperature at constant φ. Reddy and Rao [80] measured thermal conductivity of TiO_2 in EG-water host fluid (40 %:60 % and 50 %:50 % by weight) in the temperature range of 30–70 °C. They observed that the thermal conductivity increased with φ and also with temperature. Vajjha et al. [81] experimentally investigated the thermal conductivity of three different nanofluids of Al_2O_3, CuO and ZnO_2, where the nanoparticles were suspended in EG and water mixture. Studies were conducted for φ = 10 % between the temperature ranges of 298 *K* and 363 *K*. Results showed that the enhancement in thermal conductivity is achieved

with increase in temperature of nanoparticles. Syam Sundar et al. [82] prepared EG and water mixture based Fe_3O_4 magnetic nanofluid and the experiments were conducted in the temperature range from 20–60 °C and φ = 0.2–2.0 %. Thermal conductivity was enhanced by 46 % at 2.0 % of φ of nanoparticles dispersed in 20:80 % EG and water mixture compared to other base fluids. Timofeeva et al. [83] observed that the increase in thermal conductivity with increase in temperature from 10 to 60 °C in water and EG-based Al_2O_3 nanofluid (φ = 5 %). Few reports have shown that the thermal conductivity decreases with increase in temperature for TiO_2-water based nanofluid [72] and hexane based Bi_2Te_3 nanorods [84]. It can be concluded that the thermal conductivity enhancement is a strong function of temperature, increasing with rise in temperature.

1.3.2.3. Effect of particle size

Strong effect of nanoparticle size on enhancement of thermal conductivity of nanofluid has been observed by several researchers – the effect is found more predominant for smaller particle size. Brownian motion of nanoparticles and liquid layering around nanoparticles are two important mechanisms for the enhancement of thermal conductivity of nanofluids. When the particle size decreases, the above mentioned mechanisms are very active and influence the thermal conductivity of nanofluids. An enhancement in thermal conductivity with decrease in particle size was reported in Al_2O_3-water-based nanofluids for three different particle diameters of 20, 50 and 100 nm [85]. Mintsa et al. [56] observed that the thermal conductivity of Al_2O_3-water nanofluid of 36 and 47 nm and CuO-water nanofluid of 29 nm; the effective thermal conductivity increased with decrease in particle size. Kailash et al. [86] observed a strong dependence of thermal conductivity on particle size for CuO-water-based nanofluid. A decrease in thermal conductivity with increase in particle size was reported in TiO_2-water-based nanofluids [87]. Chopkar et al. [65, 88] conducted experiments with Al_2Cu and Ag_2Al nanofluids in water and EG at 300 K to study the effects of particle size on thermal conductivity, where they also observed similar phenomenon. Thermal conductivity study in EG-based nanofluid also showed an increase in thermal conductivity with decrease in particle size [89]. Experiments with ZnO and TiO_2 nanoparticles in water and EG were conducted by Kim et al. [90]. The measured thermal conductivity was found to be inversely proportional to the mean diameter of

the suspended particles and reveals the size dependence for both nanofluids. Li and Peterson [91] evaluated experimentally the effect of particle size (36 nm and 47 nm diameter) on thermal conductivity of Al_2O_3-water nanofluid for φ = 0.5–6.0 % and T = 27–37 ˚C. They found that at φ = 6 %, the thermal conductivity enhancement (over the base case of pure host fluids) rose from 26 % to 28 %, when the nanoparticle size was decreased from 47–36 nm. He et al. [87] experimentally measured the thermal conductivity, heat transfer coefficient (HTC) and flow behavior of TiO_2 (anatase + rutile)-water (i.e., a mixture of anatase and rutile nanoparticles) nanofluids with different particle size and φ. Results showed that the effective thermal conductivity increased with φ and decreased with increase in particle size. Wang et al. [64] dispersed Al_2O_3 (28 nm) and CuO (23 nm) in different types of base fluid. They mentioned that the thermal conductivity is higher for CuO compared to Al_2O_3 due to the smaller particle size of CuO particles. However, there are few contradictory results that appear in the literature as well. Beck et al. [92] have conducted experiments with Al_2O_3 nanoparticles of five different sizes in water and EG in the range of 8–282 nm and found that the thermal conductivity enhancement decreased as the particle size decreased; they attributed it to phonon scattering at the solid-liquid interface. Shalkevich et al. [93] reported that the thermal conductivity decreased with decrease in particle size (in the size range of 2–40 nm) for water-based gold nanofluids. A larger thermal conductivity was observed for larger particle size in water-based silicon carbide (SiC) nanofluids with four different particle sizes 20, 30, 35 and 90 nm [94]. Xie et al. [95] studied the thermal conductivity enhancement using spherical and cylindrical shaped SiC nanoparticles of size 26 nm and 600 nm suspended in water, respectively. A 22.9 % enhancement of thermal conductivity was observed at φ = 4 % for cylindrical particles (600 nm), but only 15.8 % increment was reported at φ = 4.2 % for spherical particles (26 nm). Results showed higher enhancement at larger particle size, which contradicted the prior results. This anomaly may have occurred due to clustering of nanoparticles. Up to a certain level of clustering, thermal conductivity is augmented while excessive clustering may create an opposite effect; finally, sedimentation of nanoparticles occurs. Feng et al. [96] supported the above statement by showing the effect of clustering, which was observed to be more pronounced in smaller size of nanoparticles. However,

contradictory results were found from literature, as evidence, the decrease in thermal conductivity with decrease in particle size, mainly due to the clustering of small nanoparticles [97]. Shima et al. [98] also observed an increase in thermal conductivity with particle sizes (2.8–9.5 nm). For φ = 5.5 %, the enhancement was about 5 % and 25 %, for 2.8 and 9.5 nm respectively. They attributed the thermal conductivity enhancement due to the agglomeration of nanoparticles. Studies related to particle agglomeration were carried out by using the fractal theory [99]. Karthikeyan et al. [67] dispersed CuO nanoparticles in water and EG at φ = 1 %. The results showed that the thermal conductivity increased with increase in particle size and mono-dispersity of nanoparticles. They mentioned that the size of cluster not only depends on average particle diameter but also on φ. As φ in the fluid was higher, the inter-particle distance between the particles was smaller, increasing the probability of agglomeration due to van der Waals attraction. From the above studies it can be concluded that the thermal conductivity enhancement is a strong function particle size.

1.3.2.4. Effect of particle shape

Particle shape is also one of the factors which could affect the thermal conductivity of nanofluids. In the field of nanofluids, most of the nanoparticles used are of spherical and cylindrical shapes. Xie et al. [95] studied the thermal conductivity enhancement using spherical (26 nm) and cylindrical (600 nm) shaped SiC nanoparticles suspended in water. A 22.9 % increase in thermal conductivity was observed for SiC-H_2O with cylindrical particles at φ = 4 %, but only 15.8 % increase is found for SiC-H_2O with spherical particles at φ = 4.2 %. Kim et al. [100] investigated the effect of particle shape on suspension stability and thermal conductivities of water-based bohemite Al_2O_3 nanofluids. The thermal conductivity of nanofluids with brick, platelet, and blade shaped particles are maximally enhanced up to 28 %, 23 %, and 16 % at 7.0 %, respectively. Murshed et al. [53] performed studies on the effect of particle shape using spherical and cylindrical TiO_2 nanoparticles. Results showed that the enhancement of thermal conductivity was greatly influenced by the shape of the nanoparticles. An enhancement of 29.7 % was obtained for spherical shape nanoparticles, whereas 32.8 % enhancement was observed for rod-shaped nanoparticles at φ = 5.0 %, respectively. Figure 1 shows the effect of particle shape studies using two different shapes of SiC-26 (spherical) and SiC-

600 (cylindrical) nanoparticles dispersed in water. From the results it is evident that cylindrical nanoparticles provide higher thermal conductivity enhancement than spherical particles. The only difference between the two suspension systems is on the particle morphology (shape and size). Here the particle shape affects heat transfers between the solid particles and the base liquid. Hence, it can be concluded that the cylindrical shape (rod-shaped) nanoparticles possess higher thermal conductivity enhancement compared to spherical shape nanoparticles due to larger surface area and rapid heat transport along relatively long distances due to the greater length, usually of the order of micrometers.

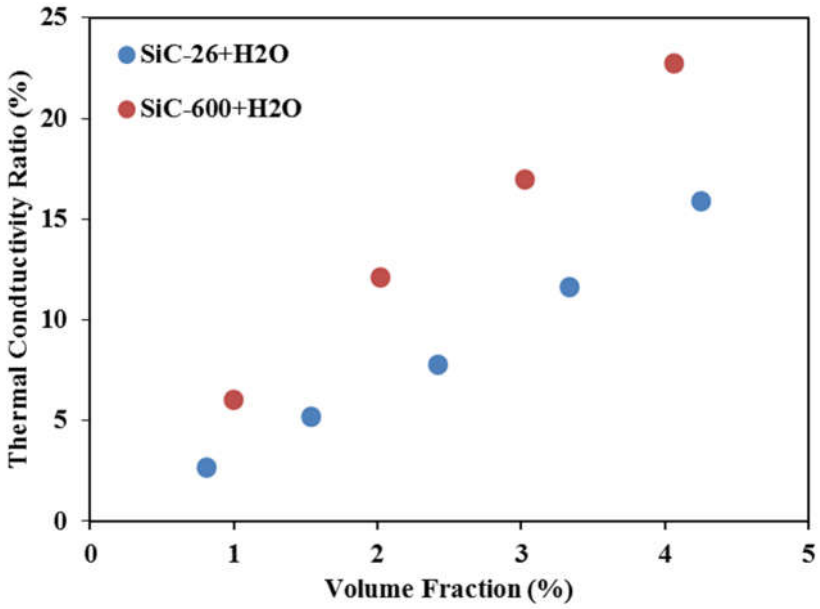

Figure 1 Thermal conductivity ratios of two suspensions containing two different solid particles of SiC-26 and SiC-600 in DI-H_2O [95]. (Reproduced from [95] with permission by Elsevier).

1.3.2.5. Effect of base fluid

Thermal conductivity of the base fluid also affects the heat transfer enhancement of nanofluids. In case of nanofluids, the situation is complicated, as the Brownian motion is affected by the viscosity of the base fluid, which affects the thermal conductivity [135]. Lee [101] found a new concept, suggesting that the electrical double layer (EDL) formed around the nanoparticles influences the thermal conductivity, he also observed that thermal conductivity and thickness of the layer depend on the type of base fluid. Wang et al. [64] measured thermal conductivity of nanofluids by dispersing

Al_2O_3 and CuO nanoparticles in different base fluids such as water, EG, vacuum pump oil, and EO. The highest value of thermal conductivity was observed for Al_2O_3-water nanofluid, whereas the highest thermal conductivity ratio was obtained for Al_2O_3-EG nanofluid. Sonawane et al. [102] synthesized TiO_2 (anatase) nanofluids (5 nm) by using different base fluids, e.g. water, EG, and paraffin oil, to measure the effect of sonication time on thermal conductivity at different φ (1–6 %). They found that water-based nanofluids provide the highest thermal conductivity enhancement of 22 % as compared to other base fluids at highest φ. Ruan and Jacobi [103] reported that the thermal conductivity enhancement for both water-based and EG-based MWCNT nanofluids was around 9 % at φ = 0.24 %. Agarwal et al. [104] dispersed Al_2O_3 in distilled water and EG to prepare nanofluid and studied the thermal conductivity enhancement based on the base fluid. Result showed that the value of thermal conductivity of water-based nanofluids exhibit an almost constant rate of thermal conductivity with increase of φ and temperature; EG-based nanofluids are more sensitive to increase of φ as compared to temperature change. Thus water-based nanofluids would be more efficient in heat transfer applications where the rise in temperature is more prominent, whereas EG-based nanofluids would be better used in high φ nanofluid samples for Al_2O_3 nanoparticles. Similar type of studies was found in [62, 70, 105, 106] which portrayed the thermal conductivity enhancement in nanofluids. It was observed that the effective thermal conductivity ratio decreases with increase in base fluid of thermal conductivity and the enhancement of thermal conductivity is lowest when water is used as a base fluid. It is difficult to conclude the quantitative effect of base fluid on the thermal conductivity enhancement, primarily due to contradicting results and also for fewer studies. Experiments are required to be carried at a given particle concentration to clearly demonstrate the effect of base fluid alone for all nanoparticles.

1.3.2.6. Effect of surfactants

Surfactants or additives are used for better stabilization of nanofluids and prevent the nanoparticles from agglomeration. Most of the reports have shown that an optimum concentration of additives will enhance the thermal conductivity of nanofluid. Additive makes an insulation layer around nanoparticles and could help them to be dispersed in the base fluid, but performances may

deteriorate at high temperature [107]. Wang et al. [108] also reported that an optimal concentration of sodium dodecylbenzenesulfonate (SDBS) can result in an enhanced thermal conductivity in water-based Cu and Al_2O_3 nanofluids. Angayarkanni and Philip [109] characterized the variation of k_{nf} / k_f and the % of decrease in thermal conductivity as a function of surfactant concentration for SDS, CTAB, NP9 and NP10 with water (Figure 2). For all the cases, the k_{nf} / k_f was found to decrease with the increase in surfactant concentration. As the surfactant concentration increased, the number of micelles in the system increased, leading to an increase in the degree of disorder. This resulted in a decrease in k_{nf} / k_f with increase in surfactant concentration, because micellar system is a disordered system. Eastman et al. [24] found a drastic improvement in thermal conductivity for Cu-EG based nanofluid stabilized with thioglycolic acid, compared to that of non-acid-containing nanofluids. They observed about 40 % enhancement of thermal conductivity at φ = 0.3 % for thioglycolic acid-based nanofluid. Saleh et al. [110] prepared TiO_2 (anatase) water-based nanofluids (33 nm), using three different types of surfactants i.e., cetyl trimethyl ammonium bromide (CTAB), sodium dodecyl sulfate (SDS) and sorbitan monooleate (Span80), by two-step method and measured the thermal conductivity and HTC of the prepared nanofluids. However, the enhancement in the relative thermal conductivity exhibits a nonlinear relationship with respect to the φ of nanoparticles and temperature. Mueller [111] has suggested that the strength of the inter-atomic binding force is related to thermal conductivity. Greater the strength of this binding force, greater is the thermal conductivity. The binding force is weak in the case of micellar systems due to its disordered structures, leading to a lower thermal conductivity. At low φ, the number of micelles in the system is less so that the interfacial thermal resistance is also lower. The lower interfacial thermal resistance at lower φ might be a probable reason for the observed large deviation from theoretical fit at lower φ [111]. For φ above 0.02, the experimental data fits well with the effective medium theory (EMT) for all surfactants. The long alkyl chain group of non-ionic surfactants, micelles were found to be very poor thermal conductors at very low φ, with large interfacial tension, compared to their anionic counterparts. The thermal property of a nanofluid in the presence of surfactant and nanoparticles depend only on the thermal conductivity of nanoparticles in the fluid. The addition of surfactant

beyond the optimal or critical micellar concentration (CMC) could deteriorate the thermal conductivity of nanofluids. From the above studies, it can be stated that by using surfactants at a concentration below the CMC, the thermal conductivity may be enhanced. However, the literature still has a few contradiction in this regard [108, 109]. Therefore, extensive study is required for finding the actual surfactant effects on thermal conductivity enhancement.

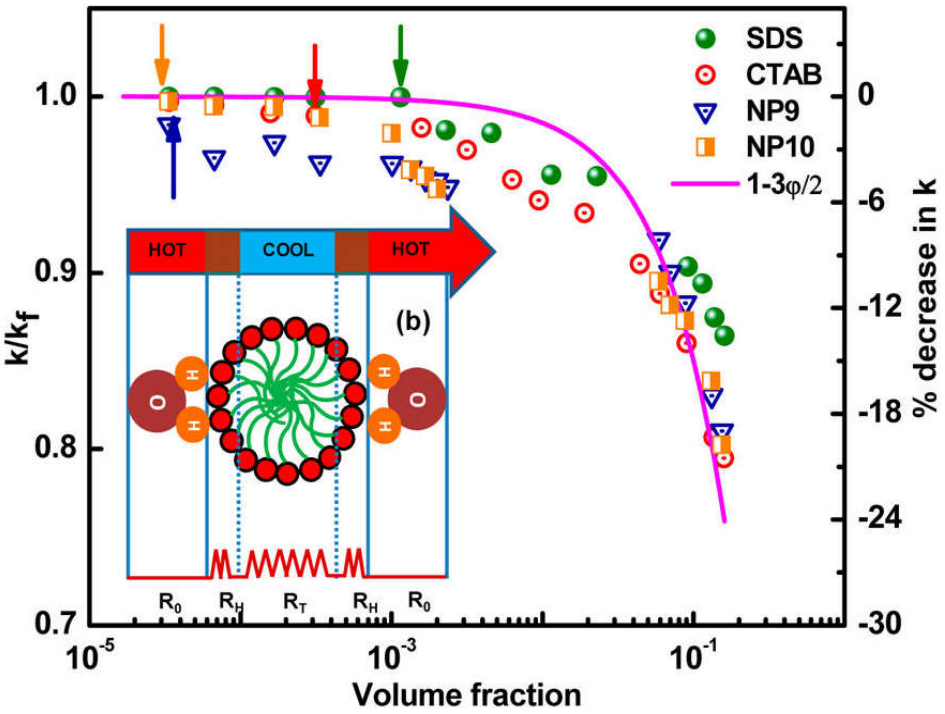

Figure 2 The variation of thermal conductivity as a function of volume fraction for SDS, CTAB, NP9, and NP10 along with the theoretical fit following effective medium theory. The inset in the figure shows the schematic representation of micelles and the possible thermal resistive contributions from different moieties. (Reproduced from [109] with permission by Elsevier)

1.3.2.7. Effect of pH

While the thermal conductivity and viscosity of nanofluids have received much attention in the research community, a careful review of literature reveals that not enough report has been published on the impact of pH of the base fluid on thermal conductivity of nanofluid. pH is also one important factors which could affect the thermal conductivity of nanofluids. When metal oxide particles are suspended with water, hydroxyl radicals (OH^-) are formed at the surface of the particle

[112]. The interaction between the water and particles depends on the pH of water, in acidic or alkaline range. In acidic water, the particle surface assumes positive charge, as a hydrogen ion (H^+) which combine with hydroxyl radical (OH^-); in alkaline water it has a negative charge due to the removal of hydrogen ion. At a certain value of pH, the mixture of particle and water reaches a point where the number of +ve ions and the –ve ions are equal. This state of the mixture is called equipotential or iso-electric point. The iso-electric point depends on the type of metallic oxide particles used in dispersion. If the pH of the fluid nanoparticle mixture is close to the iso-electric point, the particles will agglomerate and affect the thermal conductivity of the nanofluid. Xie et al. [105] prepared nanofluids by dispersing Al_2O_3 nanoparticles in EG and water to investigate the effect of pH value of the suspension on nanofluid thermal conductivity. They observed that an increase in difference between the pH value and isoelectric point or decrease in pH for Al_2O_3 particle resulted in thermal conductivity enhancement. Li et al. [113] observed that the surface charge increases when the pH of nanofluid moves away from the iso-electric point, because of more frequent attacks to the surface hydroxyl groups and phenyl sulphonic group (in SDBS) by potential determining ions (H^+, OH^- and phenyl sulphonic group). They found that the colloidal particles were stable and eventually they altered the thermal conductivity of the nanofluid. They hypothesized that more surface charges at pH value in the optimum range of 8.5–9.5 led to the attainment of the maximum value of thermal conductivity [113]. Wang et al. [108] found that the value of thermal conductivity ratio was dependent on the pH value of nanofluid. Due to the higher thermal conductivity of Cu nanoparticles (compared to that of Al_2O_3 nanoparticles), thermal conductivity enhancement of Cu-water nanofluids is greater than that of Al_2O_3-water nanofluids. For both nanofluids at lower pH (pH, Al_2O_3 < 7:5, pH, Cu < 9:0), the thermal conductivity ratio was found to increase as pH increased for the all φ. On the contrary, at higher pH (pH Al_2O_3 > 8:0; pH Cu > 9:5), the thermal conductivity ratio was found to decrease with pH for all φ (see Figure 3). Experiments were conducted to determine the thermal conductivity of TiO_2 nanofluid with 20 nm size particles at a pH value of 11 [87], and 15 nm size particles in the pH range of 6.2–6.8 [53]. Similar studies by others [114, 115] also showed the effect of pH on thermal

conductivity. It can be seen from the above study that, there is a strong effect of pH on thermal conductivity enhancement of nanofluids.

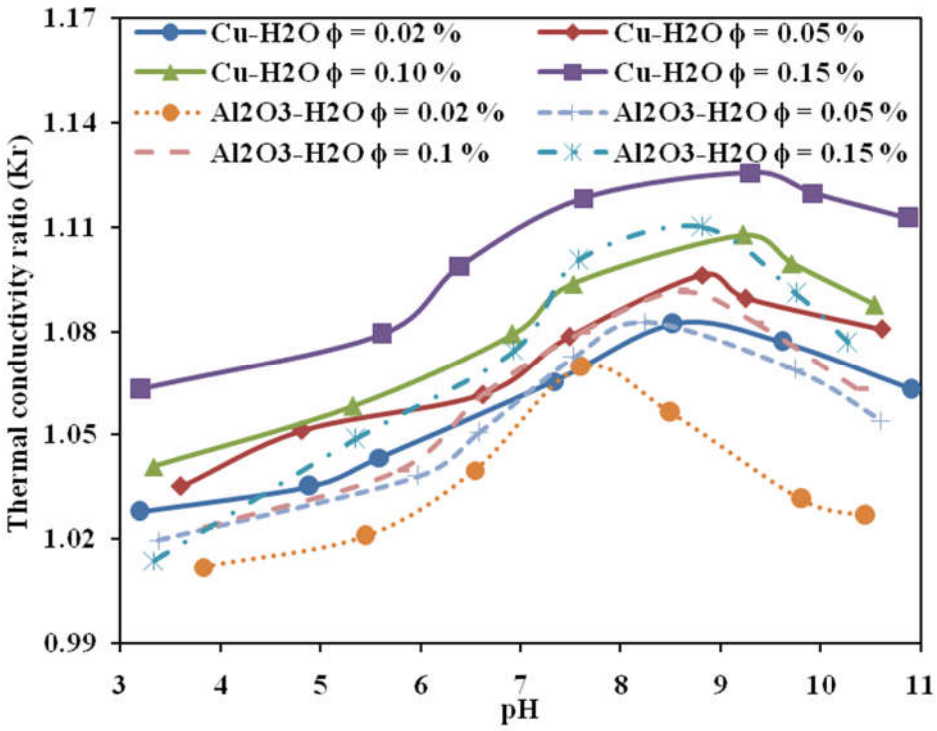

Figure 3 Effects of pH on thermal conductivity ratio (k_{nf}/k_f) of nano-suspensions with SDBS dispersants for Al_2O_3-H_2O and Cu-H_2O [108]. (Reproduced from [108] with permission by Elsevier).

1.3.2.8. Effect on sonication

Nanofluids have been considered as advantageous in heat transfer applications due to their improved thermophysical properties. Due to the inter-particle adhesion forces, nanoparticles become agglomerated and their settlement can be observed because of the gravity forces. In the presence of nanoparticle aggregates, the dispersion stability may decay with time. To increase the stable lifetime of nanofluids, ultrasonication has been widely utilized, and has been accepted as an essential step in the preparation of nanofluids. Ultrasonic vibration is a possible way to break up cluster formation of nanoparticles and help to scatter the nanoparticles into base fluids, so that ultrasonication processes is widely used for nanofluid preparation. Ultrasonication process is of two types: direct sonication, as the immersion of ultrasonic probe into the mixture, and indirect sonication, where the sample is kept inside a container that is submerged into a bath having liquid (mostly water) through which ultrasonic

waves is transmitted. There are contradictory results among the researchers about the effect of ultrasonication duration on colloidal dispersion of nanoparticles. Karthikeyan et al. [67] found that the CuO nanofluid cluster size increased up to a few μm within several minutes of sonication (20–70 minutes). As the cluster size (8 nm) increased, the sedimentation rate also increased. They also noticed formation of mesh-like structures after 60 minutes of the sonication, accompanied by a reduction in thermal conductivity. Khedkar et al. [116] observed that the thermal conductivity of CuO nanofluids (25 nm) increased slightly with the sonication until a critical time (which varied from 60 – 80 minutes, depending on the nanofluid). Thermal conductivity starts decreasing after this critical sonication time. Initially, before this critical time of sonication, the Brownian motion of nanoparticles have an increasing effect in improving the thermal conductivity, but after the critical sonication time, clustering of nanoparticles leads to decrement in thermal conductivity. Ruan and Jacobi [117] mentioned that thermal conductivity of MWCNT nanofluids (10–30 nm) increased nonlinearly with an increase in sonication (0-23 h) specific energy input. Thermal conductivity increased with sonication time/energy because the effect on breaking agglomerates was more significant than the effects related to reducing the MWCNT lengths. Dehkordi et al. [118] found that at low φ of TiO_2 nanofluids (25 nm) would become stable by low power and short period of sonication (2–20 minutes). Thermal conductivity enhancement was observed with increase the time and power of sonication as well as increase in φ of TiO_2. It is possible that increasing the sonication time and power, enhances the Brownian motion of TiO_2 nanoparticles, which improves the thermal conductivity of nanofluids. Hong and Yang [119] showed that the TiO_2 nanofluids having significant improvement in thermal conductivity ratio with sonication at different φ. Ju et al. [120] found that the Al_2O_3 particle size (20, 30, 45 nm) decreases slightly after 3 h of sonication (0–12 h) but remains constant. As the sonication time increased, particle size decreases. No significant change in DLS and thermal conductivity measurements were observed even after 12 h of sonication. Thermal conductivity of nanofluid prepared with the surfactant does increase appreciably after 6 h of sonication. Buonomo et al. [121] experimentally investigated the effect of sonication time (0–120 minutes) on thermal conductivity of Al_2O_3 nanofluid and found that thermal conductivity was nearly constant over a certain sonication

time for all φ. Mahbubul et al. [122] observed that the cluster size of nanofluids decreased with increase in sonication time (1-5 hours). They found that the value of thermal conductivity increased with the rise of temperature and ultrasonication durations. Thermal conductivity has been observed as unsteady for lower ultrasonication duration due to the effect of particle clustering and alignment. Four hours of ultrasonication provides steady thermal conductivity value as they are well-dispersed and overcome the effect of particle clustering and alignment. Figure 5 explains the mechanism behind the ultrasonication duration of thermal conductivity proposed by this group [122]. Kole and Dey [123] found that thermal conductivity of the ZnO nanofluid (30–40 nm) increased from ~21 % to ~40 % (φ = 3.75 %) as the sonication time (0–100 h) increased from 4 h to 60 h and then decreases to ~35 % for 100 h of sonication. They concluded that the effective thermal conductivity of ZnO-EG nanofluids increases with increasing sonication time and attains maximum after ~60 h of sonication. Yang et al. [124] suggested that the increase of ultrasonic time can disperse the Cu particles more uniformly. Beyond ultrasonication duration of 3 h, the value of thermal conductivity of Cu nanofluids (50 nm) tends to be constant. So, they concluded that 3 h of ultrasonic time is enough to disperse the Cu nanofluid. Ultrasonication (10–70 minutes) breaks nanoclusters into smaller clusters and also found that the thermal conductivity of nanofluids was related closely to the clustering of nanoparticles. From the above literature study, it can be concluded that effect of sonication was important in case of thermal conductivity, and researchers agreed that it increases with increase in sonication time upto a certain limit.

1.3.2.9. Effect of particle aspect ratio

Researchers have revealed that the thermal conductivity enhancement increased with increase in particle aspect ratio. Murshed et al. [53] observed that the rod shaped TiO_2 nanoparticles with an aspect ratio of 4 (10 nm × 40 nm) dispersed in water (φ = 5 %) shown a thermal conductivity enhancement of 32.8 %, whereas nanofluid containing spherical nanoparticles of diameter 15 nm shown an enhancement of 29 %. Buongiorno et al. [106] mentioned that the thermal conductivity enhancement of nanorod based Al_2O_3-PAO nanofluids was greater than PAO based Al_2O_3-nanofluids having spherical particles. They also identified that thermal conductivity enhancement afforded by the

tested nanofluids was increased with increase in φ, particle aspect ratio and decreased with base fluid thermal conductivity.

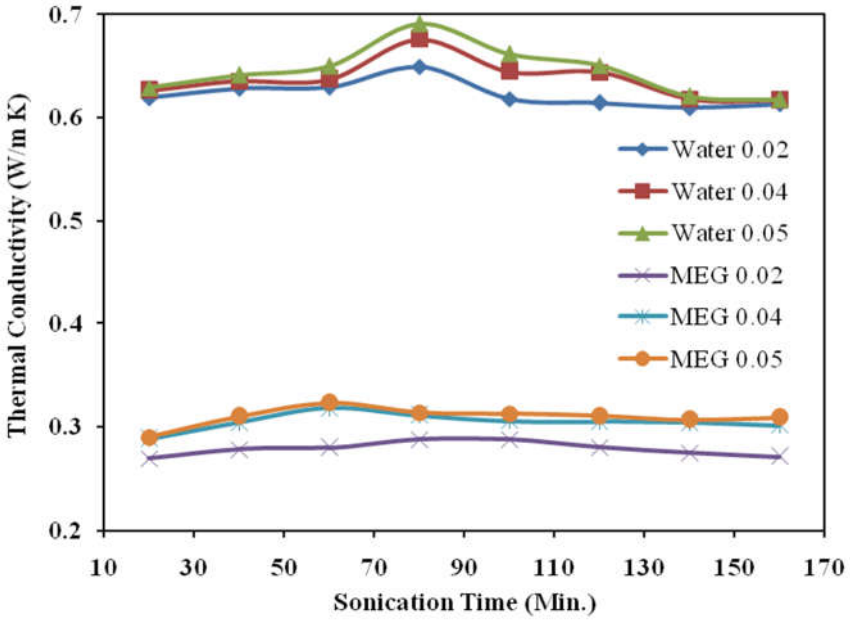

Figure 4 Effect of sonication time on thermal conductivity of CuO-water and CuO-Mono ethylene glycol (MEG) based nanofluid with different volume percent of nanoparticles [116]. (Reproduced from [116] with permission by Elsevier)

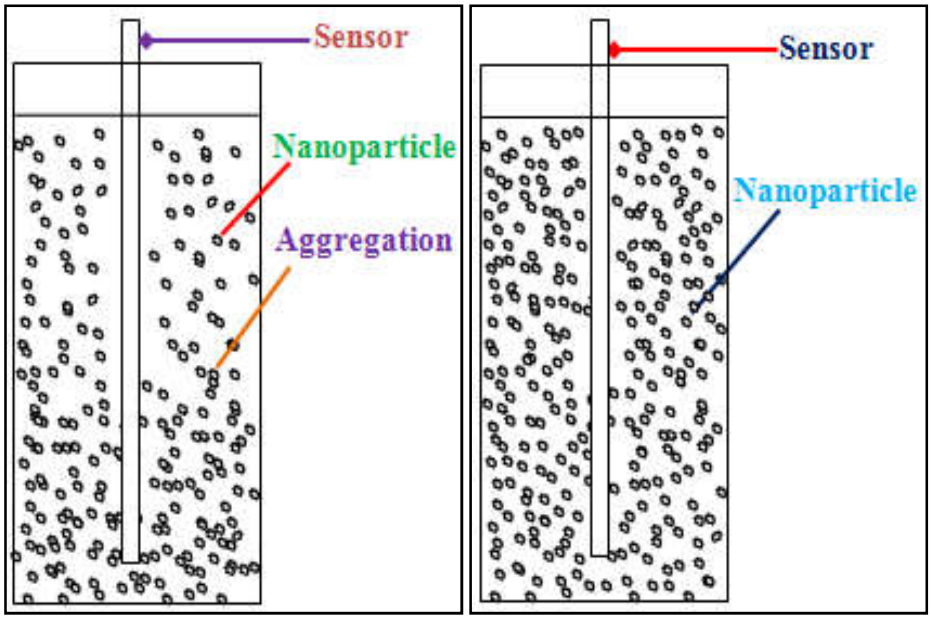

Figure 5 Influence of the duration of ultrasonication on thermal conductivity: (a) lower ultrasonication yields high aggregation and cluster, (b) longer period of ultrasonication yields less aggregation [122].

Timofeeva et al. [125] found that the thermal conductivity enhancement was about 14, 18, 38 and 48 % for the nanotube length of 0.5, 1, 1.7 and 5 μm, respectively. From the above results, it can be concluded that particles having higher aspect ratio can give a higher thermal conductivity enhancement than the spherical particle due to the effective heat transfer along the length of the rod-shaped particle.

1.3.2.10. Effect of particle type

Material of the nanoparticles is also another one important key factor, which affect the thermal conductivity of nanofluids. Several studies have concluded that particle material greatly contributes towards the thermal conductivity enhancement of nanofluids. For a specific base fluid, thermal conductivity of nanoparticles would greatly influence the thermal conductivity of one sample than the other one [4]. Higher thermal conductivity of nanoparticles is expected favor higher thermal conductivity of nanofluid. Hwang et al. [62] dispersed different types of nanoparticle such as MWCNTs, CuO and SiO_2 in water and EG to prepare nanofluids and concluded that the highest thermal conductivity enhancement was observed for an MWCNT-water nanofluid compared to any other nanoparticles. This is due to the fact that MWCNTs possess the highest thermal conductivity compared to other nanoparticles. Sinha et al. [126] reported that the thermal conductivity enhanced up to 48-70 % for the $\varphi = 1$ % in Cu nanofluids whereas Fe nanofluids showed a thermal conductivity enhancement of around 21-33 %. Chopkar et al. [65] prepared nanofluids by dispersing Al_2Cu and Ag_2Al nanoparticles into water and EG; they found that thermal conductivity of Ag_2Al nanofluid was slightly higher compared to Al_2Cu nanofluid; they attributed it to a slightly higher thermal conductivity of Ag_2Al than Al_2Cu. Wang et al. [108] reported that Cu-water based nanofluid showed higher thermal conductivity enhancement compared to Al_2O_3-water based nanofluids, because Cu has higher thermal conductivity than Al_2O_3. However, this trend is not universal. For example, although Al_2O_3 has higher thermal conductivity than SiO_2, Pang et al. [127] observed that, at $\varphi = 0.5$ %, Al_2O_3-methanol nanofluid showed inferior (10.74 %) enhancement in thermal conductivity than that of (14.29 %) for SiO_2-methanol nanofluid. This anomaly may have arisen due to the effect of clustering. Shima and Philip [128] argued that thermal conductivity of nanoparticle does not influence the

thermal conductivity enhancement in the dilute limit. So, the thermal conductivity of nanofluids was fully dependent on the φ of nanoparticle. Other researchers also reported that thermal conductivity of the nanoparticle is not a primary factor for enhancement in thermal conductivity of nanofluid [58]. Lee et al [60] found that CuO nanofluids exhibit higher thermal conductivity enhancement compared to Al_2O_3 nanofluid, despite the fact that Al_2O_3 has higher thermal conductivity than CuO. Lee et al. [60] observed that Al_2O_3 nanoparticles formed relatively larger clusters compared to CuO nanoparticles. They argued that the effect of Brownian motion reduced at higher particle size, which explained the lower enhancement of thermal conductivity. For φ = 4 %, water-based Fe_3O_4 nanofluids exhibited 38 % thermal conductivity enhancement, while water-based nanofluids containing TiO_2 or Al_2O_3 nanoparticles showed 30 % enhancement even though bulk Fe_3O_4 crystal has a lower thermal conductivity than Al_2O_3, CuO, and TiO_2 crystals [58]. At φ = 0.1 %, the thermal conductivity enhancement for water-based TiO_2 was higher than that of Al_2O_3 nanofluids, though the bulk thermal conductivity is higher for Al_2O_3 nanoparticle [61]. From the above literature study, it is clear that no direct relationship between the thermal conductivities of the nanoparticles and the corresponding nanofluids can be drawn and needs to be evaluated on a case to case basis.

1.3.3. Theoretical models of thermal conductivity of nanofluids

Literature review revealed that there are number of theoretical models available for estimating the thermal conductivity of nanofluids. From the literature survey, the existing models categorized into two groups: (i) Static and (ii) Dynamic. (i) In static models [47] stationary nanoparticles in the base fluid are assumed; thermal conductivity is predicted by conduction-based model using conductivity of phase constituents and φ. In static model the interfacial region, which is of nanometer thickness between a solid nanoparticle and the base liquid, have fluid molecules that are bonded or otherwise oriented at the particle/fluid interface. This results in unique thermophysical properties that are different from those of the both the particles and the base fluid. Hence, it is important to consider the interfacial layer as a separate component in the particle-fluid mixture in order to include its effects on the mixture (nanofluids) [47]. (ii) Dynamic models [129, 130] are based on random motion i.e., Brownian motion, of the nanoparticles in base fluid. The model assumes that the Brownian motion is

responsible for transporting energy through collision between nanoparticles leading to micro liquid convection and mixing, which in turn enhances the transport of thermal energy. Dynamic models also take into consideration the factors that influence the Brownian motion, e.g., the DLVO potential, and models the dynamic part of effective thermal conductivity [47]. Murshed et al. [47] presented a combined model for evaluation the effective thermal conductivity of nanofluids and also provides all mechanisms for the enhanced thermal conductivity of nanofluids. The model includes the effect of particle size, nanolayer, Brownian motion, particle surface chemistry and interaction potential covered for combined static and dynamic mechanisms. If there is no interaction between the nanoparticles and the interfacial layer, the equation resembles Maxwell model. Maxwell [49] derived an expression of effective thermal conductivity for two phase solid-liquid mixtures given by Eq. (1). This model becomes the basis for the evaluation of thermal conductivity for nanofluids. The model satisfactorily predicts the thermal conductivity of nanofluids bearing spherical particles at low φ and ambient conditions.

$$\left[\frac{K_{nf}}{K_{bf}}\right] = \left[\frac{K_p+2K_{bf}+2\varphi(K_p-K_{bf})}{K_p+2K_{bf}-\varphi(K_p-K_{bf})}\right]. \quad (1)$$

Bruggeman [131] proposed a model to analyze the interactions among randomly distributed particles. The interactions among the randomly distributed particles are considered in the development of an equation in an implicit form and given as Eq. (2).

$$\left[\left(\frac{K_p-K_{nf}}{K_p+2K_{nf}}\right)\varphi + (1-\varphi)\left(\frac{K_{bf}-2K_{nf}}{K_{bf}+2K_{nf}}\right)\right] = 0. \quad (2)$$

This model can be applied to spherical particles with no limitations on the concentration of inclusions. For low φ, the Bruggeman model results in almost the same results as the Maxwell model. After long years of Maxwell equation, another researcher named Hamilton and Crosser (HC) [132] modified that model to determine the effective thermal conductivity of non-spherical particles by applying a shape factor (n). These extensions take into account various factors related to thermal conductivity, like particle shape, particle distribution, high φ, particle shell structure, and interface contact resistance. The equation for determining the nanofluids thermal conductivity is given as Eq. (3).

$$\left[\frac{K_{nf}}{K_{bf}}\right] = \left[\frac{K_p+(n-1)K_{bf}-(n-1)(K_{bf}-K_p)\varphi}{K_p+(n-1)K_{bf}+\varphi(K_{bf}-K_p)}\right]. \quad (3)$$

where n denotes the shape factor, $n = 3/\psi$, ψ is the sphericity. Sphericity is defined as the ratio of the surface area of a sphere with volume equivalent to that of the average particle to the surface area of the particle, $\psi = 1.0$ and $\psi = 0.5$ for spherical and cylindrical shapes, respectively. The model of Hamilton and Crosser [132] reduces to Maxwell's model when $\psi = 1$ and is found to be in agreement with experimental data for $\varphi < 0.3$. The model is valid as long as the conductivity of the particles is larger by a factor of 100 compared to the conductivity of the continuous phase. The influence of particle size and the temperature are not considered in the model. The value of thermal conductivity predicted by this model for nanofluids are generally lower than the values obtained from experiments. Wasp et al. [133] developed an expression Eq. (4) for calculation the effective thermal conductivity of solid-liquid mixtures. This equation is a special case of Hamilton and Crosser model with $\psi = 1$.

$$\left[\frac{K_{nf}}{K_{bf}}\right] = \left[\frac{K_p + 2K_{bf} - 2\varphi(K_{bf} - K_p)}{K_p + 2K_{bf} + \varphi(K_{bf} - K_p)}\right]. \quad (4)$$

The interfacial layer thickness results in a larger effective φ of the particle-layered liquid structure and a higher thermal conductivity than liquid, which would tend to enhance thermal conductivity. Yu and Choi [134] proposed a renovated Maxwell model for nanofluid applications, where large range of φ can be considered. They studied the effect of interfacial nanolayers to the thermal conductivity of nanofluids and found significance for particle diameter less than 10 nm. They found that the thermal conductivity increased up to eight-folds with the inclusion of nanolayers in the analysis. The value was higher than the Maxwell model without the nanolayer. The thermal conductivity enhancement was found to depend on the nanolayer thickness for K_{layer} less than $10K_{bf}$. They combined the thermal conductivities of nanoparticles and the nanolayers to generate net thermal conductivity of particle, shown in Eq. (5),

$$\left[\frac{K_{nf}}{K_{bf}}\right] = \left[\frac{K_p + 2K_{bf} + 2\varphi(K_p - K_{bf})(1+\beta)^3}{K_p + 2K_{bf} - \varphi(K_p - K_{bf})(1+\beta)^3}\right]. \quad (5)$$

where β is the ratio of the nanolayer thickness to the diameter of the nanoparticle. Xuan et al. [135] established a model, by modifying Maxwell model for the estimation of thermal conductivity of nanofluid, considering the Brownian motion and clusters of nanoparticles, so that

$$\left[\frac{K_{nf}}{K_{bf}}\right] = \left[\frac{K_p + 2K_{bf} + 2\varphi(K_p - K_{bf})}{K_p + 2K_{bf} - 2\varphi(K_p - K_{bf})}\right] + \frac{1}{2K_{bf}}\rho_p C_{pp}\varphi\sqrt{\frac{K_B T}{3\pi\mu_{bf} r_c}}. \quad (6)$$

where K_B denotes the Boltzmann constant and r_c is the mean radius of the cluster (which in turn depends on the dimensions of the cluster structure). The smaller the radius of gyration of clusters suspended in the fluid, the larger is the thermal conductivity of the nanofluid at a given temperature. This happens because the smaller clusters move faster and farther per unit time and invoke a stronger energy transport inside the nanofluid. Therefore, relative contribution of Brownian motion increases in augmentation of the thermal conductivity of nanofluid. Later, Koo and Kleinstreuer [136] developed a model for effective thermal conductivity of nanofluids by considering kinetic energy of the nanoparticles due to the Brownian movement along the effects of particle size, φ, temperature and properties of the base fluid. The model Eq. (7) for Brownian contribution is given by,

$$\left[\frac{K_{nf}}{K_{bf}}\right] = \left[\frac{K_p+2K_{bf}+2\varphi(K_p-K_{bf})}{K_p+2K_{bf}-2\varphi(K_p-K_{bf})}\right] + \frac{5\times10^4}{K_{bf}}\theta\rho_{bf}C_{pbf}f(T,\varphi)\varphi\sqrt{\frac{K_BT}{\rho_p d_p}}. \quad (7)$$

where θ is the fraction of the liquid volume which travels with particle. The fraction, θ decreases with φ because of the viscous effect of the moving particles. An empirical equation for $f\ (T,\ \varphi)$ was proposed, using the experimental data of Das et al. [50] for CuO nanofluids and valid in the range of $0.01 < \varphi < 0.04$ and $300 < T < 325K$, as follows:

$$f(T,\varphi) = (-6.04\ \varphi + 0.4705)T + (1722.3\ \varphi - 134.63). \quad (8)$$

A theoretical model of nanoparticles, proposing shells between the surface of solid particle and the surrounding liquid, was suggested by Xue and Xu [137]. Based on this model, an implicit relationship for the determination of thermal conductivity for CuO-water and CuO-EG nanofluids was developed as follows:

$$\left(1-\frac{\varphi}{\alpha}\right)\frac{K_{nf}-K_{bf}}{2K_{nf}+K_{bf}} + \frac{\varphi}{\alpha}\frac{(K_{nf}-K_i)(2K_i+K_p)-\alpha(K_p-K_i)(2K_i+K_{nf})}{(2K_{nf}+K_i)(2K_i+K_p)+2\alpha(K_p-K_i)(K_i-K_{nf})} = 0. \quad (9)$$

where $\boldsymbol{\alpha} = \left[\frac{\boldsymbol{d_p}}{\boldsymbol{2t_1}}\right]^{\boldsymbol{3}}$, K_i and t_1 represents the thermal conductivity and thickness of interfacial shell, respectively. The value depends on the type of nanofluids. Prasher et al. [130] included the Brownian motion effect as a correction factor to the Maxwell equation for predicting the enhanced thermal conductivity. The proposed thermal conductivity ratio is shown as:

$$\left[\frac{K_{nf}}{K_{bf}}\right] = \left(1 + 4\times10^4 Re_B^m Pr_{bf}^{0.33}\varphi\right) + \left(\frac{[K_p(1+2\alpha_B)+2K_m]+2\varphi[K_p(1-\alpha_B)-K_m]}{[K_p(1+2\alpha_B)+2K_m]-\varphi[K_p(1-\alpha_B)-K_m]}\right). \quad (10)$$

where $K_m = K_{bf}(1 + 0.25Re_B Pr)$, is the matrix conductivity, $Re_B = \frac{1}{\vartheta}\sqrt{\frac{18K_B T}{\pi \rho_p d_p}}$, is the Brownian-Reynolds number, m = 2.5 % ± 15 % for water-based nanofluids, $\alpha_B = \frac{d_p}{2R_b K_m}$ is the nanoparticle Biot number, R_b = interfacial thermal resistance between nanoparticle and the surrounding fluid. Jang and Choi [129], derived expression for the effective thermal conductivity of nanofluids based on the kinetic theory and using the Nusselt number relation for flow past a sphere, including different modes that contribute to the energy transfer. The resulting expression for the effective thermal conductivity of nanofluids is (11):

$$\frac{K_{nf}}{K_{bf}} = (1-\varphi) + \beta\varphi\frac{K_p}{K_{bf}} + (18\times 10^6)\frac{d_{bf}}{d_p}Re^2_{d_{nano}}\varphi Pr_{bf}. \quad (11)$$

where β is a constant related to Kapitza resistance, $Re_{d_{nano}} = C_{RM}d_p/\vartheta$ and $C_{RM} = K_B T/3\pi\mu_{bf}d_p l_{bf}$. The equivalent diameter and mean free path at 300 K for water-based nanofluids are considered as d_{bf} = 0.384 nm and, l_{bf} = 0.738 nm, respectively. Kumar et al. [138] proposed a comprehensive model based on diffusive heat transport in both liquid and solid phases, based on Stokes-Einstein formula, and kinetic theory as:

$$\left[\frac{K_{eff}}{K_{bf}}\right] = 1 + c\frac{2k_b T}{\pi\eta d_p^2}\frac{\varphi r_f}{k_{bf}(1-\varphi)r_a}. \quad (12)$$

The temperature dependence is attributed to the variation of Brownian velocity of the particles, which varies in proportion to T/η. Leong et al. [139] established an expression for the effective thermal conductivity based on the solution of two dimensional, steady-state heat conduction equations in spherical coordinates and making use of spatial averages of the heat fluxes and temperature gradients. This model takes into account the effect of interfacial layer thickness $\gamma = h/a$ so that

$$k_{eff} = \frac{(k_p - k_{lr})\phi_1 k_{lr}[2\beta_1^3 - \beta^3 + 1] + (k_p + 2k_{lr})\beta_1^3[\phi_1\beta^3(k_{lr} - k_f) + k_f]}{\beta_1^3(k_p + 2k_{lr}) - (k_p - k_{lr})\phi_1[\beta_1^3 + \beta^3 - 1]}. \quad (13)$$

where $\beta = 1 + h / rp$, $\beta_1 = 1 + h / 2rp$. By considering steady state heat condition, the temperature fields within nanoparticle, nanolayer and fluid are governed by steady state heat conduction equations. Xie et al. [140] decomposed the average heat flux into contributions coming from the fluid, nanoparticles and nanolayers and deduced expression for effective thermal conductivity of nanofluid using the Fourier's law of heat conduction, so that

$$k_r = 1 + 3\Theta\varphi_e + \frac{3\Theta^2\varphi_e^2}{1-\Theta\varphi_e}. \quad [14]$$

where $\Theta = \frac{\beta_{1f}\left[(1+\gamma)^3 - \frac{\beta_{pl}}{\beta_{fl}}\right]}{(1+\gamma)^3 + 2\beta_{1f}\beta_{pl}}$, γ denotes the thickness ratio of nanolayer and β represents the functions of thermal conductivities of particle, base fluid, and nanolayer. This equation is the proposed model deduced for evaluating the effect of nanolayer on the effective thermal conductivity of nanoparticle-fluid mixtures. The expression is valid for linear thermal conductivity variation across nanolayer and in the absence of higher order pair interaction. A unit cell model for the effective thermal conductivity of nanofluid containing carbon nanofibers was proposed by Yamada and Ota [141], and it is expressed as:

$$\frac{k}{k_f} = \frac{\frac{k_p}{k_f} + K - K\varphi\left(1 - \frac{k_p}{k_f}\right)}{\frac{k_p}{k_f} + K + \varphi\left(1 - k_p/k_f\right)} k_f. \quad (15)$$

where K, the shape factor, and $K = 2\varphi^{0.2}\left(l_p/d_p\right)$ for the cylindrical particle with length (l_p), and diameter (d_p) of the cylindrical particle. Hesselman and Johnson [142] proposed a new model for thermal conductivity of dilute nanofluids by considering the thermal barrier resistance at the interface between the materials for spherical, cylindrical and flat plate particle, which is shown as:

$$\frac{k}{k_f} = \frac{[\alpha(1+2\beta+2)] + 2\varphi[\alpha(1-\beta)-1]}{[\alpha(1+2\beta+2)] - \varphi[(1-\beta)-1]}. \quad (16)$$

where $\beta = R_k\, k_f / k_p$, and R_k is the Kapitza resistance. By considering the thickness liquid layer and Brownian motion of the dispersed particle, Wang et al. [143] modified the Maxwell model,

$$\frac{k}{k_f} = \frac{(1-\varphi) + 3\varphi \int_0^\infty \frac{k_{cl}(r)n(r)}{k_{cl}(r)+2k_f} dr}{(1-\varphi) + 3\varphi \int_0^\infty \frac{k_f n(r)}{k_{cl}(r)+2k_f} dr}. \quad (17)$$

where $k_{cl}(r)$ is the effective thermal conductivity of clusters and $n(r)$ is the radius distribution function. By considering the freezing point of the base fluid, Corcione [144] developed a correlation as:

$$\left[\frac{K_{nf}}{K_{bf}}\right] = 1 + 4.4 Re_p^{0.4} Pr_{bf}^{0.66} \left(\frac{T}{T_{fr}}\right)^{10} \left(\frac{K_p}{K_{bf}}\right)^{0.03} \varphi^{0.66}. \quad (18)$$

where $Re = \frac{2\rho_{bf}K_{bf}T}{\pi\mu_{bf}^2 d_p}$, T is the nanofluid temperature, T_{fr} is the freezing point of the base liquid. Shukla and Dhir [145] proposed a microscopic model which takes into account the dependence of size

of the nanoparticles and temperature. The contribution from the inter-particle potential was analysed through calculations involving DLVO interaction between the electric double layers on spherical nanoparticles. A general theoretical framework was presented for the derivation of the effective thermal conductivity of a nanofluid suspension by accounting for the Brownian motion and pair wise additive inter-particle potential between various nanoparticles. The effective thermal conductivity of the nanofluid suspension is mentioned as:

$$\lambda_{eff} = \lambda_f \left\{\frac{\lambda_p+2\lambda_f+2\varphi(\lambda_p-\lambda_f)}{\lambda_p+2\lambda_f-\varphi(\lambda_p-\lambda_f)}\right\} + \varphi\frac{\rho C k_B T}{\gamma} + \left\{\frac{nk_B^2T}{\gamma}\right\} \times \left\{\frac{(1-\varphi)Z}{8(1+(\rho_i/nZ))}\right\}\left\{\frac{3.29(\alpha k_D)^2+3.61\alpha k_D+1.89}{\alpha k_D(1+\alpha k_D)^2}\right\} +$$

$$\varphi\left\{\frac{\rho C k_B T}{\gamma}\right\}\left\{\frac{(1-\varphi)Z}{16(1+(\rho_i/nZ))}\right\} \times \left\{\frac{9.87(\alpha k_D)^2+21.64\alpha k_D+17.05}{\alpha k_D(1+\alpha k_D)^2}\right\} + \left\{\frac{\rho C k_B T}{\gamma}\right\} \times \left\{\frac{(1-\varphi)^2Z^2}{48(1+(\rho_i/nZ))^2}\right\} \times$$

$$\left\{\frac{1.92(\alpha k_D)^4+1.8(\alpha k_D)^3+1.05(\alpha k_D)^2+0.29\alpha k_D}{(1+\alpha k_D)^4}\right\}. \quad (19)$$

where ρ and C denote the density and specific heat capacity of the solid, respectively, nanoparticle size = 10 nm at φ = 0.01 % in water at a temperature of 300 *K*. Murshed et al. [47] proposed a combined (static and dynamic mechanisms-based) model for predicting the effective thermal conductivity of nanofluids. In this model they included the particle size, nanolayer, Brownian motion, particle surface chemistry, and interaction potential which are the static and dynamic mechanisms responsible for the enhanced effective thermal conductivity of nanofluids. The effects of these mechanisms are treated to be additive in this model. The combined model for the effective thermal conductivity of nanofluids is $\left(k_{eff-nf} = k_{st} + k_{dy}\right)$, which may be expressed as:

$$k_{eff-nf} = \left\{k_f \frac{\varphi_p\omega(k_p-\omega k_f)[2\gamma_1^3-\gamma^3+1]+(k_p+2\omega k_f)\gamma_1^3[\varphi_p\gamma^3(\omega-1)+1]}{\gamma_1^3(k_p+2\omega k_f)-(k_p-\omega k_f)\varphi_p[\gamma_1^3+\gamma^3-1]}\right\} + \left\{\varphi_p^2\gamma^6 k_f\left(3\Lambda^2 + \frac{3\Lambda^2}{4} +\right.\right.$$

$$\left.\left.\frac{9\Lambda^3}{16}\frac{k_{cp}+2k_f}{2k_{cp}+3k_f} + \frac{3\Lambda^4}{2^6} + \cdots\right)\right\} + \left\{\frac{1}{2}\rho_{cp}C_{p-cp}d_s\left[\sqrt{\frac{3K_{BT}(1-1.5\gamma^3\varphi_p)}{2\pi\rho_{cp}\gamma^3 r_p^3}} + \frac{G_T}{6\pi\gamma r_p d_s}\right]\right\}. \quad (20)$$

A few other semi-empirical models for effective thermal conductivity of nanofluids are summarized in Table 1.

Table 1: Semi-empirical models for effective thermal conductivity of some nanofluids.

References	Semi empirical models
[146]	$\left[\frac{K_{nf}}{K_f}\right] = 4.97\varphi^2 + 2.72\varphi + 1$ (21)
[83]	$\left[\frac{K_{nf}}{K_{bf}}\right] = (1 + 3\varphi)$ (22)
[147]	$\left[\frac{K_{nf}}{K_{bf}}\right] = \left[\frac{\{2(1-\gamma)+(1+\beta)^3(1+2\gamma)\}\gamma}{-(1-\gamma)+(1+\beta)^3(1+2\gamma)}\right]$ (23)
[148]	$\left[\frac{K_{nf}}{K_f}\right] = \left[1 + \frac{K_p}{K_f}\frac{A_p}{A_f} + C\frac{K_p}{K_f}\frac{A_p}{A_f}Pe\right]$ (24) where $\frac{A_p}{A_f} = \frac{d_f}{d_p}\frac{\varphi}{(1-\varphi)}$, and $Pe = \frac{U_p d_p}{\propto_f}$, Here $U_P = \frac{2K_b T}{\pi\mu_f d_p^2}$
[76]	$\left[\frac{K_{nf}}{K_{bf}}\right] = 1 + 64.7\varphi^{0.7460}\left(\frac{d_{bf}}{d_p}\right)^{0.3690}\left(\frac{K_p}{K_{bf}}\right)^{0.7476} Pr_{bf}^{0.9955} Re^{1.2321}$ [25] where $Re = \frac{\rho_{bf} K_B T}{3\pi\mu_{bf}^2 l_{bf}}$
[149]	$\left[\frac{K_{nf}}{K_{bf}}\right] = 0.8938\left(1 + \frac{\varphi}{100}\right)^{1.37}\left(1 + \frac{T_{nf}}{70}\right)^{0.2777}\left(1 + \frac{d_p}{150}\right)^{-0.0336}\left(\frac{\alpha_p}{\alpha_{bf}}\right)^{0.01737}$ (26)
[150]	$\left[\frac{K_{nf}}{K_f}\right] = 1 + 7.47\varphi$ (Al_2O_3 nanofluid) (27) $\left[\frac{K_{nf}}{K_f}\right] = 1 + 2.92\varphi - 11.99\varphi^2$ (TiO_2 nanofluids) (28)
[79]	$\left[\frac{K_{nf}}{K_f}\right] = 0.7644815\varphi + 0.018689T + 0.537853$, ($Al_2O_3$ nanofluid), (29) $\left[\frac{K_{nf}}{K_f}\right] = 3.761088\varphi + 0.017924T + 0.69266$, (CuO nanofluid), (30)
[56]	$\left[\frac{K_{nf}}{K_f}\right] = 1 + 1.72\varphi$ (Al_2O_3 nanofluid) (31) $\left[\frac{K_{nf}}{K_f}\right] = 0.99 + 1.74\varphi$ (CuO nanofluid) (32)

1.3.4. Viscosity of nanofluids

Besides thermal conductivity, viscosity is also an important property of the nanofluids as it is relevant for estimating the pumping power requirement to ensure the flow of nanofluid in the flow

circuits of the relevant engineering applications [151]. If the viscosity of the nanofluid increases, the pressure drop across the flow section also increases, resulting in a decrease of the flow and heat transfer rate. Experimental investigation on viscosity of nanofluids reveals the rheological behavior that has equal importance in proposing theoretical models of viscosity as well as the predicting the flow behaviour in practical heat transfer applications. Several experiments on this particular topic show that particle shape and size, particle loading, temperature, surfactants and pH have direct impacts on the viscosity of nanofluids. A detail review of the experimental investigations is provided in the following sections.

1.3.4.1. Effect of volume fraction

Several studies have been reported regarding the effect of solid volume fraction (φ) on viscosity of nanofluids, which show that the nanofluid viscosity is a function of φ – even at low φ of nanofluid, the viscosity differ significantly from that of the base fluid. Chevalier et al. [152] observed that as φ increased, the viscosity also increased. They also investigated the rheological behaviors of SiO_2-ethanol nanofluids in microchannels and found a constant Newtonian behavior of the nanofluid over the range of φ = 1.1–7 % and shear rate = 5×10^3 – 5×10^4 s^{-1}. Viscosity of Al_2O_3-PG at three different φ was experimentally investigated by Prasher et al. [97] and the data were compared with Das et al. [73] and Wang et al. [64]. The study showed a strong dependence of viscosity on φ. It was further reported that at φ less than 4 %, the behavior of the nanofluid was Newtonian and the value of viscosity increased with increase in φ. Different sizes and φ of Al_2O_3 nanoparticles were dispersed in different base fluids and their viscosities were studied by several researchers experimentally [153, 72, 59, 154]. They agreed that the nanoparticle loading increases the viscosity of nanofluids. Anoop et al. [154] mentioned that the viscosity ratio increases more for water-based nanofluids as compared with EG-based nanofluid. Duangthongsuk and Wongwises [72] found an enhancement of 4–15 % of viscosity for TiO_2-water nanofluid with φ = 0.2–2.0 % at T = 15–53 °C. Chandrasekar et al. [59] studied the viscosity of Al_2O_3-water nanofluids at φ = 0.33–5 % and mentioned that viscosity increased as φ increases. Schmidt et al. [155] dispersed Al_2O_3 nanoparticles in decane and isoparaffinic polyalphaolefin (PAO) and reported that viscosity increased when φ increases from

0.25–1 %. Hojjat et al. [156] investigated the rheological behavior of various suspensions of Al_2O_3, TiO_2 and CuO nanoparticles in aqueous solution of carboxymethyl cellulose at different temperatures. They found that the viscosity of nanofluids to be the function of φ and T. They also observed that the viscosity of Al_2O_3 and TiO_2 nanofluids increased with increase in φ, but the viscosity of CuO nanofluid was almost independent of φ. Wang et al. [64] also measured viscosity of Al_2O_3-water nanofluids at φ = 3 % and observed 20–30 % higher viscosity compared to that of the base fluid. Turgut et al. [157] have measured the viscosity of TiO_2-water based nanofluid with φ at the range of 0.2–3 %. They found that the viscosity increased with increase in φ. Similar type of results were also reported by Bobbo et al. [158], Jarahnejad et al. [159] and Yiamsawas et al. [160] for TiO_2-water nanofluids. He et al. [87] observed that viscosity of the nanofluid increased with φ and particle size. They found a shear thinning behavior, where the shear viscosity tends to be constant at shear rates above 100 s^{-1} for TiO_2 (anatase + rutile) nanofluids. Chadwick. [161] studied the effect of φ on viscosity for TiO_2-EG (uncoated anatase) and found that the value of viscosity increased with φ. They did not examine the effect of temperature on viscosity, which is important for heat transfer application. They also found a shear thinning behaviour at low shear rate and shear thickening behaviour at high shear rate. Saleh et al. [110] found that the viscosity increased with φ, and showed an independent behavior with temperature for TiO_2 (anatase) water-based nanofluids. Tseng and Lin [162] investigated the rheological behavior of TiO_2 (anatase) water-based nanofluids (φ = 0.05–0.12 %) and reported a pseudoplastic flow for most of the shear rates (10–1000 s^{-1}). It can be concluded that viscosity enhancement is a strong function of φ.

1.3.4.2. Effect of temperature

Temperature has an inherent relation with viscosity. Many researchers admitted that the viscosity of nanofluids decreased with increase in temperature. Generally heating of liquids contributes to increase the random motion and weakening of intermolecular forces, leading to a reduction in viscosity. Turgut et al. [157] measured the viscosity of TiO_2-water based nanofluids with a temperature range of 13–55 °C and found that viscosity of nanofluid decreased with increase in temperature. Similar trend was observed for water-based Al_2O_3 and CuO nanofluids when the

temperature is raised from 21 °C to 75 °C [153]. Sekhara and Sharma [163] reported the effect of variation of temperature (25–45 °C) on viscosity of Al_2O_3-water nanofluid at low φ (0.01–1.0 %) and found a nonlinear increment of viscosity with φ, which attributed to the aggregation of particles. Anoop et al. [154] experimentally measured the EG-based Al_2O_3 and CuO nanofluids and observed decreasing nature in temperature range of 20–50 °C for different φ. Duangthongsuk and Wongwises [72] reported the variation in viscosity of TiO_2-water nanofluids of different φ (0.2–2 %) at different temperatures (15–35 °C). The results showed that the measured viscosity of nanofluids decreased with increase in nanofluid temperatures. Sahoo et al. [164] considered Al_2O_3-EG-water nanofluid for its rheological characteristics and mentioned that in higher temperature range (273–363 *K*), the nanofluid behaves as a Newtonian fluid. As the temperature increased, viscosity of the nanofluid decreased exponentially for all the φ. From the above study it can be reported that the value viscosity enhancement is a strong function of temperature. However, a few researchers [97, 165] have also found that the viscosity of nanofluids may be independent of temperatures, which is contradiction in general trend.

1.3.4.3. Effect of particle size

The viscosity of nanofluid suspension with the same nanoparticles varies with the particle size. Nguyen et al. [166] investigated the particle size effect on the viscosity of Al_2O_3 (average particle sizes of 36 and 47 nm) water-based nanofluids. The results showed that for $\varphi < 4$ %, the viscosity of Al_2O_3-water nanofluid was independent of particle size. However, for higher φ, viscosity increased with increase in particle size. He et al. [87] measured the viscosity of TiO_2-water nanofluids for two different particle sizes (95 nm, 145 nm), and found that the viscosity increased with increase in particle size. Contrary to that, Namburu et al. [167] reported that the value of viscosity reduced with increase in particle size for SiO_2 nanoparticles. Chevalier et al. [152] also found results similar to that of Namburu et al. [167], while examining the viscosity of SiO_2-ethanol nanosuspensions of three different particle sizes of 35, 94 and 190 nm. Same trend was observed by Anoop et al. [154] for Al_2O_3-water nanofluids. Fan et al. [168] prepared Al_2O_3-EG nanofluids and found that the smaller particles enhanced the viscosity more as compared to the larger particles. Hence, it can be concluded

from the above study that the value of viscosity of the nanofluid is strongly depend on the nanoparticle size.

1.3.4.4. Effect on surfactants or additives

A few studies have been conducted by the researchers about the effect of surfactants on viscosity of nanofluids, because surfactants or dispersants are mainly used to improve stabilization of the nanofluids. But these surfactants may alter the physical properties (viscosity, thermal conductivity and surface tension) of the nanofluids. Dispersant, usually a long-chain hydrocarbon, consists of a hydrophobic tail portion, and a hydrophilic polar head group. Two opposing forces control the self-association process with tail-water interactions. In aqueous phase, hydrophobic tail portion constitutes the core portion of the aggregates forming micelles, and the hydrophilic head portion are in contact with the enclosing liquid medium creating a level of continuity between the nanoparticles and base fluid [169]. Drzazga et al. [170] prepared CuO nanofluids by adding two different nonionic surfactants, i.e. Rocacet O7 and Rokanol K7. They mentioned that the addition of surfactant increased the value of dynamic viscosity. Hung et al. [171] found that addition of chitosan in MWCNTs-water nanofluids increased the viscosity of those nanofluids. The chitosan at 0.4 wt. % concentration provided a good suspension performance for all φ of MWCNTs. A maximum viscosity enhancement of 233% occurs when the φ of MWCNTs is 1.5 wt. % and that of chitosan is 0.4 wt. %. From the study it can be mentioned that the value of viscosity enhancement is a strong function of surfactants.

1.3.4.5. Effect on Sonication

Sonication is the simple way to break up agglomerates and promote dispersion of nanoparticles into base fluids It is the most widely utilized process in the literature to increase the stability of nanofluids. The nanofluid suspension is sonicated for sufficient time to reduce the nanoparticle agglomerate. If the suspension is sonicated too long, fragmentized nanoparticles can reagglomerate due to the effect of high surface energy. Thus, an optimal sonication time needs to be determined to achieve optimal agglomeration size and stability for different combinations of nanoparticle, base fluid, and for different φ [172]. Adi et al. [173] prepared Al_2O_3-glycol nanofluid and measured the effect of sonication on viscosity. They found that the viscosity of the nanofluids

reduced as the ultrasonication energy increased upto an optimum value. Mahbubul et al. [174] investigated the effects of ultrasonication duration (180 minutes) on viscosity of Al_2O_3-water nanofluid for φ = 0.5 %. They found that the viscosity of the nanofluid increased to a maximum, when the ultrasonication duration was of 60 minutes and then decreased with increase in sonication time. They also mentioned that by using possible higher ultrasonication durations, more stable and lower–viscosity nanofluids can be obtained. Overall, inconsistent outcomes have been reported in the literature even for the same type of nanofluid. can be mentioned that the effect of sonication is necessary to lower the viscosity value.

1.3.4.6. Effect of shear rate

Shear rate plays an important role on the viscosity of nanofluids. Rheological behaviour of any fluid is explained as the relationship between shear stress (τ) and shear rate (γ). Shear stress is defined as the tangential force applied per unit area and the shear rate is stated as the change of shear strain per unit time. The fluid behaviour is categorized into two types (i) Newtonian and (ii) non–Newtonian. The value of viscosity remains constant with shear rate and the stress exhibits linear relation with shear rate for Newtonian behaviour. For non-Newtonian fluid, the viscosity may vary with shear rate; the correlation between shear stress and strain rate may be non-linear, or it may follow linear profile with Bingham plastic behaviour. With an increase in shear rate, the particle-particle interactions become weaker and are even broken down, and the nanofluid shows Newtonian behavior [175]. Aladag et al. [176] investigated the effects of temperature and shearing time on the rheological properties of nanofluids for low temperature range (2–10 °C). They clearly revealed that for both Al_2O_3-water and CNT-water nanofluids a viscosity hysteresis phenomenon was observed when the stress is gradually loaded. Results showed that Al_2O_3-water-based nanofluid was non-Newtonian and CNT water-based nanofluid was Newtonian only for high shear rate. Sahoo et al. [164] investigated the rheological characteristics of Al_2O_3-EG-water nanofluids and found that the nanofluids showed non-Newtonian behavior at low temperature. This behavior specifically fitted into the characteristics of a Bingham plastic and was more pronounced as φ of the nanoparticles increased. Tseng and Lin [162] investigated the rheology of TiO_2-water nanofluid and reported that within φ =

5–12 %, the nanofluid exhibited non-Newtonian viscoplastic fluid behavior. As nanoparticles were added to the base fluid up to φ = 5 %, an initial yield stress was needed to be exceeded before flow could be achieved. This feature puts the nanofluids in the viscoplastic non-Newtonian regime. Namburu et al. [177] showed that CuO nanoparticles in water and EG behaved as Newtonian fluids. Chen et al. [165] found that EG-based-TiO_2 nanofluids were Newtonian with the shear viscosity depending strongly on temperature and φ. Mahbubul et al. [178] studied the rheological behaviours of Al_2O_3-R141b nanorefrigerants for φ = 0.05–0.15 %, with the temperature range of 4 to 16 °C upto 305.75 s^{-1} shear rate. In their study, nanorefrigerants showed non-Newtonian behaviour (dilatant or shear thickening fluid) with low shear rates, but at high shear rates almost Newtonian trend was observed. With the increase of shear rate, the sedimentation formed during the particle agglomeration easily break down to form a dispersed suspension with near Newtonian behaviour. Richmond et al. [179] found that mixing of TiO_2 in SiO_2-water nanofluid changes its flow behaviour from Newtonian to non-Newtonian. Penkavova et al. [180] investigated the rheological behaviour of TiO_2-water nanofluid and the result showed Newtonian behaviour. Al_2O_3-water-nanofluid showed non-Newtonian behaviour [181]. Similar findings on generalized Newtonian behaviour [158, 97, 77] of nanofluids have been reported, while a few others observed non-Newtonian shear thinning trend [162, 182].

1.3.5. Theoretical model of viscosity of nanofluids

Literature review have revealed that there are number of theoretical models available for estimating the viscosity of nanofluids. Some representative viscosity models are discussed in this section, followed by selected empirical models which were obtained by fitting experimentally observed viscosity data of particular type of nanofluids. The earliest model for nanofluid viscosity dates back to 1906 when Einstein [183] proposed an equation to predict the viscosity of nanofluids; applicable for ($\varphi \leq 0.01$) dilute suspension of spherical particles, he suggested the ratio of the viscosity of nanofluid (μ_{nf}) to that of the base fluid (μ_{bf}) as:

$$\frac{\mu_{nf}}{\mu_{bf}} = [1 + 2.5\varphi]. \quad (33)$$

Taylor [184] established another model by extending the Einstein model. The author considered the liquid drops to be spherical.

$$\frac{\mu_{nf}}{\mu_{bf}} = 1 + 2.5\varphi\left(\frac{\mu' + \frac{2}{3}\mu}{\mu' + \mu}\right). \quad (34)$$

μ' denotes as the velocity of the liquid. Brinkman [185] extended and modified the Einstein model for denser suspensions, i.e., for up to $\varphi \leq 4$ %, which states:

$$\frac{\mu_{nf}}{\mu_{bf}} = \left[\frac{1}{(1-\varphi)^{2.5}}\right]. \quad (35)$$

Frankel and Acrivos [186] developed a model using asymptotic technique to describe the viscosity of the nanofluids in terms of the actual φ to the maximum attainable particle loading φ_m such that

$$\mu_{eff} = \mu_o \frac{9}{8}\left[\frac{(\varphi/\varphi_m)^{1/3}}{1-(\varphi/\varphi_m)^{1/3}}\right]. \quad (36)$$

Graham [187] model is the modified form of Franken-Acrivos model, considered the particle diameter d_p and interparticle spacing h. Brownian motion, van der Waals, and electro-viscous forces were considered in this model.

$$\frac{\mu_{nf}}{\mu_{bf}} = \left(1 + 2.5\varphi + 4.5\left[\frac{1}{\left(\frac{h}{d_p}\left(2+\frac{h}{d_p}\right)\right)\left(1+\frac{h}{d_p}\right)^2}\right]\right). \quad (37)$$

Azmi et al. [188] developed a viscosity correlation based on φ, temperature T_{nf} and particle size d_p.

$$\frac{\mu_{nf}}{\mu_o} = C_1\left(1 + \frac{\varphi}{100}\right)^{\alpha}\left(1 + \frac{T_{nf}}{70}\right)^{-\lambda}\left(1 + \frac{d_p}{170}\right)^{-\sigma}. \quad (38)$$

where C_1 is empirical constant and the value of α, λ, and σ exponents are 11.3, 0.038, and 0.061, respectively. Khanafer and Vafai [189] proposed a correlation to calculate the viscosity of Al_2O_3-water nanofluid as function of φ, temperature and particle size as

$$\mu_{nf} = -0.4491 + \frac{28.837}{T} + 0.574\varphi - 0.1634\varphi^2 + 23.053\frac{\varphi^2}{T^2} + 0.0132\varphi^3 - 2354.735\frac{\varphi}{T^3} +$$

$$23.498\frac{\varphi^2}{d_p^2} - 3.0185\frac{\varphi^3}{d_p^2}. \quad (39)$$

Hosseini et al. [190] obtained a new dimensionless model for calculating the viscosity of nanofluids. They considered the hydrodynamic volume fraction φ_h of nanoparticles, and thickness r of capping layer, diameter d of the nanoparticle, and temperature T.

$$\frac{\eta_{nf}}{\eta_{bf}} = exp\left[m + \alpha\left(\frac{T}{T_o}\right) + \beta(\varphi_h) + \gamma\left(\frac{d}{1+r}\right)\right], \quad (40)$$

where T_o is a reference temperature taken to be 20 °C, and m is a system property constant that is a function of types of nanoparticles, types of base fluids, and the interactions between them. α, β and γ are empirical constants obtainable from the experimental data.

Corcione [191] developed a model to calculate the viscosity of nanofluids.

$$\mu_{nf} = \mu_o \left(\frac{1}{1-34.87\left(d_p/d_f\right)^{-0.3} \varphi^{1.03}} \right). \quad (41)$$

d_f is the equivalent diameter of a base fluid molecule, $d_f = 0.1\left(\frac{6M}{N\pi\rho f}\right)^{1/3}$, where M is the molecular weight of the base fluid, N is the Avogadro number, and ρ_f is the mass density of the base fluid calculated at room temperature. Sharma et al. [192] proposed a viscosity model for SiC and metal oxide nanofluids, and they also considered the value of C_1 = 1:4, for SiC nanofluids and C_1 = 1.0, for metal oxide nanofluids.

$$\frac{\mu_{nf}}{\mu_f} = C_1 \left\{ \left(1 + \frac{\varphi}{100}\right)^{11.3} \left(1 + \frac{T_{nf}}{70}\right)^{-0.038} \left(1 + \frac{d_p}{170}\right)^{-0.061} \right\}. \quad (42)$$

Sekhar and Sharma [193] proposed a model to calculate the viscosity of Al_2O_3-water nanofluid.

$$\mu_{nf} = 0.935\mu_o \left(1 + \frac{T_{nf}}{70}\right)^{0.5602} \left(1 + \frac{d_p}{80}\right)^{-0.05915} \left(1 + \frac{\varphi}{100}\right)^{10.51}. \quad (43)$$

The above equation is valid for in the temperature range of T = 20–70 °C, particle diameter d_p = 13–100 nm, and φ = 0.01–5.0 %. Abu-Nada [194] developed a temperature dependent viscosity model, valid for Al_2O_3 nanofluids.

$$\mu_{nf} = -0.155 - \frac{19.582}{T} + 0.794\varphi + \frac{2094.47}{T^2} - 0.192\varphi^2 - 8.11\frac{\varphi}{T} - \frac{27463.86}{T^3} + 0.127\varphi^3 + 1.6044\frac{\varphi^2}{T} + 2.1754\frac{\varphi}{T^2}. \quad (44)$$

A few other models for viscosity of nanofluids are summarized in Table 2.

Table 2: Summary of the models for viscosity of nanofluids.

References	Viscosity model
Mooney [195]	$\frac{\mu_{nf}}{\mu_{bf}} = exp\left(\frac{2.5\varphi}{1-\upsilon\varphi}\right)$ (45)
Ward and Whitmore [196]	$\frac{\mu_{nf}}{\mu_f} = \left[1 + \eta\left(\varphi_{eff} + 2.5\eta + (2.5\eta)^2 + \cdots\right)\right]$ (46)
Batchelor [197]	$\frac{\mu_{nf}}{\mu_{bf}} = [1 + 2.5\varphi + 6.5\varphi^2]$ (47)

References	Viscosity model
Saito [198]	$\frac{\mu_{nf}}{\mu_{bf}} = (2.5\varphi + 14.1\varphi^2)$ (48)
Booth [199]	$\mu_{eff} = \mu_0 \left[1 + 2.5\varphi \left\{1 + \sum_1^\infty b_I \left(\frac{e\zeta}{K_b T}\right)^I\right\}\right]$ (49) b_I is the characteristics of electrolyte, e is the electronic charge on particles, K_b is the Boltzmann constant, and T is the absolute temperature.
Krieger and Dougherty [200]	$\frac{\mu_{nf}}{\mu_{bf}} = \left(1 - \left(\frac{\varphi}{\varphi_m}\right)\right)^{-[\eta]\varphi_m}$ (50) φ_m is the maximum concentration and η is the intrinsic viscosity = 2.5.
Lundgren [201]	$\frac{\mu_{nf}}{\mu_{bf}} = \left(1 + 2.5\varphi + \frac{25}{4}\varphi^2 + f(\varphi^3)\right)$ (51)
Thomas and Muthukumar [202]	$\frac{\mu_{nf}}{\mu_{bf}} = (1 + 2.5\varphi + 4.83\varphi^2 + 6.4\varphi^3)$ (52)
Vand [203]	$\frac{\mu_{nf}}{\mu_{bf}} = (1 + 2.5\varphi + 7.349\varphi^2 + \cdots)$ (53)
Roscoe [204]	$\frac{\mu_{nf}}{\mu_{bf}} = (1 - 1.35\varphi)^{-2.5}$ (54)
Kitano et al. [205]	$\frac{\mu_{nf}}{\mu_{bf}} = \frac{1}{\left[1-\left(\frac{\varphi}{\varphi_m}\right)\right]^2}$ (55)
Bicerano [206]	$\mu_r = (1 + \eta\varphi + k_H\varphi^2)$ (56) μ_r is the ratio of dispersion to the dispersing fluid, η is the intrinsic viscosity, and K_H is the Huggins coefficient.
Tseng and Chen [207]	$\mu_{nf} = \mu_f \times 0.4513e^{0.6965\varphi}$ (57)
Buongiorno [150]	$\mu_{nf} = \mu_f(1 + 39.11\varphi + 533.9\varphi^2)$ Al_2O_3 nanofluid (58) $\mu_{nf} = \mu_f(1 + 5.45\varphi + 108.2\varphi^2)$ TiO_2 nanofluid (59)
De Bruijn [208]	$\frac{\mu_{nf}}{\mu_f} = \frac{1}{1-2.5\varphi+1.552\varphi^2}$ (60)
Song et al. [209]	$\mu_{nf} = \mu_f(1 + 56.5\varphi)$ (61)
Chen et al. [210]	$\frac{\mu_{nf}}{\mu_f} = \left(1 - \frac{\varphi_a}{\varphi_m}\right)^{-2.5\varphi_m}$ (62) $\varphi_a = \varphi\left(\frac{a_a}{a}\right)^{3-D}$, φ_a = effective volume fraction of agglomerates, D = fractal index; a_a and a are the radii of the agglomerates and primary particles.
Masoumi et al. [211]	$\mu_{nf} = \mu_f\left(1 + \frac{\rho_N V_b d_N^2}{72C\delta\mu_f}\right)$ (63)
Maiga et al. [212]	$\mu_{nf} = \mu_f(1 + 0.19\varphi + 306\varphi^2)$, Al_2O_3-EG (64) $\mu_{nf} = \mu_f(1 + 7.3\varphi + 123\varphi^2)$ Al_2O_3-water (65)
Nguyen et al. [213]	Al_2O_3-water nanofluid

References	Viscosity model
	$\mu_{nf} = \mu_o \times 0.904e^{0.1483\varphi}$ (for 47 nm particle size) (66) $\mu_{nf} = \mu_o(1 - 0.025\varphi + 0.015\varphi^2)$ (for 36 nm particle size) (67) CuO-water nanofluid $\mu_{nf} = \mu_o(1.475 - 0.319\varphi + 0.051\varphi^2 + 0.009\varphi^3)$ (68)
Nielsen [214]	$\frac{\mu_{nf}}{\mu_{bf}} = (1 + 1.5\varphi)e^{\frac{\varphi}{(1-\varphi_m)}}$ (69) valid for φ more than 0.02. where φ_m is the maximum packing fraction (0.64) which is approximately 0.64 for randomly dispersed spheres.
Nguyen et al. [213]	$\mu_{nf} = \mu_o(1.125 - 0.0007T)$ for φ = 1 %, (70) $\frac{\mu_{nf}}{\mu_f} = (2.1275 - 0.0215T + 0.00027T^2)$ for φ = 4 %, (71)
Smoluchowski [215]	$\mu_{eff} = \mu_o\left[1 + 2.5\varphi\left\{1 + \frac{1}{k\mu_o a^2}\left(\frac{\zeta D_E}{2\pi}\right)^2\right\}\right]$ (72) k = specific conductivity of the electrolyte, a = radius of the solid particles, D_E = dielectric constant of the water, and ζ = zeta potential of the particle with respect to the electrolytic medium.
Kulkarni et al. [216]	$\ln(\mu_{nf}) = -(2.8751 + 53.548\varphi - 107.12\varphi^2) + \frac{(1078.3+15857\varphi+20587\varphi^2)}{T}$ CuO-water nanofluids (73)
Prasher et al. [217]	$\mu_{nf} = \mu_o + \frac{\rho_p V_B d_p^2}{72C_1\delta}$, (74) $V_B = \frac{1}{d_p}\sqrt{\frac{18k_bT}{\pi\rho_p d_p}}$, $\delta = \sqrt[3]{\frac{\pi}{6\varphi}}d_p$
Rashin and Hemalatha [218]	$\mu_{nf} = \mu_o(1 + A\varphi - B\varphi^2)$ CuO-coconut oil (75) $\mu_{nf} = Ce^{-0.03T}$ (76) For φ = 0.5–2.5 % and T = 35–55 °C. A, B, and C are parameters.
Heyhat et al. [219]	$\frac{\mu_{nf}}{\mu_o} = Exp\left(\frac{5.989\varphi}{0.278-\varphi}\right)$ Al_2O_3-water (77)
Suganthi and Rajan [220]	$\mu_{nf} = \mu_o(1 + 2.5\varphi_a)$, (78) where $\frac{\varphi_a}{\varphi} = \left(\frac{D_a}{d_p}\right)^{3-D}$
Suganthi et al. [221]	$\mu_{nf} = A\theta^{-B}$ ZnO-PG nanofluid (79) θ = Temperature in degree Celsius, A and B are empirical constants are different for different φ.
Singh et al. [222]	$\mu_{nf} = \mu_{\infty,T} exp\left(\frac{E_a}{R_g T}\right)$, (80) where μ_∞, T is the viscosity at infinite temperature, E_a is the activation

References	Viscosity model
	energy to viscous flow, R_g is the universal gas constant.
Yiamsawas et al. [223]	$\mu_{nf} = A\varphi^B T^C \mu_0^E$, (81) TiO_2 and Al_2O_3 EG-water nanofluid, where $\mu_0 = 2.3775 - 0.0461T + 0.0003T^2$. A, B, C, and E are the empirical constants.
Namburu et al. [177, 167]	$Log(\mu_{nf}) = Ae^{-BT}$, (82) (T = -35–50 °C) and φ (1–10 %) for CuO-EG-water. A and B are empirical curve fit parameters and in this case are functions of φ, with R^2 = 0.99. For CuO nanofluids, $A = 1.8375\varphi^2 - 29.643\varphi + 165.56$, $B = 4 \times 10^{-6}\varphi^2 - 1 \times 10^{-3}\varphi + 1.86 \times 10^{-2}$, For SiO_2 nanofluids, $A = 0.1193\varphi^3 - 1.9289\varphi^2 - 2.245\varphi + 167.17$, $B = (-7 \times 10^{-6})\varphi^2 - 0.0004\varphi + 0.0192$,
Hemmat Esfe and Saedodin [224]	$\frac{\mu_{nf}}{\mu_o} = 0.98118\, e^{(5.49\varphi - 0.00001359T^2)} + 0.0303\, ln(T)$, (83)
Tseng and Lin [225]	$\mu_{nf} = \mu_o \times 13.47e^{35.98\varphi}$ (84)
Duangthongsuk and Wongwises [226]	$\mu_{nf} = \mu_o(A + B\varphi + C\varphi^2)$ TiO_2-water (85) A, B, and C are empirical constants obtained from curve fitting at three different temperatures.
Kole and Dey [227]	$log(\mu_{nf}) = Aexp(-BT)$, Al_2O_3 nanofluids (86) $A = -225.245\varphi^2 + 18.404\varphi + 1.749$, $B = 575.835\varphi^3 - 32.101\varphi^2 + 0.148\varphi + 0.011$,
Kole and Dey [228]	$\mu_{nf} = \mu_o \left(1 - \frac{\varphi}{0.5}\left(\frac{a_a}{a}\right)^{1.3}\right)^{-1.25}$ CuO-gear oil (87) $ln(\mu_{nf}) = A + \frac{1000B}{(T+C)}$ (88) a_a and a are the aggregates and primary particles, respectively. A, B, and C are empirical curve fit constants.
Chen et al. [229]	$\mu_{nf} = \mu_o(1 + 10.6\varphi + (10.6\varphi)^2)$ TiO_2-EG (89)
Chen et al. [229]	$ln(\eta) = A + \frac{1000B}{(T+C)}$ (90) η is the shear viscosity of nanofluids, and A, B, and C are empirical constants varying with φ.
Noni et al. [230]	$\frac{\mu_{nf}}{\mu_f} = 1 + b\left(\frac{\varphi}{1-\varphi_m}\right)^n$ Al_2O_3-water (91)

References	Viscosity model
	b and n are the empirical coefficients which was calculated by least squares regression method. The values of the coefficients b and n were 1631 and 2.8, respectively.
Chandrasekar et al. [231]	$\mu_{nf} = \mu_o \left(1 + A \left(\frac{\varphi}{1-\varphi}\right)^n\right)$ Al_2O_3-water (92) By using Noni et al.'s [230] model with the same n = 2.8, and a fixed value of coefficient b = 5300 with temperature range of 5–50 °C.
Hernandez Battez et al. [232]	$\eta_r(cp) = 52.8 - 9.76 \times 10^{-7}\gamma + 0.172\,\varphi - 0.912\,T + 1.02 \times 10^{-8}\gamma T + 4.24 \times 10^{-3}T^2$ ZnO nanofluid (93) $\eta_r(cp) = 53.78 - 9.25 \times 10^{-7}\gamma + 0.202\,\varphi - 0.937\,T + 9.65 \times 10^{-9}\gamma T + 4.39 \times 10^{-3}T^2$ ZrO_2 nanofluids (94) γ = shear rate.

1.3.6. Surface tension and contact angle of nanofluids

Surface tension can be explained in terms of forces between molecules that develop at the interface between two immiscible fluids and lies on the plane of interface. This property is also important when analyzing the performance of a thermal system and has a wide range of applications including in boiling heat transfer [233]; boiling HTC has been observed to increase with reduction in surface tension [234]. Surface tension also plays a vital role in drops and bubble formation [235], oil recovery [236], capability of cleaning oil spills, etc. Adding nanoparticles in the liquid alters its surface energy and wettability on common solid surfaces [235]. Despite its importance, surface tension of TiO_2 nanofluid has not been characterized well and the studies of surface tension of nano fluids are limited in the literature. Murshed et al. [107] showed that surface tension of TiO_2-water nanofluids was lower than that of pure water at room temperature. The reduction in surface tension was attributed to the Brownian motion and the adsorption of nanoparticles at the interfaces. Ravera et al. [237] argued that the presence of nanoparticles in surfacted liquid has two competing effects: (i) the nanoparticles adsorb the surfactant, leading to an increase of the interfacial tension, and (ii) the nanoparticles tend to attach themselves to the interface, thereby reducing the overall interfacial tension. Similarly, other researchers found that the surface tension of nanofluids decreased with increase in φ and temperatures [238, 239]. Chinnam et. al. [240] found that surface tension of TiO_2,

SiO_2, ZnO and Al_2O_3 nanofluids decreased as the temperature and φ increases. They attributed the reduction in the surface tension of nanofluid (compared to the corresponding base liquid) to the downward pulling of host liquid molecules by the nanoparticles, leading to a local rarefaction on the interface. On the other hand, Vafaei et al. [241] reported that the surface tension of nanofluids first decreased with the particle loading, reached a minimum and then increased again at larger values of φ. Moosavi et al. [242] showed that the surface tension of ZnO-EG nanofluid increased by ~7 % at φ = 3 %. With Al_2O_3 nanoparticles, Kim et al. [235] observed an increase in surface tension beyond φ = 0.01 %, while Golubovic et al. [243] and Das et al. [77] observed no significant change in surface tension with respect to φ. On the other hand, Tanvir and Qiao [244] observed that the surface tension of nanofluids increases linearly with increase in φ. Similar types of results were found by [235, 245, 246]. Besides that, Vafaei et al. [241] mentioned that the surface tension of nanofluids first decreased with the particle loading, reached a minimum and then increased again at larger values of φ. Thus, contradictory results exist regarding the variation of surface tension of nanofluids. From the above literature survey, it can be observed that there is a contradiction among the researchers regarding effect of φ and temperature on surface tension of nanofluids.

Droplet impact on solid surfaces is a key element of a wide variety of phenomena encountered in applications, such as inkjet printing and rapid spray cooling of surfaces. It also can be used in other applications, such as fire suppression by sprinklers, internal combustion engines, spray painting and coating, plasma spraying, and crop spraying. Many studies have been carried out to determine the parameters influencing the behavior of a single drop impact, in order to characterize their respective influence. Various parameters such as impact velocity, droplet diameter, liquid viscosity, surface tension, and substrate wettability have been investigated to correlate the droplet impact with the spreading process [247, 248, 249, 250]. The study of the shape of a liquid droplet, and the droplet contact angle in particular, has considerable scientific interest, since simple analysis of a fluid droplet can help to deduce important properties of the fluid itself. There are already established theoretical frameworks to link other physical properties to the mathematical equations governing droplet contact angle [251, 252, 253, 254]. However, there is a lack of consistent experimental studies comparing the

effects of concentration of different water-based nanofluids with stabilizing surfactants on their respective contact angles. Most of the recent developments have shown some similar results for different concentrations of nanofluids.

1.3.7. Application of nanofluids on solar thermal collector (STC)

Solar thermal collector collects heat by absorbing sunlight whereas collector is a device for capturing solar radiation. Solar radiation is energy in the form of electromagnetic radiation from the ultraviolet to the infrared wavelengths. Solar water heating systems is one of the most widely deployed renewable energy technologies used mostly in residential buildings, can reduce the use of fossil fuels. Nanofluid-based direct absorption solar collectors are solar thermal collectors where nanoparticles in a liquid medium can scatter and absorb solar radiation. Applications of nanofluids in solar collectors were investigated for the energy efficiency, economic and environmental aspects. Nanofluids have the following advantages over the conventional fluids for use in solar collectors:

A. Suspended nanoparticles will increase the surface area; however, it decreases the heat capacity of the fluid.
B. Suspended nanoparticles will enhance the thermal conductivity, which helps to improve the efficiency of heat transfer systems.
C. Absorption of solar energy will be maximized with change of the particle size, shape, material and φ of the nanoparticles and the properties of the nanofluid can be changed by varying φ of nanoparticles.

Researchers and scientists have continuously made an effort to increase the performance of solar collectors, which is the main components of any solar system [255, 256]. Initially Tyagi et al. [257] numerically investigated a nanofluid-based, low-temperature direct absorption solar collector (DASC). They used aluminum nanoparticle suspensions in water as the working fluid and showed an efficiency enhancement of around 10 % in comparison with a conventional flat plate solar collector. Otanicar et al. [2] also numerically evaluated the performance of low-temperature DASC. They considered three different nanofluids (graphite, silver, and CNT) for the simulation and found efficiency improvements of up to 5 % by utilizing nanofluids as the absorption medium. Luo et al

[258] investigated the effect of nanofluid on the performance of a solar flat collector based on direct absorption collection. They observed that by using the nanofluids, the solar efficiency could be enhanced upto about 2–25 %. Moradi et al. [259] developed a model of DASC using computational fluid dynamics (CFD) analysis of the flow and temperature. They found that there is a non-uniform dependence of the collector efficiency on the φ of nanoparticle. Taylor et al. [15] investigated the application of nanofluid-based DASC to high-temperature, concentrated solar power plants. They found that the use of a nanofluid in the receiver can improve the efficiency by 10 %, if operating conditions were chosen carefully.

1.4. GAP AREA

The above discussion points out to the fact that the thermophysical properties of the nanofluids play a major role in the performance of DASC. While the studies on nanofluids properties have increased prolifically over the past couple of decades, the literature is still replete with contradictory results and insufficient explanation of such results. For example, He et al. [87] and Wang et al. [64] showed that the effective thermal conductivity decreased with increase in particle size, while Beck et al. [92] and Shalkevich et al. [93] reported a reverse trend. Wang et al. [108] found that an optimal concentration of surfactant can enhanced thermal conductivity, while Angayarkanni and Philip [109] observed that the k / k_f decreased with the increase in surfactant loading. Xie et al. [105] observed that the value of thermal conductivity enhanced with decrease in pH value, but Wang et al. [108] found that the thermal conductivity ratio decreased at higher pH value. Mahbubul et al. [122] observed that the value of thermal conductivity increased with the rise of temperature and ultrasonication durations, while Kole and Dey [123] mentioned that the thermal conductivity of nanofluids increased with increase in sonication time and saturates at a maximum value beyond ~60 h of sonication. Wang et al. [108] reported that Cu-water nanofluid has a higher thermal conductivity enhancement than Al_2O_3-water nanofluid, because Cu nanoparticles exhibit higher thermal conductivity than Al_2O_3 nanoparticles. On the contrary, Lee et al [60] found that CuO nanofluids possess higher thermal conductivity compared to Al_2O_3 nanofluids, despite a lower thermal conductivity of CuO nanoparticles in comparison to Al_2O_3 nanoparticle. Hence, to understand the

suitability of any nanofluid for a specific application, unambiguous knowledge of its thermophysical properties is essential. Besides, our literature survey indicates a paucity of research data on the stability of TiO_2, Al_2O_3-water based nanofluids. Since the stability of nanofluids also depend on the specific mode of synthesis (which varies slightly from one group to another), it is imperative that the same needs to be verified in-house. In order to predict the performance of DASC with an in-house synthesized nanofluids, it is imperative that the ambiguities on the pertinent nanofluid properties are dispelled beforehand. For application of nanofluids in DASC, the study of the stability of these nanofluids are also needed. All these are possible if the entire study of synthesis, characterization and performance study (realistic DASC configuration) are carried out together. To the best of the author's knowledge, an all-encompassing study involving the above attributes has not been carried out before.

1.5. OBJECTIVE

The present study focuses on detailed characterisation of TiO_2, Al_2O_3 and TiO_2 (anatase) nanofluids. Titanium dioxide (TiO_2) nanoparticles have the inherent advantage of having high chemical and physical stability, low cost and commercial availability, besides being free from health hazards. Therefore, TiO_2 nanofluids can be pitched as a promising heat transfer medium. The rationale of choosing Al_2O_3 nanoparticle as the dispersed phase of the nanofluid is its high chemical and physical stabilities, low cost, easy availability and feasibility of large-scale industrial production. Al_2O_3 nanofluid in water has also been pitched as a promising heat transfer medium. Therefore, the present study attempts to characterize the thermophysical properties of Al_2O_3 and TiO_2 nanofluids for their use in DASC. The objectives of the thesis in terms of preparation, stability and measurable parameters described as follows.

- Synthesis of TiO_2 (21 nm), Al_2O_3 (51 nm), and TiO_2-anatase (25 nm) water-based nanofluids with and without surfactants. Testing the suitability of different surfactants, e.g., cetyl trimethyl ammonium bromide (CTAB), acetic acid glacial (AA) (99–100 %), oleic acid (OA), sodium dodecyl sulphate (SDS), and sodium dodecylbenzenesulfonate (SDBS) in stabilizing the nanofluids.

- Checking stability of the prepared nanofluids and particle distribution and morphology of the nanofluids by Zeta Potential, DLS and TEM method respectively.
- Determination of thermophysical properties (thermal conductivity, viscosity, surface tension) of the nanofluids for different φ (0.1–2.0 %) and temperature (20–60 °C).
- Performance analysis, through numerical study, of direct absorption solar collector (DASC) using nanofluids.

CHAPTER-2

2. Experimental methods

In this chapter, experimental methods on the synthesis process, characterization techniques, and property measurements of nanofluids have been discussed. The algorithm proposed for preparation of nanofluids is described in Figure 6.

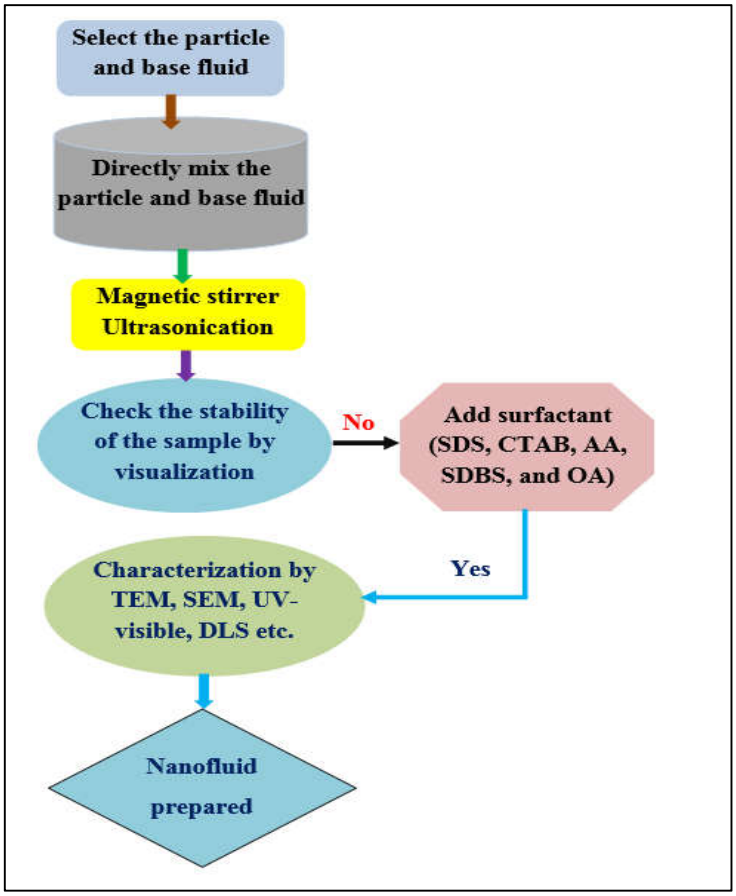

Figure 6 Algorithm for preparation of nanofluids following two-step method.

2.1. Preparation of nanofluids

For synthesis of nanofluids, various types of nanoparticles and surfactants have been considered. The properties of the base fluid (water) and nanoparticles are summarized in Table 3. Selection of suitable surfactant depends mainly upon the properties of the solutions and particles. Surfactants typically lower the interfacial tension between two liquids or between a solid and a liquid, or between a liquid and a gas. Surfactants may act as detergents, wetting agents, emulsifiers, foaming agents, and dispersants. Various types of surfactants are available; it depends on the charge on the head group of surfactants. A few examples of surfactants are mentioned in Table 4.

Table 3: Properties of nanoparticles

Types of particle	Particle size (nm)	Density (Kg/m^3)	Thermal conductivity (W/m *K*)
TiO_2	21	4260	8.4
Al_2O_3	50	3960	40
TiO_2 (anatase)	25	3900	8.9
Water		1000	0.613 (30 °C)

Table 4: Different types of surfactants

Types of surfactants	Examples
Anionic	Carboxylates, Sulphonates, Petroleum Sulphonates, Ammonium lauryl sulphate, Sodium dodecylbenzene sulphonate (SDBS), Sodium dodecyl sulphate (SDS), Sodium stearate, Sodium laureth sulfate, Potassium lauryl sulphate, Alkyl–benzene–sulphonates, Olefin Sulphonates, Sulphated Esters, Sulphated Alkylphenols, , etc.
Cationic	Quaternary Ammonium Salts; Cetyl trimethyl ammonium bromide (CTAB), Benzalkonium chloride (BAC), Cetylpyridinium chloride (CPC), Benzethonium chloride (BZT), Distearyl dimethylammonium chloride, Dioctadecyldimethylammonium bromide (DODAB), Amines with Amide Linkages, Alicyclic Amines, etc..
Nonionic	Polyethylene Glycol (PEG) Esters, Ethoxylated Aliphatic Alcohol, Polyoxyethylene Fatty Acid Amides, Carboxylic Acetic acid (AA), Gum arabic (GA), Poly vinyl pyrrolidone (PVP), Tween 80, Tween X–100, Stearyl alcohol, Oleic acid (OA), Oleyl amine, etc.
Amphoteric/Zwitterionic	Both cationic and anionic. Sodium lauroamphoacetate, Cocamidopropyl betaine, Lecithin, Hydroxysultaine,Phospholipids phosphatidylserine, Phosphatidylcholine, Sphingomyelins, Phosphatidylethanolamine, etc.

2.1.1. Synthesis of TiO_2 nanofluids

TiO_2 nanoparticles purchased from Sigma Aldrich Chemicals Limited, Germany, and the base fluid consisted of distilled water (Merck Millipore) of 99.7 % purity were used to prepare the nanofluids. Surfactants or dispersants like CTAB, AA glacial (99–100 %), OA and SDS were purchased from Merck Millipore used to improve the stability of the suspensions. Two-step method was adopted for the preparation of nanofluid. The desired solid volume fractions (φ) of nanofluids

were obtained by dispersing a carefully measured mass of nanoparticle in the host liquid. A high-precision electronic balance (Sartorius, BSA 224S-CW, max 220 g, d = 0.1 mg) was used for this purpose. The resulting solid φ is obtained using the formula mentioned in Eq. (95),

$$\varphi = \left[\frac{\left(\frac{w}{\rho}\right)_p}{\left(\frac{w}{\rho}\right)_p + \left(\frac{w}{\rho}\right)_{bf}}\right], \tag{95}$$

where ρ_p denotes the density of the TiO_2 nanoparticles, w_p is the weight of the nanoparticle, ρ_{bf} denotes the density of the host fluid, and w_{bf} is the weight of host fluid used. The measured quantity of nanoparticles were mixed with the host fluid and agitated for 2 h in an ultrasonic bath (Misonix, 40 KHz), and the suspensions were observed for several hours to check if the particles settled under gravity. To stabilize the nanofluids, different surfactants were used. It required selection of suitable surfactant with appropriate amount. Efficacies of CTAB, AA, SDS and OA have been tested as the possible surfactants. For CTAB and AA, the nanoparticle to surfactant mass ratio of 1:10 was found to give the best suspensions. For SDS and OA ranges of particle to surfactant mass ratio (from 1:2, to 1:10) were tried, but they did not exhibit satisfactory stabilization. First, the surfactant was mixed with distilled water and stirred in a magnetic stirrer for 1–2 h to ensure homogenous mixing of surfactant with the base fluid. Then the nanoparticles were added and stirred for another 2 h in the magnetic stirrer so that the particles get dispersed homogeneously within the mixture. Finally, the nanofluid mixture was dispersed in the ultrasonic bath for about 2–3 h at 30 °C to break the agglomerates retained even after stirring. The prepared samples using CTAB and AA were found to remain stable for several days with negligible disturbance. The prepared nanofluids were tested for their stability against settling through visual observations. Nanofluid samples were stored in vials for several days without disturbance and were imaged periodically shown in Figure 7.

2.1.2. Synthesis of Al_2O_3 nanofluids

Al_2O_3 nanoparticles (Sigma Aldrich Chemicals Limited, Germany) were used as the dispersed phase and distilled water was used as base fluid. Different surfactants viz., CTAB, SDBS and SDS were used to help disperse the particles and improve the stability of suspensions. Nanofluid samples were prepared by dispersing the Al_2O_3 nanoparticles in distilled water by two-step method. Measured

masses of nanoparticles were dispersed into appropriate base liquid of 100 ml to prepare nanofluid samples of varying φ, ranging from 0.1–2.0 %. Gravimetric measurements of nanoparticles and dispersant were performed using a high-precision electronic balance. The resulting φ of synthesized nanofluid was calculated by using the formula mentioned in Eq. (95). Where ρ_p denotes the density of the Al_2O_3 nanoparticles, W_p is the weight of the Al_2O_3 nanoparticle, ρ_{bf} denotes the density of the host fluid (100 ml), and W_{bf} is the weight of host fluid used. For preparing the non–surfacted nanofluid, appropriate volume of Al_2O_3 nanoparticles were added in distilled water and the mixture was stirred in a magnetic stirrer for 1 h so that the particles get dispersed homogeneously. The resulting suspension was sonicated for 15 minutes using a probe sonicator (PCI Analytics, PKS–750FM, at a power input rate of 0.167 J/s) to break the agglomerates remaining in the sample even after stirring. The sonicated suspensions, bearing different particle loadings, were observed for several hours to check if the particles settled under gravity. Another set of nanofluid samples was prepared that contained any of the three surfactants, viz., SDBS, SDS, and CTAB. For these samples, the concerned surfactant was first mixed with distilled water and stirred in the magnetic stirrer for 1 h to ensure homogenous mixing of surfactant with the host fluid. Measured quantity of nanoparticles was then added to the surfactant-water mixture and stirred and sonicated following the same protocol described above. For all three types of surfactants, different ranges of particle to surfactant mass ratios were tried; CTAB and SDS did not exhibit satisfactory stabilization with Al_2O_3 nanoparticle, whereas SDBS (at a particle to surfactant mass ratio of 2:1) showed better stabilization. The prepared samples using SDBS was found to remain stable for several hours with negligible particle agglomeration and settling; periodic stirring (every 40–60 minutes) further ameliorated the issue of particle sedimentation. The prepared nanofluids were tested for their stability against settling through visual observations. Nanofluid samples were stored in vials for several days without disturbance and were imaged periodically. Figure 7 and Figure 8 show the settling behaviours of the TiO_2 and Al_2O_3 nanofluids as the samples are maintained on a vibration-free platform over several hours. It is observed from Figure 7 that both the AA- and CTAB- stabilized nanofluids maintain very good stability over the span of 15 days. Figure 8 shows that the non-surfacted Al_2O_3 Nanofluids show slight

stratification, indication of cluster formation and gravitational settling. The SDBS-stabilized Al_2O_3 nanofluid exhibits an apparent phase separation. While the top phase shows a clear host fluid bulk, the heavier phase of a stable colloidal suspension is observed to separate out at the bottom, which quickly re-suspends upon mild stirring (without sonication).

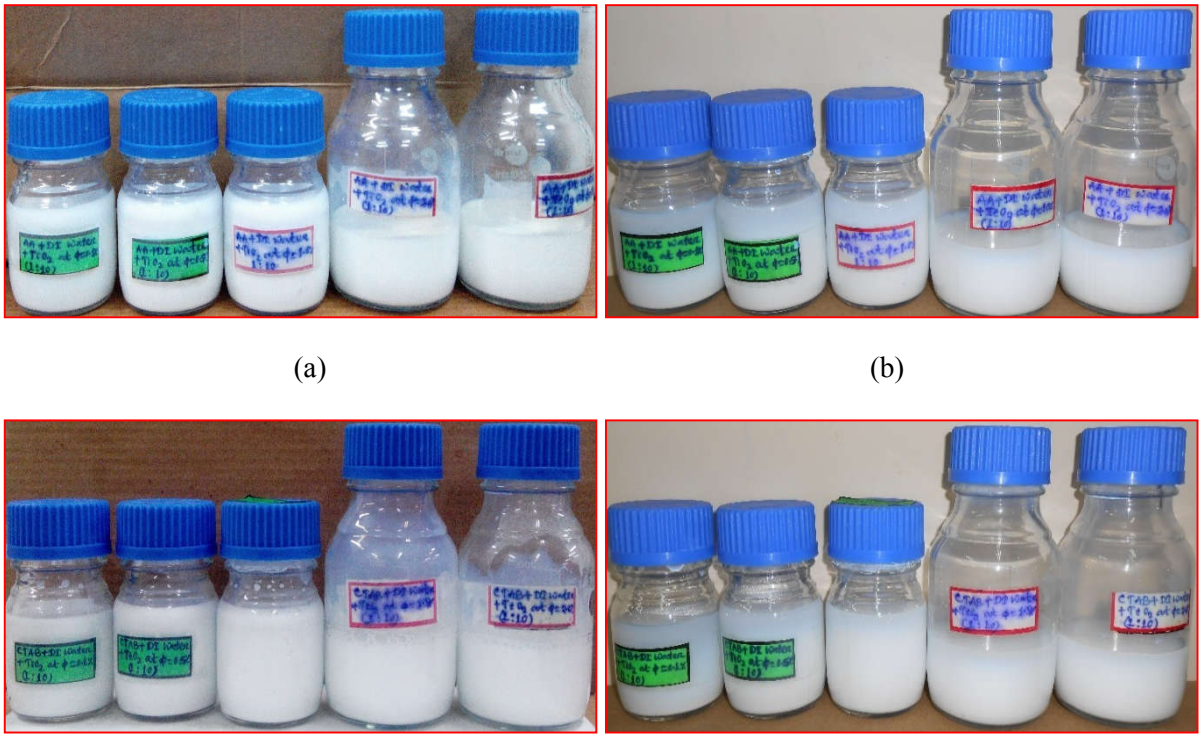

(a) (b)

(c) (d)

Figure 7 TiO_2 AA nanofluids (a) freshly prepared, and (b) after 15 days; TiO_2 CTAB nanofluids (c) freshly prepared, and (d) after15 days.

(a) (b) (c) (d)

Figure 8 Al_2O_3 nanofluid (without surfactant) (a) freshly prepared, and (b) after 1 day; Al_2O_3 -SDBS nanofluid (c) freshly prepared, and (d) after 1 day.

2.1.3. Synthesis of TiO_2 anatase nanofluids

Anatase grade TiO_2 nano powders (Sigma Aldrich Chemicals Limited, Germany) were used as dispersant and distilled water used as base fluid, whereas different surfactants, e.g., CTAB, AA, and SDS were purchased from Merck Millipore and used to help disperse the particles to improve stability of the suspensions. Nanofluid samples were prepared by dispersing the TiO_2 (anatase) nanoparticles in distilled water by two-step method. The nanoparticles were dispersed into the base liquid of 100 ml, to prepare nanofluid samples of varying φ (0.1–1.0 %). A high-precision electronic balance was used for measuring the accurate amount of nanoparticles and dispersants with an accuracy of 0.1 mg. The resulting φ of the prepared nanofluid was calculated by using the formula mentioned in Eq. (95). Where ρ_p denotes the density of the TiO_2 (anatase) nanoparticles, W_p is the weight of the TiO_2 (anatase) nanoparticle, ρ_{bf} denotes the density of the base fluid (100 ml), and W_{bf} is the weight of base fluid used. Different surfactants were used to prepare nanofluids. Initially, the appropriate amount of surfactant was mixed with distilled water and stirred in the magnetic stirrer for 1 h to ensure homogenous mixing of surfactant with the host fluid. Then appropriate amount of TiO_2 (anatase) nanoparticles was added to the surfactant–water mixture and stirred for another 1 h in the magnetic stirrer. For sample preparation, a fixed mass ratio r of surfactant to particle was used. The corresponding mass ratio x_s of surfactant to water was evaluated as,

$$[x_s] = \left[r \times \frac{\rho_p}{\rho_f} \times \left\{ \frac{\varphi}{1-\varphi} \right\} \right], \tag{96}$$

where ρ_p is the density of the nanoparticle, and $r = m_s / m_p$. Finally, the nanofluid mixture was sonicated in the probe sonicator for about 15 minutes. For all types of surfactants, different ranges of particle to surfactant mass ratios were tried. Visual observation shows that AA did not exhibit satisfactory stabilization for the TiO_2 (anatase) nanoparticle, whereas SDS and CTAB (at a surfactant to particle ratio *r = 1:10*) showed better stabilization.

2.2. Characterization of nanofluids

Characterization of nanofluids includes transmission electron microscope (TEM), dynamic light scattering (DLS), zeta potential, UV spectroscopy etc.

2.2.1. Morphology of nanofluids

Several techniques were used to characterize the nanopowder samples. In order to visualize the morphology of the nanoparticles, dry samples were analyzed by Transmission Electron Microscopy (TEM; JEOL JEM–2100, operating at an acceleration voltage of 200 kV). The TEM was used here to provide high-resolution images that can reach approximately 0.1 nm in case of lattice images. Droplet (~1 μL) of freshly prepared nanofluid were cast on transparent and thin carbon–coated, 300 mesh copper grids for TEM analysis. The samples were first air-dried (for ~ 2–3 minutes) in a controlled environment and further dried in a desiccator (for ~24 h). Figure 9 (a) and (b) shows the TEM images of the prepared TiO_2-water nanofluids, with CTAB as the stabilizer, for two different φ, viz., 0.1 % and 1.5 %, respectively. It is evident from the micrographs that the average size of the particles for both the cases ranges of 10–40 nm. Figure 9c shows the TEM image of a representative cluster in the TiO_2-water nanofluid (with AA as a stabilizer) sample for φ = 2.0 %. The high resolution-TEM images of a single nanoparticle and a cluster are shown in the insets of Figure 9c. Both of the TEM and HRTEM figures show the TiO_2 particles in the form of black spots. A well-defined thin surfactant layers covering the particles and their clusters can be observed in Figure 9a-c. HRTEM images show that the particle diameter in the TiO_2-AA water nanofluid lies in the range of 10–30 nm.

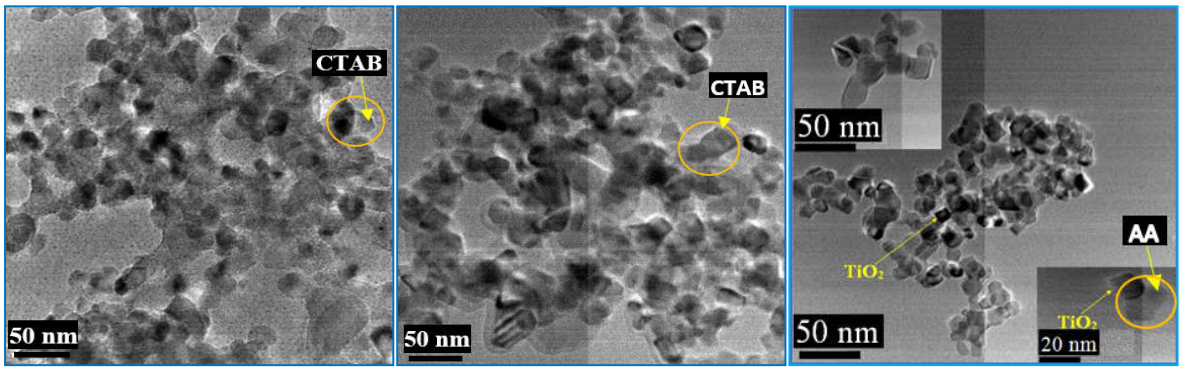

(a) (b) (c)

Figure 9 TEM image of CTAB–stabilized TiO_2-water nanofluid for (a) φ = 0.1 % and (b) φ =1.5 %; (c) TEM and HRTEM (insets) images of AA–stabilized TiO_2–water nanofluid for φ = 2.0 %.

Figure 10a and Figure 10b shows the TEM images of Al_2O_3–water and Al_2O_3–SDBS water nanofluids, respectively, for φ = 0.5 %. Figure 10a shows Al_2O_3 nanoparticles appearing as black rod–

like formations, where the particle size is found to vary in the range of 20–60 nm. The TEM image of SDBS–stabilized Al_2O_3 nanofluids (Figure 10b) shows the black spots of the particle varying in the size range of 30–70 nm. DLS analysis was used to get a quantitative estimate of the particle size distribution. The analysis was conducted at 25 °C, with freshly prepared dilute sample. Figure 11a and Figure 11b shows the TEM images of the anatase-SDS and anatase-CTAB nanofluids, respectively, for φ= 0.5 %. TEM images of SDS-stabilized anatase nanofluid samples (Figure 11a) show nearly-spherical particles (the darker spots) varying in the range of 10−40 nm in size. TEM images of CTAB-stabilized anatase nanofluids (Figure 11b) shows particles in the size range of 20−40 nm.

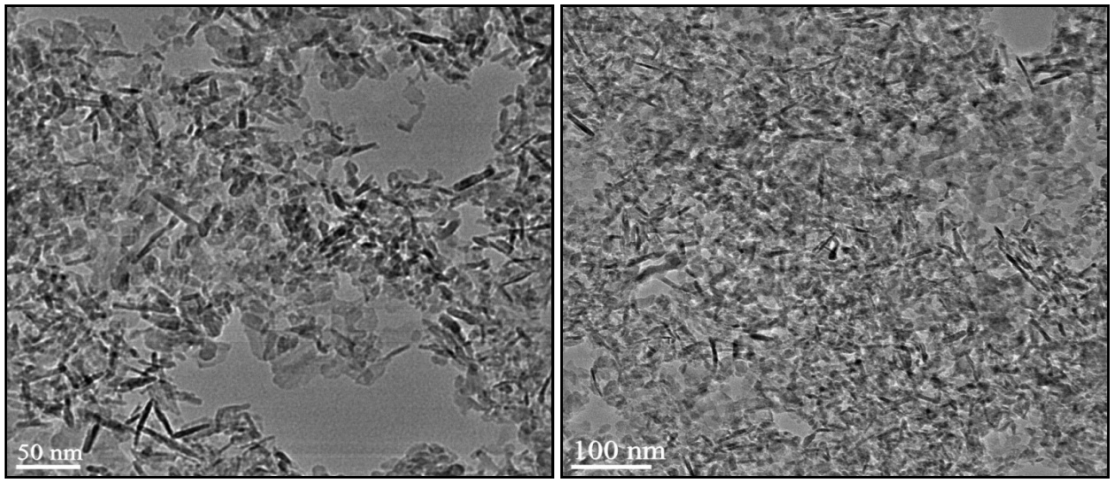

(a) (b)

Figure 10 TEM images showing the microstructure of (a) Al_2O_3 and (b) Al_2O_3-SDBS water nanofluid for φ = 0.5 %. The elongated dark spots represent the Al_2O_3 particles.

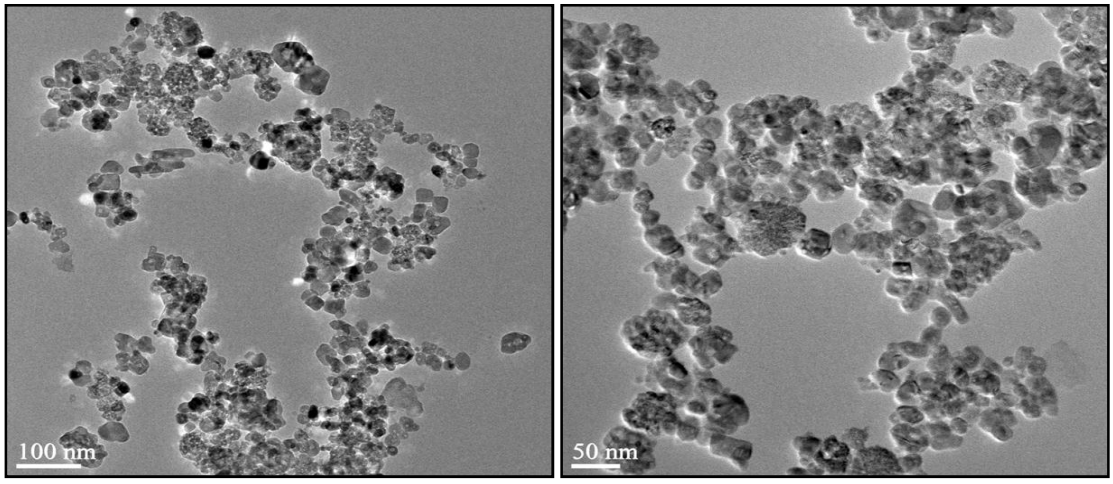

(a) **(b)**

Figure 11 TEM images of TiO_2 (anatase) nanofluid samples with (a) SDS and (b) CTAB as surfactants, at φ = 0.5 %.

2.2.2. Particle size distribution of nanofluids

Particle size distribution in the nanofluid samples were analyzed using dynamic light scattering (DLS, Zetasizer Nano ZS, Malvern, 0.3 nm–10.0 μm) instrument. DLS provides a clear insight and precise information about particle size distribution. All measurements were performed at 25 °C. DLS provides a clear insights and precise information about particle size distribution. Figure 12a displays a cumulative result for AA-stabilized TiO_2-water nanofluid at φ = 1.5 %; it shows an average diameter of 147.6 nm. This is much larger than the specified nanoparticle size (21 nm), indicating the possible formation of thermodynamically stable clusters of particles. The polydispersity index, defined as the ratio of the mass-weighted average particle diameter to the number-weighted average particle diameter, is a measure of width of particle size distribution. For the present case, it is found to be 0.271 directly from the DLS measurement (instrument data), implying that the nanofluids exhibits trend of monodispersity [260]. Figure 12b displays cumulative results for CTAB-stabilized TiO_2-water nanofluids at φ = 1.0 %; this shows an average diameter of 207.7 nm and polydispersity index of 0.232, denoting the stability of the nanofluids. Particle size distribution for the Al_2O_3-water nanofluid is shown in Figure 13a; the DLS analysis shows a number-averaged particle size of 222 nm while the polydispersity index is 1.23. The observed particle size is much larger than the specified nanoparticle size (50 nm), indicating the possibility of formation of thermodynamically stable clusters of particles. Figure 13 shows the number distribution of particles in the SDBS-stabilized Al_2O_3-water nanofluid; the plot shows a number-averaged diameter of 75 nm and a polydispersity index is 1.19 – both lower than those of the non-surfacted type. The reduced value of polydispersity index of the surfacted nanofluid is indicative of a better homogeneity and lower clustering; the average particle size appears slightly larger than the specified nanoparticle size possibly because of the surfactant layer.

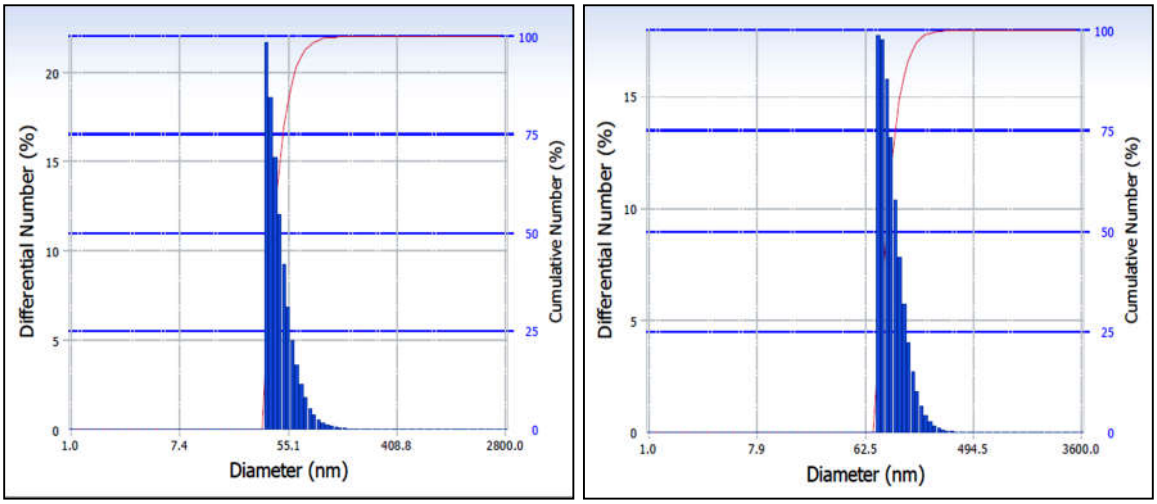

(a) (b)

Figure 12 Particle size distribution of TiO_2-water nanofluids with (a) AA stabilization at φ = 1.5 % and (b) CTAB stabilization at φ = 1.0 %.

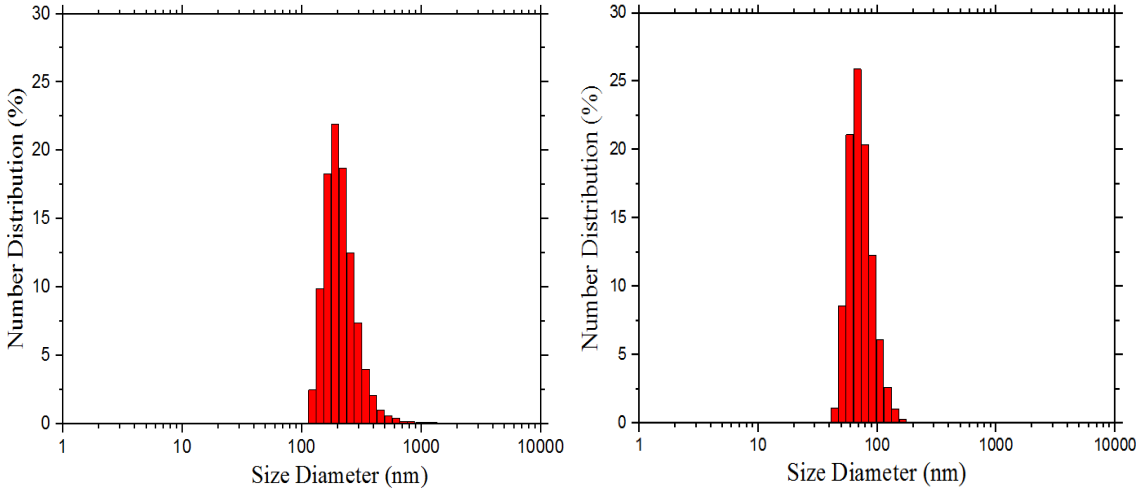

(a) (b)

Figure 13 Particle size distribution through DLS in Al_2O_3-water nanofluids (a) without surfactant, and (b) with SDBS surfactant.

Figure 14a and Figure 14b presents the particle size distribution of SDS and CTAB based TiO_2 (anatase) nanofluid at φ = 0.5 %, respectively. DLS analysis shows a number averaged particle size of 265 nm and 226 nm for SDS and CTAB based nanofluids, respectively. Figure 14a and Figure 14b presents the particle size distribution of SDS- and CTAB-based TiO_2 (anatase) nanofluids, respectively, at φ = 0.5 %. The analysis was conducted at 25 °C, with freshly prepared sample. DLS analysis shows a number-averaged particle size of 265 nm and 226 nm for SDS- and CTAB-based nanofluids, respectively. It is important to note here that the apparent particle size in DLS

measurement exceeds that observed through TEM. This is a common observation [261, 262]. Transmission electron microscope (TEM) calculates the primary size of the particles in the sample in dried state. On the contrary, dynamic light scattering (DLS) relies on Rayleigh scattering from the suspended nanoparticles that undergo Brownian motion and it calculates the hydrodynamic diameter of the sample in solvated state; the scattering intensity-based measurement includes the solvation diameter and the thickness of the surfactant layer that engulf the particle [263]. Besides, stable suspensions of particles clusters (where small clusters of multiple particles, instead of a single particle, remain suspended in the sample) may also be responsible for the larger average particle size data found from DLS measurement [264]. The intensity of the scattered light in DLS measurement scales with the sixth power of the particle diameter. Therefore, even with a small presence of agglomerates, the scattered light from the agglomerates may strongly overlay that of smaller particles [265]. Hence, we observed a particle size difference between DLS and TEM.

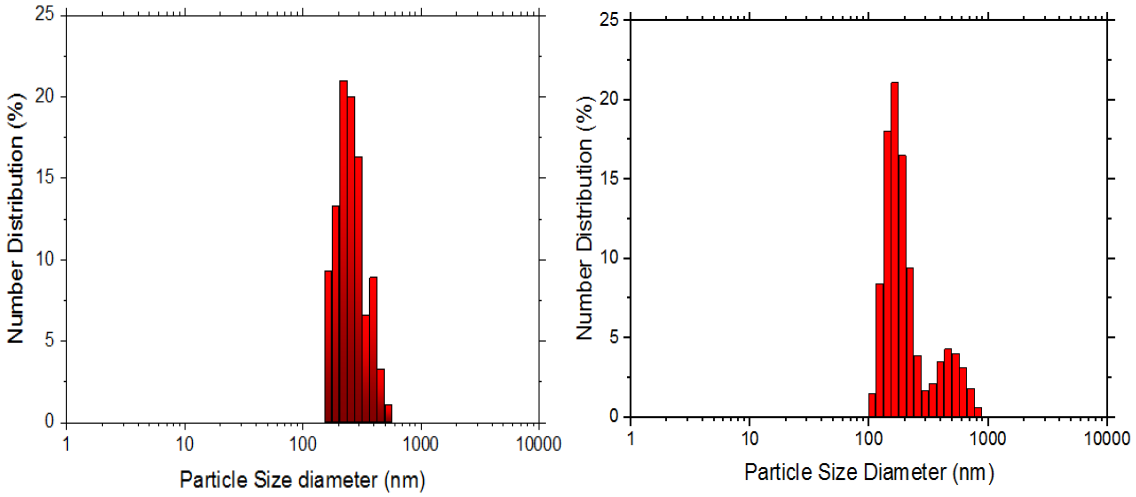

(a) (b)

Figure 14 Particle size distribution for TiO_2 (anatase) nanofluids with (a) SDS and (b) CTAB as surfactants at φ = 0.5 %.

2.2.3. Stability of nanofluids

Another important parameter to be considered to confirm the stability of the nanofluid is its Zeta potential. Stability of a colloidal system mainly depends on two forces: (i) attractive force and (ii) repulsive force. If the attractive force is bigger than the repulsive force between two particles, the particles will collide and if the repulsive force is greater than the attractive forces, then the particles

will repel each other. Zeta potential, known as electro-kinetic potential, is the potential in the interfacial double layer (at the location of slipping or shear plane) of a colloid particle moving under electric field [266], it shows the potential difference between the dispersion medium and the stationary layer of fluid attached to the dispersed particle. Colloids with high zeta potential (±) are electrically stabilized; while at low zeta potential, the particles tend to flocculate. The implication of zeta potential value on the nanofluid stability is described in Table 5. Figure 15a and Figure 15b shows the stability measurement of TiO_2-AA and TiO_2-CTAB nanofluids, where zeta potentials of 25.5 mV and 14.1 mV, respectively, are observed. Here, the AA based nanofluid has marginally better stability than the CTAB nanofluid. Figure 15c and Figure 15d shows the stability measurement of Al_2O_3 water and Al_2O_3-SDBS nanofluids, where zeta potentials of 40.3 mV and –29.5 mV, respectively, are observed. Here, the Al_2O_3 based nanofluid has marginally better stability than the SDBS nanofluid. Figure 15e and Figure 15f shows the stability measurement of anatase-SDS and anatase-CTAB nanofluids, where zeta potentials of –17.8 mV and –21.1 mV, respectively, are observed. Therefore, the anatase-CTAB nanofluid has marginally better stability than the anatase-SDS nanofluid. Though all the nanofluids exhibit limited stability with slow settling. Zeta potential values of both the nanofluids imply that they have limited colloidal stability, and hence, particle agglomeration cannot be ignored. This is corroborated by our experimental observation, where both the nanofluids were found to exhibit slow, diffusion-limited [162, 267] settling (settling time ~ 6 h). As per the theory of diffusion-limited cluster aggregation (DLCA) model, particle aggregation at short time scale occurs due to the Brownian motion. At a larger time scale, aggregating suspension settles down under gravity. It has been shown in the literature [267] that for extremely dilute suspensions, long-term settling takes place in the form of cluster deposition. For particle volume fraction exceeding a threshold (φ^*) the aggregates settle down collectively as a gelled suspension. For the present case of a well-sonicated suspension of anatase nanoparticles having particle diameter ~100 nm, the threshold $\varphi^* \sim (4\pi\Delta\rho g a^4 \,/\, 3K_B T)$, (where $\Delta\rho$ denotes the density difference between the dispersed and the continuous phases, g the acceleration due to gravity, a the particle radius, K_B the Boltzmann constant, and T is the absolute temperature) is estimated to be around ~ 0.023 (i.e., 2.3 %). Therefore, for the

range of particle volume fraction investigated in the present case ($0.001 \leq \varphi \leq 0.01$), the particles settle down in the mode of individual cluster deposition.

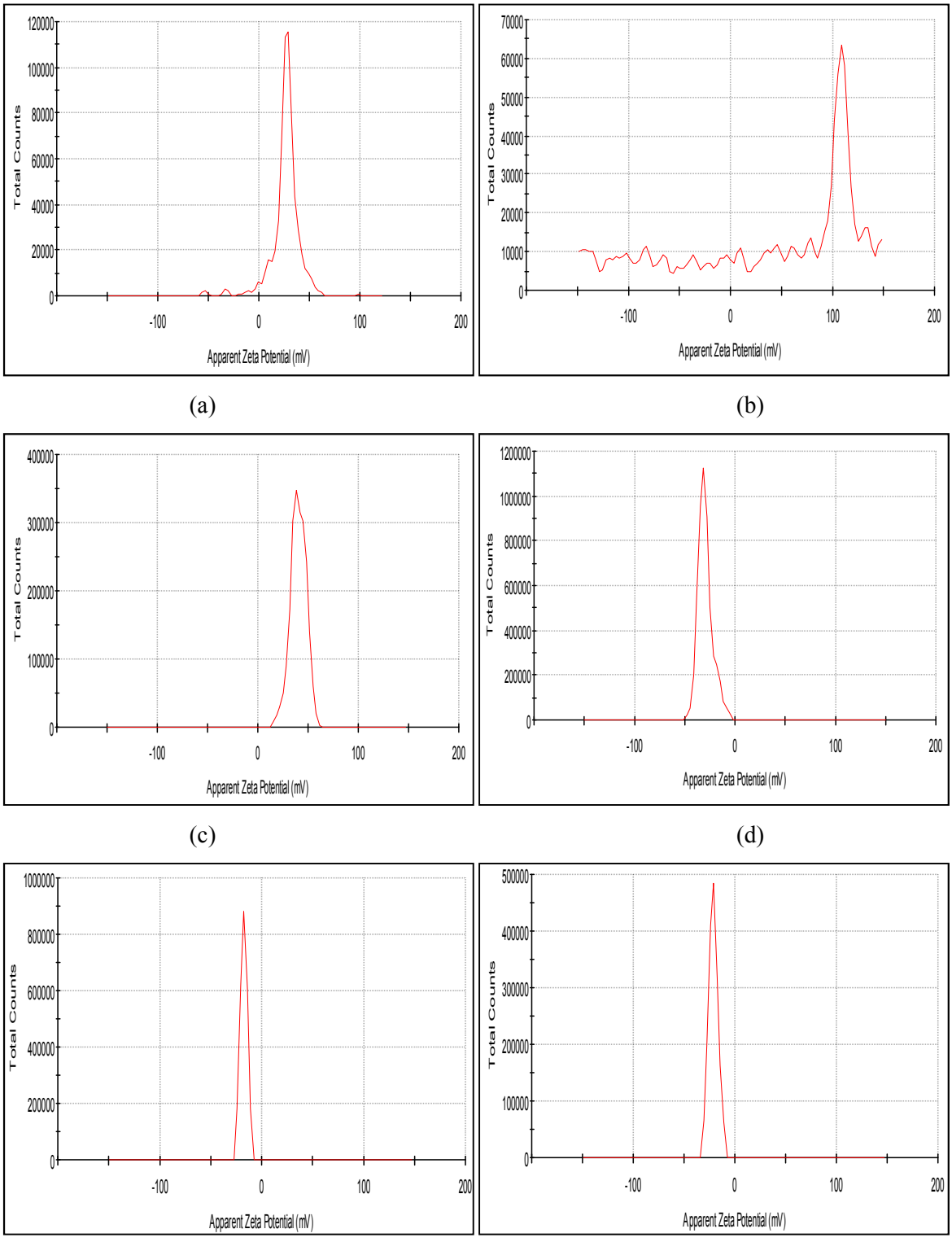

Figure 15 Zeta potential of (a) TiO_2-AA (b) TiO_2-CTAB (c) Al_2O_3 (d) Al_2O_3-SDBS, (e) TiO_2-anatase-SDS (f) TiO_2-anatase-CTAB, at φ = 0.1 %.

Table 5: Implication of zeta potential on stability [268]

Zeta potential (± mV)	Stability behavior of the colloid
0 to 5	No stability, rapid agglomeration occurs
10 to 30	Limited stability; particles settle down slowly
30 to 40	Moderate stability
40 to 60	Good stability; yet some possibility of settling
more than 60	Excellent stability, little settling likely

Besides, ultraviolet-visible spectroscopy (UV-Vis) was used to quantitatively determine the stability of the nanofluid. UV-Vis refers to absorption or reflectance spectroscopy in the ultraviolet-visible spectral region. This is the measurement of attenuation of light after it passes through a sample or after reflection from a sample surface. A beam of light from a visible or UV light source is separated into its component wavelengths by a prism or diffraction grating. The measurements were performed by pouring the nanofluid sample in a cuvette cell through which electromagnetic radiation was passed. This cuvette had two highly polished faces to minimize reflection and scatter losses. The other two faces were transparent to allow incident light beam. After preparation, a sample was drawn from prepared nanofluid, and then, was poured into the cuvette for testing. The spectral transmittance of nanofluid dispersions are typically measured by using a spectrophotometer, over a range of wavelengths from 200–1100 nm. The most common spectrophotometers are used in the ultra-violet ($\lambda < 380$ nm) and visible ($380 < \lambda < 780$ nm) ranges of the electromagnetic spectrum, and some could also operate in the near-infrared ($780 < \lambda < 1500$ nm) region. The output of UV-Vis spectroscopy for any material bears a relation between absorbance of light and the incident wavelength. A Shimadzu UVPC-1601 UV-Visible Absorption Spectrophotometer of wavelength range (200 – 1100 nm), has been used for the spectral transmittance measurement. A schematic diagram of the relevant setup is shown in Figure 16.

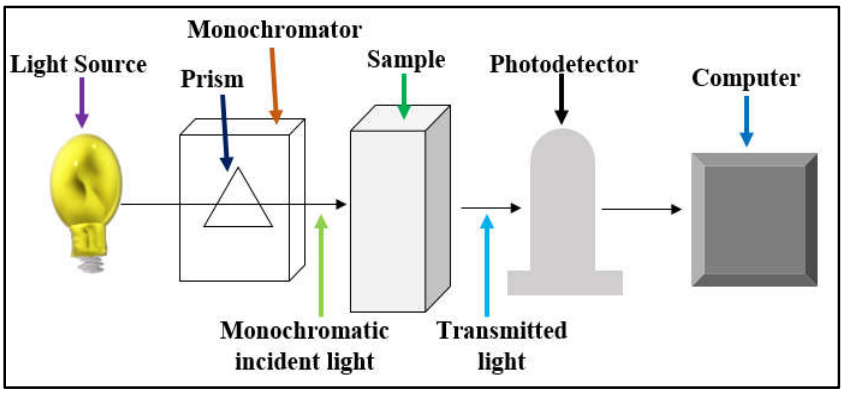

Figure 16 A schematic diagram of the UV-Visible spectroscopy.

The sample is placed in a quartz vial when a halogen light is passed through the monochromator. The probing light signal, generated from the monochromator (a combination of prism and grating system) is allowed to pass through the sample, and the transmitted light is picked up by a photodetector, and analysed.

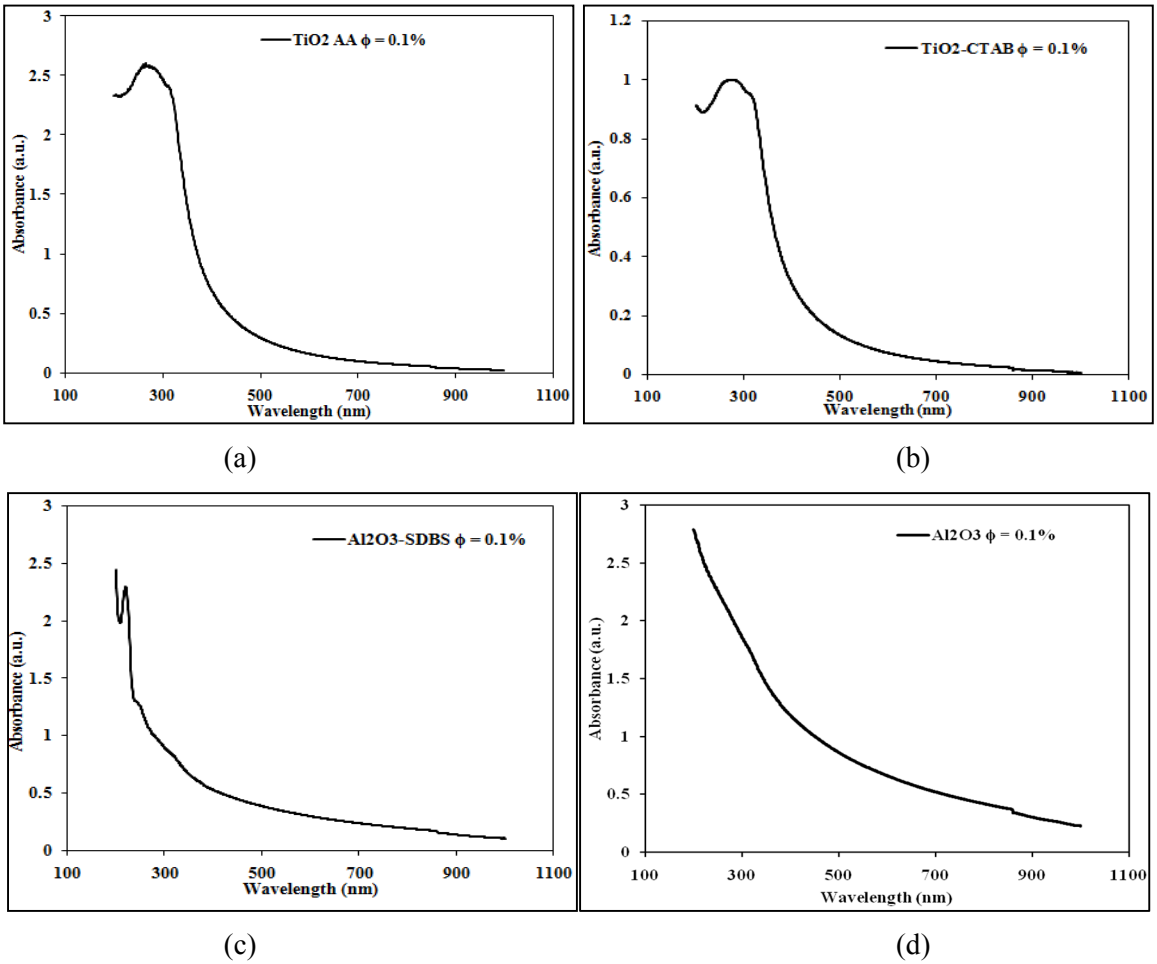

Figure 17 Figure shows the UV visible spectroscopy for (a) TiO_2-AA, (b) TiO_2-CTAB, (c) Al_2O_3-SDBS, (d) Al_2O_3-water-based nanofluids at $\varphi = 0.1$ %.

Figure 17 shows the UV-visible spectroscopy data for (a) TiO_2-AA, (b) TiO_2-CTAB, (c) Al_2O_3-SDBS, (d) Al_2O_3 water-based nanofluids at φ = 0.1 % respectively. For TiO_2-AA nanofluids the maximum amount of sample's absorption occurred in the wavelength range of 266 nm and this amount is equal to 2.598, as shown in Figure 17a. For TiO_2-CTAB nanofluids the maximum amount of absorption from the sample occurred in the wavelength of 278 nm and this amount is equal to 0.999, (Figure 17b). Similarly, for Al_2O_3-SDBS nanofluids, the peak absorptions occurred in the wavelength of 200 nm and 218 nm (amounting to 2.44 and 2.28, respectively, shown in Figure 17c); for Al_2O_3 water-based nanofluids the peak absorption (equal to 2.78) was 200 nm (see Figure 17d). From the figure it is identified that the strongest absorption band wavelength in the studied nanofluids lie in the ranges from 280–350 nm.

2.3. Property measurement techniques

The property measurements techniques included thermal conductivity, viscosity, surface tension, contact angle and pH of nanofluids described below.

2.3.1. Measurement of thermal conductivity of nanofluids

Thermal conductivity (TC) of the TiO_2, Al_2O_3 and TiO_2 (anatase) nanofluids, for different φ (0.1–2.0 %) and temperature (20–60 °C), was measured using a KD2 Pro thermal analyzer (Decagon Devices, WA, USA). A thermostatic bath (Model no.-CTB 07) was used to maintain the sample temperature (within a range of ± 0.1 °C of the set value). Figure 18 describes the experimental set–up for conductivity measurement. TC measurement was based on transient hot wire technique using a sensor (KS–1), which has an accuracy of ± 5 %. The thermal analyzer runs on battery, comes with a handheld microcontroller and sensor needles. During measurement, the 60 mm long and 1.3 mm diameter stainless-steel probe, which served both temperature sensor and line heat source, was fully immersed into the nanofluid sample, which was kept in a cylindrical glass container (25 mm diameter and 80 mm height). In order to obtain accurate results, the vessel and probe were maintained at a constant temperature for 10 minutes to reach equilibration before each measurement. The samples were maintained at different stipulated temperatures by immersing them in the constant temperature bath. Before analyzing the thermal characteristics of the prepared nanofluids, the sensor was

calibrated every time with the base liquid (water) and glycerine at a room temperature of 25 °C. The experimental set up of TC meter was placed on a horizontal plane with adequate vibration isolation (to avoid any vibration induced convection at the probe tip) to obtain accurate result. Thermal conductivity measurement at a given φ and temperature lasted for 30–40 minutes (excluding the time taken for thermally equilibrating the thermostatic bath and the nanofluid sample), when 5 to 8 runs were taken (and the average values were reported). With every sample of nanofluid (i.e., at a given φ), measurements were also made at different sample temperatures. Measurements were performed at different temperatures and particle loadings of the nanofluids. For each sample, temperature was varied from 20–60 °C at increments of 5 °C.

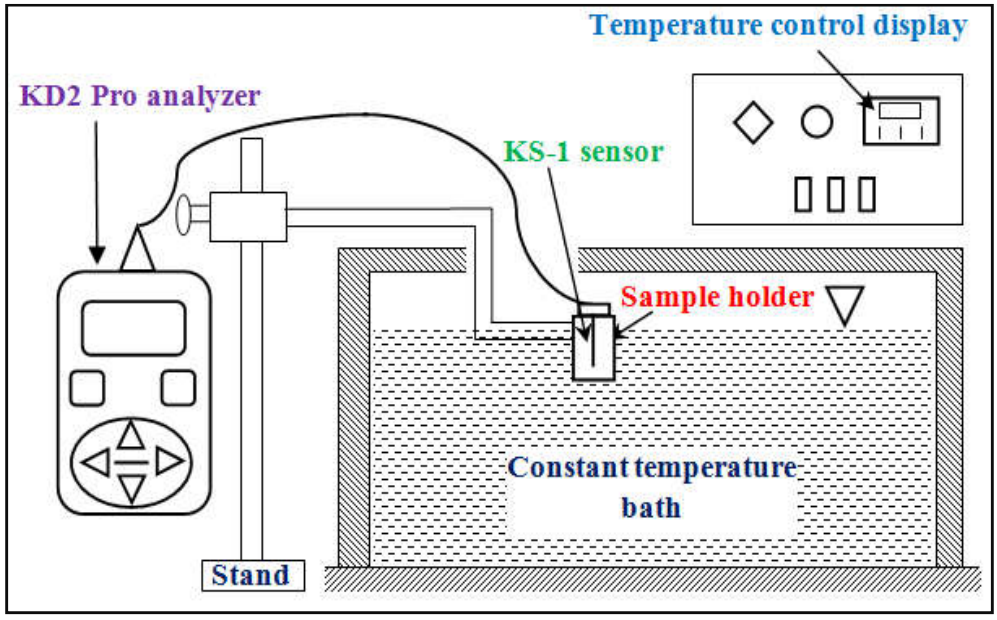

Figure 18 Schematic diagram of experimental setup used to measure the thermal conductivity of nanofluids.

An uncertainty analysis has been carried out by using the standard technique [269]. The contributing factors towards the overall uncertainty ($W_{k,T}$) in the measured thermal conductivity are the individual uncertainties in measurement of particle volume fraction (w_φ), nanofluid temperature (w_T), and the device uncertainty of the thermal conductivity meter itself (w_k). Therefore,

$$W_{K,T} = \sqrt{\left(\frac{\partial k}{\partial \varphi} w_\varphi\right)^2 + \left(\frac{\partial k}{\partial T} w_T\right)^2 + (w_k)^2}, \quad (97)$$

where $\frac{\partial k}{\partial \varphi}$ and $\frac{\partial k}{\partial T}$ denotes the variation of thermal conductivity with respect to φ and temperature, respectively. The maximum uncertainty in measured thermal conductivity of the TiO_2-AA, and TiO_2-CTAB water nanofluid samples were found to be ± 5.0 %, for Al_2O_3-water nanofluid samples, with and without SDBS surfactant, were found to be ± 5.0 % and for TiO_2-water nanofluid samples, SDS and CTAB surfactant, were found to be ± 5.25 % and ± 5.21 %, respectively.

2.3.2. Measurement of viscosity of nanofluids

A standard programmable viscometer (model DV–II + Pro, Brookfield Instruments) was used to measure the viscosity of the nanofluid samples. Figure 19 describes the experimental set-up of the viscometer. A spindle (S18, range of 1–2000 cp), was connected to the viscometer and inserted into the corresponding chamber, which contained a minimum of 16 ml of sample. The machine was connected to a computer through an RS232 cable, and RHEOCALC V3.3 software was used for data collection and storage. Measurements were performed at different temperatures and particle loadings of the nanofluids. For each sample, temperature was varied from 20–60 °C at increments of 5 °C while the measurements were taken at a fixed shear rate of 122.3 s^{-1} and the precisions of temperatures were maintained in the range of ± 0.5 °C. The same thermostatic bath (used in TC measurement) was attached to the viscometer cup to maintain the temperature within ± 0.1 °C of the set value. For each sample, temperature was varied at increments of 5 °C, the viscosity and shear stress data of all samples were measured within a shear rate range of 12–232 s^{-1}, while the spindle rotation was 10–190 rpm. Speed of the viscometer was changed by 10 RPM (12.23 s^{-1} shear rate) and it was held for 30 s at each speed. The experiments were conducted at least ten times for generating the datasets for the analysis. Similar to the case of thermal conductivity (see Eq. (97)), an uncertainty analysis in measurement of viscosity data has also been carried out.

2.3.3. Measurement of pH of nanofluids

pH of the nanofluids at different temperatures and φ was measured using a pH meter (Sartorius Mechatronics, Model no. PT-10). A beaker containing the nanofluid was placed on a hot plate with magnetic stirrer and covered with Teflon tape. The magnetic stirrer helps to disperse the nanoparticles uniformly, leading to consistency in reading. The temperature probe of the pH meter

was immersed to a depth of 3 cm in the nanofluid for consistent result. While immersed in the nanofluid, the pH probe measures the pH and the temperature probe measures the temperature of nanofluid. The time for each 5°C rise of the sample temperature was controlled to be within 2 to 3 min. The accuracy of the pH meter specified by the manufacturer is ±0.002% of the reading.

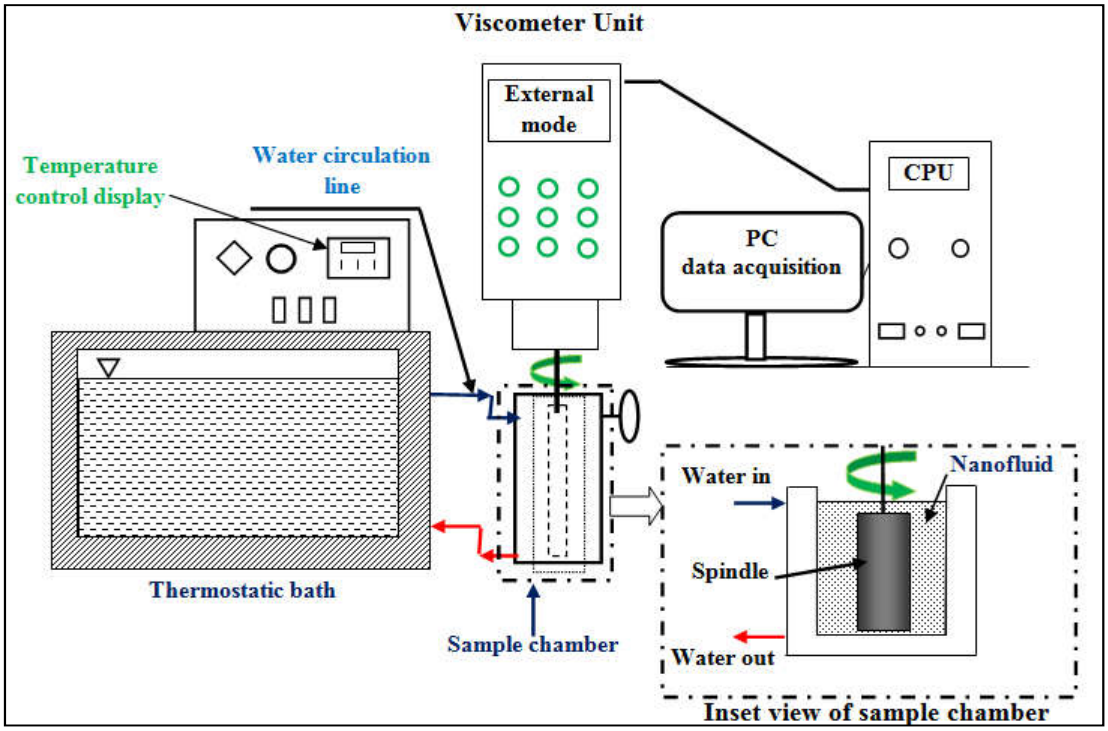

Figure 19 Schematic diagram for viscosity measurement set-up.

2.3.4. Measurement of surface tension and contact angle of nanofluids

Effects of φ and temperature on the surface tension of the nanofluids were measured by using a platinum ring type tensiometer (Jencon India). The tensiometer was calibrated against distilled water. The platinum ring was thoroughly cleaned and dried before each measurement. Surface tensions of the nanofluids were measured to characterize the surface properties nanofluids. Du-nouy ring method is a popular, simple and reliable method of measuring the interfacial tension between two liquids [270, 271]. Surface tension of TiO_2-AA, TiO_2-CTAB, Al_2O_3-water, and Al_2O_3-SDBS based nanofluids were measured by using platinum ring type tensiometer for different φ (0.1–2.0 %), at a constant temperature. In the Du-nouy ring method, a surface tensiometer is used, and the tensiometer is placed horizontally on a vibration-less table. A very sensitive thin platinum ring is used for the

tensiometer. The ring is placed near the surface of the liquid sample, and an upward force is exerted on the ring. At equilibrium, the upward force is balanced with the surface tension applied on the on ring by the liquid which gives the measurement of surface tension of the liquid. Because of the movement of the ring during the measurement, this method can be quasi-static in nature which may result incorrect measurement in surface tension. Therefore, it is required that the movement of ring is restrained. The ring is made of inert material of almost null mass so that to alleviate the effects of gravity. Before each measurement the tensiometer was calibrated against the base fluid, the platinum ring was thoroughly cleaned and dried. For each sample, 4 to 6 measurements were taken at a constant temperature and the corresponding average value was recorded.

Contact angle was measured from sessile droplets by using the principle of a standard direct optical Goniometer. In this set-up a droplet is gently put on a smooth mirror-finish homogeneous substrate. The images of the corresponding droplets on the surfaces are then analyzed to measure its contact angle with the surface. The surface must be horizontal in order to avoid hysteresis and to ensure this, the experiment was conducted on a horizontal and vibration-less table top. An image of the droplet on the surface is taken using a high resolution high speed camera (CMOS camera, Model: Basler acA2000–340kc), having a full pixel resolution of 2046 × 1086 at a frame rate of 340 fps. In this experiment, we have used a hydrophilic glass substrate to measure the contact angle and consider that the surface is entirely clean. The sessile drop profile was captured by the high-speed camera and then was analyzed using two similar algorithms: Low-Bond Axisymmetric Drop Shape Analysis and Drop-snake. Drop-snake and LBADSA are available as simple plugins of ImageJ (Java coded) to plot the boundary of a sessile droplet with appreciable accuracy. Drop-snake, a method based on B-spline snakes (active contours) to shape the drop is more mathematical, While LBADSA method, which follows the Young Laplace equation is used in this particular series of analysis of sessile drops. Following the Young Laplace equation to trace out the droplet boundary by adjusting the radii of curvature with the image of sessile drop conveniently provides the contact angle. However, it is obvious that in the sessile drop analysis all the combinations of interacting elements namely the solid (the surface), liquid and the vapour (air) affect the contact angle, i.e. the drop shape.

Therefore, Dupre's equation is required to accurately determine the surface tension of the unknown liquid in this analysis. Finally, Young-Drupe's equation was implemented for verification of our experiment. This method is called the direct optical method which has its advantages: it is fairly simple and only small quantities of fluid (a few microlitres) and small surface substrates (a few square mm) are required. Also, it must be mentioned that there is an impact of impurities due to the small size of the liquid and substrate. The direct optical method fundamentally relies of observing the tangent of a curve optically and therefore is prone to errors in the observations. So, a background light along with a diffuser screen was used to assist observation, while a cold light source was selected to avoid undesired heating of the liquid or substrate. A micrometer syringe with a narrow-gauge stainless steel and Teflon needle was used to slowly create a droplet of around 4-5 mm diameter. The needle was very close to the surface of substrate where the drop fell in order to avoid undesired vibrations and also, the needle opening was small enough to prevent the drop from getting distorted forcibly. Also, the imaging device only focuses on the largest meridian section of the sessile drop, which means the profile image reflects only the contact angle at the point in which the meridian plane intersects the three-phase line. Contact angle measurements were made inside an enclosed chamber to avoid airborne contamination, external forces due to flowing air and establish equilibrium vapour pressure of the liquid tested. Figure 20 shows the experimental setup for contact angle measurement.

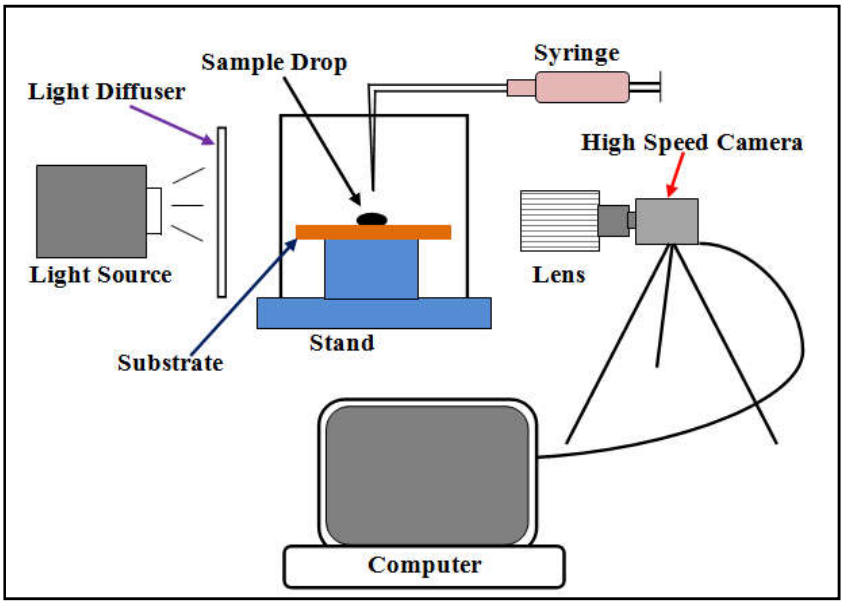

Figure 20 Schematic diagram of the contact angle measurement setup.

CHAPTER 3

3. Thermophysical properties of nanofluids

The salient thermophysical properties of the TiO_2 and Al_2O_3 nanofluids synthesised following the methods described in chapter 2 are reported here. A comprehensive characterization of thermal conductivity, viscosity, surface tension, contact angle and pH of nanofluids have been provided for each type of nanoparticle and surfactant. The properties of nanofluids were measured at different temperature (20–60 °C) and solid volume fraction (φ = 0.1–2.0 %).

3.1. Thermal conductivity of nanofluids

3.1.1. TiO_2 nanofluids

In order to estimate the heat transfer enhancement upon use of the nanofluid, thermal conductivity of TiO_2-water nanofluid was measured at different temperatures (20–60 °C) and φ (0.1–2.0 %). Figure 21a and Figure 21b shows the variation of thermal conductivity with φ at different temperature for AA-stabilized nanofluid and CTAB-stabilized nanofluid respectively. Minimum ten numbers of runs have been taken to calculate the standard deviation, for plotting the error bar. The result shows that the thermal conductivity of the nanofluid increases with increase in φ and temperature. The enhanced effect of temperature on thermal conductivity may be attributed to the increased intensity of the particle Brownian motion with the increase of temperature and clustering of nanoparticles [64]. The van der Waals force and electrostatic force also play important role.

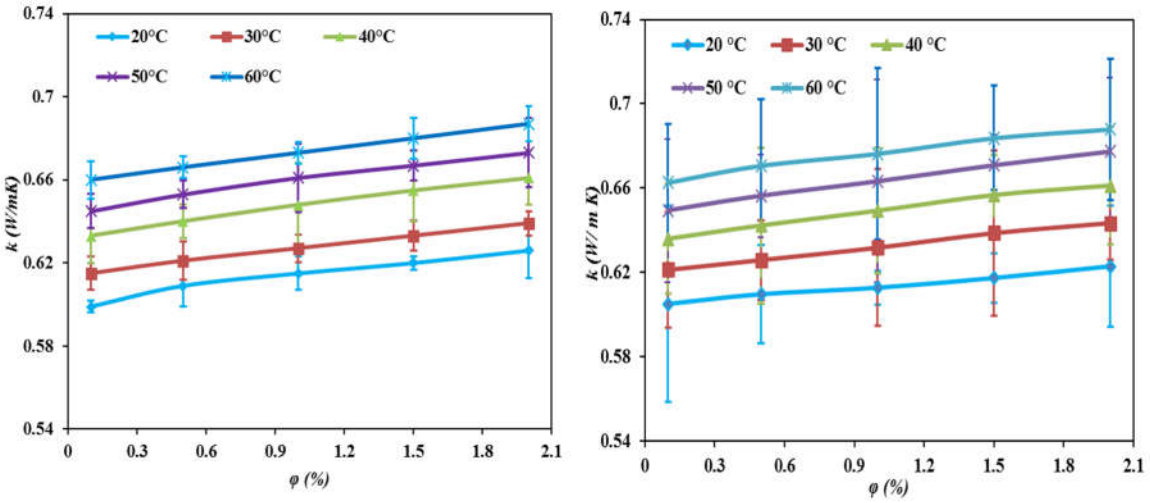

(a) (b)

Figure 21 Variation of thermal conductivity with φ for (a) AA-stabilized, and (b) CTAB-stabilized TiO_2-water nanofluid at different temperature.

Figure 22a and Figure 22b shows the thermal conductivity ratio (the ratio of effective thermal conductivity of the nanofluid to that of water) of AA-stabilized nanofluids and CTAB-stabilized as function of φ at different temperatures (viz., 20, 30, 40, 50 and 60 °C) respectively, and compares the observed thermal conductivity values with those predicted from three well-known thermal conductivity models for nanofluids. The three models, viz., Maxwell [49], Timofeeva et. al. [83] and Yu and Choi [134] describe the thermal conductivity of nanofluids as function of φ shown in Eq. (1), Eq. (22), and Eq. (5), respectively. In Eq. (5), β denotes the ratio of the nano-layer thickness to the original particle radius. Normally, $\beta = 0.1$ is used to calculate the thermal conductivity of nanofluid [134]. It is observed that for the temperature range and φ reported in Figure 22a and Figure 22b, the models proposed by Maxwell (Eq. 1), Timofeeva (Eq. 22) confirms to the experimental observation, while the Yu and Choi model (Eq. 5) slightly overpredicts the thermal conductivity values. This may be attributed to the departure of the assumed β from the actual one. This is in contrast to the observation of Yu and Choi [134], who found their model largely underpredicts the thermal conductivity of surfacted (ternary) nanofluid suspension systems. This anomaly may be attributed to the difference in surface chemistry of the nanoparticles in the surfacted host fluid.

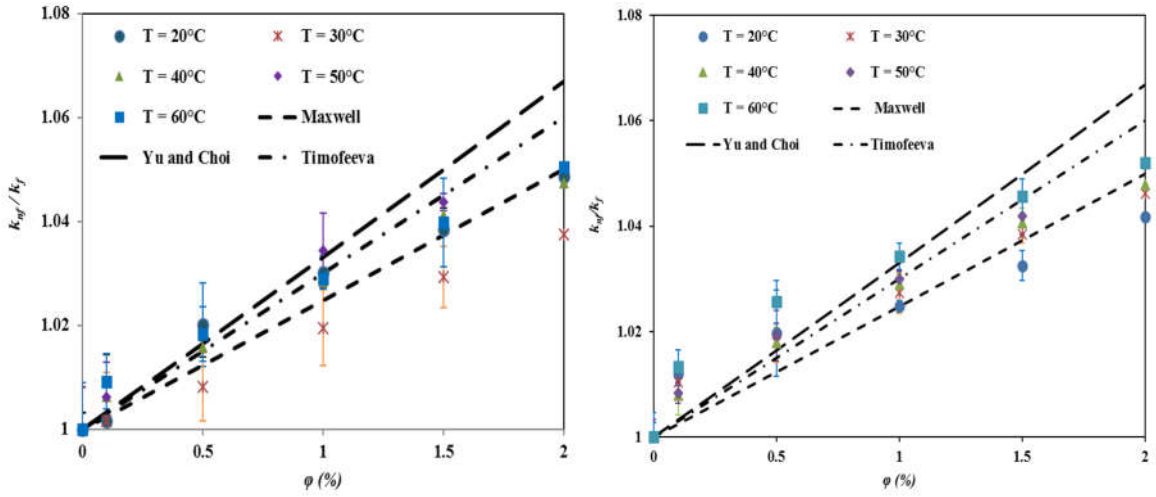

(a) (b)

Figure 22 Thermal conductivity ratio of TiO_2 nanofluids (a) AA-stabilized and (b) CTAB-stabilized, plotted against φ at different temperatures; the trend compares with well existing thermal conductivity models for nanofluids.

3.1.2. Al_2O_3 nanofluids

Thermal conductivity of Al_2O_3 nanofluid was measured at different temperatures (20–60 °C) and φ = 0.1–2.0 %. Figure 23a and Figure 23b shows the variation of thermal conductivity with φ, at different temperatures, for Al_2O_3-water nanofluid samples without surfactant and with SDBS surfactant stabilization. Thermal conductivity measurements for each φ and at each temperature was repeated 5 to 8 times; the largest standard deviation in thermal conductivity data was found to be ± 0.047 W/m–*K*. Result shows that thermal conductivity of nanofluid increases with the temperature as well as φ. The enhancing effect of temperature on thermal conductivity may be attributed to the increased intensity of the Brownian motion of nanoparticles with the increase of temperature. Microscopic motion of suspended nanoparticles is due to Brownian, van der Waals, and electrostatic forces also plays significant role. Nanofluids exhibit higher thermal conductivity than their base fluids even at very low φ of suspended nanoparticles. Thermal conductivity of liquids enhances due to both static and dynamic factors [272]. Brownian motion is caused by the random bombardment of liquid molecules, causing the particles to randomly move through the liquid, thereby enabling stronger transport of heat. This translates into an enhanced effective thermal conductivity. When the size of the nanoparticles in a nanofluid becomes less than the phonon mean-free path, phonons no longer diffuse across the nanoparticle but move ballistically without any scattering [272]. However, the mechanism responsible for ballistic phonon transport to be more effective than a very-fast diffusion phonon transport is still nebulous, falling short of explaining the anomalously high thermal conductivity of nanofluids at low φ [272]. Jang and Choi [129] also explained the role of Brownian motion in enhancing the thermal conductivity of nanofluids and attributed it to the collision between nanoparticles. As can be seen from Figure 23, the average value of thermal conductivity of non-surfacted Al_2O_3-water nanofluid at each temperature and φ is higher than that of SDBS-stabilized nanofluid. Although this is in line with prior findings that the thermal conductivity of SDBS-water mixture decreases with the increasing SDBS concentration [273] – the dispersants effectively suppress the thermal conductivity of the base fluid [274]. The result is somewhat inconclusive as the

difference in TC (less than 2 %) is smaller than the uncertainty of TC prediction (5 %). Error bars in Figure 23 show the standard deviation of thermal conductivity of data.

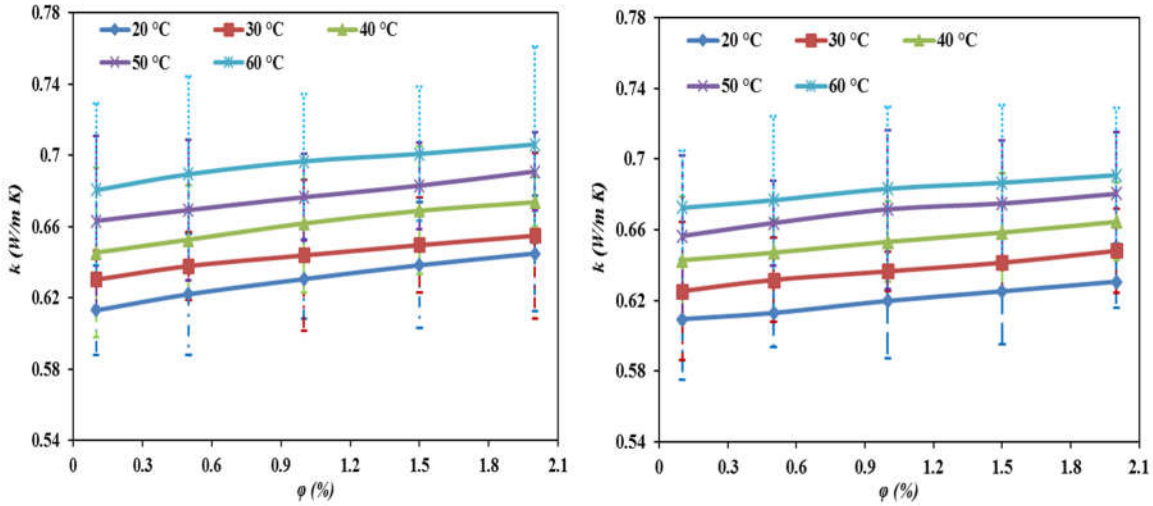

Figure 23 Variation of thermal conductivity with φ at different temperatures for Al_2O_3-water nanofluids (a) without surfactant, and (b) with sodium dodecylbenzenesulfonate (SDBS) surfactant.

Figure 24 shows the thermal conductivity ratio (the ratio of effective thermal conductivity of the nanofluid to that of the base fluid), i.e., (k_{nf} / k_f) of the Al_2O_3-water nanofluids, both without and with the surfactant (SDBS), as function of φ at various temperatures (viz., 20, 40 and 60 °C). The measured thermal conductivity of nanofluids was used for comparison with those obtained from the existing correlations proposed by Maxwell [49], Timofeeva et. al. [83] and Yu and Choi [134], respectively, which describe that the thermal conductivity of nanofluids as functions of φ. It is observed that for the temperature range and φ reported in Figure 24, the models proposed by Maxwell (Eq. 1), Timofeeva (Eq. 22), and Yu and Choi (Eq. 5) underpredicts the thermal conductivity values, particularly at low values of φ. Several factors may be attributed to this observed enhancement of thermal conductivity of the tested nanofluid samples. For example, the size and clustering of the particles, the favourable influence of the nano-layer between the nanoparticles and base fluids, or even the difference in surface chemistry of the nanoparticles in the surfacted host fluid. These factors have been considered in the model proposed by Patel et al. [148], since it accounts for the Brownian

velocity of the nanoparticles, as described in Eq. (24). Thus, unlike the models of Maxwell [49], Timofeeva [83] and Yu & Choi [134], Patel model implicitly accounts for temperature dependence of the nanofluid thermal conductivity. In this Eq. (24) the factor C was determined from the experimental data. Figure 25 shows the variation of thermal conductivity ratio (k_{nf}/k_f) of Al_2O_3-water and Al_2O_3-SDBS water nanofluids as a function of φ at different temperatures (viz., 20, 40 and 60 °C). The experimental values of thermal conductivity ratio for $\varphi > 1.0$ % are well predicted by Patel model [148] for C = 25,000. However, even this model underpredicts the k_{nf}/k_f ratio for the lower range of φ investigated here. A more comprehensive model that takes into account the influence of surfactant and particle size would require consideration of a larger spectrum of parametric study, involving particles of different size and shape, nature of surfactant, and host fluid, which is beyond the scope of current work.

The predicted models have considered only solid volume fraction in the evaluation of thermal conductivity, and have ignored the influence of other parameters like the effects of particle size and shape, and the molecular-level liquid layering on the bare and/or non-surfacted particles. This may have led to the difference in the observed results from the prevalent models. Several factors may be attributed to this observed enhancement of thermal conductivity of the tested nanofluid samples. For example, the size and clustering of the particles, the favourable influence of the nano-layer between the nanoparticles and base fluids, or even the difference in surface chemistry of the nanoparticles in the surfacted host fluid. As already mentioned before, the thermal conductivity of nanofluid is influenced both by the static (contribution due to higher intrinsic thermal conductivity of the nanoparticles) as well as the dynamic (Brownian transport) factors [275]. Therefore, the enhanced thermal conductivity at low φ be attributed to the dynamic factors. Dynamic effect becomes more tangible at very low nanoparticle volume fractions, when the phonon mean-free path in the nanofluid exceeds the nanoparticle size, and the phonons, instead of diffusing across the nanoparticles, move ballistically without scattering [129]. Nevertheless, the exact mechanism of how ballistic phonon transport supersedes diffusion phonon transport is still not well defined, and hence, the above

hypothesis only qualitatively explains the high thermal conductivity of nanofluids at low concentrations [129].

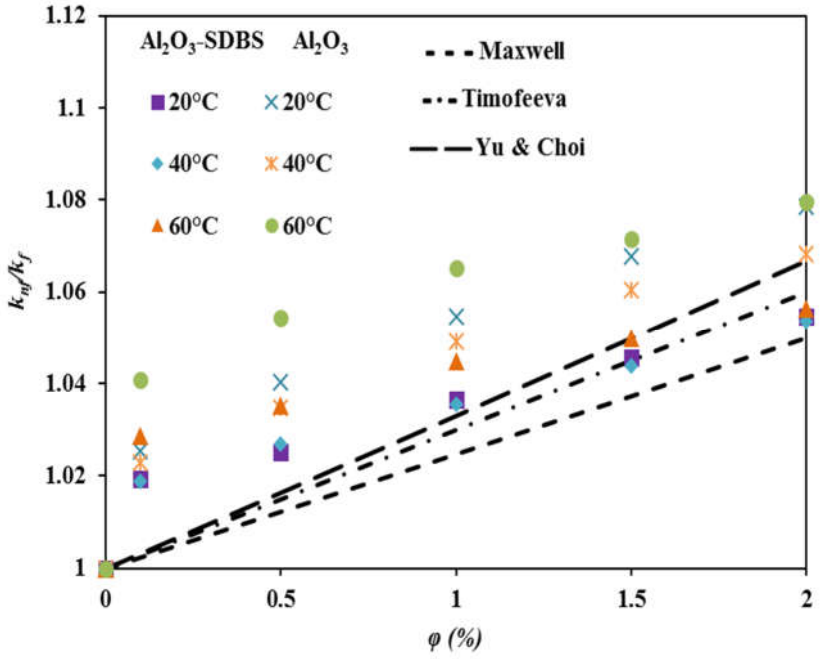

Figure 24 Variation of thermal conductivity ratio with φ, both without (marked as Al_2O_3) and with (marked as Al_2O_3-SDBS) surfactant, at different temperatures; existing thermal conductivity models underpredicts the k_{nf}/k_f ratio, particularly at low φ.

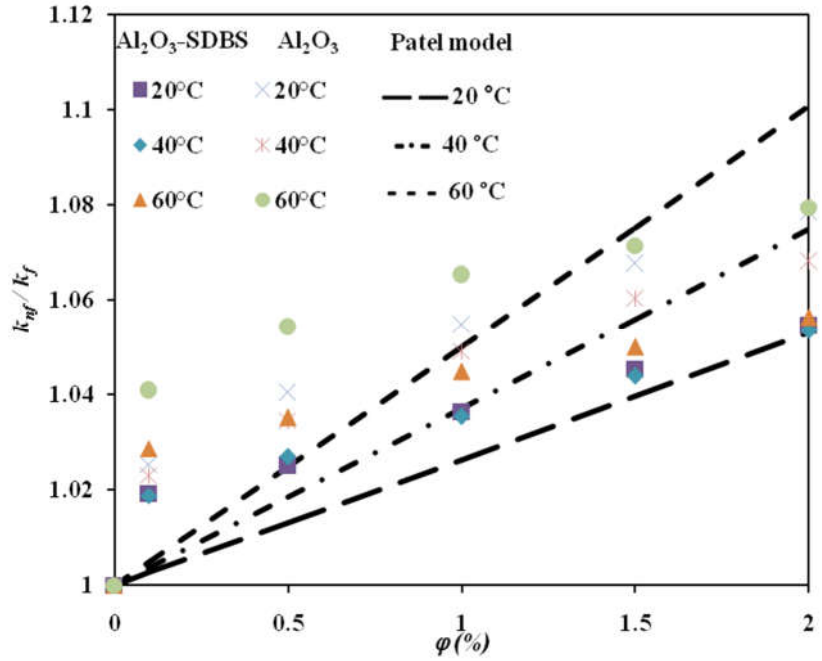

Figure 25 Variation of thermal conductivity ratio with φ, both without (marked as Al_2O_3) and with (marked as Al_2O_3-SDBS) surfactant, at different temperatures for Patel model [148], (C = 25000).

3.1.3. TiO_2-anatase nanofluids

Thermal conductivity of the TiO_2 (anatase) nanofluid was measured at different temperatures (20–60 ºC) and φ (0.1–1.0 %). Figure 26a and Figure 26b shows the variation of thermal conductivity with temperature at different φ, for SDS- and CTAB-surfacted nanofluids, respectively; the measured thermal conductivity of nanofluid is also compared with that of the base fluid [276]. It is observed that an increase in either temperature or φ results in an increase of the thermal conductivity of the nanofluid. The enhanced effect of temperature on thermal conductivity attributed to the increased intensity of the Brownian motion of nanoparticles with the increase of temperature, microscopic motion of suspended nanoparticles due to Brownian. Figure 26 clearly shows that the thermal conductivity of the nanofluid exceeds that of the base fluid (water) even at very low φ of suspended nanoparticles. This increase is attributed to the static (contribution due to higher intrinsic thermal conductivity of the nanoparticles) as well as the dynamic (Brownian transport) factors [272]. At least 5–8 runs were taken to plot both the vertical and horizontal error bars, which denote the standard deviation of thermal conductivity of data, in Figure 26. It can be seen from the figure that the value of thermal conductivity of TiO_2-SDS-water nanofluid is higher than that of CTAB stabilized TiO_2-water nanofluid for all temperature and φ.

Figure 27 shows the thermal conductivity ratio of anatase-SDS and anatase-CTAB nanofluids as a function of φ at two different temperatures, viz., 30 and 40 °C, and compares the observed thermal conductivity values with the well-known thermal conductivity models for nanofluids. In 1881, Maxwell [49] derived an expression of effective thermal conductivity for two-phase solid-liquid mixtures given by Eq. (1). The model satisfactorily predicts the thermal conductivity k_{nf} of the nanofluid in terms of the thermal conductivities of the base fluid (k_f) and the particles (k_p) for spherical particles at low φ and ambient conditions. More recently, Patel et al. [148] developed a model shown in Eq. (24) for thermal conductivities of nanofluids by taking into account the specific surface area and Brownian motion of nanoparticles, in addition to particle concentration. The relative variation of thermal conductivity ratio with φ, i.e., $\left[\frac{\partial}{\partial\varphi}\left(\frac{k_{nf}}{k_f}\right)\right]_T$ match well between the two models

described by Eq. (1) and (24). However, the conductivity ratio at low particle loading shows a sudden jump, and both the models underpredicts the $\frac{k_{nf}}{k_f}$ ratio for all φ (see the vertical shift in the experimental plots from the model predictions in Figure 27). Clearly, the Maxwell model does not take into consideration the dynamic factor, while the Patel model underpredicts the same (see Figure 27). The difference between the experimentally observed k_{nf}/k_f values and those predicted from the two models can be attributed to the limitations in accounting for the correct dynamic factor.

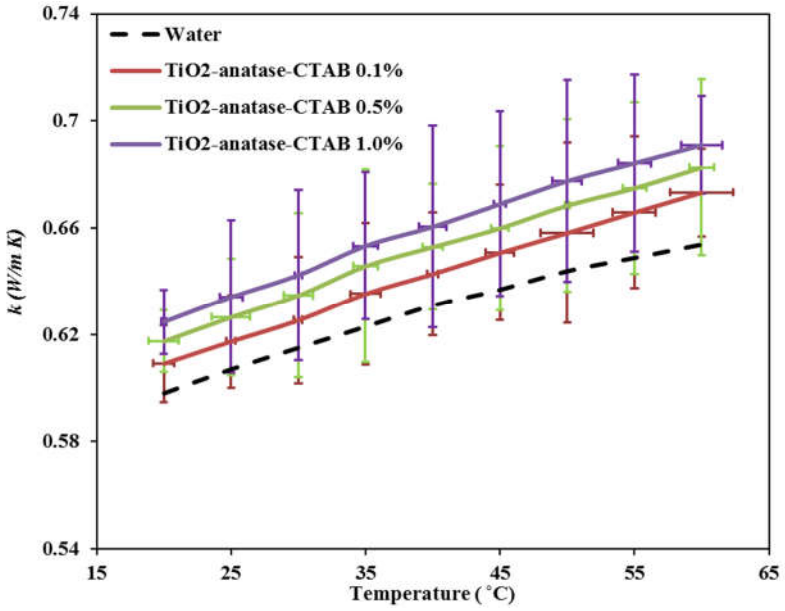

(a)

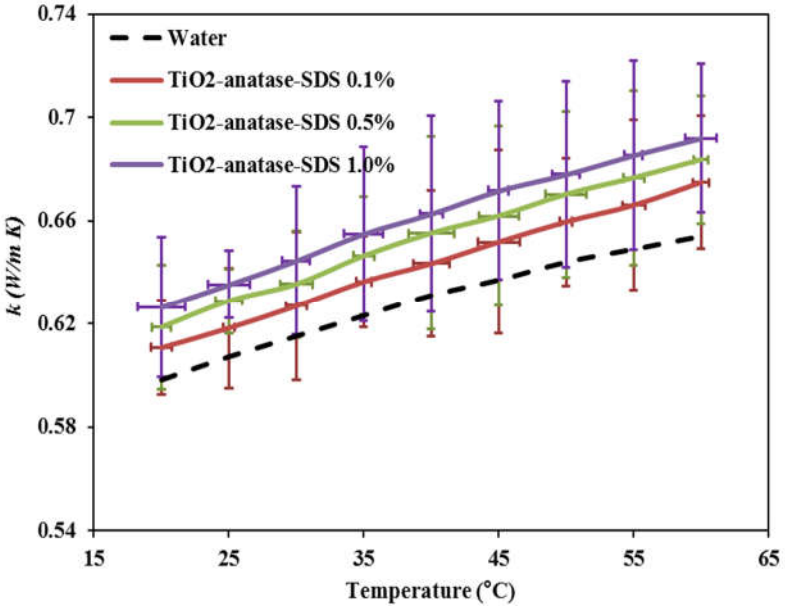

(b)

Figure 26 Variation of thermal conductivity with temperature for (a) SDS- and (b) CTAB- stabilized anatase-water nanofluids at different φ.

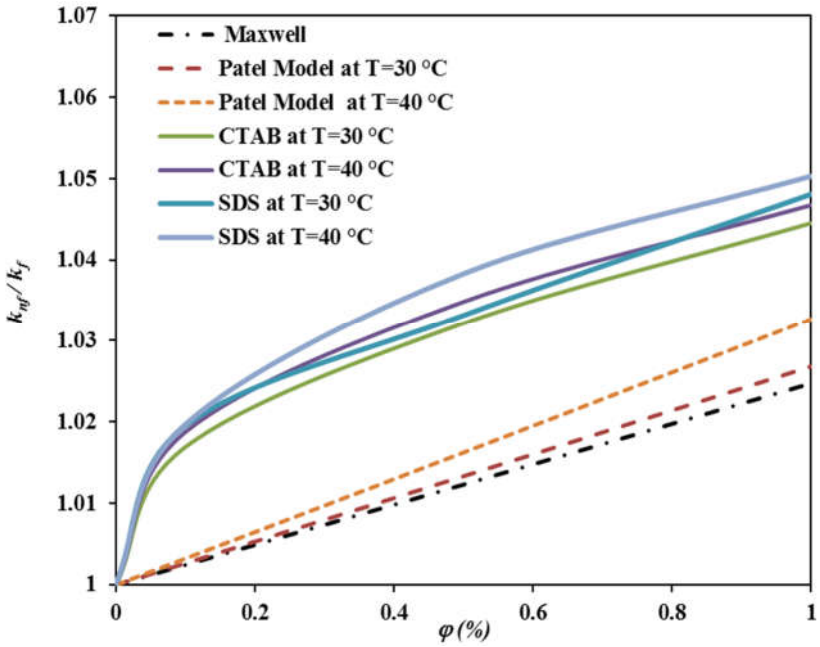

Figure 27 Variation of thermal conductivity ratio of CTAB- and SDS-stabilized anatase-water nanofluids with φ at different temperatures and comparison with existing thermal conductivity models.

Figure 28 shows the percentage of thermal conductivity enhancement for SDS and CTAB based TiO_2-anatase nanofluids at a temperature range of 20–60 °C. The enhancement of thermal conductivity was estimated from the measured thermal conductivity data as follows:

$$\text{Enhancement} = \frac{(k_{nf}-k_f)}{k_f} \times 100, \qquad (98)$$

where k_{nf} and k_f are the thermal conductivities of nanofluid and water, respectively. From the Figure 28, it was observed that the thermal conductivity enhancement increased with temperature and φ. At φ = 1.0 % and T = 60 °C, a maximum 5.8 % of thermal conductivity enhancement was found for SDS-surfacted nanofluids, which is slightly greater than that exhibited by the CTAB-surfacted nanofluids (enhancement of 5.4 %). For both SDS- and CTAB- surfacted nanofluids, the enhancement shows almost linear relationship with temperature. The possible explanation of an anomalous increase in the thermal conductivity are the effects of interfacial layer, Brownian motion, nanoparticles clustering, particle aggregation and the nature of heat transport in nanoparticles.

In Figure 26, it is seen that the thermal conductivity of water increases linearly in the range 20 °C to 40 °C and then increases at a somewhat reduced rate. However, the thermal conductivity of the

nanofluids with 0.1 % anatase increases almost linearly all through the measured temperature range. This results in a nearly constant enhancement in thermal conductivity, compared to neat base liquid, at low temperatures seen in Figure 27. As the temperature increases, the surface energy of the particles reduces and hence, agglomerated particles are separated which in turn increases Brownian motion of the suspended particles. Their collision with the fast-moving atoms or molecules increases the effective thermal conductivity of nanofluid [50, 277]. This compensates for the slight reduction in $(\partial k/\partial T)$ for pure water at the higher temperature range (as observed in Figure 26) and results in nearly linear rise of k_{nf} with temperature.

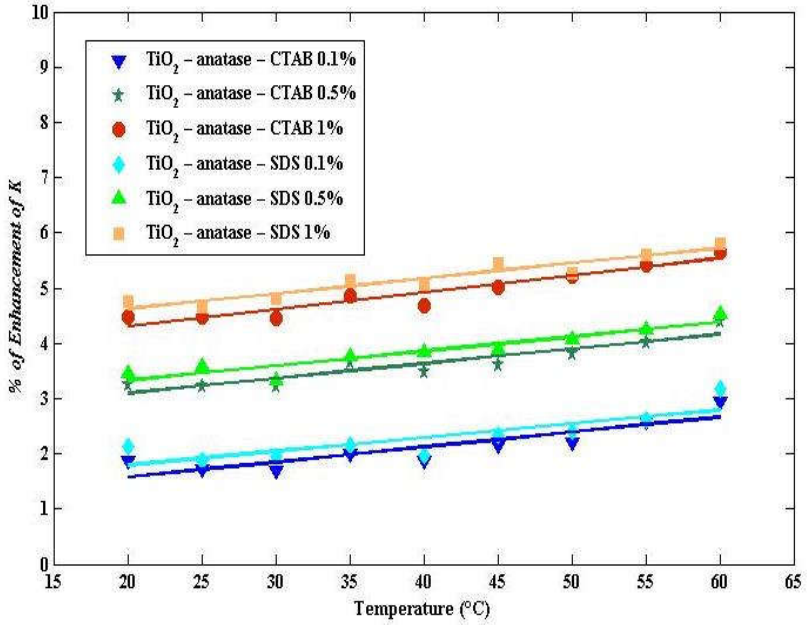

Figure 28 Variation of % enhancement of k_{nf} with temperature for different nanofluids.

3.1.4. Consolidation with existing correlation

In the previous section, the thermal conductivities of different nanofluids were compared with standard models; while it was observed that the results mapped well with the models at some values of φ, the properties differed significantly at other φ. For example, for Al_2O_3-water and Al_2O_3-SDBS-water nanofluids, the experimental values of thermal conductivity ratio for φ > 1.0 % were well-predicted by Patel model [148] for C = 25,000. However, this model underpredicts the k_{nf}/k_f ratio for the lower range of φ investigated here. The plot shown in Figure 25 following Patel model did consider C = 25,000 for φ > 1.0%. However, fitting the experimentally observed values of k_{nf}/k_f

ratios to Patel model for lower range of φ would warrant a different value of C. For example, Figure 29 shows a variation of C as function of φ for different temperatures for the non-surfacted Al_2O_3-water nanofluid. A mode comprehensive model that takes in to account the influence of surfactant and particle size would require consideration a larger spectrum of parametric study, involving particles of different size and shape, nature of surfactant, and host fluid, which is beyond the scope of current work.

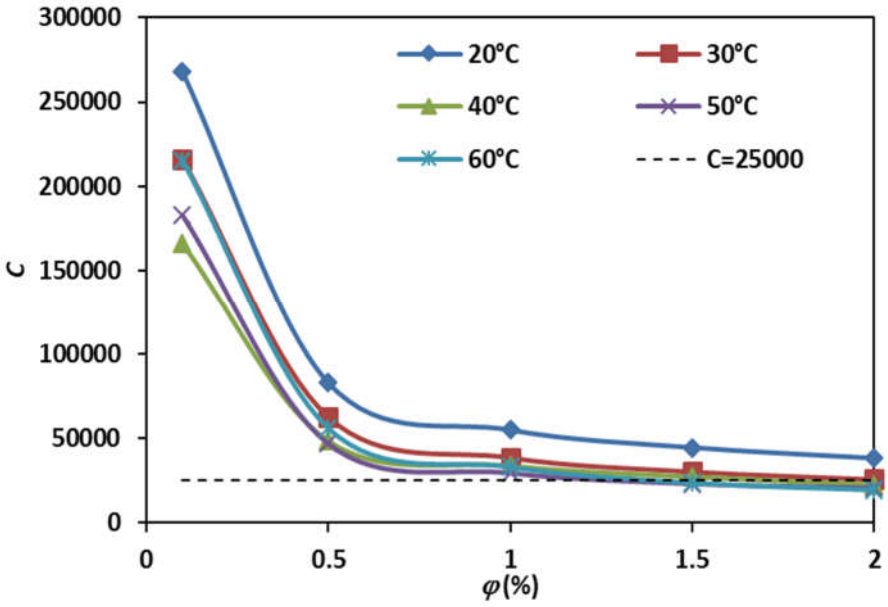

Figure 29 Variation of the empirical parameter C as a function of φ for the best fit of the k_{nf}/k_f ratio data for the non-surfacted Al_2O_3 nanofluid. The $C = 25000$ value assumed in the Patel model matches best at high temperature and φ values.

3.2. Viscosity of nanofluids

3.2.1. TiO_2 nanofluids

Figure 30 (a) and (b) indicates the variation of viscosity of the CTAB-stabilized and AA-stabilized TiO_2-water nanofluids, respectively, as functions of φ and temperature. The results show that the viscosity of nanofluid decreases with increase of temperature and, at the same time, increases with the φ. The nanofluid viscosities at $\varphi = 2.0$ % for CTAB-stabilization and AA-stabilization are found to be 1.65 mPa.S and 1.54 mPa.S, respectively. It may be inferred that this difference is due to the effect of surfactants. Figure 30 (c) compares the viscosity (as function of φ) of the CTAB- and AA-stabilized nanofluids at temperatures of 20, 40 and 50 °C. At 20 °C, CTAB-stabilized nanofluids

exhibit higher viscosity than its AA-stabilized counterpart and their difference increases with φ. However, at higher temperature this difference is not prominent and the choice of surfactant (between CTAB and AA) has negligible reflection in the pumping power requirement in a practical application. It is important to note that this difference in viscosities at various φ decreases with increase in temperature. This suggests that at higher temperature, increasing the particle loading entails less increase in viscosity. Data-point in Figure 30 was obtained from runs that were repeated at least 5 times, when the variance was found to be less than 0.03 %.

3.2.2. Al_2O_3 nanofluids

Figure 31a and Figure 31b shows the variation of viscosity of Al_2O_3-water nanofluid, without and with the SDBS surfactant, respectively, as functions of temperature (20–60 ^oC), for different φ (0.1–1.0 %) at a constant shear rate (122.3 s^{-1}). Data-points in Figure 31a and Figure 31b were obtained from runs that were repeated for at least 10 times, when the standard deviation was found to be less than 0.03 %. Therefore, the error bars in Figure 31 are not discernable. The result shows that the viscosity of nanofluid decreases with increase of temperature while the same increases with the φ. The viscosity of nanofluid at φ = 1.0 %, for Al_2O_3-water and Al_2O_3-SDBS-water nanofluids are found to be 1.5 mPa. S and 3.23 mPa.S, respectively. Comparing Figure 31a and Figure 31b, it emerges that the viscosity of Al_2O_3-SDBS-water nanofluid is greater than the nanofluid without surfactant for all temperature and φ values. Figure 31a shows that for the non-surfacted nanofluid, the increase of viscosity with φ is marginal at 25 °C – the viscosity increases from 1.32 cP to 1.46 cP as φ increases from 0.1–1.0 %. On the contrary, the viscosity of the surfacted nanofluid increases from 1.38 cP to 3.05 cP at the same temperature. The presence of micelles in the surfacted fluid may be implicated to the increased viscosity [278]. Increment of surfactant concentration above the critical micelle concentration (CMC) in nanofluids has been found to form multilayer adsorption of surfactant molecules on the surface of nanoparticles, while the surplus molecules scattered in the water forms surfactant micelles [278]. For long chain surfactants, viscosity increases quickly at low or moderate concentrations. In this situation, the size of micelles grows gradually with the increase of concentration [279]. The CMC of SDBS surfactants is 3 *mM* at room temperature [280]. In the present

experiment, the surfactant is added in proportion with the nanoparticles. The concentration of SDBS surfactant in our nanofluid samples increased from 0.57 *mM* at $\varphi = 0.1$ to 11.62 *mM* for $\varphi = 1.0$. This clearly indicates that at higher φ, the micellar concentration increases. This is why the viscosity of the surfacted nanofluids significantly increases at higher φ.

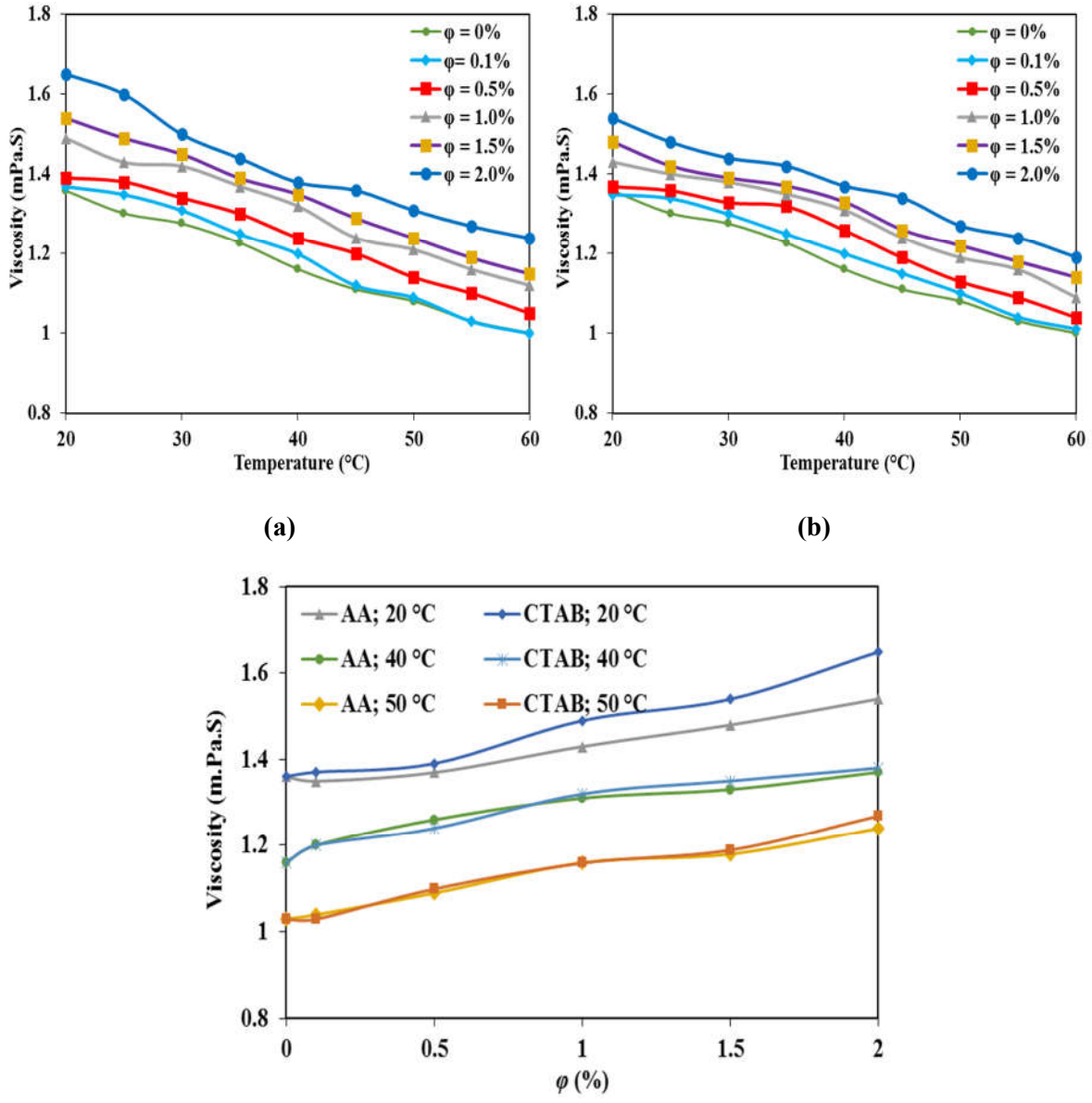

Figure 30 Variation of viscosity with temperature for (a) CTAB- and (b)AA-stabilized nanofluids at different φ for a constant shear rate of 122.3 s^{-1}, (c) Comparative plots of viscosity of CTAB- and AA-stabilized nanofluids as function of φ at temperatures of 20 °C, 40 °C and 50 °C.

Figure 32 shows the variation of viscosity ratio μ_{nf} / μ_f (i.e., the nanofluid viscosity to the viscosity of its corresponding base fluids) as a function of φ, for both Al_2O_3-water and Al_2O_3-SDBS-water nanofluids, at 30 °C. As already mentioned before, that the presence of SDBS-micelles significantly alters the viscosity of the base fluid. Therefore, for the case surfacted nanofluids, viscosity of water-surfactant mixtures (with the same mass ration of SDBS to water as in the original surfacted nanofluid) was treated as the base fluid viscosity μ_f. The experimental values of viscosity ratio are compared with two well-established models proposed by Buongiorno [150], and Maiga [212], which are represented by Eq. (58) and (64), respectively. It is clear from the figure that both the models underpredicts the increase in viscosity with φ. The experimental values differ from the models primarily at very low concentrations. The models have considered the influence of only the solid volume fraction to predict the viscosity. But in practice, the viscosity of nanofluid depends not only on solid volume fraction but also on various other parameters such as temperature, particle size, shape, surfactants etc., which influences the viscosity through the dynamic effect explained before (while explaining the sudden jump in thermal conductivity). Here, the models of Maiga and Buongiorno both applied the Al_2O_3 nanoparticles.

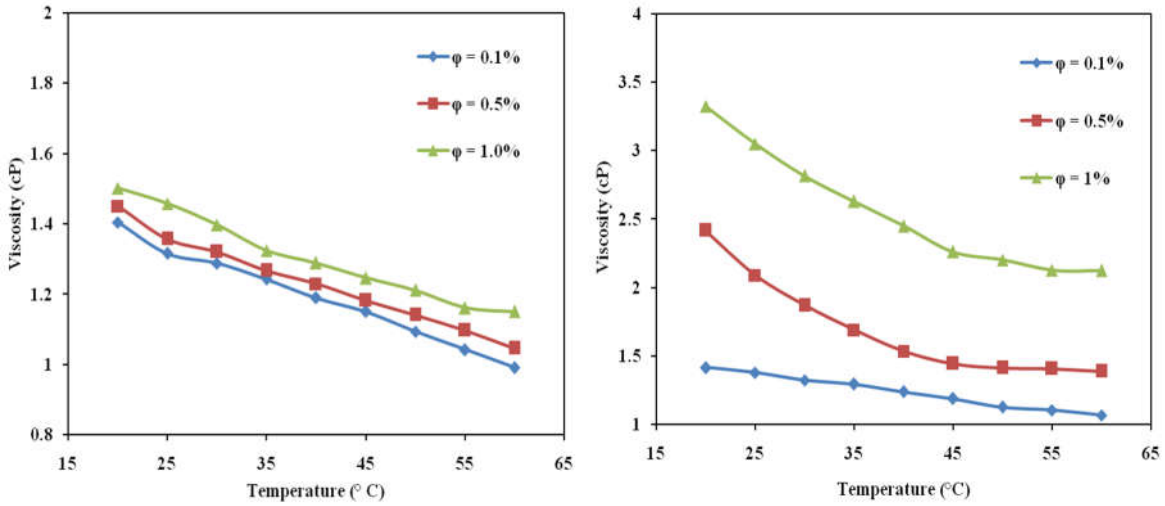

(a) (b)

Figure 31 Variation of viscosity with temperature for at different φ for the nanofluids (a) without surfactant, and (b) with SDBS surfactant.

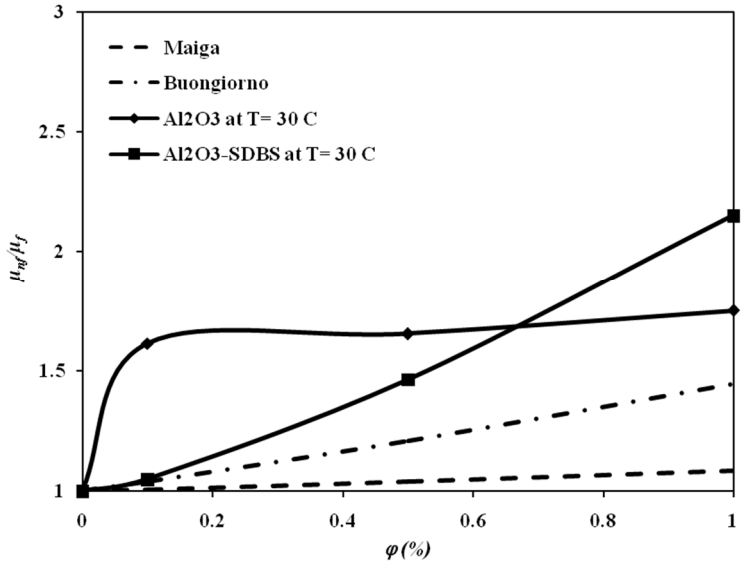

Figure 32 Variation of viscosity ratio of Al_2O_3 nanofluids (with and without SDBS surfactant) with φ at two different temperatures and compared with two models [150, 212].

Figure 33a and Figure 33b shows the variation of Prandtl number of the Al_2O_3-water nanofluids, both without and with SDBS surfactant, respectively, with temperature for different φ. The Prandtl numbers of both types of nanofluids are found to increase with φ and decrease with temperature. Prandtl number is defined as:

$$Pr = \frac{\mu_{nf} C_{pnf}}{K_{nf}} \tag{99}$$

where μ_{nf}, and C_{pnf} denote the viscosity and specific heat of the nanofluid, respectively. The viscosity value is obtained directly from Figure 31, while the specific heat and density (ρ_{nf}) are evaluated using the mixing rule, i.e.,

$$C_{p_{nf}} = \frac{\left[\varphi(\rho C_p)_p + (1-\varphi)(\rho C_p)_f\right]}{\rho_{nf}}, \text{ and} \tag{100}$$

$$\rho_{nf} = \varphi\rho_p + (1-\varphi)\rho_f. \tag{101}$$

As apparent from Figure 33, *Pr* decreases with increase in temperature since the thermal conductivity increases and viscosity goes down with increase in nanofluid temperature. For the non-surfacted nanofluids, particle loading is found to have little effect on the Prandtl number (Figure 33a); for all values of φ, the *Pr* decreases nearly to the same extent from ~9.5 at 20 ^oC to ~ 6.4 at 60 ^oC. On

the contrary, *Pr* values of the surfacted nanofluid strongly depend on the particle loading (and hence the surfactant concentration). At large surfactant loading (large φ), the high value of viscosity (see Figure 31b), results in the high *Pr*. For lower surfactant loading ($\varphi = 0.1$), the *Pr* versus temperature curve resembles that of the non-surfacted nanofluid. Figure 30b provides important information regarding selection of the appropriate φ of the nanofluid for a particular heat transfer application. It is imperative that for applications warranting high *Pr* fluids, SDBS-surfacted Al_2O_3-water nanofluids may be used, although it might call for higher pressure drop to induce forced convection. For applications involving quick circulation cycles, and where intermittent sonication or stirring of nanofluid may be provided (to facilitate particle suspension), non-surfacted nanofluid may be preferred because of their low viscosity.

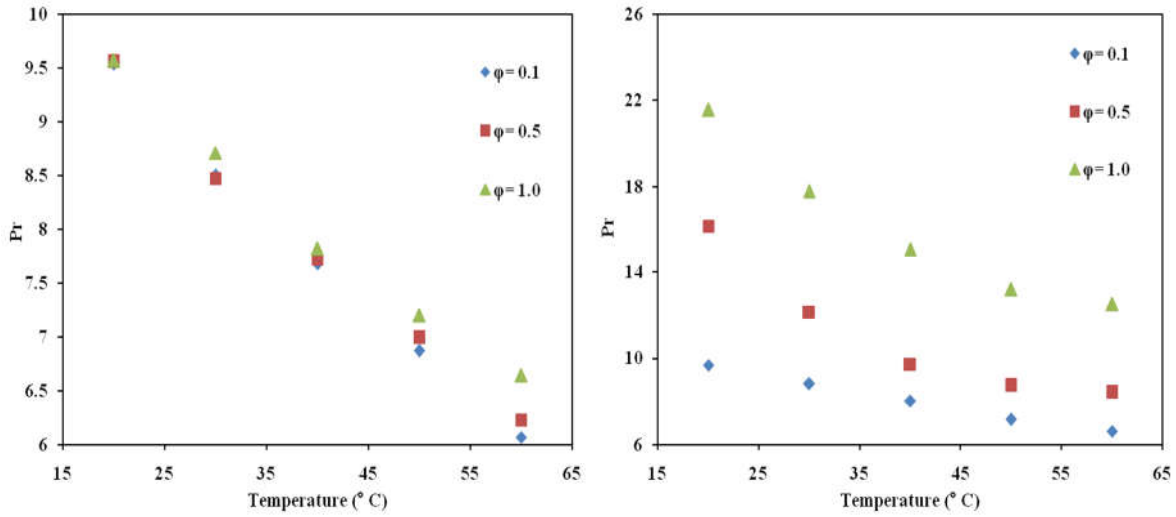

Figure 33 Variation of Prandtl number with temperature at different φ for Al_2O_3-water nanofluids (a) without surfactant, and (b) with SDBS surfactant.

3.2.3. TiO_2 anatase nanofluids

It is already identified that viscosity is one of the most important properties of nanofluids, which indicates the resistance of fluid. Literature study reveals that the viscosity of nanofluid depends on φ, particle size, and shear rate. In this study the viscosity of TiO_2-anatase water (SDS and CTAB) based nanofluids were measured at different temperatures and φ. Figure 34a and Figure 34b shows the

variation of viscosity with temperature (20–60 °C) for SDS and CTAB surfacted water and the corresponding nanofluids (at 0.1 % < φ < 1.0 %), respectively, at a constant shear rate of 122.3 s^{-1}. It can be observed from Figure 34 that the viscosity of nanofluids are slightly higher than their respective surfacted water solutions and it increases with φ. The viscosity also decreases with increase of temperature. Comparing Figure 34a and Figure 34b it is observed that the viscosity values are almost independent of the type of surfacted used in the study. Data-points for Figure 34a and Figure 34b were obtained from several runs (at least 10 times for each condition), where the standard deviation was found to be less than 0.03 %; the error bars in Figure 34 are therefore hardly visible.

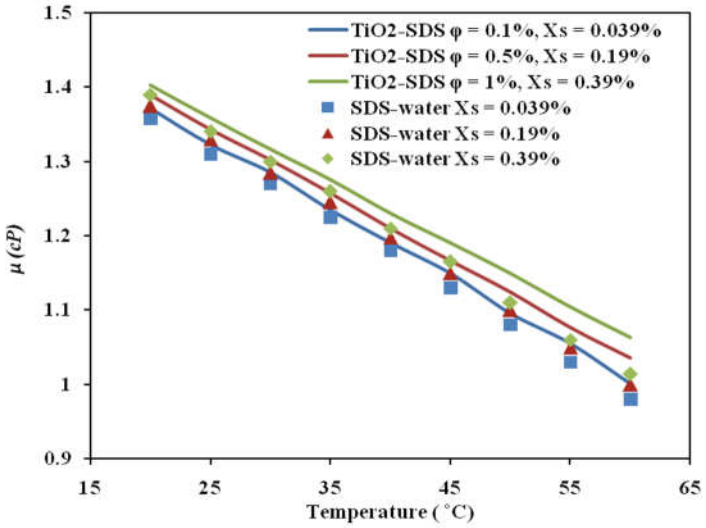

(a)

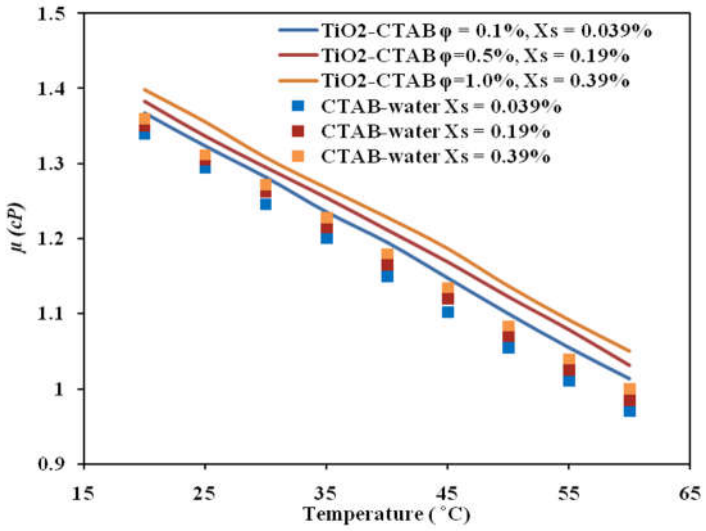

(b)

Figure 34 Variation of viscosity with temperature for with and without nanoparticle at different φ, with (a) SDS and (b) CTAB used as surfactant.

Various theoretical correlations have been developed to predict the viscosity of nanofluids. In 1926, Einstein [183] first developed a correlation based on the liquid-particle interaction, which calculate the effective viscosity of liquids in low φ having spherical suspended particles (see Eq. 33).

$$\frac{\mu_{nf}}{\mu_{bf}} = [1 + 2.5\varphi], \quad (102)$$

Subsequently, advanced correlations were developed by Roscoe [204] (Eq. 54), Batchelor [197] (Eq. 47) to better predict nanofluid viscosity at high φ. More recently, some correlations have been proposed specifically for TiO_2 nanofluids, such as Buongiorno [150] (Eq. 58), and Bobbo et al. [158] (Eq. 103).

$$\mu_{nf} = \mu_o(1 + A\varphi + B\varphi^2), \quad (A \text{ and } B \text{ are empirical values}) \quad (103)$$

The measured property values from the present experimental study have been compared with these correlations to validate the study. Figure 35 shows the variation of viscosity ratio (i.e., the nanofluid viscosity to the viscosity of its corresponding base fluids) as a function of φ for TiO_2-SDS and TiO_2-CTAB based nanofluids, at 25 °C. The experimental values of viscosity ratio are compared with the above established models. It can be seen from the Figure 35 that beyond φ=0.4%, the models presented by Buongiorno [150] overpredict the viscosity ratio of nanofluid while that of Bobbo et al. [158] underpredicts the value. However, at lower φ, all the models underpredict the viscosity ratio.

3.3. Effect of shear-rate on viscosity of nanofluids

Figure 36a and Figure 36b shows the variation of viscosity of CTAB and AA-stabilized nanofluids respectively, as functions of shear rate (ranging from 76–760 s^{-1}) at a given temperature (24 °C) for different φ. It is found that below a shear rate 400 s^{-1} the value of viscosity shows shear thinning in nature. But beyond this, the viscosity gradually increases with the φ and shear rate of the nanofluids, thus exhibiting a shear thickening behavior. This may be attributed a Taylor-Couette regime of flow transition [124]. It is also observed that the value of viscosity with CTAB-stabilizer is slightly greater than that with AA-stabilizer for high value of φ and shear rate.

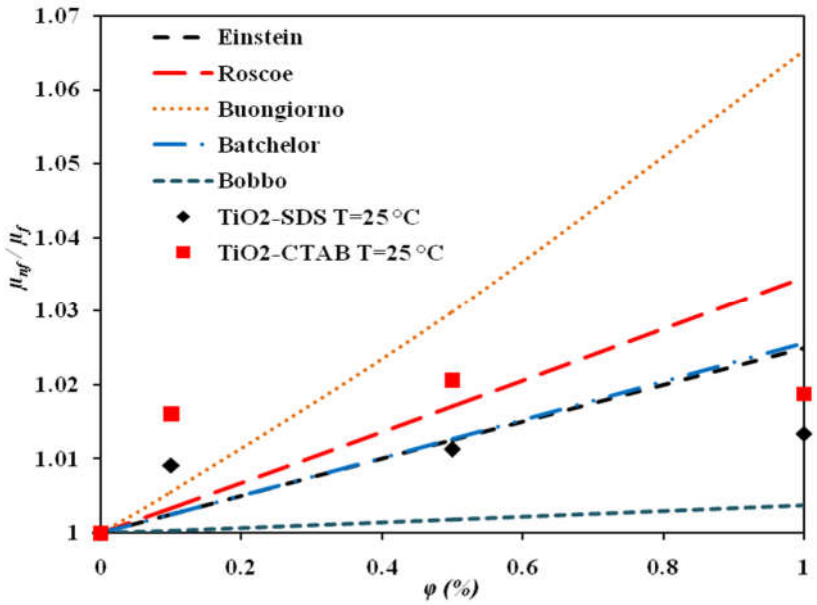

Figure 35 Variation of viscosity ratio with φ for two different surfactant-stabilized nanofluids at a shear rate of 122.3 s^{-1}; observed data are compared with established models.

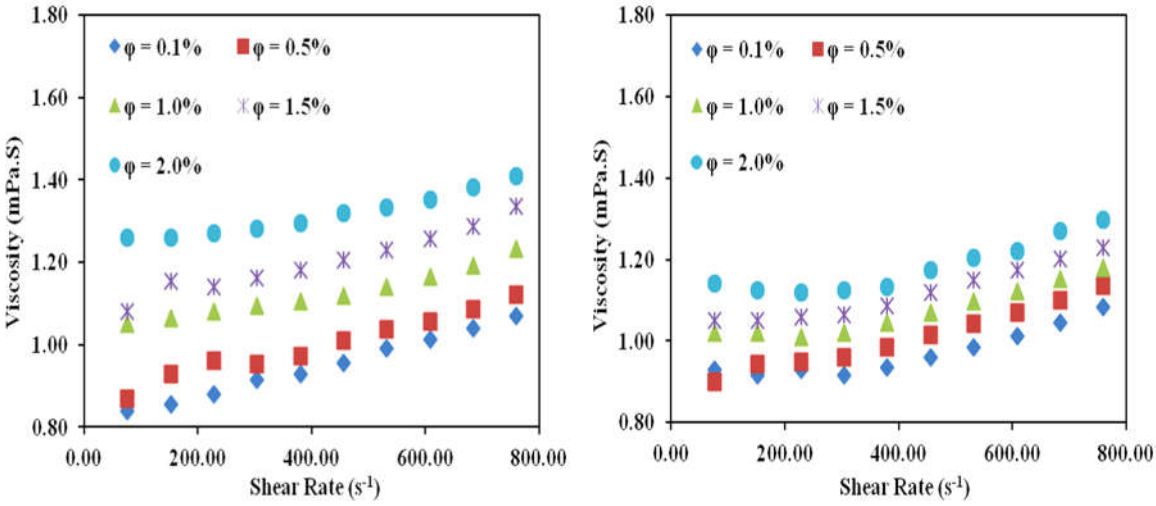

(a) **(b)**

Figure 36 Viscosity plots as a function of shear rate for TiO_2; (a) CTAB- and (b) AA-stabilized nanofluid for a constant temperature (24 °C) at different φ.

Apart from the above study, the effects of nanoparticle φ and temperature on rheological behavior of water-based nanofluids of Al_2O_3, TiO_2-AA, TiO_2-CTAB were investigated. Viscosity of a particular nanofluid at a given temperature was measured at different shear rates. Figure 37 (a-e) shows the variation of viscosity of Al_2O_3-water nanofluids with different shear rates in the

temperature range (2060 °C) for φ = 0.12.0 %. It has been observed, for each case, that upto a certain shear-rate the nanofluid shows Newtonian behaviour above which it shows non-Newtonian shear thickening behaviour. So, a critical shear rate exists above which the fluid become non-Newtonian. The value of the critical shear rate depends on the particle loading (φ) and nanofluid temperature. It is also observed that for a particular φ the critical shear rate decreases with increase in temperature. For φ = 0.1 %, it is 110 s^{-1} at 20 °C, while it is 12 s^{-1} for 60° C (Figure 37a). The same value is 110 s^{-1} and 36 s^{-1} respectively for φ = 0.5 % (Figure 37b). For φ = 1.0 %, 1.5 % and 2.0 % the value of critical shear rate at 20 °C are 134 s^{-1}, 183 s^{-1} and 183 s^{-1} respectively, while at 60 °C it is 61 s^{-1}, 61 s^{-1} and 85 s^{-1} respectively (Figure 37c, Figure 37d, Figure 37e).

Similar trend was also observed for different φ and temperatures. Viscosity of TiO_2-CTAB and TiO_2-AA-water based nanofluids at different shear rates and temperatures, which are shown in Figure 38 and Figure 39, respectively. Dilatancy is strongly related to the size, shape, and surface of the particles used in dilatant system. It was observed that due to the hydrocluster mechanism, shear thickening occurs [281, 282] for colloidal suspensions. The attractive and repulsive forces act between the particles in the colloidal suspension, thereby forming cluster. The distance between the colloidal particles reduces due to the external shear forces at high shear rates. As particles get in closer, they stick together and form large clusters, so-called hydroclusters. These hydroclusters prevents the flow and causes the shear thickening behavior of the suspensions. Shear thickening can be stamped out by reducing the interactions between particles [283]. Structure and rheological behavior of the suspension changes according to the shear flows. The experimental result of this study did not match the mechanism which was found from the literature, for shear thickening behavior. Figure 37, Figure 38 and Figure 39, also demonstrated that viscosity decreased with increase in temperature and decreased with φ for Al_2O_3-water, TiO_2-CTAB and TiO_2-AA nanofluids. High temperature increases the Brownian motion of nanofluid and weaker the interparticle adhesion forces [107]. The interaction time between neighboring molecules of a fluid decreases due to increased velocities of individual molecules. With the increase of temperature, heat provides extra energy that separates the molecules, resulting in the decrease of attractive forces between particles. Similar types of result for Al_2O_3-water

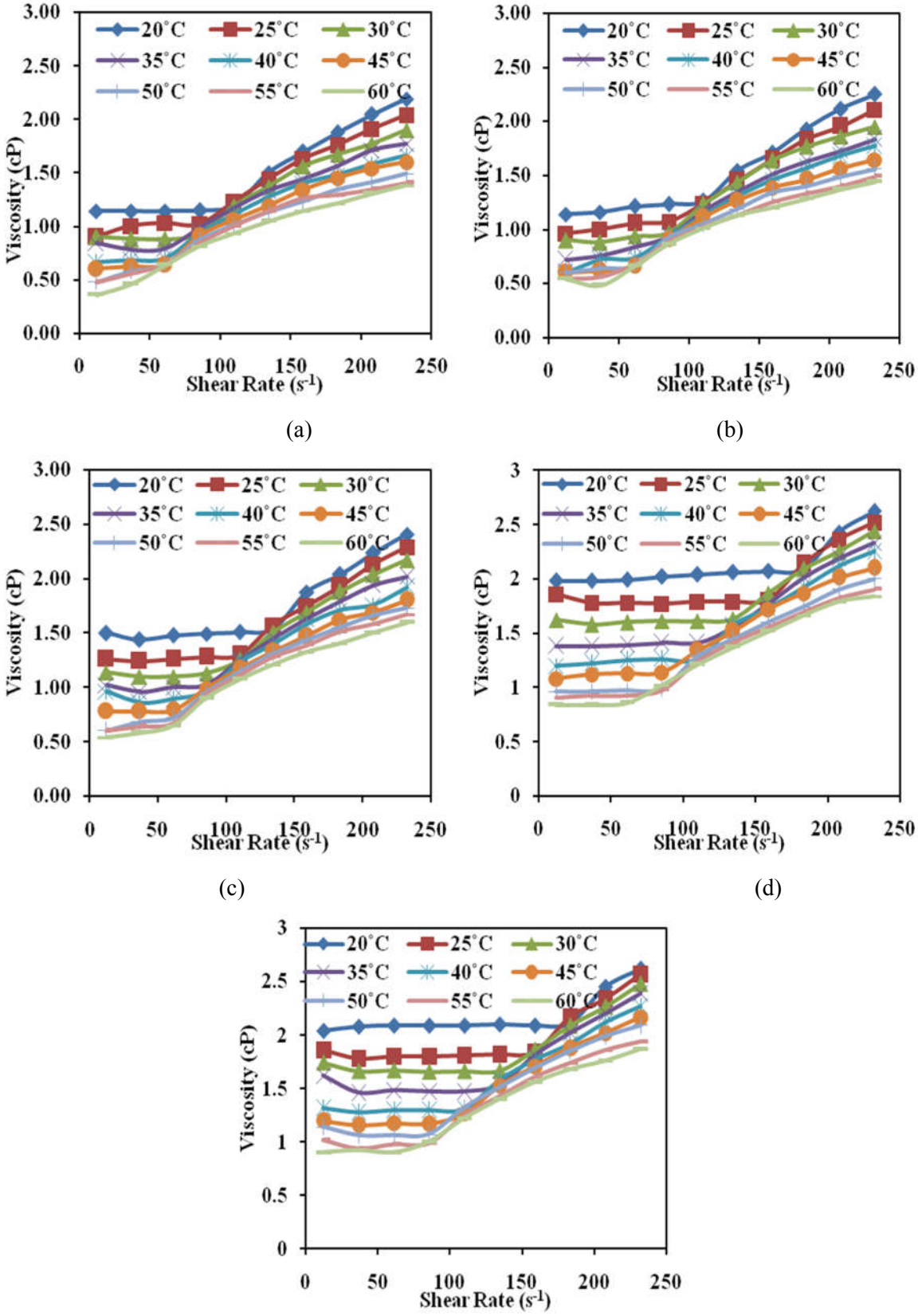

Figure 37 Viscosity at different shear rate for the Al_2O_3–water nanofluid at (a) $\varphi = 0.1$ % (b) $\varphi = 0.5$ % (c) $\varphi = 1.0$ % (d) $\varphi = 1.5$ % (e) $\varphi = 2.0$ %.

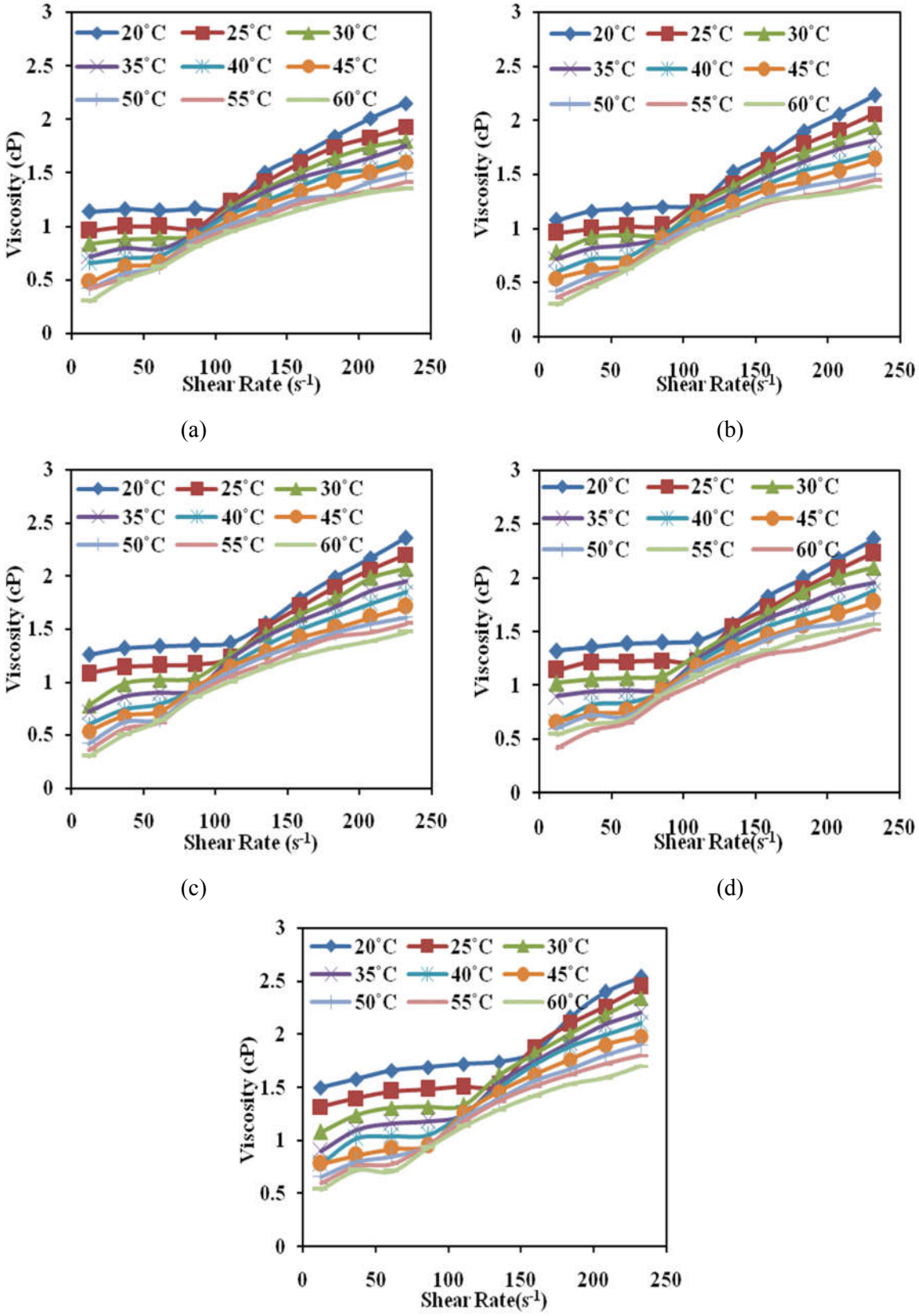

Figure 38 Viscosity at different shear rate for the TiO_2-CTAB stabilized water nanofluid at (a) φ = 0.1 % (b) φ = 0.5 % (c) φ = 1.0 % (d) φ = 1.5% (e) φ = 2.0 %.

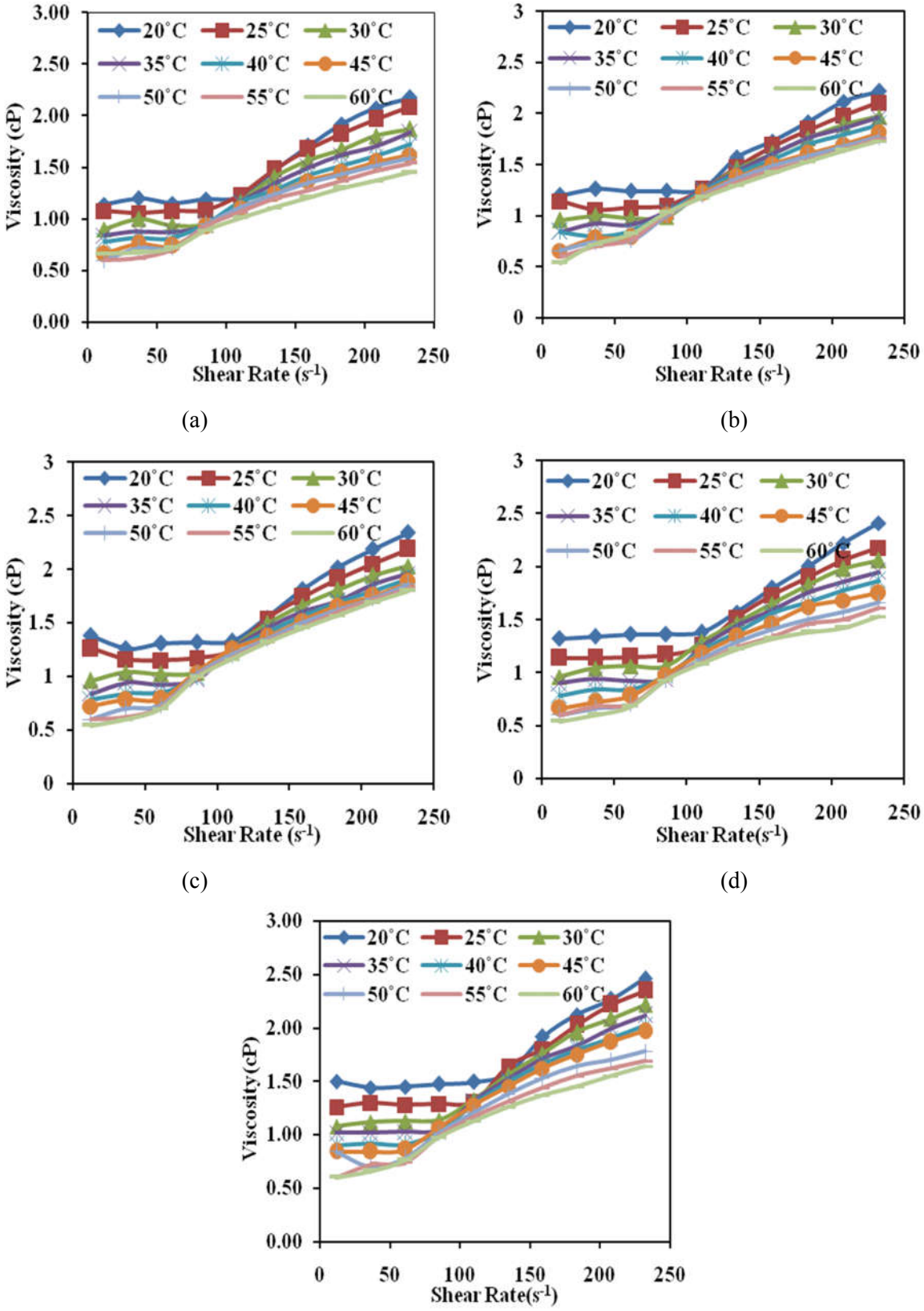

Figure 39 Viscosity at different shear rate for the TiO_2-AA stabilized water nanofluid at (a) $\varphi = 0.1$ % (b) $\varphi = 0.5$ % (c) $\varphi = 1.0$ % (d) $\varphi = 1.5$ % (e) $\varphi = 2.0$ %.

based nanofluid have been presented by Mahbubul et. al. [284] at a constant φ (= 0.5 %), for different temperature from 10–50 °C and different sonication times. They found that viscosity of nanofluid decreased with the increase in temperature. At lower temperature and lower shear rates, nanofluid showed Newtonian behavior, while at higher temperature and higher shear rate, nanofluid showed non-Newtonian behavior.

3.4. Surface tension and contact angle of nanofluids

The interfacial tension of nanofluids have measured to characterize the surface properties of the nanofluids. Surface tension is the elastic tendency of a fluid surface which makes it acquire the least surface area possible. Figure 40a and Figure 40b shows the variation of surface tension as function of φ, at different nanofluid temperatures (viz., 30, 40, 50 and 60 ^{o}C) with CTAB and AA-stabilizers, respectively, for TiO_2 nanofluids. It is important to note that the presence of surfactants plays a major role in altering the surface tension of the nanofluid from that of water. For example, at 30 ^{o}C, 0.1 % (w/w) CTAB in water decreases the surface tension from 71 mN/m to 40.5 mN/m. The same percentage of AA in water at 30 ^{o}C yields a surface tension of 69.8 mN/m. It is evident from both the figures that the presence of nanoparticles further lowers the surface tension. For example, in CTAB-stabilized host fluid at 30 ^{o}C, presence of nanoparticles at a meager φ = 0.1 % lowers the surface tension from 40.8 to 40.5 mN/m. A similar dip (of surface tension due to addition of nanoparticles) is also observed in AA-surfacted water (see Figure 40b), where the surface tension at 30 ^{o}C drops from 70.2 to 69.8 mN/m at φ = 1 % of nanoparticles).

The presence of particles at the air-water interface has been found to alter the cohesive force between the host liquid molecules and the adhesive force between the host liquid molecule and nanoparticles at the liquid-air interface, causing a reduction in the surface tension of nanofluid [285]. On the other hand, the adsorption of surfactant on the nanoparticles, ensuing from migration of the particles to the nanofluid interface may lead to a reduction of surfactant concentration at the interface and cause an effective increase in surface tension. The decreasing trends of surface tension in Figure 40a and Figure 40b implies that the second effect is negligible as compared to the former [244]. It is apparent from Figure 40a and Figure 40b that TiO_2-nanofluid shows lyophilic nature in presence of

both the surfactants. For both types of nanofluids, the surface tension is found to decrease with increase of temperature. This is intuitive, since an increase in temperature not only decreases the surface tension of the host fluid, but also increases Brownian transport of particles to the surface.

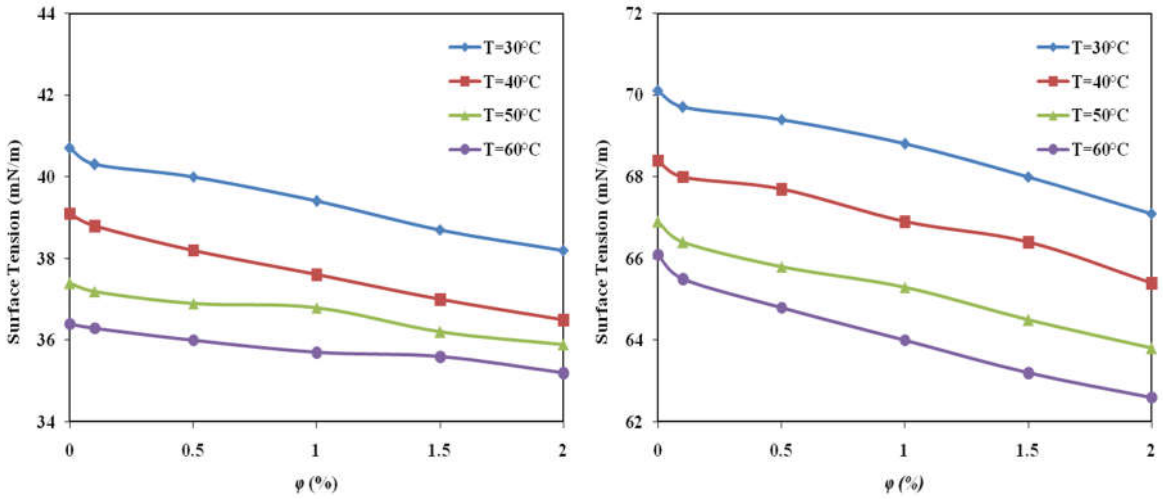

Figure 40 Variation of surface tension with φ at different temperatures for (a) CTAB- and (b) AA-stabilized nanofluids. Variation of pH with temperature for (c) CTAB- and (d) AA-stabilized nanofluids at different φ.

Figure 41a and Figure 41b shows the variation of surface tension as a function of φ, at different temperatures (viz., 30, 40, 50 and 60 ^{o}C) for Al_2O_3 water and Al_2O_3-SDBS water-based nanofluids respectively. Figure 41a represents that at T = 30 ^{o}C and φ = 0.1 %, the value of surface tension is 71.1 mN/m, while at the same temperature as the φ increases from 0.1–2.0 %, the value of surface tension decreases from 71.1 mN/m to 63 mN/m. At temperature, T = 60 ^{o}C, the value of surface tension decreases from 65.3 to 55.4 mN/m as the φ increases from 0.1–2.0 %. Also, the surface tension of the Al_2O_3-water nanofluid decreases as the temperature and φ of the nanofluids increases. Figure 41b shows that the value of surface tension at T = 30 ^{o}C is 35.2 mN/m at φ = 0.1 %, reduced to 31.8 mN/m at φ = 2.0 %. At T = 60 ^{o}C, the value of surface tension decreases from 32.7 to 30.2 mN/m as the φ increases from 0.1–2.0 %. Here also the same trend was found, as the temperature and φ of the nanofluid increases the value of surface tension decreases. Comparing these two; Figure

41a and Figure 41b, it can be noticed that the value of surface tension decreased from 71.1 mN/m to 35.2 mN/m for a constant T = 30 ^{o}C, and φ = 0.1 %, and it happens due to the effect of surfactants. It can be noted that the presence of surfactants plays a major role in altering the surface tension of the nanofluid from that of water.

Figure 42a shows the variation of surface tension as function of temperature at different φ (viz., 0.1 %, 0.5 % and 1.0 %) for SDS-water and anatase-SDS water based nanofluids. It can be seen from Figure 42a that an increase in temperature and φ of nanoparticles reduces the surface tension of nanofluids. Figure 42b shows the variation of surface tension with temperature for anatase-CTAB water-based nanofluids (at different φ) and CTAB-water solutions (at the same x_s value corresponding to the nanofluid samples). It is important to note that the presence of surfactant plays a major role in altering the surface tension of the nanofluid from that of water. It can be seen from Figure 42a and Figure 42b that the surface tension value of surfacted fluid is greater than the surfacted nanofluids (despite bearing the same concentration of surfactant). Therefore, it is evident from both the figures that the presence of nanoparticles further lowers the surface tension. The nanoparticle concentration on the liquid-air interface depends on the equilibrium between repulsive and attractive forces among nanoparticles, as well as forces driving the diffusion of nanoparticles near the interface. The electrostatic force serves as repulsive force, while the van der Waals force is attractive in nature. Nanoparticle agglomeration and assembly near the liquid-air interfaces has been attributed to this change in the effective liquid–air surface tension of nanofluids [241]. The presence of nanoparticles at the air-water interface alters the cohesive force between the host liquid molecules. The adhesive force between the host liquid molecules and nanoparticles at the liquid-air interface causes a reduction in the surface tension of nanofluid [285]. For both types of nanofluids, surface tension is found to decrease with increase of temperature. An increase in temperature lowers the surface tension of the host fluid and also increases Brownian transport of particles to the surface; both these factors lead to reduction in the effective surface tension.

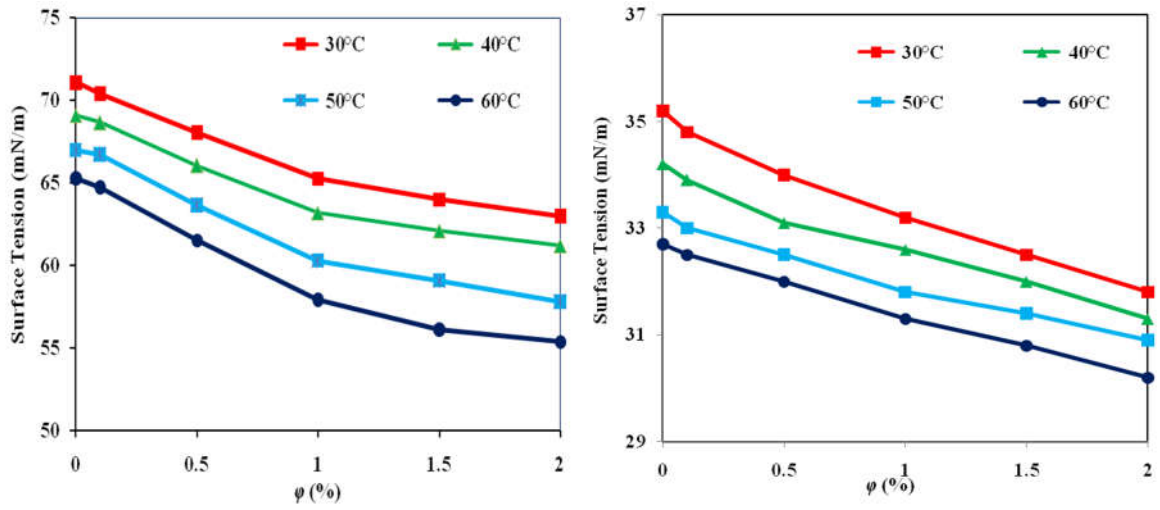

(a) (b)

Figure 41 Variation of surface tension with φ for (a) Al_2O_3-water and (b) Al_2O_3-SDBS water-based nanofluids for different temperature.

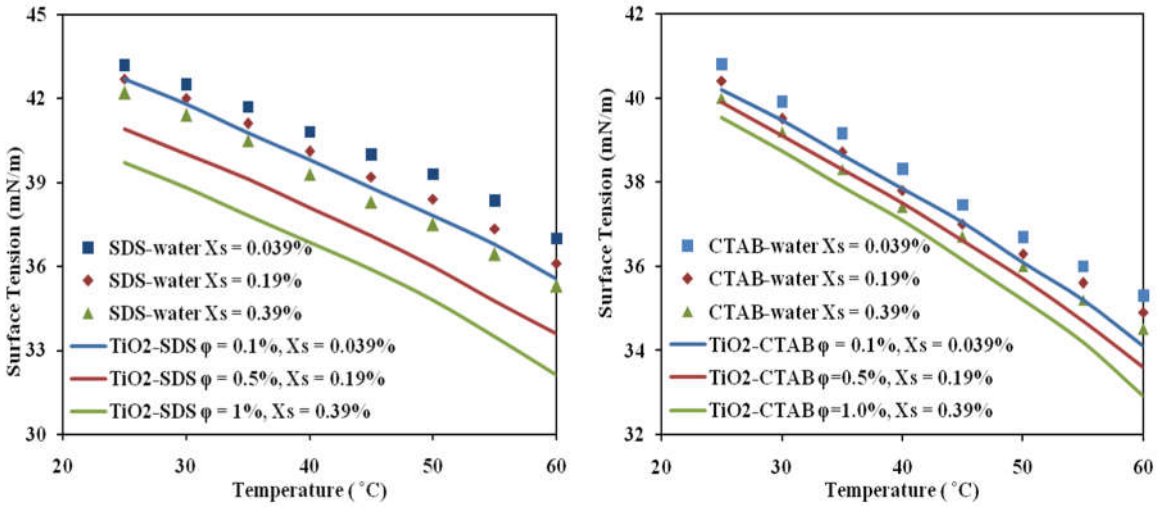

(a) (b)

Figure 42 Variation of surface tension with temperature for with and without nanoparticle (anatase) at different φ, where (a) SDS used as surfactant, (b) CTAB used as surfactant at different φ.

Besides measurement of the nanofluid surface tension, a detailed study of the interaction of the nanofluids with standard solid substrates have also been carried out. This is important to identify the nanofluid behaviour on open surfaces, or for phase change heat transfer problems associated with

the nanofluids [286]. We investigated the shape of sessile droplets of nanofluids on a smooth glass surface that was cleaned with DI water and then by acetone.

Spreading of liquid droplets on a solid surface is attributed to adhesion, and the adhesion is related to the surface energy. When a liquid droplet is deposited on a solid surface exposed to air, the liquid may spread indefinitely (complete wetting), spread to an extent (partial wetting) or may not spread at all (de-wetting). The behavior is strongly linked to the relative magnitudes of the interfacial energies σ_{SV}, σ_{SL} and σ_{LV} (denoting vapor, liquid and solid by *V*, *L* and *S*, respectively) that exist at the interfaces of the solid-vapor, solid-liquid and liquid- vapor, respectively. For the case of partial wetting, the liquid droplet dispensed on the solid surface will spread to some extent until it acquires an equilibrium shape specified by the contact angle, θ. The equilibrium contact angle may be obtained by striking a balance of the interfacial tension forces at the triple line (the intersection of the liquid droplet, solid surface and gaseous medium) along the horizontal direction and is given by Young's formula (See Figure 43 (a)) [287].

$$\sigma_{SV} = \sigma_{SL} + \sigma_{LV} cos\theta \quad (104)$$

This is combined with Dupre's equation [287] expressing the solid-liquid work of adhesion W_{SL} to obtain:

$$W_{SL} = \sigma_{SV} + \sigma_{LV} - \sigma_{SL} = \sigma_{SL}(1 + cos\,\theta) \quad (105)$$

This indicates that the contact angle is directly related to the strength of adhesion between liquid and solid and suggests that contact angle measurements can be used to estimate adhesion energies. Intuitively, the contact angle of a sessile nanofluid droplet will depend on the type of solid substrate used, the nanoparticle-dispersant-host fluid combination, particle size and the particle and surfactant loadings [288]. Figure 43 shows the contact angle images (on clean, smooth glass surface) of Al_2O_3-nanofluids, TiO_2-CTAB nanofluids, and TiO_2-AA nanofluids at φ = 0.1 % and 2.0 %. It can be confirmed from the table that the contact angle image of the nanofluids for φ = 2.0 % is smaller than φ = 0.1 %. Figure 44 shows that variation of contact angle with solid volume fraction for TiO_2-AA, TiO_2-CTAB, Al_2O_3-water, AA-water, and CTAB-water, solutions. Nanofluids have shown great difference in surface wettability on a solid surface from that of the base fluid [289, 290]. It can be

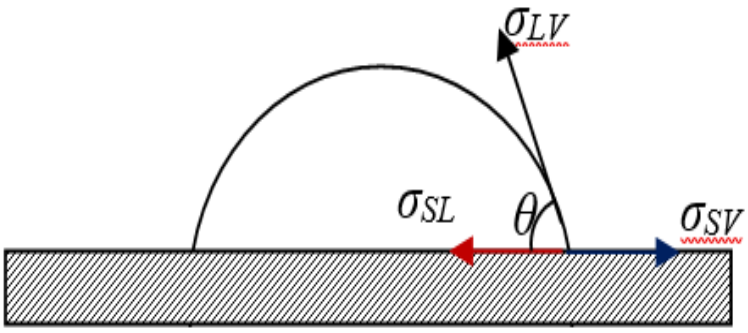

(a)

Contact angle (θ)	at φ = 0.1%	at φ = 0.1%
Al_2O_3-nanofluids	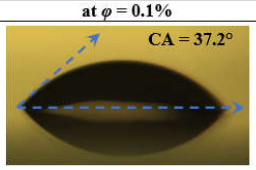	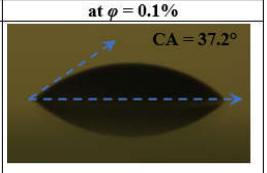
TiO_2-CTAB nanofluids	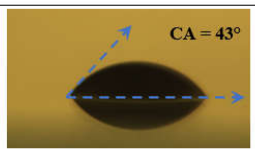	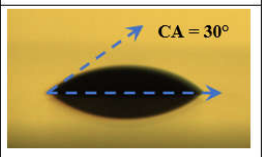
TiO_2-AA nanofluids	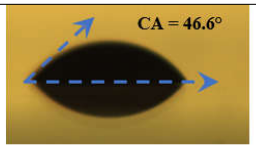	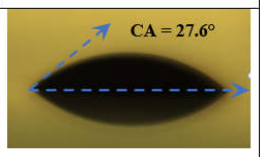

(b)

Figure 43 (a) Force balance on the triple line of a sessile droplet, (b) Contact angles of sessile nanofluid droplets on cleaned glass surfaces.

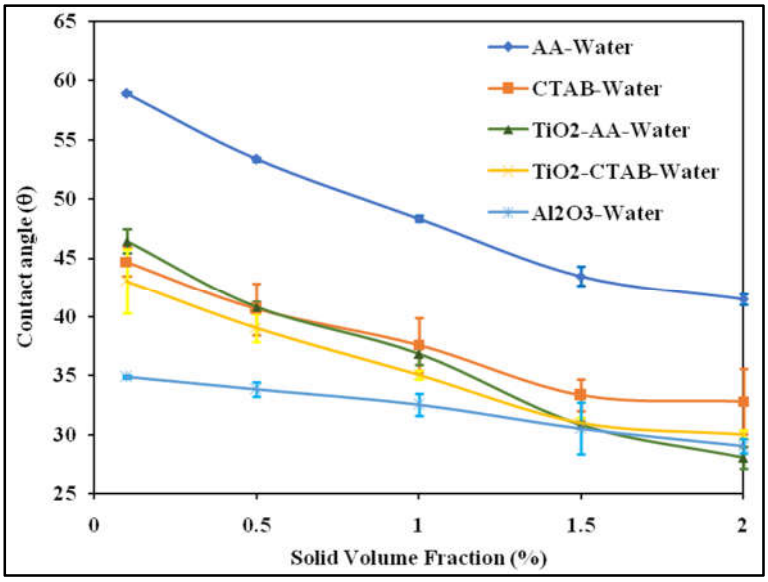

Figure 44 Variation of sessile droplet contact angle (on cleaned glass surface) with φ for different nanofluid and surfactant-water solutions.

seen from Figure 44 that the contact angle of nanofluids decreases with increase in φ. This may be attributed to the change in surface tension with the particle loading. The contact angle trend in Figure 44 matches with the plots showing the variation of surface tension with φ (see Figure 40, Figure 41, Figure 42). Contact angles of the AA-water and CTAB-water solutions are also found to decrease with increasing surfactant loading, since the observed concentrations were below their respective.

3.5. pH of nanofluids

Figure 45a and Figure 45b shows the pH values of TiO_2-water nanofluid with AA and CTAB surfactants. The pH values are found to fall within range of 2.8–3.7 and 3.9–4.9, respectively, for AA & CTAB-stabilized nanofluids, for the φ range of 0.1–2.0 %. This shows that the nanofluid pH is relatively insensitive to temperature; the pH decreases with increase φ and temperature. Besides, the pH value remains nearly unaffected at different temperatures.

Figure 45c and Figure 45d shows the variation of pH with φ at different temperature for Al_2O_3-water and Al_2O_3-water-SDBS nanofluids respectively. While the pH value of both non-surfacted and surfacted nanofluids remains nearly insensitive to particle loading (pH decreases marginally with increased φ due to selective adsorption of the OH^- ions at the Stern layer on the Al_2O_3-nanoparticles [291]), it has a more pronounced effect of temperature for the non-surfacted nanofluid. The ionic dissociation of water increases with temperature, resulting in higher H^+ loading (leading to lowering of pH) [292]. On the other hand, being an anionic surfactant, aqueous SDBS solution exhibits a strong basic nature, which is observed from the high value of pH (>10) for the surfacted nanofluid (see Figure 45d). Since the particle to SDBS mass ratio was held constant (2:1), the amount of surfactant was increased with particle loading, leading to an increase in the pH with φ. The pervasive presence of SDBS also masks out the effect of temperature on the pH, and hence the isothermal pH curves in Figure 45d runs close to each other.

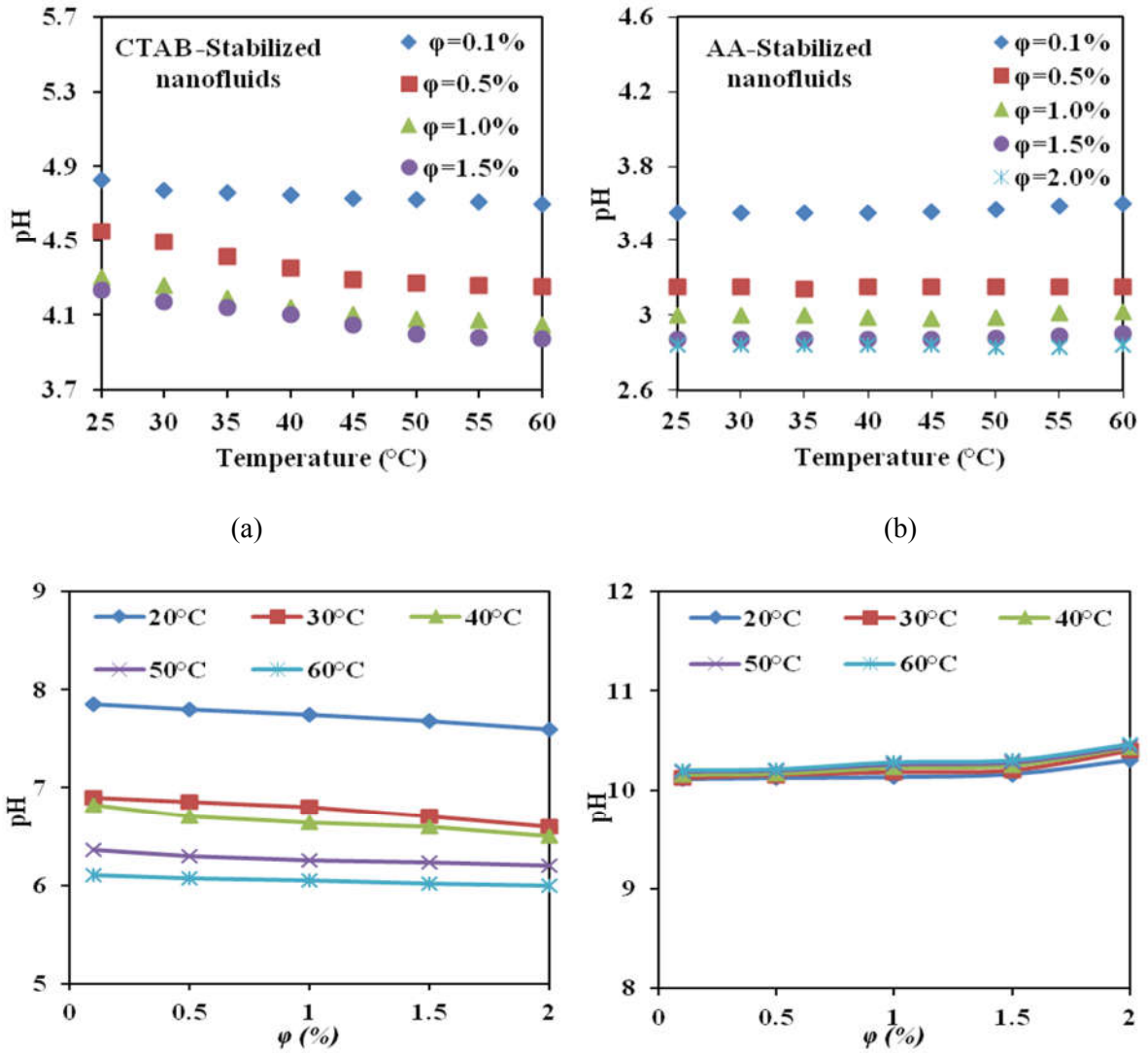

Figure 45 Variation of pH with temperature for TiO_2 (a) CTAB- and (b) AA-stabilized nanofluids at different φ. Variation of pH with φ for (c) Al_2O_3-water nanofluid (without surfactant) and (d) Al_2O_3-SDBS stabilized nanofluid at different temperature.

CHAPTER 4

4. Numerical modelling of direct absorption solar collector

4.1. Background

This chapter aims at developing a framework of numerical simulation for analysing thermal transport using the nanofluids whose thermophysical properties have been characterised in the foregoing chapter. Design of a DASC would warrant comprehensive numerical analysis in representative realistic configurtions employing the thermophysical property correlations from the literature as well as those developed from the current study.

4.2. Introduction

Several researchers have investigated the heat transfer behavior of flow of nanofluids through different geometrical configurations. Numerical studies have been conducted for investigation of heat transfer coefficient (HTC) of nanofluids with different nanoparticles. Numerical methods are also extensively used to predict the performance of various heat transfer devices using nanofluids. The device includes microchannel heat sink, direct absorption solar collector (DASC) etc.

Zhao et al. [293] presented a three-dimensional numerical analysis to study the laminar heat transfer and flow characteristics of Al_2O_3-water nanofluids through a flat tube at constant heat flux boundary condition. The single-phase based numerical results showed higher HTC and pressure drop of Al_2O_3-water nanofluids than the base fluid. Both the convective HTC and pressure drop enhanced with increase in nanoparticle concentration (φ) and decrease in nanoparticle size. The heat transfer and pressure drop enhancements of nanofluids were more obvious at smaller Reynolds number (*Re*) and higher temperature. Ghale et al. [294] investigated laminar forced convective heat transfer of Al_2O_3-water nanofluids in a straight microchannel was studied numerically using CFD modeling. Single-phase and two-phase models were used for prediction of temperature profile and fluid flow distribution and calculation of friction factor and Nusselt number. The HTC of nanofluids increased with increase in the φ and *Re*. Increase in the φ from 1 % to 2 %, resulted in 16.1 % increase in the Nusselt number. Manay et al. [295] numerically studied the heat transfer and hydraulic characteristics of CuO-water and Al_2O_3-water nanofluids inside a microchannel with square duct using the mixture model. The result showed that the heat transfer rate enhanced with the increase of φ and *Re*. Kalteh et

al. [296] numerically studied the laminar forced convective heat transfer of Cu-water nanofluid inside an isothermally heated microchannel. Heat transfer increased with increase in *Re* and φ, while the pressure drop increased slightly for all the cases. Moraveji and Esmaeili [297] numerically investigated the forced convection heat transfer with laminar flow condition for Al_2O_3-water nanofluids flow inside a circular tube, under constant heat flux from the wall for 100 nm nanoparticles concentration φ = 1 % and 4 %. They found that the rate of heat transfer increased with increase in φ and *Re*. Similar result was obtained by Bajestan et al. [298], Tahir et al. [299], Davarnejad et al. [300], Heris et al. [301]. Tahir and Mital [299], also showed similar result but they observed non-linear parabolic decrease in heat transfer with increase in particle size. Bianco et al. [302] numerically investigated the laminar forced convection flow of Al_2O_3-water nanofluid in a circular tube, at a constant and uniform heat flux at the wall. Both single-phase and two-phase methods have used for this simulation. Result showed that, at φ = 4.0 % two-phase model has about 11 % of enhancement in average HTC compared to pure water. Similar kind of study has numerically analyzed the heat transfer behavior of water based Al_2O_3 and TiO_2 nanofluids in a pipe for Eulerian-Eulerian mixture-phase model. Higher heat transfer rate was found while using the multi-phase model than the single-phase model. They also found that TiO_2-water nanofluid was the most energy efficient coolant than Al_2O_3-water nanofluid [303]. Moraveji and Ardehali [304] numerically investigated the laminar forced convection of Al_2O_3-nanofluid, with particle size equal to 33 nm and φ = 0.5, 1 and 6 %, through mini-channel heat sink considering both single phase and two-phase model. The two-phase model represented a better approximation of the experimental data comparing to the single-phase model and they observed that, increased in *Re* and φ led to enhanced heat transfer. Akbarinia and Behzadmehr [305] numerically studied the fully developed laminar mixed convection of Al_2O_3-water nanofluid in a horizontal curved tube. They found that increased in nanoparticle φ have a positive effect on the HTC at different *Re–Gr* (Grashof number) combinations.

Namburu et al. [306] numerically studied the HTC of CuO, Al_2O_3 and SiO_2 EG-water nanofluids with different φ flowing through a tube under constant heat flux condition for turbulent flow. They measured the nanofluid viscosity and developed a correlation for the nanofluid viscosity as

a function of temperature up to φ = 10 %. Their results showed that the HTC increased with increase in φ of nanoparticles. Bianco et al. [307] investigated the turbulent forced convection flow of Al_2O_3-water nanofluid in a circular tube, subjected to a constant and uniform temperature at the wall. Two-phase mixture model was employed to simulate the nanofluid convection, and particles were assumed to be spherical with diameter of 38 nm. They found that convective HTC for nanofluids were greater than that of the base liquid, and the heat transfer enhancement increased with the increment of particle φ and *Re*. Similar type of result was obtained by Hejazian and. Moraveji [308], Yarmand et al. [309], Behroyan et al. [310], Colla et al. [311]. Moraveji et al. [312] investigated the effects of nanofluids (cooling performance and pressure drop) in micro channel heat sink. The results showed that HTC became greater with increase in nanoparticle φ and *Re*. Abdellahoum et al. [313] presented a numerical investigation of turbulent forced convection of nanofluid over a heated cavity in a horizontal duct. They found that the average Nusselt number increased with φ for all ranges of *Re*. Behesti et al. [314] numerically investigated the turbulent convection of Al_2O_3-water and TiO_2-water nanofluids inside an annular channel. Single-phase and two-phase models used for prediction of thermal behavior of the nanofluids. Result showed that Nusselt number increased with nanoparticle φ and *Re.* They also observed that for all nanoparticle φ, two-phase models shown better prediction to experimental data comparing to single-phase model. Hussein et al. [315] studied the forced convection heat transfer under turbulent flow by numerical simulation with uniform heat flux boundary condition. Friction factor and heat transfer enhancement of different types of nanofluids flow through horizontal three shapes of tubes evaluated numerically. The friction factor increased with increase in φ of nanofluid and decreased with increase of *Re*. In addition, the friction factor of circular tube was higher than others followed by elliptical and flat tube. The HTC increased with increase of φ and *Re*. They concluded that the flat tube has the highest values of HTC compared by elliptical and circular tube.

Kumar et al. [316] numerically investigated the heat transfer enhancement of Al_2O_3-water nanofluid through pipe, using single phase approach for constant wall temperature condition. Both the experimental and numerical prediction showed that the enhancement in the laminar regime was not as

significant as in the turbulent regime. Delavari and Hashemabadi [317] numerically studied heat transfer in nanofluids (Al_2O_3 particles in water and EG-based fluid) passed through a flat tube in 3D using CFD for single and two-phase approaches in turbulent and laminar flow. As presented in their investigations, a small difference in the friction factors of the tube was observed between the two approaches and the two-phase model better predicted the Nusselt number for the experimental data than the single-phase approach. Additionally, whether in laminar or turbulent flow, the volumetric flow for the same heat transfer rate decreased and less pumping power was required for the nanofluids. Celen et al. [318] studied the pressure drop of pure water and TiO_2-water nanofluid flowing inside plain and micro-fin pipes by CFD analysis. Result showed that the pressure drop of TiO_2-water nanofluids was higher compared to pure water for both plain and microfin pipes. Pressure drop of TiO_2-water nanofluids flowing in microfin tube was greater than plain pipes. Ziaei-Rad [319] studied the laminar and turbulent forced convection heat transfer and pressure drop between horizontal parallel plates for Al_2O_3-water nanofluid. Result showed that the effect of nanoparticle φ on hydraulic and thermal parameters was significant in laminar flow. The rate of heat transfer for the laminar flow with nanoparticles was greater than that of the base liquid. Rostamani et al. [320] numerically analyzed the turbulent flow of CuO, Al_2O_3, TiO_2 nanofluids with different φ of nanoparticles flowing through a two-dimensional duct under constant heat flux condition. Result showed that by increase in φ, the wall shear stress and heat transfer rate increased. For a constant φ and *Re*, the effect of CuO nanoparticles to enhance the Nusselt number is better than Al_2O_3 and TiO_2 nanoparticles. Demir et al. [321] numerically investigated the forced convection for TiO_2 and Al_2O_3 nanofluids in a horizontal tube with constant wall temperature. Result showed that the use of nanofluids can significantly increase heat transfer capabilities even for relatively small φ. Nanofluids with higher φ have higher heat transfer enhancement and also have higher pressure drop.

In the present study, flow and heat transfer characteristics in a simplified DASC configurations is investigated. Two different methods are adopted, which calculate the fluid properties using single phase model and mixture phase model. Also, comparison of DASC performance is made between the results obtained using nanofluid property values taken from the literature vis-à-vis those

obtained from the in-house measurements. A set of mathematical model equations were first developed that represent the conservation laws. These equations are then solved using a commercial CFD software to obtain the flow variables throughout the computational domain. ANSYS FLUENT version 13.0 was used for all the simulations presented in this thesis. FLUENT uses a finite-volume discretization of the coupled mass, momentum and energy equations with an unstructured mesh to compute the flow dynamics within a given computational domain. This unstructured mesh allows for much easier mesh creation, especially with complicated geometries. Validation of CFD models is carried out by comparing numerical results with available benchmark experimental data.

4.3. Governing equations

In this study both the single-phase models and multiphase (mixture phase) models are used for solving the respective problems.

4.3.1. Single phase model

A single-phase model for the nanofluid treats the medium as a homogeneous fluid with effective properties calculated by standard correlations available in the literature. The single-phase model equations include the equation of continuity, momentum equation and energy. The continuity and momentum equations are used to calculate velocity vector. The energy equation is used to calculate temperature distribution and wall HTC. The conservation equations solved to estimate the dependent flow variables (e.g., the flow velocity and temperature) are:

Continuity equation:

$$\nabla.(\rho\vec{v}) = 0 \tag{106}$$

Momentum equation:

$$\nabla.(\rho\vec{v}\vec{v}) = -\nabla p + \nabla.(\mu_t\nabla\vec{v}) + \rho g, \text{ and} \tag{107}$$

Energy equation:

$$\nabla.\left(\rho\vec{v}c_pT\right) = \nabla.(k\nabla T) \tag{108}$$

4.3.2. Mixture phase model

The mixture model is a simplified multiphase model that can be used in different ways. The mixture model allows for selecting granular phases and calculates all properties of the granular

phases. This is applicable for liquid-solid flows. Mixture model solves the continuity, momentum and energy equations for the mixture as well as a volume fraction equation for the secondary phases. Then it uses a correlation to calculate the relative velocity between the phases. The steady state governing equation describing a mixture fluid flow and heat transfer in micro channel are presented as follows [322].

Continuity equation:

$$\nabla.(\rho_m v_m) = 0 \tag{109}$$

Momentum equation:

$$\nabla.(\rho_m.V_m.V_m) = -\nabla p + \nabla.(\mu_m.\nabla V_m) + \nabla.\left(\sum_{k=1}^{n} \varphi_k \rho_k V_{dr,k} V_{dr.k}\right) - \rho_{m,i}\beta_m g(T - T_i) \tag{110}$$

Fluid energy equation:

$$\nabla.\sum_{k=1}^{n}\left(\rho_k.C_{pk}.\varphi_k.V_k.T\right) = \nabla.(K_m.\nabla T) \tag{111}$$

Energy equation:

$$\nabla.\left(\sum_{k=1}^{n} \varphi_{k.}\rho_k.H_k.\overrightarrow{V_k}\right) = -\nabla.q_m - \tau_t:\nabla\overrightarrow{V_m} \tag{112}$$

Particle φ equation:

$$\nabla.\left(\varphi_p \rho_p V_m\right) = -\nabla.\left(\varphi_p \rho_p V_{r,p}\right) \tag{113}$$

Here, V_m denotes the mass average velocity, which can be defined as:

$$V_m = \frac{\sum_{k=1}^{n} \varphi_k \rho_k V_k}{\rho_m} \tag{114}$$

In Eq. (115), $V_{dr.k}$ is the drift velocity for the secondary phase *k*, which is related to the relative velocity as:

$$V_{dr.k} = V_{pf} - V_m \tag{115}$$

Slip velocity is defined as the velocity of a secondary phase (*p*) relative to the primary velocity (*f*):

$$V_{pf} = V_p - V_f \tag{116}$$

The drift velocity is related to the relative velocity as:

$$V_{dr,p} = V_{pf} - \sum_{k=1}^{n} \frac{\varphi_k \rho_k}{\rho_m} V_{fk} \tag{117}$$

$$V_{pf} = \frac{\rho_p d_p^2}{18 f_{drag} \mu_f} \frac{(\rho_p - \rho_m)}{\rho_p} a^* \tag{118}$$

$$f_{drag} = \begin{cases} 1 + 0.15.Re_p^{0.687} & Re_p \leq 1000 \\ 0.0183.Re_p & Re_p > 1000 \end{cases} \quad (119)$$

where $a^* = g - (V_m.\nabla).V_m$ and $Re_p = {(V_m d_p)}/{V_{nf}}$

From Eq. (118) the relative velocity can be determined, as proposed by Manninen et al. [323], while from Eq. (119) we can calculate the drag function, as proposed by Schiller and Naumann [324].

4.3.3. Thermo-physical properties of nanofluids

The fluid properties of nanofluids vary when nanoparticles are suspended in them. In this present simulation the thermo-physical properties of nanofluids are calculated from the following equations:

Density $\left[\frac{\rho_{nf}}{\rho_f}\right] = \varphi\rho_p + (1-\varphi)$ (120)

Specific heat $\left[\frac{C_{pnf}}{C_{pf}}\right] = \varphi C_{pp} + (1-\varphi)$ (121)

Viscosity $\left[\frac{\mu_{nf}}{\mu_f}\right] = exp\left(4.91\varphi/(0.2092-\varphi)\right)$ (122)

Thermal Conductivity $\left[\frac{k_{nf}}{k_f}\right] = 1 + \left(\frac{Kp}{Kf}\right)\left(\frac{Ap}{Af}\right) + cPe\left(\frac{Kp}{Kf}\right)\left(\frac{Ap}{Af}\right)$ (123)

where $\left(\frac{Ap}{Af}\right) = \frac{d_f}{d_p}\frac{\varphi}{(1-\varphi)}$ and $p_e = \frac{u_p d_p}{\propto_f}$, where u_p is the velocity of the particles $u_p = \frac{2k_bT}{\pi\mu f d_p^2}$, where k_b the Boltzmann constant, φ is the volume fraction of the nanoparticles, ρ, C_p, μ and K are density, specific heat, viscosity and thermal conductivity respectively. Eq. (120) and (121) are based on the correlations from Pak et al. [112] and Maiga et al. [146] respectively. Eq. (122) was obtained for the calculation of viscosity Rea et al. [325], and Eq. (123) is the effective thermal conductivity of fluid has been determined by the model proposed Patel et al. [148]. Also the property values from Chapter 3 have been used and the performance of DASC is evaluated.

4.4. Performance analysis of direct absorption solar collector using multiphase model

4.4.1. Flow geometry and boundary condition

Figure 46 shows a schematic diagram (top view and side view) of the DASC having dimension of 150 μm (height) × 3 cm (width) × 5 cm (length) used for computational domain. The collector channel is fed through an inlet port of 1 mm diameter. The TiO_2 nanoparticle diameter was taken as 95 nm.

Both single phase and Mixture phase models were considered for this simulation with different physical properties (density, viscosity, specific heat and thermal conductivity). For mixture phase model water and TiO_2 is considered as primary phase and secondary phase, respectively. At the inlet port of the DASC, velocity was specified (calculated from *Re* which varies from 100-2000). The inlet temperature is assumed to be 22°C. Zero-slip velocity boundary condition was specified at all the walls. A specified heat flux (1000 W/m^2) boundary was imposed on the top glass wall, emulating the direct solar radiation; bottom and side walls were considered adiabatic. The physical properties of required material are shown in the Table 6. Properties of water was calculated by interpolation method and the values were taken from [276].

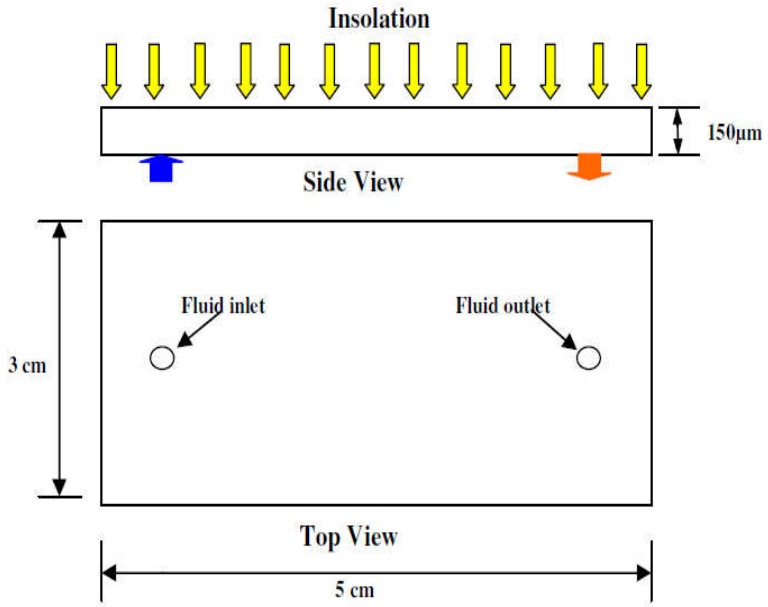

Figure 46 Schematic of the computational domain in the DASC Collector.

Table 6. Physical properties of water and nanoparticles.

Properties/Particles	**Water**	**Al_2O_3**	**TiO_2**
Density (Kg/m^3)	997.6	3970	4250
Specific heat (J/kg. K)	4181.2	765	686.5
Conductivity (W/m. K)	0.6016	40	8.95
Viscosity (Kg/m s)	0.000963		

Structured meshing method done in the ANSYS Workbench was used for meshing the geometry. Several grid sizes have been used for the grid independence test. The grid size for the present calculation consists of 35352 numbers of nodes and 104140 numbers of elements (in *x*, *y* and *z* directions) were found to be suitable for calculations by comparing with other two grid sizes (70345 and 150385). In Figure 47 the meshed profiles of the geometry have shown with different boundary name.

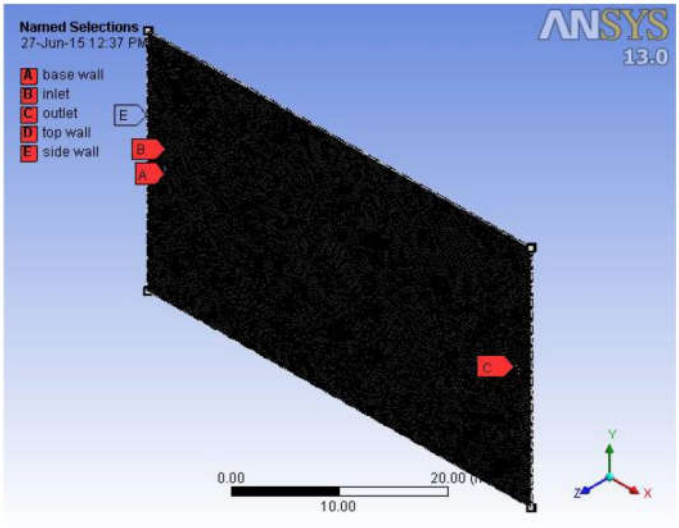

Figure 47 Meshed profile of the DASC geometry.

4.4.2. Performance parameters

As it discussed earlier, FLUENT 13.0 was used to solve the numerical solution. SIMPLE scheme and standard initialization method was taken to solve this geometry. After solving the governing equations, the other useful quantities such as average *Nu*, Pressure drop and average HTC can be determined by the following equations. *Nu* can be obtained by using eq. (124), HTC calculated as eq. (125), *Re* calculated as eq. (126) and pressure drop as eq. (128):

$$Nu = \frac{hD}{K_{nf}} \tag{124}$$

$$h = \frac{q''}{(T_w - T_m)} \tag{125}$$

$$Re = \frac{\rho.v.D}{\mu}, \tag{126}$$

where *v* denotes the average flow velocity calculated as

$$v = \frac{2}{R^2}\int_0^R u(r)dr \tag{127}$$

$$\Delta P = P_{inlet} - P_{outlet} \quad (128)$$

4.4.3. Results and Discussion

Figure 48 shows, for validation of the present simulation, the comparison of HTC vs. *Re* plots for water and TiO_2 nanofluids between the present study (single phase and mixture phase model) and the experimental work of He. et al. [87] where a cylindrical geometry has been chosen. The value of numerical HTC results matches well with the experimental one. Convective HTC has been calculated at a normalized distance of x/D = 151 from the inlet plane of the cylindrical configuration. As can be seen from Figure 48, the convective HTC increases with *Re*. Here the mixture phase model shows better enhancement of HTC than the single-phase model. Figure 49 shows the contour plot of temperature and gauge pressure at a mid-plane position (z = 75 μm) in the DASC flow for TiO_2 nanofluid (φ = 2.0 %). The nanofluid properties were considered using the mixture phase model and a *Re* = 1500. The average HTC was computed based on the computed bulk mean temperature of the nanofluid flowing and the temperature of the top surface where the heat-flux boundary condition was specified. Figure 50 shows the variation of HTC with *Re*, which indicates that with the gradual increase of *Re* at a given φ, the average HTC also increased. The average HTC was found to yield a very small enhancements at low *Re.* Mixture phase model shows a better enhancement of average HTC (compared to the single-phase model). Figure 51 shows the comparison between average *Nu* and *Re* for water, single phase and water, single phase and mixture phase model, and φ is considered as 2.0 %. It was observed that *Nu* increases as the value of *Re* increased. For higher *Re* the mixture model gives better enhancement than others. Little enhancement of *Nu* was found at low *Re* for all models. It is interesting to note that the single-phase model significantly underpredicts the Nu. At *Re* > 500. The HTC at 500 < *Re* < 2000 falls slightly even below that with pure water. This may be attributed to the fact that the increment of *k* exceeds the increase in HTC. For φ = 2.0 %, and temperature of 25 ^{o}C, estimation of nanofluid thermophysical parameters using single phase model predicts a *Pr* of 6.25 for the nanofluid, as opposed to 6.69 for water. For a given *Re*, this leads to a 2 % reduction in the estimated *Nu*. On the contrary, the mixture phase model estimates the local thermophysical properties based on local particle φ and reflects more realistic enhancement in HTC.

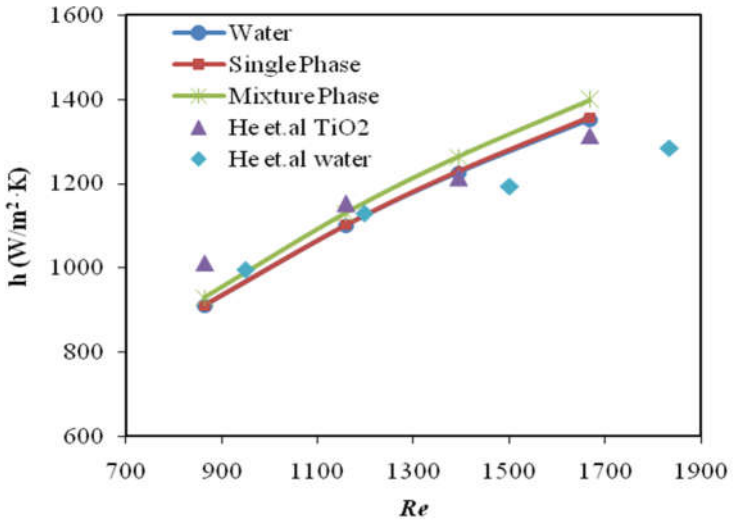

Figure 48 Comparison of HTC (at x/D = 151) with TiO_2-water nanofluid (φ = 0.6 %) between the present simulation and He et al. [87].

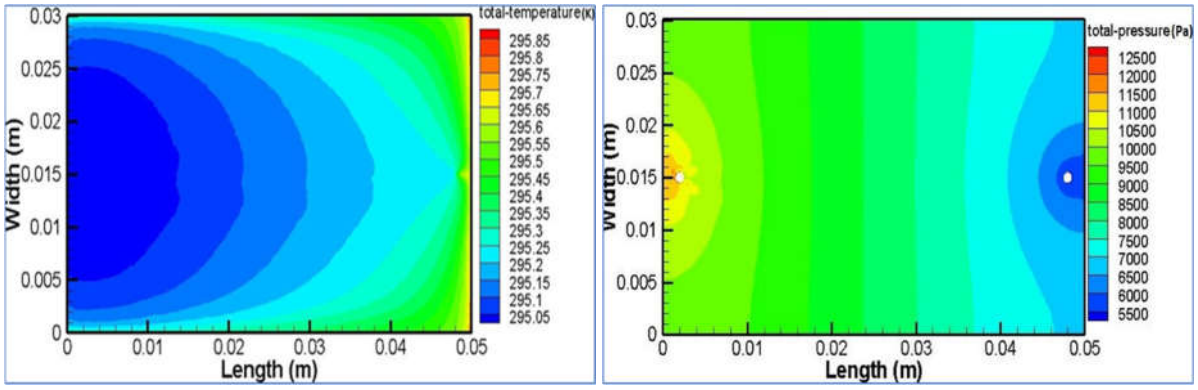

(a) (b)

Figure 49 Flow profile of TiO_2 nanofluid (φ = 2.0 %) along the z = 75 μm plane: (a) temperature contours and (b) gauge pressure contour, at *Re* =1500, for mixture model.

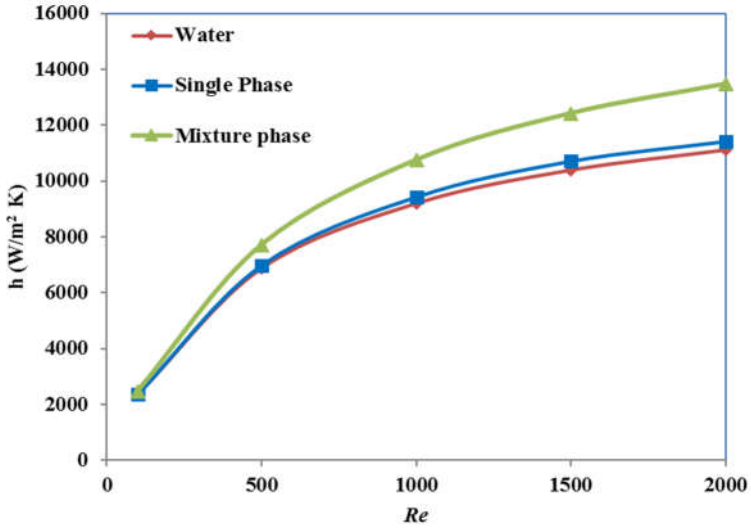

Figure 50 Average HTC as a function of *Re* at φ = 2.0 % for water, single-phase and mixture-phase model.

Figure 52 shows the variation of pressure drop for different *Re* for water, single and mixture phase model at constant φ = 2.0 %. Pressure drop increases as *Re* increased for water and for nanofluids with both the models. Very small difference in pressure drop for all models was observed. Figure 53 shows the comparison of average HTCs and average Nusselt numbers with different φ for constant *Re* at 1500 and 2000, applying both single phase and mixture phase models. The average HTC and Nu both increase as the φ and *Re* increases. Single phase model shows very less enhancement of HTC and Nu than that predicted by the mixture phase model for different *Re*. It is observed from Figure 54 that with increase in *Re* average HTCs and Nu increase for a particular φ. Moreover, average HTC and Nu of the collector increases with increase in φ. At *Re* = 2000, the HTC increases by 18.12 % if the φ increases from 0.24 % to 2.0 %, for mixture phase model.

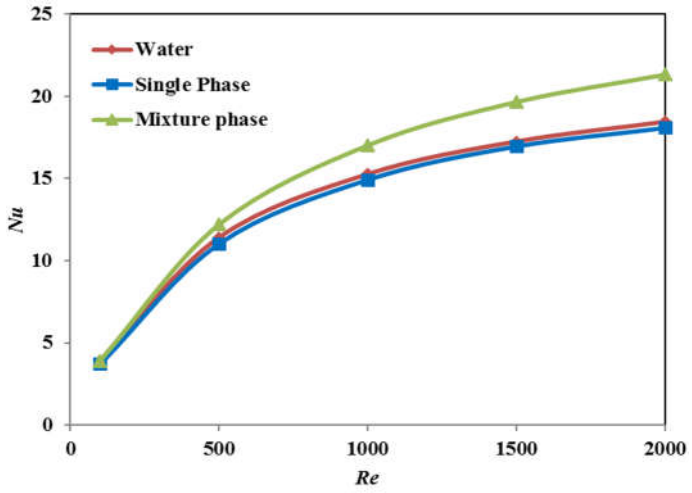

Figure 51 Average *Nu* as a function of *Re* at φ = 2.0 % for water, single phase and mixture phase model.

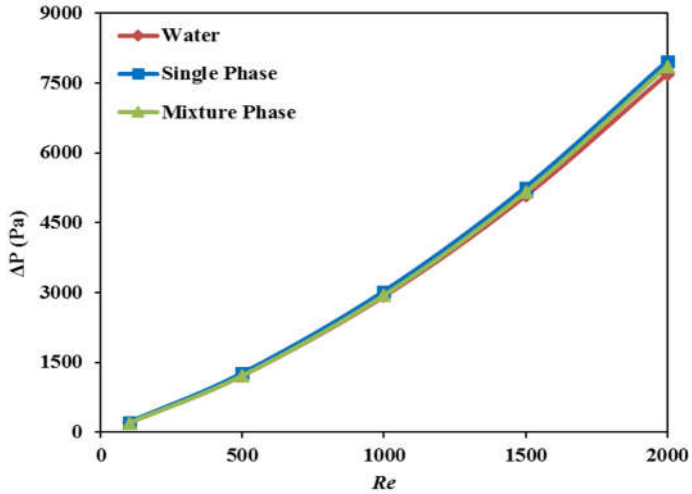

Figure 52 Pressure drop as a function of *Re* with φ of 2.0 % mixture phase model.

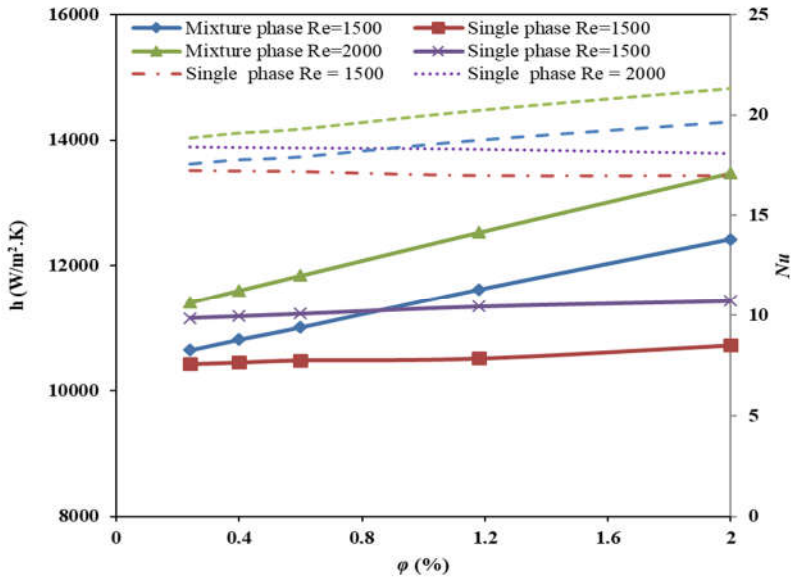

Figure 53 Average HTC and average Nusselt number as a function of φ with constant *Re* of 1500 and 2000 for single phase and mixture phase model (dotted line Represents *Nu* Vs. φ).

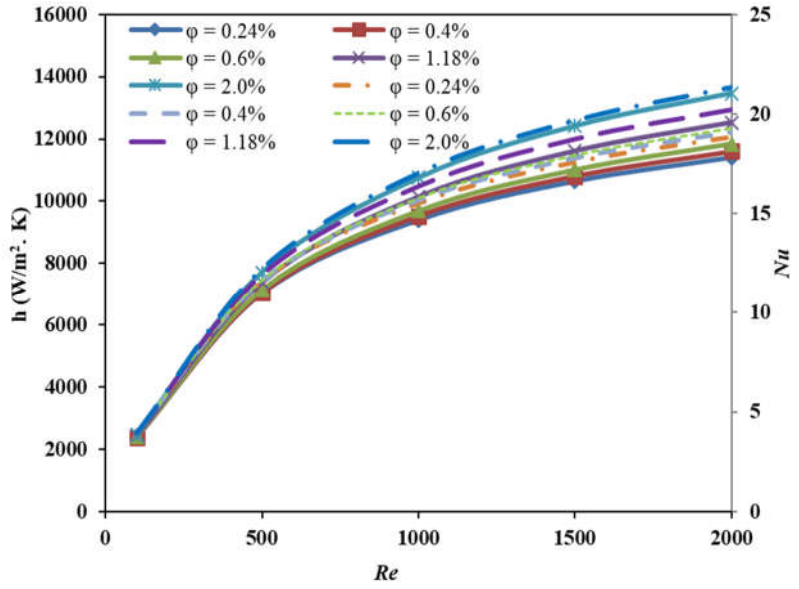

Figure 54 Average HTC and average Nusselt number as a function of *Re* for mixture phase model at different φ (dotted line represents *Nu* vs. Re).

4.4.4. DASC performance using in-house property values

Figure 55 shows the comparison of HTC with *Re* for two different nanofluids (TiO_2 and Al_2O_3) and φ (0.1 % and 0.24 %) for single phase and mixture phase models. HTC values for TiO_2-CTAB, TiO_2-AA and Al_2O_3-water nanofluids are predicted by using the nanofluid property values

taken from the literature (considering the single-phase model with φ = 0.1 %), vis-à-vis those from the experiments performed in house. The obtained result was also compared with the single phase and mixture phase models at φ = 0.24 % for TiO_2 nanofluids. The results indicate that the HTC calculated from the experimentally-obtained property values value is more than the that using the theoretical property values. Similarly, Figure 56 shows the comparison of HTC vs *Re* plots for the cases with the experimental value-based HTC and theoretical value at φ = 2.0 %. As the value of *Re* increases, HTC

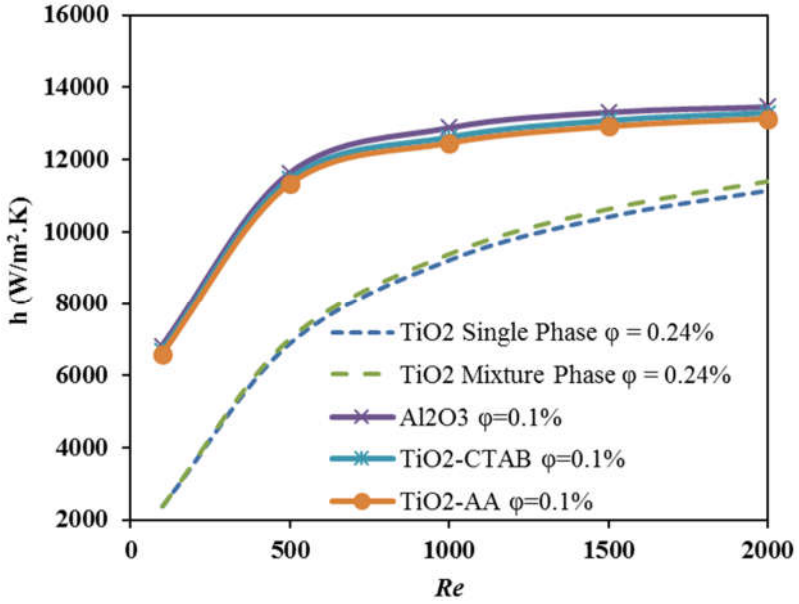

Figure 55 HTC vs *Re* for different nanofluids at low φ.

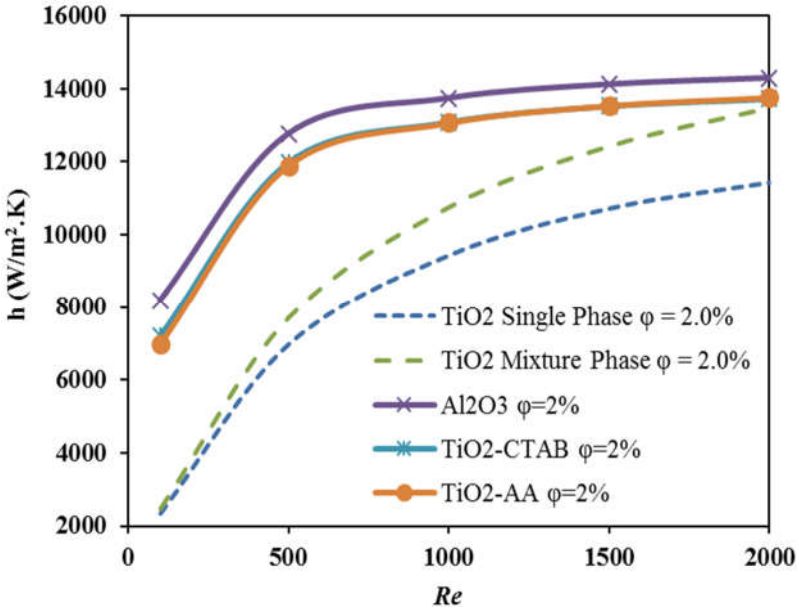

Figure 56 HTC vs *Re* for different nanofluids at higher φ.

increases, and Al_2O_3-water nanofluid shows higher HTC than TiO_2 nanofluids. This corroborates to the observation in Chapter 3, where the thermal conductivity of Al_2O_3-water nanofluid was found to be higher than the TiO_2 nanofluids. The results of Figure 56 also shows that, the HTC values using the experimentally observed property data exceeds those obtained using the single-phase and mixture-phase models adopted from the literature. However, at higher *Re*, the difference between the HTC values decrease.

Results from the numerical simulations indicate that the DASC exhibits higher thermal performance when the thermophysical property data measured in-house are used for the nanofluids. This trend is particularly higher at low φ and low *Re*, when the effect of dynamic fluctuations of the nanoparticles become more tangible.

CHAPTER 5

5. CONCLUSION AND RECOMENDATION FOR FUTURE WORK

Synthesis and characterization of few relevant nanofluids for application in direct absorption solar collectors (DASC) have been performed. Although the literature is rich in studies on thermophysical properties of nanofluids, the results are often inconclusive or contradictory. Therefore, a comprehensive characterization of the properties was warranted for accurate performance prediction of the DASC. The following section highlights the salient findings of the study.

5.1. Synthesis and characterization of TiO_2, Al_2O_3, and TiO_2 (anatase) nanoparticles

- TiO_2, Al_2O_3, and TiO_2-(anatase) nanoparticles were suspended in water for preparing nanofluid by two-step method. Nanofluids with different particle volume fractions (φ = 0.1 %, 0.5 %, 1.0 %, 1.5 % and 2.0 %) were prepared. Different surfactants were tried for stabilizing the nanofluids, e.g., acetic acid (AA), sodium dodecylbenzenesulfonate (SDBS), oleic acid (OA), sodium dodecyl sulfate (SDS), and cetyl trimethyl ammonium bromide (CTAB). Transmission electron microscopy (TEM), Dynamic light scattering (DLS), Zeta potential (ZP) were performed on the synthesized nanofluids to characterize the particle morphology, size distribution, and the nanofluid-stability, respectively.
- For TiO_2 nanofluid, CTAB and AA showed the best stabilization (stable for exceeding 500 h). TEM data showed a particle size in the range of 10–40 nm, while the DLS measurement indicated the existence of stable clusters having average size of 147 nm and 207 nm.
- For Al_2O_3 nanofluid, SDBS surfactant offered the best stabilization for the Al_2O_3-water nanofluids. TEM image of Al_2O_3-water and Al_2O_3-SDBS-water nanofluids indicated the presence of rod-like nanoparticles ranging between 20–70 nm. DLS measurement of the nanofluid samples showed that the number-averaged particle sizes for the non-surfacted and surfacted nanofluids were 222 nm and 75 nm, respectively, while the polydispersity indices for the samples were 1.23 and 1.19, respectively. Presence of surfactant lowered the extent of clustering and ensured a better homogeneity of particle size distribution; albeit, effective particle diameter was found to be slightly higher due to the presence of surfactant layers.

- For TiO_2 (anatase) nanofluids, CTAB and SDS were found to provide stable suspensions. TEM images of the SDS and CTAB-stabilized TiO_2 nanofluids indicated the presence of sphere-like nanoparticles of size ranging between 10–40 nm. DLS measurements showed that the number-averaged particle sizes for the surfacted nanofluids were 265 nm and 226 nm with SDS and CTAB stabilization, respectively.
- The value of zeta potentials of TiO_2-AA, TiO_2-CTAB, Al_2O_3-water, and Al_2O_3-SDBS based nanofluids were 29.5, 14.1, 40.3 and 25.5 mV, respectively. From these zeta potential values, it was confirmed that the nanofluids produced stable suspensions.

5.2. Thermophysical property measurements of the prepared nanofluids

5.2.1. TiO_2 nanofluids

- Thermal conductivity of the CTAB- and AA-stabilized TiO_2-nanofluid increased monotonically with φ and temperature. At φ = 2.0 %, and T = 60 °C, the enhancement in effective thermal conductivity was 6 %, for AA-based nanofluids.
- Viscosity of the TiO_2 nanofluids increased with its φ and decreased with temperature. The nanofluid viscosity also showed mild shear thickening at a constant temperature for both CTAB and AA surfactant-stabilized nanofluid beyond a critical shear rate. The critical shear rate decreased with increase in temperature and increased with increase in φ.
- pH of the nanofluids decreased with increase in temperature and φ.

5.2.2. Al_2O_3 nanofluids

- Thermal conductivity of Al_2O_3-nanofluids was found to increase monotonically with φ and temperature. At low φ (below φ = 1.0 %), the measured k_{nf} exceeded the predicted values using standard models. Dynamic contribution arising out of the particle Brownian motion have been attributed to this deviation.
- The viscosity of Al_2O_3-water and Al_2O_3-SDBS-water nanofluid increased with φ and decreased with temperature. The increase of viscosity with φ was far more pronounced in surfacted nanofluids than the non-surfacted ones. This was attributed to the formations of

multilayer adsorption of the surfactant molecules on the surface of nanoparticles and presence of scattered micelle of the surfactant in the nanofluid at high φ, augmenting the viscosity.

- Prandtl number (*Pr*) of the nanofluids decreased monotonically with temperature, as viscosity decreased and thermal conductivity increased with temperature. The *Pr* of the non-surfacted nanofluids exhibited little dependence on φ, while that for the surfacted nanofluid increased considerably with φ (and hence the SDBS concentration). Depending upon the particle loading and SDBS concentration, Al_2O_3 nanofluids offer a wide range of *Pr* to suite specific heat transfer applications.

5.2.3. TiO_2 (anatase) nanofluids

- The measured thermal conductivity of the nanofluids increased monotonically with φ and temperature. The maximum enhancement in thermal conductivity of nanofluids is 5.8 %, at φ = 1 % and temperature of 60 °C for SDS based nanofluids with respect to that of the base fluid.
- Viscosity of both the SDS- and CTAB-stabilized nanofluids increased to a very small extent with φ and decreased monotonically with temperature.

Besides describing the important thermophysical characteristics, the study also provided a few important insights for preparing anatase nanofluids with favourable thermophysical properties. For example, it ensued from the study that the effect of variation of particle loading on viscosity is less pronounced with CTAB than that with SDS. Also, the CTAB-surfacted nanofluid exhibited slightly lower viscosity than the SDS-stabilized one over the temperature range of 15–60 °C. Therefore, for better operation of a heat transfer device deploying nanofluid, it is imperative to use CTAB, instead of SDS, for stabilizing the nanofluids at relatively high particle loading. The ratio of thermal conductivity to viscosity is also higher at lower φ. Therefore, for optimizing heat transfer related applications, e.g., in forced flow heat exchangers, it is more prudent to work at the φ in the range of 0.1 %.

5.3. Nanofluid surface tension and contact angle on solid substrates

The surface tension and contact angles of water-based nanofluids were measured experimentally.

- Surface tension of nanofluids decreased with increase in φ as well as temperature.
- TiO_2-AA stabilized nanofluid showed significantly higher surface tension compared to that by TiO_2-CTAB stabilized nanofluid for same φ and T.
- Al_2O_3 water nanofluid showed higher surface tension than Al_2O_3-SDBS stabilized nanofluid.
- SDS-stabilized nanofluids have higher surface tension than CTAB-stabilized nanofluids.
- At a given temperature, surface tension of nanofluids decreased with increase in φ. TiO_2-AA and Al_2O_3-water have higher surface tension than TiO_2-CTAB, and Al_2O_3-SDBS based nanofluids.
- Results indicate that contact angle of surfacted-water solutions (without the nanoparticles) were more than the corresponding nanofluids, and the value of contact angle of TiO_2-AA, TiO_2-CTAB, Al_2O_3-water, nanofluids decreased with increase in φ.

5.4. Application of nanofluid on direct absorption solar collector (DASC)

Forced convection heat transfer due to flow of different nanofluids was studied numerically under various configurations and boundary conditions that are relevant to solar thermal applications. The governing transport equations (continuity, momentum and energy) were solved numerically using a commercial CFD software, ANSYS FLUENT 13.0. Both the single phase and mixture phase models built-in the software were employed to analyze heat transfer performance of nanofluids. Nanofluid properties were either adopted from the existing literature or taken from the in-house data from the measurements. All the thermo-physical properties of nanofluids were assumed to be temperature-dependent.

- Performance analysis of direct absorption solar collector (DASC) was simulated. Heat transfer in forced-flow arrangement has been investigated on DASC configuration. The effects of nanoparticle concentrations and flow rate were investigated. It was found that

average HTC increased with increase in φ and flow rate. Mixture phase model showed better enhancement of *Nu* and average HTC compared with single phase model for TiO_2-nanofluid.

- Results from the numerical simulations indicate that the DASC exhibits higher thermal performance when the thermophysical property data measured in-house are used for the nanofluids. This trend is particularly higher at low φ and low *Re*, when the effect of dynamic fluctuations of the nanoparticles becomes more tangible.

An experimental setup comprising of a DASC and flow loop has been developed in-house to investigate the performance improvement of DASC using different nanofluids (see the next section).

5.5. Recommendations for future research

The present work has provided a comprehensive characterization of the thermophysical properties of a few nanofluids and a numerical study portraying the thermal performance of representative heat transfer device configurations using those nanofluids. Figure 57 shows the image of a nanofluid-based table-top DASC loop experimental setup developed for measurement of heat transfer performance of different nanofluids. Comprising of a DASC module, a circulation pump, a thermostatic bath and temperature controller, the setup is capable of operating under sunlight or artificial halogen light and logging the temperature and the flow data for estimation of overall system thermal performance. The following future works are proposed.

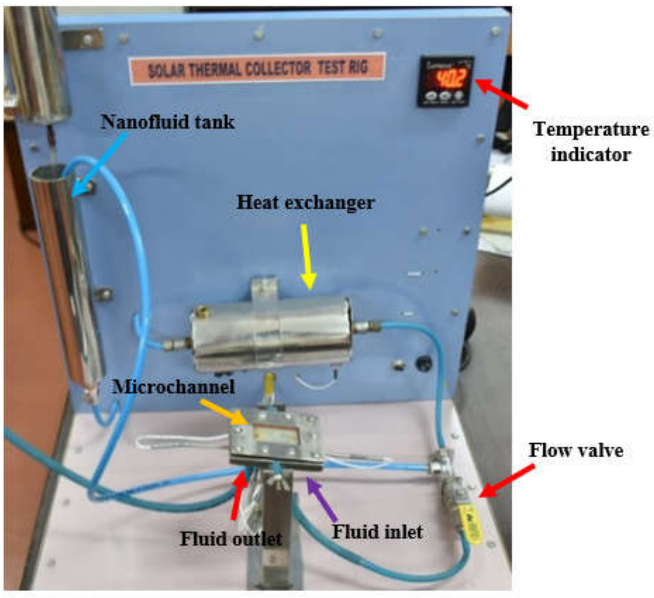

Figure 57 Experimental setup for performance study of a DASC setup using nanofluid.

- The thermal performance of the direct absorption solar collector (DASC) module using the nanofluids characterized in this thesis needs to be investigated as the immediate future work. As a future extension, more types of nanofluids, e.g., Cu, CuO, carbon nanofiber (CNF) nanofluid, etc may be tested in the DASC setup. Also, the performance of heat transfer and thermosiphonic pumping using magnetic nanofluid is prescribed as a future exercise.
- In the numerical simulation side, the current model does not consider radiation heat transfer due to absorption by the nanoparticles. This may be included in the future investigations through incorporating appropriate radiation model and invoking the user-defined function (UDF) in FLUENT. Also, different multiphase models may be tested. The result obtained can be compared with experimental result.
- Ferrofluid, a nanofluid of superparamagnetic ferrous nanoparticles in a nonmagnetic liquid, can be used as DASC fluid and temperature-dependent magnetic susceptibility gradient of ferrofluid to create an unbalanced Kelvin body force to pump the fluid through the DASC can be harnessed.
- As a long-term roadmap, coupling the nanofluid-based STCs with different engineering applications, e.g. organic Rankine cycle (ORC) for generating power, may be studied. This will show directions of developing energy-efficient systems that will deploy nanofluids for reducing the use of conventional energy and consumption of fossil fuel.

Appendix

Numerical simulation in benchmark configurations

A. Simulation of laminar forced convection heat transfer of Cu-water nanofluids inside a vertical tube

(a) Flow geometry, grid and boundary conditions

Figure 58 shows a schematic representation of the flow configuration. A cylindrical geometry of diameter (D) of 4.5 mm and length (L) of 1.01 m was chosen for the simulation. Considering the axisymmetric nature of the flow, a two-dimensional CFD model is developed based on single phase fluid system. For the simulation of steady state flows in a vertical tube, the thermal performance of two different nanofluids and pure water, as base fluid passing through it. The nanofluid properties were chosen from the literature [326] to mimic Al_2O_3-water and Cu-water suspensions having ~ 100 nm diameter. The fluid enters with a uniform axial velocity and the inlet temperature was chosen at 295 *K*. The nanofluid was assumed as a single-phase fluid with specified physical properties (density, viscosity, specific heat and thermal conductivity). The density of Al_2O_3 and Cu nanoparticles was 3920 and 8954 kg/m^3 respectively. Specific heat of Al_2O_3 and Cu were 880 and 383.1 J/kg. *K*, respectively. The thermal conductivity of and Al_2O_3 and Cu were 40 and 401 W/m. *K*, respectively. The properties of water were taken from standard handbook [276]. On the tube wall, no-slip condition and a constant heat flux were imposed following Saberi et al. (200 W) [326]. The geometry and the grid were generated using Ansys fluent 13.0. A grid with 400 nodes for z-direction and 40 nodes in r-direction was found to produce grid-independent result for this configuration.

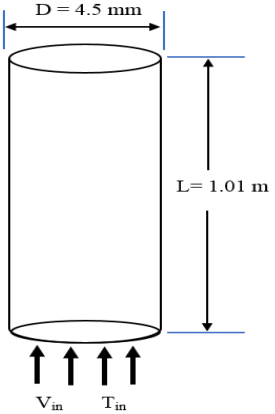

Figure 58 Schematic representation of the pipe flow configuration.

(b) Results and Discussion

Considering the heat flux values, pipe dimensions and the thermophysical properties assumed herein, the Grashof number for the internal flow inside the vertical tube is estimated to be ~200. This implies that the heat transfer is primarily by force convection. This implicitly means that the vertical orientation does not influence the result. The average Nusselt number (*Nu*) and HTC of nanofluids were calculated using the following Eq. (127) and (128) respectively. Re for this flow configuration were calculated from Eq. (129).

Figure 59 and Figure 60 shows a comparison of present work with Saberi et al [326]. Figure 59 shows the variation of HTC and *Re* for water, while the Figure 60 shows the variation of HTC and *Re* for Al_2O_3-water nanofluid at φ of 1.32 %. Figure 61 shows the variation of convective HTC of Cu-water nanofluid (0.64 %, 1.32 % and 2.76 %) with different *Re*. The HTC increases according to the increase of φ and *Re*. Figure 62 shows the comparison between the convective HTC of water, Al_2O_3-water and Cu-water nanofluid (φ = 1.32 %) with *Re*. Comparing between these two nanofluids and water, Cu-water nanofluid has shown a good increment of HTC. Figure 63 shows the comparison of Nusselt number verses *Re* for water, Al_2O_3-water and Cu-water nanofluid with φ = 2.76 %. The results show that the relative differences between average Nusselt number of water and nanofluid inside the tube was increased as the *Re* increased. Al_2O_3-water nanofluid (φ = 2.76 %) shows better Nusselt number compared to Cu-water nanofluid (φ = 2.76 %) and water.

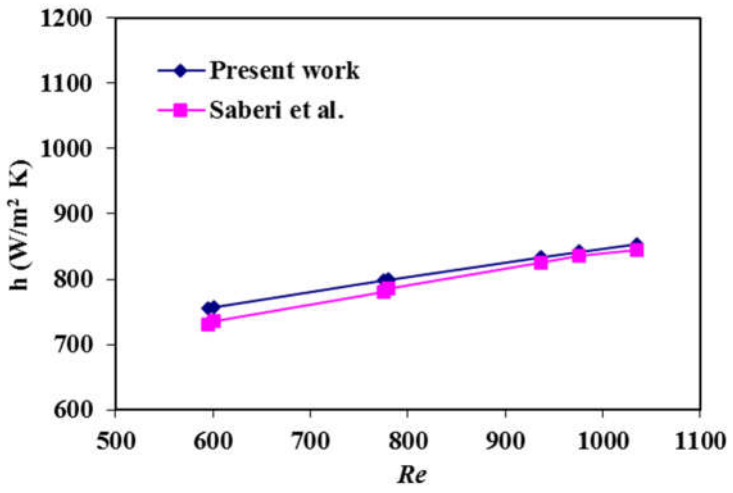

Figure 59 Comparison of convective HTC of water with different *Re*.

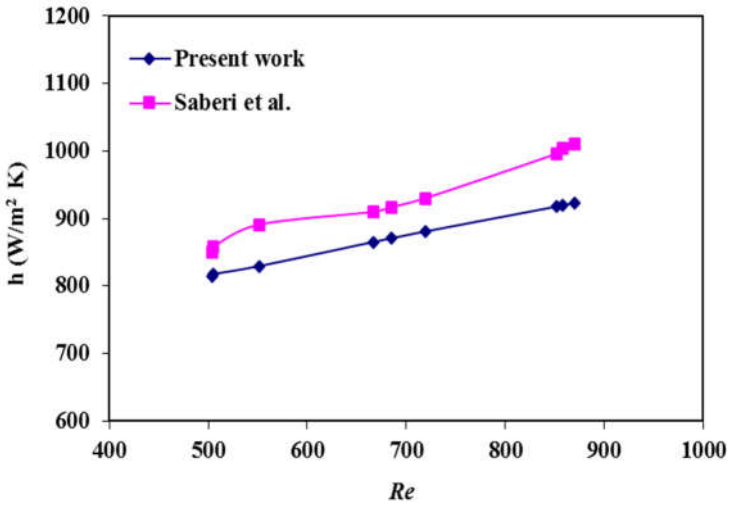

Figure 60 Comparison of convective HTC of Al_2O_3-water (φ = 1.32 %) nanofluid with *Re*.

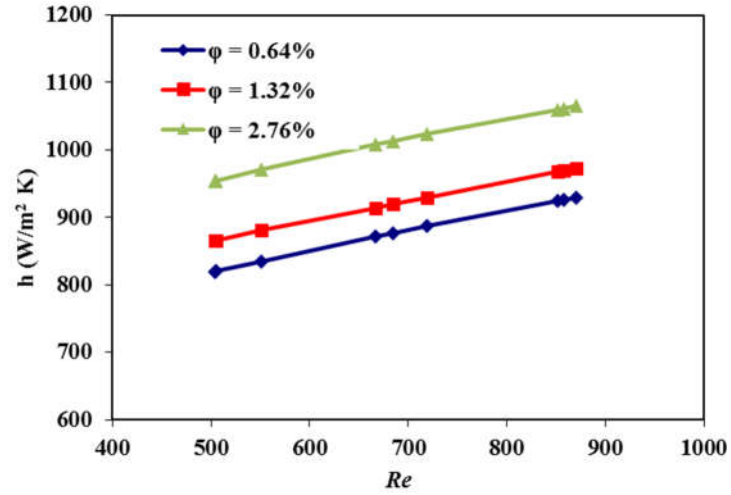

Figure 61 Variation of convective HTC of Cu-water nanofluids at different φ, with *Re*.

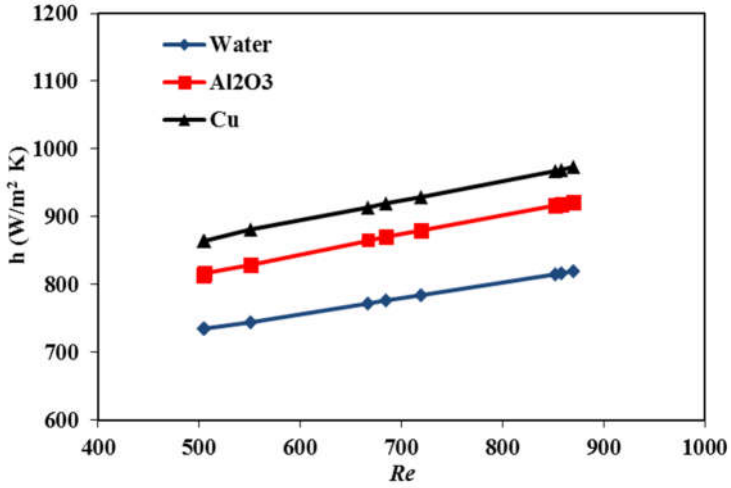

Figure 62 Comparison of convective HTC of water, Al_2O_3-water and Cu-water nanofluid (φ = 1.32 %) with *Re*.

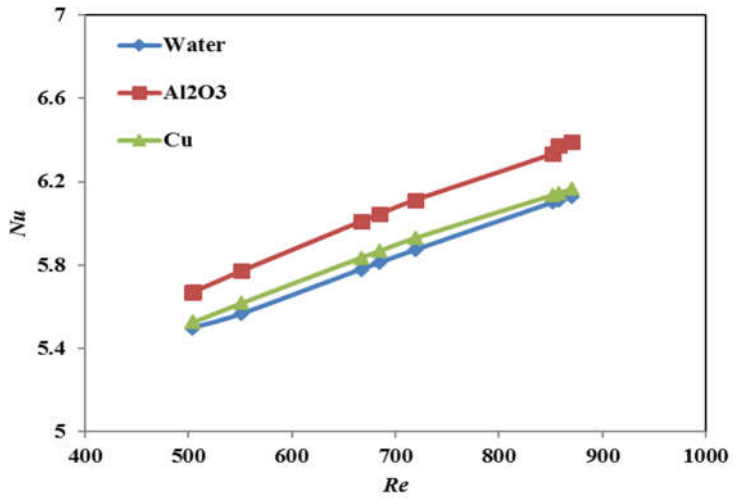

Figure 63 Comparison of Nusselt numbers of water, Al_2O_3-water and Cu-water nanofluid (φ = 2.76 %) with *Re*.

The foregoing study of laminar forced convection heat transfer of Cu-water and Al_2O_3-water nanofluids inside the vertical tube, with constant heat flux boundary condition, shows that the HTC and Nusselt number increases with increase in *Re* as well as φ. Wall shear stress also increases with increase in *Re* and φ. For the same *Re* and φ, Cu-water nanofluid shows better heat transfer than that of Al_2O_3 nanofluid, while the wall shear stress is more for Al_2O_3 nanofluid at a particular flow condition.

B. Numerical investigation of HTC of nanofluids flow through a vertical pipe

(a) Flow geometry and boundary conditions

A vertical circular pipe was modelled and simulated by CFD method. The diameter (D) and length (L) of the pipe was 3.97 mm 1834 mm respectively. Thermal performance of two different nanofluids and pure water as base fluid passing through the pipe were studied. Two nanofluids were considered i.e., Al_2O_3-water and TiO_2-water, and particle diameter was taken as 95 nm. The nanofluid for this simulation was considered as single-phase fluid with different physical properties. At inlet of the pipe, average flow velocity was calculated from *Re*, which was varied from 100-7000. Several grid sizes have been tried when a mesh comprising 50,000 nodes and 197166 elements were found to produce grid-independent results.

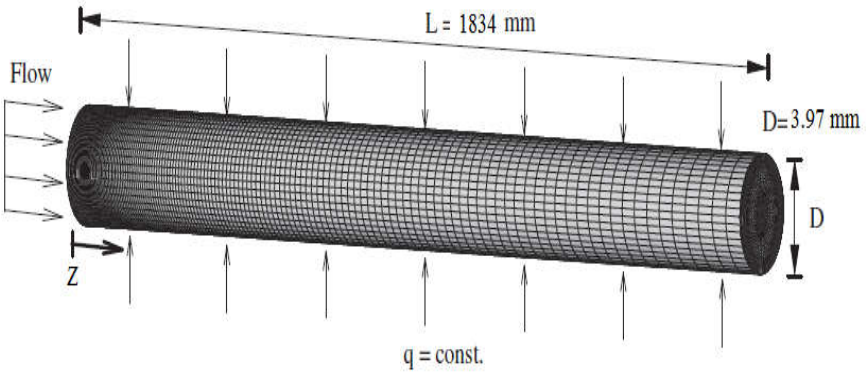

Figure 64 Flow geometry and numerical grid distribution of the model.

(b) Turbulence model

The governing equations for laminar flow is already discussed in Chapter 4. For turbulent flow regimes in the present numerical analysis, *k*-*ε* turbulent model was applied with enhanced wall functions. The *k*-*ε* turbulent model announces two additional equations; i.e. turbulent kinetic energy and rate of dissipation [327]. The equations for turbulent kinetic energy (k) and rate of dissipation (ε) are given by the following equations.

$$\nabla.\left(\rho.k.\vec{V}\right) = \nabla.\left[\left(\mu + \frac{\mu_{tu}}{\sigma_k}\right).\nabla k\right] + G_k - \rho.\varepsilon \tag{129}$$

$$\nabla.\left(\rho.\varepsilon.\vec{V}\right) = \nabla.\left[\left(\mu + \frac{\mu_{tu}}{\sigma_\varepsilon}\right).\nabla\varepsilon\right] + C_{1\varepsilon}.\left(\frac{\varepsilon}{k}\right).G_k + C_{2\varepsilon}.\left(\frac{\varepsilon^2}{k}\right).\rho \tag{130}$$

where G_k represents the generation of turbulent kinetic energy due to mean velocity gradients; σ_k and σ_ε are effective Prandtl numbers for turbulent kinetic energy and rate of dissipation, respectively; $C_{1\varepsilon}$ and $C_{2\varepsilon}$ are constants; and μ_{tu} is the eddy viscosity.

$$\mu_{tu} = \rho.C_\mu.\frac{k^2}{\varepsilon} \tag{131}$$

Here C_μ is a constant and its value is 0.09. Some constants are used in Eq. (120) and (121). Whose values are $C_{1\varepsilon} = 1.92$, $C_{2\varepsilon} = 1.92$, $\sigma_k = 1.0$, and $\sigma_\varepsilon = 1.3$. Further information is available in Launder and Spalding [328].

(c) Thermophysical properties

As already mentioned before, a single-phase model was considered for representing the thermophysical properties of the nanofluid. It is important to note that all properties of a given

nanofluid will depend on the φ and the corresponding properties of the base fluid and nanoparticles. The density and specific heat of the nanofluid were calculated form the individual properties of the host fluid and the nanoparticles, using the Eq. (123) and Eq. (124), respectively. Since the properties of base fluid are temperature dependent, the corresponding properties of the nanofluids are also temperature dependent.

The effective thermal conductivity and viscosity of nanofluids were determined by using Maxwell [49] and Einstein [183] models, mentioned in Eq. (1) and Eq (33), respectively (both are different from the models chosen in the previous simulation). Inlet temperature was taken as 22 °C and heat flux at the wall was taken according to the experimental data [87]. The wall motion and the shear conditions are set to be stationary and no-slip respectively. Standard *k*-epsilon model was selected for turbulent flow. At the inlet, the average flow velocity was specified, while the turbulence intensity and hydraulic diameter of 4 % and 0.00397 m were chosen, respectively, as the *k* and the epsilon boundary conditions. Pressure outlet was selected as the outflow boundary condition. The properties of water were taken by interpolation method from [276]. Other properties of Al_2O_3 and TiO_2 nanoparticles shown in Table 6. Figure 64 shows the mesh generated profile of the model.

(d) Results and Discussions

Figure 65 (a) compares the HTC vs. *Re* plots for water and different nanofluids between the present study and the experimental [87] results for laminar flows. Figure 65 (b) compares the HTC vs. *Re* plots for water and different nanofluids between present study and the experimental [87] results for turbulent flows with water and TiO_2-water based nanofluid at φ = 0.6 %. Both the results (for laminar and turbulent flows) show that the model underpredicts the heat transfer coefficients for the nanofluids at low *Re*. However, for both cases, the HTC increases with *Re* and the simulated results match better with the experiment at higher *Re*. The difference at low *Re* may be attributed mainly to the underprediction of thermal conductivity of the nanofluids, since conduction component becomes more pervasive at low *Re*.

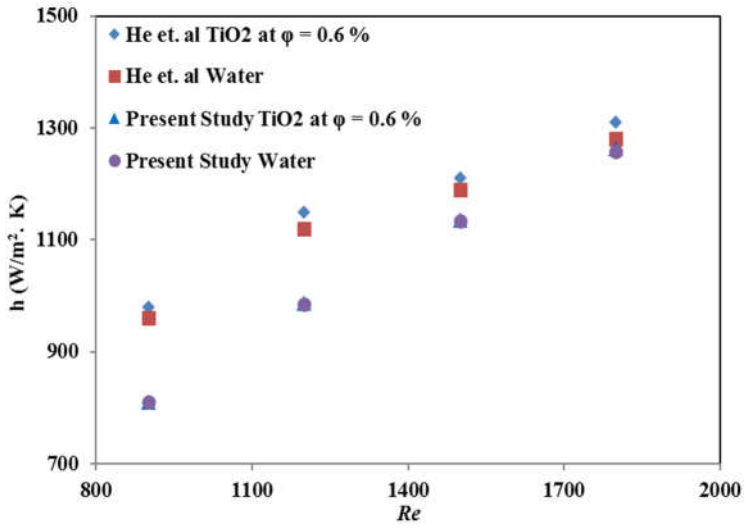

(a)

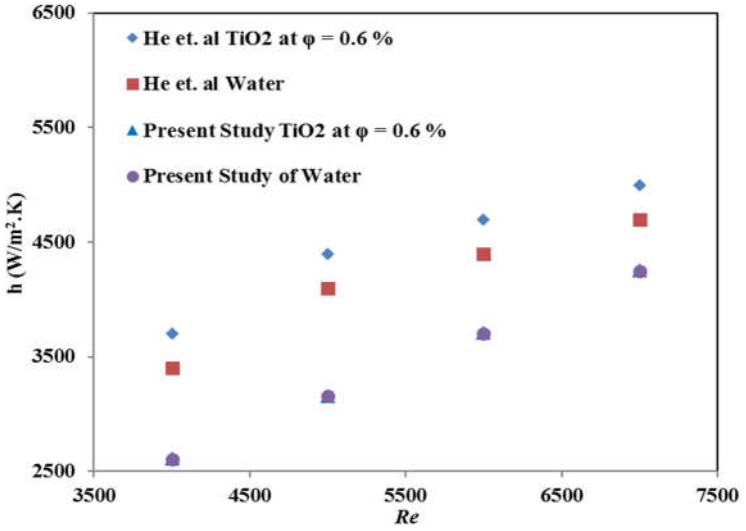

(b)

Figure 65 Comparison of HTC (at x/D = 151) for water and TiO_2-water nanofluid at (a) laminar flow and (b) turbulent flow for present study and experimental data [87].

Figure 66 (a) **c**ompares the HTC, plotted as functions of *Re*, of water, TiO_2 and Al_2O_3-water based nanofluid for laminar flows and φ were considered as 0.24 % and 2.0 %. It shows that the increase of *Re* and φ, HTC also increased for all fluids gradually. Al_2O_3-water based nanofluid shows better enhancement of HTC compared with water and TiO_2-water based nanofluid with same φ. Figure 66 (b) compares the HTC, plotted as functions of *Re*, of water, TiO_2 and Al_2O_3-water based nanofluid for turbulent flows. It shows that the increase of *Re*, HTC also increased for all fluids.

Al_2O_3-water based nanofluid shows a better enhancement of HTC compared with other fluids. Figure 67 (a) shows the comparison between HTC and φ for water and other two nanofluids at constant Re = 2000. The φ were varied from 0.24 % to 2.0 %. HTC increases as φ of the particle increased for all fluids. Here the Al_2O_3-water based nanofluid shows better increment of HTC compared with water and TiO_2-water based nanofluid. Figure 67 (b) shows the comparison between HTC and φ for water and other two nanofluids at constant Re = 7000. The φ were varying from 0.24 % to 2.0 %. HTC increases as the φ increased for all fluids. Here the Al_2O_3-water based nanofluid shows better increment of HTC compared with other fluids.

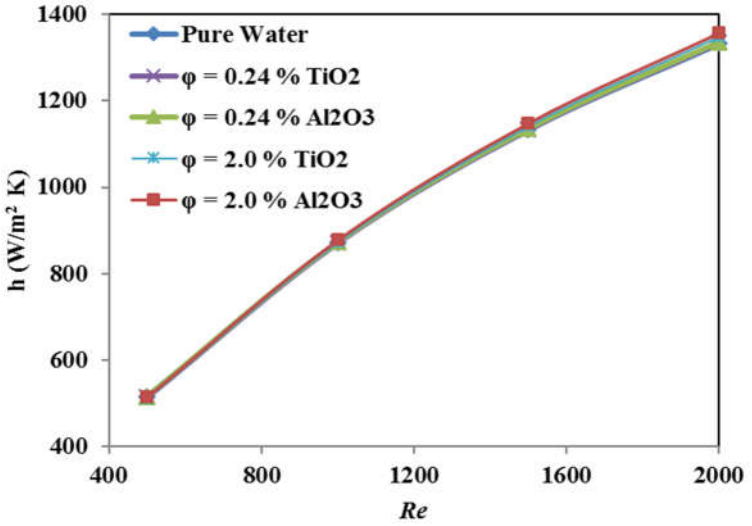

(a)

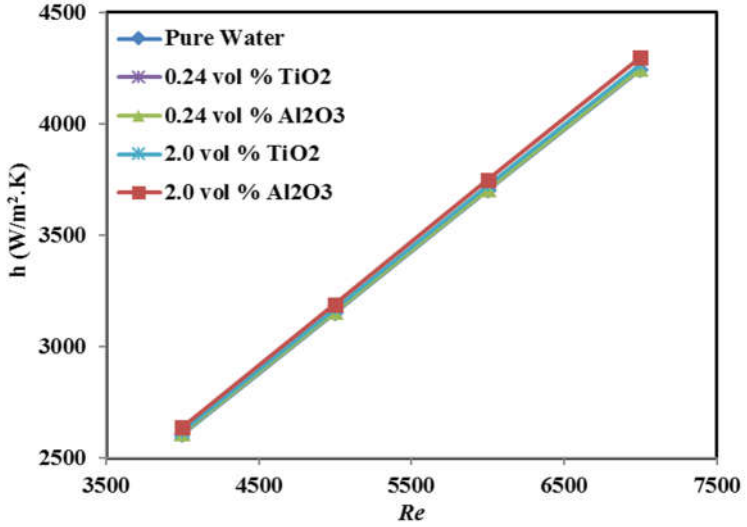

(b)

Figure 66 HTC as a function of Re with different particle φ (at x/D = 151) for (a) laminar flow and (b) turbulent flow.

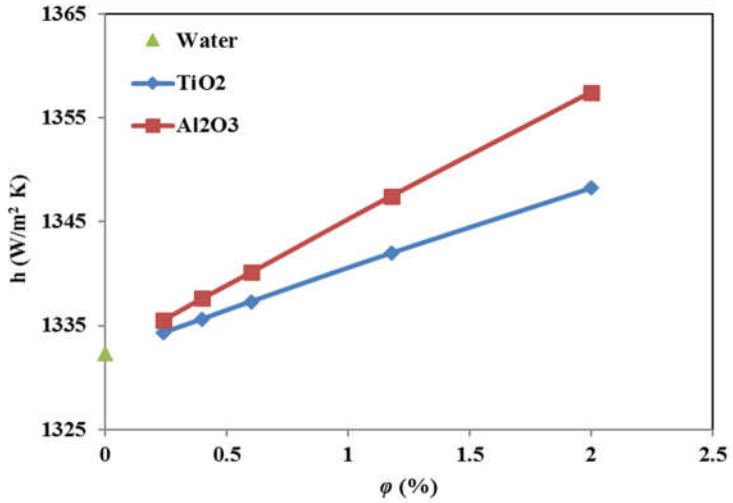

(a)

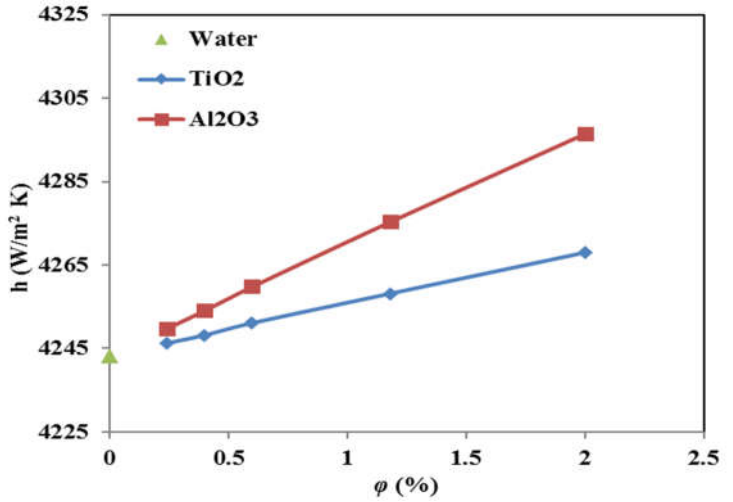

(b)

Figure 67 Variation of HTC with φ for Al_2O_3-water and TiO_2-water nanofluids at (a) *Re* of 2000, and (b) *Re* of 7000.

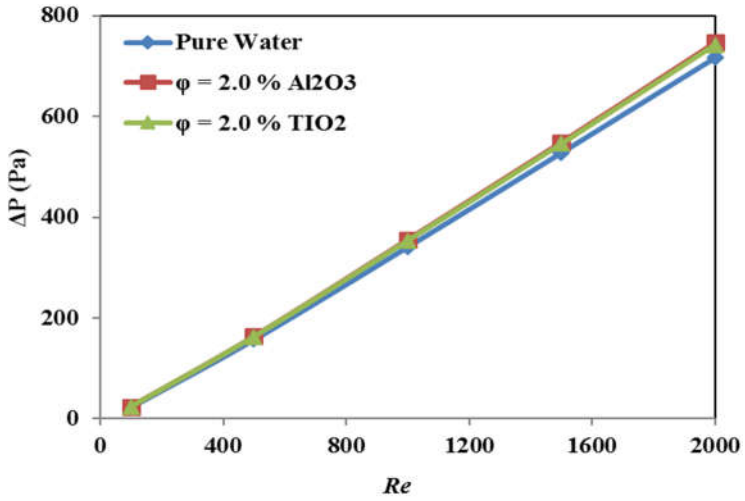

Figure 68 Comparison of pressure drop and *Re* between water and nanofluids (at x/D = 151) for laminar flow.

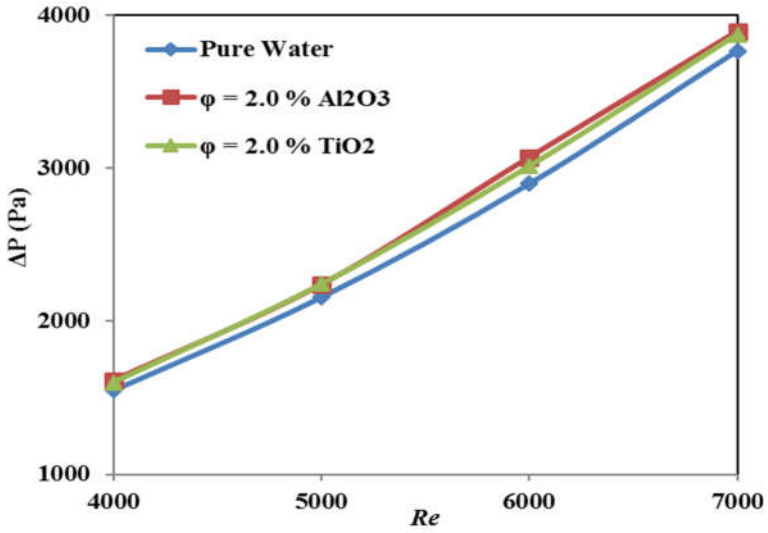

Figure 69 Comparison of Pressure drop and *Re* between water and nanofluids (x/D = 151) for turbulent flow.

Both laminar and turbulent flows of nanofluid through the vertical pipe shows that Al_2O_3-water nanofluid yields higher heat transfer than TiO_2-water nanofluid for the same *Re* and φ. However, the effect of particle φ appears more tangible in the turbulent flow regime than the laminar one.

REFERENCE

[1] S.A. Kalogirou, Solar thermal collectors and applications, Progress in Energy and Combustion Science 30 (2004) 231–295.

[2] T.P. Otanicar, P.E. Phelan, R.S. Prasher, G. Rosengarten, R.A. Taylor, Nanofluid based direct absorption solar collector, Journal of Renewable and Sustain. Energy 2 (2010) 033102.

[3] S.U.S. Choi, J.A. Eastman, Enhancing thermal conductivity of fluids with nanoparticle, ASME International Mechanical Engineering Congress & Exposition San Francisco 12–17th November 23 (1995) 199–105.

[4] P.K. Das, A review based on the effect and mechanism of thermal conductivity of normal nanofluids and hybrid nanofluids, Journal of Molecular Liquids 240 (2017) 420–446.

[5] S.P. Jang, S.U.S. Choi, Cooling performance of a microchannel heat sink with nanofluids, Applied Thermal Engineering 26 (2006) 2457–2463.

[6] P. Naphon, P. Assadamongkol, T. Borirak, Experimental investigation of titanium nanofluids on the heat pipe thermal efficiency, International Communication of Heat and Mass Transfer 35 (2008) 1316–1319.

[7] Z. Azizi, A. Alamdari, M.R. Malayeri, Convective heat transfer of Cu–water nanofluid in a cylindrical microchannel heat sink, Energy Conversion and Management 101 (2015) 515–524.

[8] C.J. Ho, W.C. Chen, An experimental study on thermal performance of Al_2O_3-water nanofluid in a minichannel heat sink, Applied Thermal Engineering 50 (2013) 516–522.

[9] A.K. Tiwari, P. Ghosh, J. Sarkar, Performance comparison of the plate heat exchanger using different nanofluids, Experimental Thermal and Fluid Science 49 (2013) 141–151.

[10] K.Q. Ma, J. Liu, Nano liquid–metal fluid as ultimate coolant, Phy. Let. A 361 (2007) 252–256.

[11] A.M. Hussein, R.A. Bakar, K. Kadirgama, K.V. Sharma, Heat transfer enhancement using nanofluids in an automotive cooling system, International Communications in Heat and Mass Transfer 53 (2014) 195–202.

[12] D.P. Kulkarni, R.S. Vajjha, D.K. Das, D. Oliva, Application of Al_2O_3 nanofluids in diesel electric generator as jacket water coolant, Applied Thermal Engineering 28 (2008) 1774–1781.

[13] S. Bi, L. Shi, L. Zhang, Application of nanoparticles in domestic refrigerators, Applied Thermal Engineering 28 (2008) 1834–1843.

[14] S. Wu, D. Zhu, X. Li, H. Li, J. Lei, Thermal energy storage behavior of Al_2O_3–H_2O nanofluids, Thermochimica Acta 483 (2009) 73–77.

[15] R. Taylor, P.E. Phelan, T.P. Otanicar, C.A. Walker, M. Nguyen, S. Trimble, R. Prasher, Applicability of nanofluids in high flux solar collectors, Journal of Renewable Sustainable Energy 3 (2011) 023104.

[16] B. Shen, A.J. Shih, S.C. Tung, Application of Nanofluids in minimum quantity lubrication grinding, Tribology Transactions 51 (2008) 730–737.

[17] Y. Mitamura, S. Arioka, D. Sakota, K. Sekine, M. Azegami, Application of a magnetic fluid seal to rotary blood pumps, Journal of Physics Condens. Matter 20 (2008) 204145(1–5).

[18] M. Heinlaan, A. Ivask, I. Blinova, H.C. Dubourguier, A. Kahru, Toxicity of nanosized and bulk ZnO, CuO and TiO_2 to bacteria vibrio fischeri and crustaceans Daphnia magna and Thamnocephalus platyurus, Chemosphere 71 (2008) 1308–1316.

[19] R. Jalal, E.K. Goharshadi, M. Abareshi, M. Moosavi, A. Yousefi, P. Nancarrow, ZnO nanofluids: Green synthesis, characterization, and antibacterial activity, Materials Chemistry and Physics 121 (2010) 198–201.

[20] A. Panacek, L. Kvitek, R. Prucek, M. Kolar, R. Vecerova, N. Pizurova, V.K. Sharma, T. Neveena, R. Zboril, Silver Colloid Nanoparticles: Synthesis, Characterization, and Their Antibacterial Activity, Journal of Physical Chemistry B 110 (2006) 16248-16253.
[21] Y. Xuan, Q. Li, Heat transfer enhancement of nanofluids, International Journal of Heat and Fluid Flow 21 (2000) 58-64.
[22] S. Yatsuya, Y. Tsukasaki, K. Mihama, R. Uyeda, Preparation of extremely fine particles by vacuum evaporation onto a running oil substrate, Jou. of Crystal Growth 45 (1978) 490–494.
[23] J.A. Eastman, S.U.S. Choi, S. Li, L.J. Thompson, S. Lee, Enhanced thermal conductivity through the development of nanofluids, Materials Res. Society Symp. Proc. 457 (1997) 3–11.
[24] J.A. Eastman, S.U.S. Choi, S. Li, W. Yu, L.J. Thompson, Anomalously increased effective thermal conductivities of ethylene glycol-based nanofluids containing copper nanoparticles, Applied Physics Letters 78 (2001) 718–720.
[25] S.U.S. Choi, W. Yu, J.R. Hull, Z.G. Zhang, F.E. Lockwood, Nanofluids for vehicle thermal management, Proceedings of the Vehicle Thermal Management Systems Conference Society of Automotive Engineers 2001.
[26] S.W. Lee, S.D. Park, I.C. Bang, Critical heat flux for CuO nanofluid fabricated by pulsed laser ablation differentiating deposition characteristics, International Journal of Heat and Mass Transfer 55 (2012) 6908–6915.
[27] T.X. Phuoc, Y. Soong, M.K. Chyu, Synthesis of Ag-deionized water nanofluids using multi-beam laser ablation in liquids, Optics and Lasers in Engineering 45 (2007) 1099–1106.
[28] H.J. Kim, I.C. Bang, J. Onoe, Characteristic stability of bare Au-water nanofluids fabricated by pulsed laser ablation in liquids, Optics and Lasers in Engineering 47 (2009) 532–538.
[29] F. Mafune, J.Y. Kohno, Y. Takeda, T. Kondow, Full Physical Preparation of Size–Selected Gold Nanoparticles in Solution: Laser Ablation and Laser-Induced Size Control, American Chemical Society 106 (2002) 7575–7577.
[30] P.X. Tran, Y. Soong, Preparation of nanofluids using laser ablation in liquid technique, ASME applied mechanics and material conference (2007).
[31] H.T. Zhu, Y.S. Lin, Y.S. Yin, A novel one-step chemical method for preparation of copper nanofluids, Journal of Colloid and Interface Science 277 (2004) 100–103.
[32] X.Q. Wang, A.S. Mujumdar, Heat transfer characteristics of nanofluids: a review, International Journal of Thermal Science 46 (2007) 1–19.
[33] S. Ananda Kumar, K.S. Meenakshi, B.R.V. Narashimhan, S. Srikanth, G. Arthanareeswaran, Synthesis and characterization of copper nanofluid by a novel one–step method, Materials Chemistry and Physics 113 (2009) 57–62.
[34] A.G. Kanaras, F.S. Kamounah, K. Schaumburg, C.J. Kiely, M. Brust, Thioalkylated tetra ethylene glycol: a new ligand for water soluble monolayer protected gold clusters, The Royal Society of Chemistry Chemical Communication (2002) 2294–2295.
[35] S.U. Sandhya, S.A. Nityananda, A Facile One Step Solution Route to Synthesize Cuprous Oxide Nanofluid, Nanomaterials and nanotechnology 3 (2013) 5(1-7).
[36] M.S. Liu, M.C.C. Lin, C.Y. Tsai, C.C. Wang, Enhancement of thermal conductivity with Cu for nanofluids using chemical reduction method, International Journal of Heat and Mass Transfer 49 (2006) 3028–3033.
[37] H. Wang, J.Z. Xu, J.J. Zhu, H.Y. Chen, Preparation of CuO nanoparticles by microwave irradiation, Journal of Crystal Growth 244 (2002) 88–94.
[38] K. Patel, S. Kapoor, D.P. Dave, T. Mukherjee, Synthesis of nanosized silver colloids by microwave dielectric heating, Journal of Chemical Science 117 (2005) 53–60.

[39] F. Bonet, K.T. Elhsissen, K.V. Sarathy, Study of interaction of ethylene glycol/PVP phase on noble metal powders prepared by polyol process, Bull. Mater. Science 23 (2000) 165–168.
[40] D. Kim, S. Jeong, J. Moon, Synthesis of silver nanoparticles using the polyol process and the influence of precursor injection, Nanotechnology 17 (2006) 4019–4024.
[41] P.Y. Silvert, R.H. Urbina, N. Duvauchelle, V. Vijayakrishnan, K.T. Elhsissen, Preparation of colloidal silver dispersions by the polyol process Part 1–Synthesis and characterization, Journal of Muter. Chemical 6 (1996) 573–577.
[42] C.H. Lo, T.T. Tsung, L.C. Chen, Shape-controlled synthesis of Cu–based nanofluid using submerged arc nanoparticle synthesis system (SANSS), J. of Cry. Growth 277 (2005) 636–642.
[43] C.H. Lo, T.T. Tsung, H.M. Lin, Preparation of silver nanofluid by the submerged arc nanoparticle synthesis system (SANSS), J. of Alloys and Comp. 434–435 (2007) 659–662.
[44] C. Wang, J. Yang, Y. Ding, Phase transfer based synthesis and thermophysical properties of Au/Therminol VP–1 nanofluids, Materials International 23 (2013) 338–342.
[45] I. Manna, Synthesis, characterization and application of nanofluid–an overview, Journal of Indian Institute of Science 89 (2009) 21–33.
[46] R. Prasher, P.E. Phelan, P. Bhattacharya, Effect of aggregation kinetics on the thermal conductivity of nanoscale colloidal solutions (nanofluid), Nano Letters 6 (2006) 1529–1534.
[47] S.M.S. Murshed, K.C. Leong, C. Yang, A combined model for the effective thermal conductivity of nanofluids, Applied Thermal Engineering 29 (2009) 2477–2483.
[48] D. Cabaleiro, J. Nimo, M.J. Pastoriza-Gallego, M.M. Piñeiro, J.L. Legido, L. Lugo, Thermal conductivity of dry anatase and rutile nano–powders and ethylene and propylene glycol–based TiO_2 nanofluids, The Journal of Chemical Thermodynamics, 83 (2015) 67–76.
[49] J.C. Maxwell, A Treatise on Electricity and Magnetism. Oxford, NY, UK: Oxford Clarendon, 1881.
[50] S.K. Das, N. Putra, P. Thiesen, W. Roetzel, Temperature dependence of thermal conductivity enhancement for nanofluids, Journal of Heat Transfer 125 (2003) 567–574.
[51] D. Zhu, X. Li, N. Wang, X. Wang, J. Gao, H. Li, Dispersion behavior and thermal conductivity characteristics of Al_2O_3-H_2O nanofluids, Current Applied Physics 9 (2009) 131–139.
[52] W. Duangthongsuk, S. Wongwises, An experimental study on the heat transfer performance and pressure drop of TiO_2–water nanofluids flowing under a turbulent flow regime, International Journal of Heat and Mass Transfer 53 (2010) 334–344.
[53] S.M.S. Murshed, K.C. Leong, C. Yang, Enhanced thermal conductivity of TiO_2–water-based nanofluids, International Journal of Thermal Science 44(4) (2005) 367–373.
[54] S.A. Angayarkanni, J. Philip, Effect of Nanoparticles Aggregation on Thermal and Electrical Conductivities of Nanofluids, Journal of Nanofluids 3 (2014) 17–25.
[55] H. Masuda, A. Ebata, K. Teramae, N. Hishinuma, Alteration of Thermal Conductivity and Viscosity of Liquid by Dispersing Ultra-Fine Particles (Dispersion of γ–Al_2O_3, SiO_2, and TiO_2 Ultra-Fine Particles), Netsu Bussei 7 (1993) 227–233.
[56] H.A. Mintsa, G. Roy, C.T. Nguyen, D. Doucet, New temperature dependent thermal conductivity data for water-based nanofluids, International Journal of Thermal Science 48 (2009) 363–371.
[57] T. Cho, I. Baek, J. Lee, S. Park, Preparation of nanofluids containing suspended silver particles for enhancing fluid thermal conductivity of fluids, Jou. of Ind. Engg. Chemistry 11 (2005) 400.
[58] H. Zhu, C. Zhang, S. Liu, Y. Tang, Y. Yin, Effects of nanoparticle clustering and alignment on thermal conductivities of Fe_3O_4 aqueous nanofluids, Applied Physics Letters 89 (2006) 023123.

[59] M. Chandrasekar, S. Suresh, A.C. Bose, Experimental investigations and theoretical determination of thermal conductivity and viscosity of Al_2O_3–water nanofluid, Experimental Thermal and Fluid Science 34 (2010) 210–216.
[60] S. Lee, S.U.S. Choi, S. Li, J.A. Eastman, Measuring thermal conductivity of fluids containing oxide nanoparticles, Journal of Heat Transfer 121 (1999) 280–289.
[61] D.H. Yoo, K.S. Hong, H.S. Yang, Study of thermal conductivity of nanofluids for the application of heat transfer fluids, Thermochim Acta 455 (2007) 66–69.
[62] Y.J. Hwang, Y.C. Ahn, H.S. Shin, C.G. Lee, G.T. Kim, H.S. Park, J.K. Lee, Investigation on characteristics of thermal conductivity enhancement of nanofluids, Current Applied Physics 6 (2006) 1068–1071.
[63] H. Jiang, H. Li, Q. Xu, L. Shi, Effective thermal conductivity of nanofluids considering interfacial nano-shells, Materials Chemistry and Physics 148 (2014) 195–200.
[64] X. Wang, X. Xu, S.U.S. Choi, Thermal conductivity of nanoparticle-fluid mixture, Journal of Thermo physics Heat Transfer 13(4) (1999) 474–480.
[65] M. Chopkar, S. Sudarshan, P.K. Das, I. Manna, Effect of particle size on thermal conductivity of nanofluid, Metallurgical and Materials Transactions A 39 (2008) 1535–1542.
[66] M, Chopkar, P.K. Das, I. Manna, Synthesis and characterization of nanofluid for advanced heat transfer applications, Scripta Materialia 55 (2006) 549–552.
[67] N.R. Karthikeyan, J. Philip, B. Raj, Effect of clustering on the thermal conductivity of nanofluids, Material Chemistry and Physics 109 (2008) 50–55.
[68] R.M. Mostafizur, M.H.U. Bhuiyan, R. Saidur, A.R.A. Aziz, Thermal conductivity variation for methanol based nanofluids, Inter. Journal of Heat and Mass Transfer 76 (2014) 350–356.
[69] G.J. Lee, C.K. Kim, M.K. Lee, C.K. Rhee, Characterization of ethylene glycol based TiO_2 nanofluid prepared by pulsed wire evaporation (PWD) method, Rev. Adv. Mater. Sci. 28 (2011) 126–129.
[70] W. Yu, H. Xie, W. Chen, Experimental investigation on thermal conductivity of nanofluids containing graphene oxide nanosheets, Journal of Applied Physics 107 (2010) 094317.
[71] V.I. Terekhov, S.V. Kalinina, V.V. Lemanov, The mechanism of heat transfer in nanofluids: state of the art (review). Part 1: Synthesis and properties of nanofluids, Thermophysics Aeromechanics 17 (1) (2010) 1–14.
[72] W. Duangthongsuk, S. Wongwises, Measurement of temperature dependent thermal conductivity and viscosity of TiO_2–water nanofluids, Experimental Thermal Fluid Science 33 (2009) 706–714.
[73] S.K. Das, N. Putra, W. Roetzel, Pool boiling of nanofluids on horizontal narrow tubes, International Journal of Multiphase Flow 29 (2003) 1237–1247.
[74] G.P. Peterson, C.H. Li, Heat and mass transfer in fluids with nanoparticle suspensions, Review Article Advanced Heat Transfer 39 (2006) 257–376.
[75] S.M.S. Murshed, K.C. Leong, C. Yang, Investigations of thermal conductivity and viscosity of nanofluids, International Journal of Thermal Sciences 47 (2008) 560–568.
[76] C.H. Chon, K.D. Kihm, S.P. Lee, S.U.S. Choi, Empirical correlation finding the role of temperature and particle size for nanofluid (Al_2O_3) thermal conductivity enhancement, Applied Physics Letters 87 (2005) 153107 (1–3).
[77] S.K. Das, N. Putra, W. Roetzel, Pool boiling characteristics of nanofluids, International Journal of Heat and Mass Transfer 46 (2003) 851–862.
[78] J.W. Gao, R.T. Zheng, H. Ohtani, D.S. Zhu, G. Chen, Experimental Investigation of Heat Conduction Mechanisms in Nanofluids Clue on Clustering, Nano Letters 9 (2009) 4128–4132.

[79] C.H. Li, G.P. Peterson, Experimental investigation of temperature and volume fraction variations on the effective thermal conductivity of nanoparticle suspensions (nanofluids), Journal of Applied Physics 99 (2006) 084314 (1–8).
[80] M.C.S. Reddy, V.V. Rao, Experimental studies on thermal conductivity of blends of ethylene glycol-water–based TiO_2 nanofluids, International Communication in Heat and Mass Transfer, 46 (2013) 31–36.
[81] R.S. Vajjha, D.K. Das, Experimental determination of thermal conductivity of three nanofluids and development of new correlations, Int. J. of Heat and Mass Transfer 52 (2009) 4675–4682.
[82] L. Syam Sundar, M.K. Singh, A.C.M. Sousa, Thermal conductivity of ethylene glycol and water mixture-based Fe_3O_4 nanofluid, Inter. Comm. Heat and Mass Transfer 49 (2013) 17–24.
[83] E.V. Timofeeva, A.N. Gavrilov, J.M. McCloskey, Y.V. Tolmachev, Thermal conductivity and particle agglomeration in alumina nanofluids: Experiment and theory, Physical Review E 76 (2007) 061203.
[84] B. Yang, Z.H. Han, Temperature-dependent thermal conductivity of nanorod–based nanofluids, Applied Physics Letters 89 (2006) 083111.
[85] T.P. Teng, Y.H. Hung, T.C. Teng, H.E. Moa, H.G. Hsu, The effect of alumina/water nanofluid particle size on thermal conductivity, Applied Thermal Engineering 30 (2010) 2213–2218.
[86] K. Nemade, S. Waghuley, A novel approach for enhancement of thermal conductivity of CuO/H_2O based nanofluids, Applied Thermal Engineering 95 (2015) 271–274.
[87] Y. He, Y. Jin, H. Chen, Y. Ding, D. Cang, H. Lu, Heat transfer and flow behaviour of aqueous suspensions of TiO_2 nanoparticles (nanofluids) flowing upward through a vertical pipe, International Journal of Heat and Mass Transfer 50 (2007) 2272–2281.
[88] M. Chopkar, S. Kumar, D.R. Bhandari, P.K. Das, I. Manna, Development and characterization of Al_2Cu and Ag_2Al nanoparticle dispersed water and ethylene glycol based nanofluid, Material Science Engineering B 139 (2007) 141–148.
[89] H.E. Patel, T. Sundararajan, S.K. Das, An experimental investigation into the thermal conductivity enhancement in oxide and metallic nanofluids, Journal of Nanoparticle Research 12 (2010) 1015–1031.
[90] S.H. Kim, S.R. Choi, D. Kim, Thermal conductivity of metal oxide nanofluids: particle size dependence and effect of laser irradiation, Journal of Heat Transfer 129 (2007) 298–307.
[91] C.H. Li, G.P. Peterson, The effect of particle size on the effective thermal conductivity of Al_2O_3–water nanofluids, Journal of Applied Physics 101 (2007) 044312 (1-5).
[92] M. Beck, Y. Yuan, P. Warrier, A. Teja, The effect of particle size on the thermal conductivity of alumina nanofluids, Journal of Nanoparticle Research 11 (2009) 1129–1136.
[93] N. Shalkevich, W. Escher, T. Burgi, B. Michel, L.S. Ahmed, D. Poulikakos, On the Thermal Conductivity of Gold Nanoparticle Colloids, Langmuir 26 (2010) 663–670.
[94] E.V. Timofeeva, D.S. Smith, W. Yu, D.M. France, D. Singh, J.L. Routbort, Particle size and interfacial effects on thermo-physical and heat transfer characteristics of water-based α-SiC nanofluids, Nanotechnology 21 (2010) 215703.
[95] H. Xie, J. Wang, T. Xi, Y. Liu, Thermal conductivity of suspensions containing nanosized SiC particles, International Journal of Thermophysics 23 (2002) 571–580.
[96] Y. Feng, B. Yu, P. Xu, M. Zou, The effective thermal conductivity of nanofluids based on the nanolayer and the aggregation of nanoparticles, Journal of Physics D: Applied Physics 40 (2007) 3164–3171.
[97] R. Prasher, D. Song, J. Wang, P. Phelan, Measurements of nanofluid viscosity and its implications for thermal applications, Applied Physics Letters 89 (13) (2006).

[98] P.D. Shima, J. Philip, B. Raj, Role of micro convection induced by Brownian motion of nanoparticles in the enhanced thermal conductivity of stable nanofluids, Applied Physics Letters 94 (2009) 2231011–3.
[99] Y. Feng, B. Yu, K. Feng, P. Xu, M. Zou, Thermal conductivity of nanofluids and size distribution of nanoparticles by Monte Carlo simulations, Journal of Nanoparticle Research 10 (2008) 1319–1328.
[100] H.J. Kim, S.H. Lee, J.H. Lee, S.P. Jang, Effect of particle shape on suspension stability and thermal conductivities of water-based bohemite alumina nanofluids, Energy 90 (2015) 1290-97.
[101] D. Lee, Thermophysical properties of interfacial layer in nanofluids, Langmuir 23 (2007) 6011–6018.
[102] S.S. Sonawane, R.S. Khedkar, K.L. Wasewar, Effect of sonication time on enhancement of effective thermal conductivity of nano TiO_2–water, ethylene glycol, and paraffin oil nanofluids and models comparisons, Journal of Experimental Nanoscience, 10 (4) (2015) 310–322.
[103] B. Ruan, A.M. Jacobi, Heat transfer characteristics of multiwall carbon nanotube suspensions (MWCNT nanofluids) in intertube falling-film flow, International Journal of Heat and Mass Transfer 55 (2012) 3186–3195.
[104] R. Agarwal, K. Verma, N.K. Agrawal, R. Singh, Sensitivity of thermal conductivity for Al_2O_3 nanofluids, Experimental Thermal and Fluid Science 80 (2017) 19–26.
[105] H. Xie, J. Wang, T. Xi, Y. Liu, F. Ai, Q. Wu, Thermal conductivity enhancement of suspensions containing nanosized alumina particles, J. of App. Physics 91 (2002) 4568–4572.
[106] J. Buongiorno, et al., A benchmark study on the thermal conductivity of nanofluids, Journal of Applied Physics 106 (2009) 094312.
[107] S.M.S. Murshed, S.H. Tan, N.T. Nguyen, Temperature dependence of interfacial properties and viscosity of nanofluids for droplet–based microfluidics, Journal of Physics D: Applied Physics, 41 085502 (2008) 1–5.
[108] X.J. Wang, D.S. Zhu, S. Yang, Investigation of pH and SDBS on enhancement of thermal conductivity in nanofluids, Chemical Physics Letters 470 (2009) 107–111.
[109] S.A. Angayarkanni, J. Philip, Role of adsorbing moieties on thermal conductivity and associated properties of nanofluids, The Journal Physical Chemistry C 117 (2013) 9009–9019.
[110] R. Saleh, N. Putra, R.E. Wibowo, W.N. Septiadi, S.P. Prakoso, Titanium dioxide nanofluids for heat transfer applications, Experimental Thermal and Fluid Science 52 (2014) 19–29.
[111] F.H. Mueller, R. Houwink, Chemie und technologie der kunststoffe, Leipzig (1942).
[112] B.C. Pak, Y.I. Cho, Hydrodynamic and heat transfer study of dispersed fluids with submicron metallic oxide particles, Experimental Heat Transfer 11 (1998) 151–170.
[113] X.F. Li, D.S. Zhu, X.J. Wang, N. Wang, J.W. Gao, H. Li, Thermal conductivity enhancement dependent pH and chemical surfactant for Cu–H_2O nanofluids, Ther. Acta 469 (2008) 98–103.
[114] H. Younes, G. Christensen, X. Luan, H. Hong, P. Smith, Effects of alignment, pH, surfactant, and solvent on heat transfer nanofluids containing Fe_2O_3 and CuO nanoparticles, Journal of Applied Physics 111 (2012) 064308.
[115] C.T. Wamkam, M.K. Opoku, H. Hong, P. Smith, Effects of pH on heat transfer nanofluids containing ZrO_2 and TiO_2 nanoparticles, Journal of Applied Physics 109 (2011) 024305.
[116] R.S. Khedkar, S.S. Sonawane, K.L. Wasewar, Influence of CuO nanoparticles in enhancing the thermal conductivity of water and monoethylene glycol based nanofluids, International Communications in Heat and Mass Transfer 39 (2012) 665–669.
[117] B. Ruan, A.M. Jacobi, Ultrasonication effects on thermal and rheological properties of carbon nanotube suspensions, Nanoscale Research Letters 127 (2012) 1–14.

[118] B. LotfizadehDehkordi, A. Ghadimi, H.S.C. Metselaar, Box–Behnken experimental design for investigation of stability and thermal conductivity of TiO_2 nanofluids, Journal of Nanoparticle Research 15 (2013) 1369.
[119] T.K. Hong, H.S. Yang, Nanoparticle dispersion dependent thermal conductivity in nanofluids, Journal of the Korean Physical Society 47 (2005) S321–S324.
[120] Y.S. Ju, J. Kim, M.T. Hung, Experimental study of heat conduction in aqueous suspensions of aluminum oxide nanoparticles, Journal of Heat Transfer 130 (2008) 092403 (1–6).
[121] B. Buonomo, O. Manca, L. Marinelli, S. Nardini, Effect of temperature and sonication time on nanofluid thermal conductivity measurements by nano–flash method, Applied Thermal Engineering 91 (2015) 181–190.
[122] I.M. Mahbubul, I.M. Shahrul, S.S. Khaleduzzaman, R. Saidur, M.A. Amalina, A. Turgut, Experimental investigation on effect of ultrasonication duration on colloidal dispersion and thermophysical properties of alumina–water nanofluid, International Journal of Heat and Mass Transfer 88 (2015) 73–81.
[123] M. Kole, T.K. Dey, Effect of prolonged ultrasonication on the thermal conductivity of ZnO–ethylene glycol nanofluids, Thermochimica Acta 535 (2012) 58– 65.
[124] J.C. Yang, F.C. Li, W.W. Zhou, Y.R. He, B.C. Jiang, Experimental investigation on the thermal conductivity and shear viscosity of viscoelastic-fluid-based nanofluids, International Journal of Heat and Mass Transfer 55 (2012) 3160–3166.
[125] E.V. Timofeeva, J.L. Routbort, D. Singh, Particle shape effects on thermophysical properties of alumina nanofluids, Journal of Applied Physics 106 (2009) 014304.
[126] K. Sinha, B. Kavlicoglu, Y. Liu, F. Gordaninejad, O.A. Graeve, A comparative study of thermal behavior of iron and copper nanofluids, Journal of Applied Physics 106 (2009) 064307.
[127] C. Pang, J.Y. Jung, J.W. Lee, Y.T. Kang, Thermal conductivity measurement of methanol based nanofluids with Al_2O_3 and SiO_2 nanoparticles, International Journal of Heat and Mass Transfer 55 (2012) 5597–5602.
[128] P.D. Shima, J. Philip, Role of Thermal Conductivity of Dispersed Nanoparticles on Heat Transfer Properties of Nanofluid, Ind. Engineering Chemical Research 53 (2014) 980–988.
[129] S.P. Jang, S.U.S. Choi, Role of Brownian motion in the enhanced thermal conductivity of nanofluids, Applied Physics Letter 84 (21) (2004) 4316-4318.
[130] R. Prasher, P. Bhattacharya, P.E. Phelan, Brownian motion–based convective conductive model for the effective thermal conductivity of nanofluids, Jou. of Heat Transfer 128 (2006) 588–595.
[131] D.A.G. Bruggeman, Berechnung verschiedener physikalischer Konstanten von heterogenen Substanzen, I. Dielektrizitatskonstanten und Leitfahigkeiten der Mischkorper aus isotropen Substanzen, Annalen der Physik, (Leipz) 24 (1935) 636–679.
[132] R.L. Hamilton, O.K. Crosser, Thermal conductivity of heterogeneous two component systems, Industrial and Engineering Chemistry Fundamentals 1 (1962) 187–191.
[133] E.J. Wasp, J.P. Kenny, R.L. Gandhi Solid–liquid flow: slurry pipe line transportation (Pumps, valves, mechanical equipment, economics) Bulk Materials Handling, Trans Tech Publication 1 (1977) 224.
[134] W. Yu, S.U.S. Choi, The role of interfacial layers in the enhanced thermal conductivity of nanofluids: a renovated Maxwell model, Journal of Nanoparticle Research 5 (2003) 167–171.
[135] Y. Xuan, Q. Li, W. Hu, Aggregation structure and thermal conductivity of nanofluids, AIChE Journal 49 (2003) 1038–1043.
[136] J. Koo, C. Kleinstreuer, A new thermal conductivity model for nanofluids, Journal of Nanoparticle Research 6 (2004) 577–588.

[137] Q. Xue, W.M. Xu, A model of thermal conductivity of nanofluids with interfacial shells, Material Chemical Physics 90 (2005) 298–301.
[138] D.H. Kumar, H.E. Patel, V.R.R. Kumar, T. Sundararajan, T. Pradeep, S.K. Das, Model for Heat Conduction in Nanofluids, Physical Review Letters 93 (2004) 144301.
[139] K.C. Leong, C. Yang, S.M.S. Murshed, A Model for the Thermal Conductivity of Nanofluids–The Effect of Interfacial Layer, Journal of Nanoparticle Research 8 (2006) 245–254.
[140] H. Xie, M. Fujii, X. Zhang, Effect of interfacial nanolayer on the effective thermal conductivity of nanoparticle–fluid mixture, Int. Journal of Heat and Mass Transfer 48 (2005) 2926–2932.
[141] E. Yamada, T. Ota, Effective thermal conductivity of dispersed materials, Heat and Mass Transfer 13 (1980) 27–37.
[142] D.P.H. Hesselman, L.F. Johnson, Effective thermal conductivity of nanocomposites with interfacial thermal barrier resistance, Journal of Composite Material 21 (1987) 508–515.
[143] B.X. Wang, L.P. Zhou, X.F. Peng, A fractal model for predicting the effective thermal conductivity of liquid with suspension of nanoparticles, International Journal of Heat and Mass Transfer 46 (2003) 2665–2672.
[144] M. Corcione, Empirical correlating equations for predicting the effective thermal conductivity and dynamic viscosity of nanofluids, Energy Conversion and Management 52 (2011) 789–793.
[145] R.K. Shukla V.K. Dhir, Effect of Brownian Motion on Thermal Conductivity of Nanofluids, Journal of Heat Transfer Copyright, (2008) ASME 130 / 042406 (1-13).
[146] S.E.B. Maiga, C.T. Nguyen, N. Galanis, G. Roy, Heat transfer behaviors of nanofluids in a uniformly heated tube, Superlattices Microstructure 35 (2004) 543–557.
[147] L.M. Schwartz, E.J. Garboczi, D.P.Bentz, Interfacial transport in porous media: Application to dc electrical conductivity of mortars, Journal of Applied Physics 78 (1995) 5898–5908.
[148] H.E. Patel, T. Sundararajan, T. Pradeep, A. Dasgupta, N. Dasgupta, S.K. Das, A micro–convection model for thermal conductivity of nanofluids, Pra. J. of physics 65 (2005) 863–869.
[149] W.H. Azmi, K.V. Sharma, R. Mamat, A.B.S. Alias, I. Izwan Misnon, Correlations for thermal conductivity and viscosity of water-based nanofluids, IOP Conference Series: Materials Science and Engineering 36 (2012) 1–6.
[150] J. Buongiorno, Convective Transport in Nanofluids, J. of Heat Transfer 128 (2006) 240–250.
[151] G. Cheraghian, L. Hendraningra, A review on applications of nanotechnology in the enhanced oil recovery part B: effects of nanoparticles on flooding, Inter. Nano Letters 6 (2016) 1–10.
[152] J. Chevalier, O. Tillement, F. Ayela, Rheological Properties of Nanofluids Flowing Through Microchannels, Applied Physics Letters 91 (2007) 233103 1–3.
[153] C.T. Nguyen, F. Desgranges, N. Galanis, G. Roy, T. Mare, S. Boucher, H.A. Mintsa, Viscosity data for Al_2O_3–water nanofluid–hysteresis: is heat transfer enhancement using nanofluids reliable?, International Journal of Thermal Science 47 (2008) 103–111.
[154] K.B. Anoop, T Sundararajan, S.K. Das, Effect of particle size on the convective heat transfer in nanofluid in the developing region, Int J Heat Mass Transfer 52 (9–10) (2009) 2189–2195.
[155] A.J. Schmidt, et al., Experimental investigation of nanofluid shear and longitudinal viscosities, Applied Physics Letter 92 (24) (2008) 244107.
[156] M. Hojjat, et al., Rheological characteristics of non–Newtonian nanofluids: experimental investigation, Int. Communication of Heat and Mass Transfer 38(2) (2011) 144–148.
[157] A. Turgut, I. Tavman, M. Chirtoc, H.P. Schuchmann, C. Sauter, S. Tavman, Thermal conductivity and viscosity measurements of water-based TiO_2–nanofluids, International Journal of Thermophysics, 30 (2009) 1213–1226.

[158] S. Bobbo, L. Fedele, A. Benetti, L. Colla, M. Fabrizio, C. Pagura, S. Barison, Viscosity of water-based SWCNH and TiO_2 nanofluids, Exp. Thermal and Fluid Science 36 (2012) 65–71.
[159] M. Jarahnejad, E.B. Haghighi, M. Saleemi, N. Nikkam, R. Khodabandeh, B. Palm, M.S. Toprak, M. Muhammed, Experimental investigation on viscosity of water–based Al_2O_3 and TiO_2 nanofluids, Rheological Acta 54 (2015) 411–422.
[160] T. Yiamsawas, O. Mahian, A.S. Dalkilic, S. Kaewnai, S. Wongwises, Experimental studies on the viscosity of TiO_2 and Al_2O_3 nanoparticles suspended in a mixture of ethylene glycol and water for high temperature applications, Applied Energy 111 (2013) 40–45.
[161] M.D. Chadwick, J.W. Goodwin, B. Vincent, E.J. Lawson, P.D. Mills, A Rheological behaviour of titanium dioxide (uncoated anatase) in ethylene glycol, Colloid. Surf. A 196 (2002) 235–245.
[162] W.J. Tseng, K.C. Lin, Rheology and colloidal structure of aqueous TiO_2 nanoparticle suspensions, Material Science Engineering A 355 (2003) 186–192.
[163] Y. Raja Sekhara, K.V. Sharma, Study of viscosity and specific heat capacity characteristics of water–based Al_2O_3 nanofluids at low particle concentrations, Journal of Experimental Nanoscience 10 (2) (2015) 86-102.
[164] B.C. Sahoo, R.S. Vajjha, R. Ganguli, G.A. Chukwu, D.K. Das, Determination of Rheological Behaviour of Aluminium Oxide Nanofluid and Development of New Viscosity Correlations, Petroleum Science and Technology 27 (2009) 1757–1770.
[165] H. Chen, Y. Ding, Y. He, C. Tan, Rheological Behaviour of Ethylene Glycol Based Titania Nanofluids, Chemical Physics Letters 444 (2007) 333–337.
[166] C.T. Nguyen, F. Desgranges, G. Roy, N. Galanis, T. Mare, S. Boucher, H.A. Mintsa, Temperature and particle-size dependent viscosity data for water-based nanofluids–Hysteresis phenomenon, International Journal of Heat and Fluid Flow 28 (6) (2007) 1492–1506.
[167] P.K. Namburu, D.P. Kulkarni, A. Dandekar, D.K. Das, Experimental investigation of viscosity and specific heat of silicon dioxide nanofluids, Micro Nano Letter 2 (2007) 67–71.
[168] W.Q. Lu, Q.M. Fan, Study for the particle's scale effect on some thermophysical properties of nanofluids by a simplified molecular dynamics method, Engineering Analysis with Boundary Elements 32 (2008) 282–289.
[169] W. Yu, H. Xie, A review on nanofluids: preparation, stability mechanisms, and applications, Journal of Nanomaterials. (2012) 435873.
[170] M. Drzazga, A. Gierczycki, G. Dzido, M. Lemanowicz, Influence of nonionic surfactant addition on drag reduction of water-based nanofluid in a small diameter pipe, Chinese Journal of Chemical Engineering 21(1) (2013) 104–108.
[171] Y.H. Hung, C. Wen–Chieh, Chitosan for suspension performance and viscosity of MWCNTs, International Journal of Chemical Engineering 3 (5) (2012) 347–353.
[172] A. Ghadimi, R. Saidur, H.S.C. Metselaar, A review of nanofluid stability properties and characterization in stationary conditions, International Journal of Heat and Mass Transfer 54 (17–18) (2011) 4051–4068.
[173] S.A. Adio, M. Sharifpur, J.P. Meyer, Influence of ultrasonication energy on the dispersion consistency of Al_2O_3−glycerol nanofluid based on viscosity data, and model development for the required ultrasonication energy, Jou. of Experimental Nanoscience 11 (8) (2016) 630−649.
[174] I.M. Mahbubul, T.H. Chong, S.S. Khaleduzzaman, I.M. Shahrul, R. Saidur, B.D. Long, M.A. Amalina, Effect of Ultrasonication Duration on Colloidal Structure and Viscosity of Alumina−Water Nanofluid, Ind. & Engineering Chemistry Research 53 (2014) 6677−6684.
[175] E.K. Goharshadi, et al.: Nanofluids for heat transfer enhancement−a review, Phys. Chem. Res 1 (1) (2009) 1–33.

[176] B. Aladag, S. Halelfadl, N. Doner, T. Mare, S. Duret, P. Estelle, S. Haleifadl, Experimental Investigations of the Viscosity of Nanofluids at Low Temperatures, Applied energy 97 (2012) 876–880.
[177] P.K. Namburu, et al.: Viscosity of copper oxide nanoparticles dispersed in ethylene glycol and water mixture, Experimental Thermal Fluid Science 32(2) (2007) 397–402.
[178] I.M. Mahbubul, S.S. Khaleduzzaman, R. Saidur, M.A. Amalina, Rheological Behavior of Al_2O_3/R141b Nano−refrigerant, Int. Journal of Heat and Mass Transfer 73 (2014) 118–123.
[179] W.R. Richmond, R.L. Jones, P.D. Fawell, The relationship between particle aggregation and rheology in mixed silica–titania suspensions, Chemical Engineering Journal 71 (1998) 67–75.
[180] V. Penkavova, J. Tihon, O. Wein, Stability and rheology of dilute TiO_2−water nanofluids, Nanoscale Research Letters 6 273 (2011).
[181] W.J. Tseng, C.H. Wu, Aggregation, rheology and electrophoretic packing structure of aqueous Al_2O_3 nanoparticle suspensions, Acta Material 50 (2002) 3757–3766.
[182] M.H. Esfe, H. Rostamian, Non−Newtonian power−law behavior of TiO_2/SAE 50 nano−lubricant: An experimental report and new correlation, Journal of Molecular Liquids 232 (2017) 219–225.
[183] A. Einstein, A new determination of molecular dimensions, Ann. Physics 19 (1906) 289–306.
[184] G.I. Taylor, The Viscosity of a Fluid Containing Small Drops of Another Fluid, Proceedings of the Royal Society 138 834 (1932) 41–48.
[185] H.C. Brinkman, The viscosity of concentrated suspensions and solution, Journal of Chemical Physics 20 (1952) 571–581.
[186] N. Frankel, A. Acrivos, On the Viscosity of a Concentrated Suspension of Solid Spheres, Chemical Engineering Science 22 (1967) 847–853.
[187] A.L. Graham, On the viscosity of suspensions of solid spheres, Applied Scientific Research 37 (3–4) (1981) 275–286.
[188] W.H. Azmi, K.V. Sharma, R. Mamat, A.B.S. Alias, I. I. Misnon, Correlations for Thermal Conductivity and Viscosity of Water-based Nanofluids, IOP Conference Series: Materials Science and Engineering 36 (2012) 012029.
[189] K. Khanafer, K. Vafai, A Critical Synthesis of Thermophysical Characteristics of Nanofluids, International Journal of Heat and Mass Transfer 54 19–20 (2011) 4410–4428.
[190] S. Hosseini, A. Moghadassi, D.E. Henneke, A New Dimensionless Group Model for Determining the Viscosity of Nanofluids, Jou. of Ther. Analysis and Cal. 100 (2010) 873–877.
[191] M. Corcione, Empirical correlating equations for predicting the effective thermal conductivity and dynamic viscosity of nanofluids, Energy Conversion and Manag. 52 1 (2011) 789–793.
[192] K.V. Sharma, P.K. Sharma, W.H. Azmi, R. Mamat, K. Kadirgama, Correlations to predict friction and forced convection heat transfer coefficients of water-based nanofluids for turbulent flow in a tube, Int. J Mic. Nanoscale Thermal Fluid Transport Phenomenon, 3 (2012) 1–25.
[193] Y.R. Sekhar, K.V. Sharma, Study of Viscosity and Specific Heat Capacity Characteristics of Water–Based Al_2O_3 Nanofluids at Low Particle Concentrations, Journal of Experimental Nanoscience 1–17 (2013).
[194] E. Abu–Nada, Effects of variable viscosity and thermal conductivity of Al_2O_3–water nanofluid on heat transfer enhancement in natural convection, International Journal of Heat Fluid Flow 30 (4) (2009) 679–690.
[195] M. Mooney, The viscosity of a Concentrated Suspension of Spherical Particles, Journal of Colloid Science113 (1951) 3–4.

[196] S. Ward, R. Whitmore, Studies of the Viscosity and Sedimentation of Suspensions Part 1, The Viscosity of Suspension of Spherical Particles, Brit. Jou. of Appl. Physics 286 (1950) 1–6.
[197] G.K. Batchelor, The effect of Brownian motion on the bulk stress in a suspension of spherical particles, Journal of Fluid Mechanics 83 (1977) 97–117.
[198] N. Saito, Concentration Dependence of the Viscosity of High Polymer Solution, Journal of the Physical Society of Japan 5 (1950) 4–8.
[199] F. Booth, The Electroviscous Effect for Suspensions of Solid Spherical Particles, Proceedings of the Royal Society A: Mathematical Physical and Engg. Science 203 1075 (1950) 533–551.
[200] I.M. Krieger, A mechanism for non-Newtonian flow in suspensions of rigid spheres, Transactions of the Society of Rheology 3 (1959) 137.
[201] T.S. Lundgren, Slow flow through stationary random beds and suspensions of spheres, Journal of Fluid Mechanics 51 (02) (1972) 273–299.
[202] C.U. Thomas, M. Muthukumar, Three–Body Hydrodynamic Effects on Viscosity of suspensions of Spheres, Journal of Chemical Physics 94 7 (1991) 5180.
[203] V. Vand, Viscosity of Solutions and Suspensions I. Theory, J. of Physical Che. (1948) 277–299.
[204] R. Roscoe, The Viscosity of Suspensions of Rigid Spheres, Jou. of App. Phys. 267 (1952) 3–6.
[205] T. Kitano, T. Kataoka, T. Shirota, An empirical equation of the relative viscosity of polymer melts filled with various inorganic fillers, Rheologica Acta 20 (2) (1981) 207–209.
[206] J. Bicerano, J.F. Douglas, D.A. Brune, Model for the viscosity of particle dispersions, Journal of Macromol. Science 39(4) (1999) 561–642.
[207] W.J. Tseng, C.N. Chen, Effect of polymeric dispersant on rheological behavior of nickel–terpineol suspensions, Material Science Engineering A 347(1) (2003) 145–153.
[208] H. De Bruijin, The viscosity of suspensions of spherical particles (the fundamental η–c and φ relations), Recueil des Travaux Chimiques des Pays–Bas 61 12 (1942) 863–874.
[209] S. Song, C. Peng, A.M. Gonzalez-Olivares, A. Lopez–Valdivieso, T. Fort, Study on hydration layers near nanoscale silica dispersed in aqueous solutions through viscosity measurement, Journal of Colloid Interface Science 287 (2005) 114–120.
[210] H. Chen, Y. Ding, C. Tan, Rheological behaviour of nanofluids, New J. Phys. 9(10) 367 (2007).
[211] N. Masoumi, N. Sohrabi, A. Behzadmehr, A new model for calculating the effective viscosity of nanofluids, Journal of Physics D: Applied Physics 42(5) (2009) 055501.
[212] S.E.B. Maiga, S.J. Palm, C.T. Nguyen, G. Roy, N. Galanis, Heat transfer enhancement by using nanofluids in forced convection flows, Int. Journal of Heat Fluid Flow 26 (2005) 530–546.
[213] C.T. Nguyen *et al.*:, Temperature and particle-size dependent viscosity data for water–based nanofluids–hysteresis phenomenon, Int. Journal of Heat Fluid Flow 28(6) (2007) 1492–1506.
[214] L.E. Nielsen, Generalized equation for the elastic moduli of composite materials, Journal of Applied Physics 41 (11) (1970) 4626–4627.
[215] M.V. Smoluchowski, Theoretishche Bemerkungen uber die Viskositat der Kolloide, Kolloidzschr 80 (1916) 190–195.
[216] D.P. Kulkarni, D.K. Das, G.A. Chukwu, Temperature dependent rheological property of copper oxide nanoparticles suspension (nanofluid), J. Nanosci Nanotechnology 6(4) (2006) 1150–1154.
[217] R. Prasher, P. Bhattacharya, P.E. Phelan, Brownian motion Based Convective Conductive Model for the Effective Thermal Conductivity of Nanofluids, Journal of Heat Transfer 128 6 (2006) 588–595.
[218] M.N. Rashin, J. Hemalatha, Viscosity Studies on Novel Copper Oxide–Coconut Oil Nanofluid, Experimental Thermal and Fluid Science, 48 (2013) 67–72.

[219] M.M.M. Heyhat et. al., Experimental Investigation of Laminar Convective Heat Transfer and Pressure Drop of Water–Based Al_2O_3 Nanofluids in Fully Developed Flow Regime, Experimental Thermal and Fluid Science 44 (2013) 483–489.
[220] K.S. Suganthi, K.S. Rajan, Temperature Induced Changes in ZnO–Water Nanofluid: Zeta Potential Size Distribution and Viscosity Profiles, International Journal of Heat and Mass Transfer 55 25–26 (2012) 7969–7980.
[221] K. Suganthi, N. Anusha, K. Rajan, Low Viscous ZnO–Propylene Glycol Nanofluid: A Potential Coolant Candidate, Journal of Nanoparticle Research 15 1986 (2013) 1–6.
[222] D. Singh, E. Timofeeva, W. Yu, J. Routbort, D. France, D. Smith, J.M. Lopez–Cepero, An Investigation of Silicon Carbide–Water Nanofluid for Heat Transfer Applications, Journal of Applied Physics 105 6 (2009) 064306.
[223] T. Yiamsawas, A.S. Dalkilic, O. Mahian, S. Wongwises, Measurement and Correlation of the Viscosity of Water–Based Al_2O_3 and TiO_2 Nanofluids in High Temperatures and Comparisons With Literature Reports, Jou. of Dispersion Science and Technology 34 12 (2013) 1697–1703.
[224] M. Hemmat Esfe, S. Saedodin, An Experimental Investigation and New Correlation of Viscosity of ZnO–EG Nanofluid at Various Temperatures and Different Solid Volume Fractions, Experimental Thermal and Fluid Science, 55 (2014) 1–5.
[225] W.J. Tseng, K. Lin, Rheology and Colloidal Structure of Aqueous TiO_2 Nanoparticle Suspensions, Materials Science and Engineering: A 355 (2003) 186–192.
[226] W. Duangthongsuk, S. Wongwises, Measurement of Temperature–Dependent Thermal Conductivity and Viscosity of TiO_2–Water Nanofluids, Experimental Thermal and Fluid Science 33 4 (2009) 706–714.
[227] M. Kole, T.K. Dey, Thermal conductivity and viscosity of Al_2O_3 nanofluid based on car engine coolant, Journal of Physics D: Applied Physics 43 (2010) 315501.
[228] M. Kole, T.K. Dey, Effect of Aggregation on the Viscosity of Copper Oxide–Gear Oil Nanofluids, International Journal of Thermal Sciences 50 9 (2011) 1741–1747.
[229] H. Chen, Y. Ding, Y. He, C. Tan, Rheological Behaviour of Ethylene Glycol Based Titania Nanofluids, Chemical Physics Letters 444 (2007) 333–337.
[230] A.D. Noni, D.E. Garcia, D. Hotza, A modified model for the viscosity of ceramic suspensions, Ceram International 28 (2002) 731–735.
[231] M. Chandrasekar, S. Suresh, A.C. Bose, Experimental Investigations and Theoretical Determination of Thermal Conductivity and Viscosity of Al_2O_3/Water Nanofluid, Experimental Thermal and Fluid Science 34 2 (2010) 210–216.
[232] A. Hernandez Battez, J.L. Viesca, R. Gonzalez, A. Garcia, T. Reddyhoff, A. Higuera–Garrido, Effect of Shear Rate, Temperature, and Particle Concentration on the Rheological Properties of ZnO and ZrO_2 Nanofluids, Tribology Transactions 57 3 (2014) 489–495.
[233] A.I. Morgan, L.A. Bromley, C.R. Wilke, Effect of Surface tension on Heat Transfer in Boiling, Industrial and Engineering Chemistry 41 12 (1949) 2767–2769.
[234] Y.M. Yang, J.R. Maa, Pool Boiling of Dilute Surfactant Solutions, ASME Journal of Heat Transfer 105 (1983) 190–192.
[235] S.J. Kim, I.C. Bang, J. Buongiorno, L.W. Hu, Surface wettability change during pool boiling of nanofluids and its effect on critical heat flux, International Journal of Heat and Mass Transfer 50 (19–20) (2007) 4105–4116.
[236] B. Suleimanov, F.S. Ismalov, E.F. Veliyev, Nanofluid for enhanced oil recovery, Journal of Petroleum Science and Engineering, 78 (2011) 431–437.

[237] F. Ravera, E. Santini, G. Loglio, M. Ferrari, L. Liggieri, Effect of Nanoparticles on the Interfacial Properties of Liquid/Liquid and Liquid/Air Surface Layers, The Journal of Physical Chemistry B 110 (2006) 19543–19551.
[238] B–j. Zhu, W–l. Zhao, J–k. Li , Y–x. Guand, D–d. Li, Thermophysical Properties of Al_2O_3–Water Nanofluids, Materials Science Forum 688 (2011) 266–271.
[239] M. Radiom, C. Yang, W.K. Chan, Characterization of surface tension and contact angle of nanofluids, Fourth International Conference on Experimental Mechanics (2009) 75221 D–1.
[240] J. Chinnam, D.K. Das, R.S. Vajjha, J.R. Satti, Measurements of the surface tension of nanofluids and development of a new correlation, Int. J. of Thermal Sciences 98 (2015) 68–80.
[241] S. Vafaei, A. Purkayastha, A. Jain, G. Ramanath, T.B. Tasciuc, The effect of nanoparticles on the liquid–gas surface tension of Bi_2Te_3 nanofluids, Journal of Colloid Interface Science 20 (185702) (2009) 1–6.
[242] M. Moosavi, E.K. Goharshadi, A. Youssef, Fabrication, characterization, and measurement of some physicochemical properties of ZnO nanofluids, International Journal of Heat and Fluid Flow 31 (2010) 599–605.
[243] M.N. Golubovic, H.D. Madhawa Hettiarachchi, W.M. Worek, W.J. Minkowycz, Nanofluids and critical heat flux, experimental and analytical study, Applied Thermal Engineering 29 (2009) 1281–1288.
[244] S. Tanvir, L. Qiao, Surface tension of Nanofluid–type fuels containing suspended nanomaterials, Nanoscale Research Letters 7 226 (2012).
[245] M. Moosavi, E.K. Goharshadi, A. Youssef, Fabrication characterization and measurement of some physicochemical properties of ZnO nanofluids, International Journal of Heat and Fluid Flow 31 (2010) 599–605.
[246] S.S. Khaleduzzaman, I.M. Mahbubul, I.M. Shahrul, R. Saidur, Effect of particle concentration temperature and surfactant on surface tension of nanofluids, International Communications in Heat and Mass Transfer 49 (2013) 110–114.
[247] Z. Yu, Y. Ge, L.S. Fan, Multi–scale Simulation of Oblique Collisions of a Droplet on a Surface in the Leidenfrost Regime, Chemical Engineering Science 62 3462 (2007).
[248] S.R. Werner, J.R. Jones, A.H. Paterson, R.H. Archer, D.L. Pearce, Droplet Impact and Spreading: Droplet Formation Effects, Chemical Engineering Science 62 2336 (2007).
[249] Y. Gu, Drop Size Dependence of Contact Angles of Oil Drops on a Solid Surface in Water, Colloids Surface A 181 215 (2001).
[250] Y.S. Joung, C.R. Buie, Scaling Laws for Drop Impingement on Porous Films and Papers, Physics Review E 89 013015 (2014).
[251] J.H. Clint, S.E Taylor, Particle Size and Interparticle Forces of Overbased Detergents–A Langmuir trough Study, Colloids Surface 65 61 (1992).
[252] J.H. Clint, N. Quirke, Contact Angles on Particles from Langmuir through Studies, Colloids Surface A 78 277 (1993).
[253] M. Peuss, H.J. Butt, Measuring the Contact Angle of Individual Colloid Particles, Journal of Colloid Interface Science 208 468 (1998).
[254] R. Mohammadi, A. Amirfazli, Contact Angle Measurement for Dispersed Microspheres using Scanning Confocal Microscopy, Journal of Dispersion Science and Technology 25 567 (2004).
[255] F.S. Javadi, R. Saidur, M. Kamalisarvestani, Investigating performance improvement of solar collectors by using nanofluids, Renewable and Sustain. Energy Rev. 28 (2013) 232–245.

[256] T. Yousefi, F. Veysi, E. Shojaeizadeh, S. Zinadini, An experimental investigation on the effect of Al_2O_3–H_2O nanofluid on the efficiency of flat–plate solar collectors, Renewable Energy 39 (2012) 293–298.
[257] H. Tyagi, P. Phelan, R. Prasher, Predicted efficiency of nanofluid–based direct absorption solar receiver, Journal of Solar Energy ASME 131 (2009).
[258] Z. Luo, C. Wang, W. Wei, G. Xiao, M. Ni, Performance improvement of a nanofluid solar collector based on direct absorption collection (DAC) concepts, International Journal of Heat and Mass Transfer 75 (2014) 262–271.
[259] A. Moradi, E. Sani, M. Simonetti, F. Francini, E. Chiavazzo, P. Asinari, Carbon nanohorn based nanofluids for a direct absorption solar collector for civil application, Journal of Nanoscience Nanotechnology 15 (2015) 3488–3495.
[260] R. Sadeghi, S.G. Etemad, E. Keshavarzi, M. Haghshenasfard, Investigation of alumina nanofluid stability by UV–vis spectrum, Microfluid Nanofluid 18 (2015) 1023–1030.
[261] T.G.F. Souza, V.S.T. Ciminelli, N.D.S. Mohallem, A comparison of TEM and DLS methods to characterize size distribution of ceramic nanoparticles, Journal of Physics: Conference Series 733 (2016) 012039 (1–5).
[262] C. Nickel, et. al., Dynamic light–scattering measurement comparability of nanomaterial suspensions, Journal of Nanoparticle Research 16 (2014) 2260 (1–12).
[263] R.F. Domingos, M.A. Baalousha, Y. J–Nam, M.M. Reid, N. Tufenkji, J.R. Lead, K.J. Wilkinson, Characterizing manufactured nanoparticles in the environment: Multi method determination of particle sizes, Environment Science and Technology 43 (2009) 7277–7284.
[264] M. Filella, J. Zhang, M.E. Newman, J. Buffle, Analytical applications of photon correlation spectroscopy for size distribution measurements of natural colloidal suspensions: capabilities and limitations, Colloids Surfaces A 120 (1997) 27–46.
[265] H. Fissan, S. Ristig, H. Kaminski, C. Asbach, M. Epple, Comparison of different characterization methods for nanoparticle dispersions before and after aerosolization, Analytical Methods 6 (2014) 7324–7334.
[266] M. Kaszuba, J. Corbett, F.M. Watson, A. Jones, High–concentration zeta potential measurements using light–scattering techniques, Philos. Transact.A Math. Physics Engineering Science 368 (2010) 4439–4451.
[267] C. Allain, M. Cloitie, M. Wafra, Aggregation and Sedimentation in Colloidal Suspensions, Physical Review Letters 74 (1995) 1478–1481.
[268] R. Choudhary, D. Khurana, A. Kumar, S. Subudhi, Stability analysis of Al_2O_3/water nanofluids, Journal of Experimental Nanoscience (2017) 1285445.
[269] J.P. Holman, Experimental methods for engineers, 5th edit., McGraw–Hill Book Com. (1989).
[270] G.G. Anil kumar, D.N. Ronald, The Effect of Wettability of Wilhelmy Plate and Du Nouy Ring on Interfacial Tension Measurements in Solvent Extraction Systems, Journal of Colloid and Interface Science 98 1 (1984).
[271] K. Lunkenheimer, K.D. Wantke, Determination of the surface tension of surfactant solutions applying the method of Lecomte du Nouy (ring tensiometer), Colloid and Polymer Science 259 (1981) 354-366.
[272] S.M.S. Murshed, K.C. Leong, C. Yang, Thermophysical and electrokinetic properties of nanofluids – A critical review, Applied Thermal Engineering 28 (2008) 2109–2125.
[273] I. Tavman and A. Turgut, An investigation on thermal conductivity and viscosity of water-based nanofluids, Microfluidics Based Microsystems: Fund. and Applications (2010) 139–162.

[274] R. Sadri, G. Ahmadi, H. Togun, M. Dahari, S.N. Kazi, E. Sadeghinezhad, N. Zubir, An experimental study on thermal conductivity and viscosity of nanofluids containing carbon, Nanoscale Research Letters 9 151 (2014).
[275] H. Fissan, S. Ristig, H. Kaminski, C. Asbach, M. Epple, Comparison of different characterization methods for nanoparticle dispersions before and after aerosolization, Analytical Methods 6 (2014) 7324–7334.
[276] N.B. Vergaftik, Handbook of Physical Properties of Liquids and Gases, Springer (1975).
[277] Li Yu–Hua, Qu Wei and F. Jian–Chao, Temperature Dependence of Thermal Conductivity of Nanofluids, Chinese Physics Letter 25 (9) (2008) 3319.
[278] M. Zhou, G. Xia, J. Li, L. Chai, L. Zhou, Analysis of factors influencing thermal conductivity and viscosity in different kinds of surfactant solutions, Experimental Thermal and Fluid Science 36 (2012) 22–29.
[279] R.G. Laughlin, The Aqueous Phase Behavior of Surfactants, Academic Press, (1994).
[280] H.M. Vale, and T.F. McKenna, Adsorption of sodium dodecyl sulfate and sodium dodecyl benzenesulfonate on poly (vinyl chloride) latexes, Colloids and Surfaces A: Physicochemical and Engineering Aspects 268 (2005) 68–72.
[281] J. Bender, N.J. Wagner, Optical measurement of the contribution of colloidal forces to the rheology of concentrated suspensions, Jou. of Colloid and Inter. Science 172 (1995) 171-184.
[282] B.J. Maranzano, N.J. Wagner, The effects of interparticle interactions and particle size on reversible shear thickening Hard sphere colloidal dispersions, Journal of Rheology 45 (2001) 1205–1222.
[283] N.J. Wagner, J. F. Brady, Shear thickening in colloidal dispersions, Phy.Tod. 62 (2009) 27–32.
[284] I.M. Mahbubul, R. Saidur, M.A. Amalina, M.E. Niza, Influence of ultrasonication duration on rheological properties of nanofluid: An experimental study with alumina–water nanofluid, International Communications in Heat and Mass Transfer, 76 (2016) 33–40
[285] R.G. Chaudhuri, S. Paria, The wettability of PTFE and glass surfaces by nanofluids, Journal of Colloid and Interface Science, 434 (2014) 141–151.
[286] V.P. Carey, Liquid-Vapor Phase–Change Phenomena, 2nd edition Hemisphere Publishing Corporation New York (2008).
[287] D. Quere, Capillarity and Wetting Phenomena: Drops, Bubbles, Pearls, Waves, Françoise Brochard-Wyart, and Pierre-Gilles de Gennes,
[288] S. Vafaei, D. Wen, T. Borca–Tasciuc, Nanofluid Surface Wettability through Asymptotic Contact Angle, American Chemical Society 27 (6) (2011) 2211–2218.
[289] K. Sefiane, J. Skilling, J. MacGillivray, Contact line motion and dynamic wetting of nanofluid solutions, Advances in Colloid and Interface Science 138 101 (2008).
[290] J.S. Coursey, J. Kim, Nanofluid boiling: The effect of surface wettability, International Journal of Heat and Fluid Flow 29 (2008) 1577–1585.
[291] R. Choudhary, D. Khurana, A. Kumar, S. Subudhi, Stability analysis of Al_2O_3/water nanofluids Journal of Experimental Nanoscience (2017) 1285445.
[292] J.D. Hem, Study and interpretations of the chemical characteristics of natural water. U.S. Geological Survey Water Supply Paper 2254 (1985) 1-263.
[293] N. Zhao, J. Yang, H. Li, Z. Zhang, S. Li, Numerical investigations of laminar heat transfer and flow performance of Al_2O_3–water nanofluids in a flat tube International Journal of Heat and Mass Transfer 92 (2016) 268–282.

[294] Z. Yari Ghale, M. Haghshenasfard, M. Nasr Esfahany, Investigation of nanofluids heat transfer in a ribbed microchannel heat sink using single-phase and multiphase CFD models, International Communications in Heat and Mass Transfer 68 (2015) 122–129.
[295] E. Manay, B. Sahin, M. Yilmaz, K. Gelis, Thermal performance analysis of nanofluids in microchannel heat sinks, World Academy of Science, Eng. Technol. 67 (2012).
[296] M. Kalteh, A. Abbassi, M. Saffar-Avvala, J. Harting, Eulerian – Eulerian two phase numerical simulation of nanofluid laminar forced convection in a microchannel, Int. J. Heat Fluid Flow 32 (2011) 107–116.
[297] M. K. Moraveji and E. Esmaeili, "Comparison between single-phase and two-phases CFD modeling of laminar forced convection flow of nanofluids in a circular tube under constant heat flux." International Communications in Heat and Mass Transfer 39, 1297–1302, 2012.
[298] E. Ebrahimnia-Bajestan, H. Niazmand, W. Duangthongsuk, S. Wongwises Numerical investigation of effective parameters in convective heat transfer of nanofluids flowing under a laminar flow regime, International Journal of Heat and Mass Transfer 54 (2011) 4376–4388.
[299] S. Tahir, M. Mital, Numerical investigation of laminar nanofluid developing flow and heat transfer in a circular channel, Applied Thermal Engineering 39 (2012) 8-14.
[300] R. Davarnejad, S. Barati, M. Kooshki, CFD simulation of the effect of particle size on the nanofluids convective heat transfer in the developed region in a circular tube, 2013.
[301] S.Z. Heris, M.N. Esfahany, G. Etemad, Numerical investigation of nanofluid laminar convective heat transfer through a circular tube, Numerical Heat Transfer, Part A, 52 2007, 1043–1058.
[302] Bianco V., Chiacchio F., Manca O., Nardini S., 2009, Numerical investigation of nanofluids forced convection in circular tubes, Appl. Thermal Eng. 29, 3632– 3642.
[303] Saha G. and Paul M. C., 2015, Heat transfer and entropy generation of turbulent forced convection flow of nanofluids in a heated pipe, Int. Com. in Heat and Mass Transfer 61, 26–36.
[304] M.K. Moraveji, R.M. Ardehali, CFD modeling (comparing single and two-phase approaches) on thermal performance of Al_2O_3/water nanofluid in mini-channel heat sink, International communications in heat and mass transfer 44, 2013, 157–164.
[305] A. Akbarinia, A. Behzadmehr, Numerical study of laminar mixed convection of a nanofluid in horizontal curved tubes, Applied Thermal Engineering 27 (2007) 1327–1337.
[306] P.K. Namburu, D.K. Das, K.M. Tanguturi, R.S. Vajjha, Numerical study of turbulent flow and heat transfer characteristics of nanofluids considering variable properties, International Journal of Thermal Sciences 48, 2, 2009, 290–302.
[307] V. Bianco, Oronzio Manca, and Sergio Nardini, Numerical Simulation of water / Al_2O_3 Nanofluid Turbulent Convection. Hindawi Publishing Corporation Advances in Mechanical Engineering Volume, 976254, 10.1155/2010/976254, 2010.
[308] M. Hejazian and M.K. Moraveji, A Comparative Analysis of Single and Two-Phase Models of Turbulent Convective Heat Transfer in a Tube for TiO_2 Nanofluid with CFD, Part A, 63 795–806, 2013, 2013.
[309] H. Yarmand, S. Gharehkhani, S.N. Kazi, E. Sadeghinezhad, and M.R. Safaei Numerical Investigation of Heat Transfer Enhancement in a Rectangular Heated Pipe for Turbulent Nanofluid, Hindawi Publishing Corporation Scientific World Journal 2014, 369593.
[310] I. Behroyan a, P. Ganesana, S. Heb, S. Sivasankaran, Turbulent forced convection of Cu–water nanofluid: CFD model comparison, Int. Comm. in Heat and Mass Transfer 67 (2015) 163–172.

[311] L. Colla, L. Fedele, O. Manca, L. Marinelli, S. Nardini, Experimental and numerical investigation on forced convection in circular tubes with nanofluids, Heat Transfer Engineering, 37 (13–14) (2016) 1201–1210.
[312] M.K. Moraveji, R.M. Ardehali, A Ijam, CFD investigation of nanofluid effects (cooling performance and pressure drop) in mini-channel heat sink, International Communications in Heat and Mass Transfer 40 (2013) 58–66.
[313] C. Abdellahouma, A. Mataoui, H. F. Oztop, Turbulent forced convection of nanofluid over a heated shallow cavity in a duct, Powder Technology 277 (2015) 126–134.
[314] A. Beheshti, M.K. Moraveji, M. Hejazian, Comparative numerical study of nanofluid heat transfer through an annular channel, Numerical Heat Transfer, 67 (2015) 100–117.
[315] A.M. Hussein, K.V. Sharma, R.A. Bakara, K. Kadirgama, The effect of cross sectional area of tube on friction factor and heat transfer nanofluid turbulent flow, International Communications in Heat and Mass Transfer, 47, (2013) 49-55.
[316] P. Kumar, A CFD Study of Heat Transfer Enhancement in Pipe Flow with Al_2O_3 Nanofluid, World Academy of Science, Engineering and Technology 57, 2011.
[317] V. Delavari, S. H. Hashemabadi, CFD simulation of heat transfer enhancement of Al_2O_3/water and Al_2O_3 / ethylene glycol nanofluids in a car radiator, Applied The. Engg. 73 (2014) 380-390.
[318] A. Celen, N. Kayaci, A. Çebi, H. Demir, A. Selim Dalkılıç S. Wongwises, Numerical investigation for the calculation of TiO_2–water nanofluids pressure drop in plain and enhanced pipes, International Communications in Heat and Mass Transfer 53 (2014) 98–108.
[319] M. Ziaei-Rad, Numerical investigation of pressure drop and heat transfer in developing laminar and turbulent nanofluid flows, IOP PUBLISHING, Phys. Scr. T155 (2013) 014021.
[320] M. Rostamani, S.F Hosseinizadeh, M. Gorji, and J.M. Khodadadi, Numerical study of turbulent forced convection flow of nanofluids in a long horizontal duct considering variable properties." International Communications in Heat and Mass Transfer 37, 1426–1431, 2010.
[321] H. Demir, A.S. Dalkilic, N.A. Kürekci, W. Duangthongsuk, S. Wongwises, Numerical investigation on the single phase forced convection heat transfer characteristics of TiO_2 nanofluids in a double-tube counter flow heat exchanger, International Journal of Heat and Mass Transfer 2011 38 218-228.
[322] H. Ounis, G. Ahmadi, J.B. McLaughlin, Brownian diffusion of submicrometer particles in the viscous sublayer, Journal of Colloid and Interface Science 143, 1991, 266–277.
[323] M. Manninen, V. Taivassalo, S. Kallio, On the Mixture Model for Multiphase Flow, In: VTT Publications, vol. 288. Technical Research Center of Finland.L. Schiller, A. Naumann, 1935, A drag coefficient correlation, Z. Ver. Deutsch. Ingenieure 77, 1996, 318-320.
[324] L. Schiller, A. Naumann, A drag coefficient correlation, Z. Ver. Deutsch. Ingenieure 77, 1935 318-320.
[325] U. Rea, T. McKrell, L. Hu, and J. Buongiorno, Laminar convective heat transfer and viscous pressure loss of alumina-water and zirconia-water nanofluids. International Journal of Heat and Mass Transfer 52, 2009, 2042-2048.
[326] M. Saberi, M. Kalbasi, A. Alipourzade, Numerical study of forced convective heat transfer of nanofluids inside a vertical tube. Inter. Jou. of the. Techno. ISSN 2013, 2277-4114.
[327] V. Bianco, O. Manca, S. Nardini, Numerical Investigation on Nanofluids Turbulent Convection Heat Transfer Inside a Circular Tube, Inter. Journal of Thermal Science, 50 2011, 341–349.
[328] B.E. Lauder, D.B. Spalding, lectures in Mathematical models of turbulence, Academic Press, London, 1972.